NASA CR112272

PROGRAM FOR ESTABLISHING LONG-TIME FLIGHT SERVICE PERFORMANCE OF COMPOSITE MATERIALS IN THE CENTER WING STRUCTURE OF C-130 AIRCRAFT

PHASE II - DETAILED DESIGN

April 1973

By W. E. Harvill, J. J. Duhig, and B. R. Spencer

Prepared under Contract No. NAS 1-11100 by
LOCKHEED-GEORGIA COMPANY
Marietta, Georgia

for

Langley Research Center
NATIONAL AERONAUTICS AND SPACE ADMINISTRATION

FOREWORD

This Phase II-Final Technical Report is submitted in fulfillment of the requirements of Contract NAS1-11100 and reports contract effort from May 1972 through March 1973. Phase II consisted of the detailed design of a composite-reinforced C-130 center wing box, and the necessary analytical and component test substantiation of the selected design. Prior to initiating the detailed design phase of program activities, extensive advanced development work was conducted in Phase I. This program activity was previously reported in NASA CR-112126. Subsequent program phases include fabrication of three C-130 center wing boxes, selectively reinforced with boron-epoxy composites, and ground/flight acceptance tests of these structures. One of the wing boxes will be subjected to a complete static and fatigue test evaluation. Two of the wing boxes will be flown on C-130 aircraft for a period of three years to demonstrate the long-time capabilities of such composite utilization.

This contract is conducted under the sponsorship of the Materials Application Branch of the Materials Division of the NASA Langley Research Center. Mr. H. Benson Dexter, Composite Section, is the NASA project monitor. Mr. W. E. Harvill is the Lockheed-Georgia Program Manager.

Major contributions to the work described herein and to this report were provided by the following Lockheed-Georgia personnel:

Design:	J. S. Bowers C. P. McElveen R. W. Coleman
Analysis:	D. C. Gibson (Static) M. G. Huff (Fatigue) H. R. Horsburgh (Fatigue) J. N. Dickson (Methods) J. B. Bailey (Flutter) R. S. Brown (Weights)
Adhesives:	A. O. Kays
Materials & Processes:	G. E. Davis
Cost/Producibility:	K. M. Barre'
Manufacturing:	E. C. Young
Structural Test:	W. M. McGee
Reliability:	J. J. Duhig
Quality Assurance:	J. B. Larsen

ABSTRACT

One of the most advantageous structural uses of advanced filamentary composites has been shown, in previous studies, to be in areas where selective reinforcement of conventional metallic structure can improve static strength/fatigue endurance at lower weight than that possible if metal reinforcement were used. These advantages are now being demonstrated by design, fabrication, and test of three boron-epoxy reinforced C-130 center wing boxes. This structural component was previously redesigned using an aluminum build-up to meet the increased severity of fatigue loadings. Direct comparisons of relative structural weights, manufacturing costs, and producibility can be obtained, and the long-time flight-service performance of the composite-reinforced structure can be evaluated against the wide background of metal-reinforced structure.

The first two phases of a five-phase NASA program to demonstrate the long-time flight service performance of a selectively reinforced center wing box have been completed. During the first phase of program activity, the advanced development work necessary to support detailed design of a composite reinforced C-130 center wing box was conducted. Activities included the development of a basis for structural design, selection and verifications of materials and processes, manufacturing and tooling development, and fabrication and test of full-scale portions of the center wing box. Phase I activities have been previously documented in NASA CR-112126.

Phase II activities described in this report consisted of preparing detailed design drawings and static strength, fatigue endurance, flutter, and weight analyses required for Phase III wing box fabrication. Some additional component testing was conducted to verify the design for panel buckling, and to evaluate specific local design areas. Development of the "cool tool" restraint concept was completed, and bonding capabilities were evaluated using full-length skin panel and stringer specimens.

CONTENTS

CONTENTS (Continued)

CONTENTS (Continued)

TABLES

FIGURES

FIGURES (Continued)

FIGURES (Continued)

FIGURES (Continued)

FIGURES (Continued)

LIST OF SYMBOLS AND ABBREVIATIONS

Symbol	Description
A	Cross section area
Al	Aluminum
α	Coefficient of thermal expansion
b	Width
c	Column end fixity factor
$\mathbb{C}$	Centerline
cm	centimeter
δ	Deflection
Δ	Incremental change
ϵ	Strain
f	Stress
^{o}F	Temperature in degrees Fahrenheit
G	Shear modulus of elasticity
g	Gram
Hg	Mercury
Hz	Frequency
I	Moment of inertia
in.	Inch
^{o}K	Temperature in degrees Kelvin
kip	One thousand pounds force
ksi	One thousand pound force per square inch
K_t	Quality level (see page 2)

Symbol	Description
L	Length
lb.	Pound (mass or force)
L/t	Length to thickness ratio
m	Meter
N	Newton (force)
N/mw	Newtons per meter width
N/m^2	Newtons per square meter
N_x	Column load per inch width
η	Shear flow parameter
ν	Poisson's ratio
μ	Micro
P	Load (force)
piw	Pounds force per inch of width
psi	Pounds force per square inch
psig	Pounds force per square inch (gage)
R	Ratio of minimum stress to maximum stress
RT	Room Temperature
σ	Stress
s.f.h.	Simulated flight hours
T	Temperature
t	Thickness
V_L	Aircraft limit (dive) speed

B

Symbol	Description
W	Weight
w	Deflection
W.S.	Wing station

Subscripts

A, a	Aluminum (also used as superscript)
B, b	Boron-epoxy (also used as superscript)
cr	Critical
i	i^{th} element
j	j^{th} element
m	Mean
o	Operating temperature
R	Restraint load
ST	Steel
v	Varying
1, 2	Normal to and in the plane of cross-section
12, 21	Refers to major and minor Poisson's ratio

PROGRAM FOR ESTABLISHING LONG-TIME FLIGHT SERVICE PERFORMANCE OF COMPOSITE MATERIALS IN THE CENTER WING STRUCTURE OF C-130 AIRCRAFT PHASE II - DETAILED DESIGN

By W. E. Harvill, J. J. Duhig, and B. R. Spencer

1.0 SUMMARY

One of the most advantageous structural uses of advanced filamentary composites is in areas where selective reinforcement of conventional metallic structure can improve static strength/fatigue endurance at lower weight than would be possible if metal reinforcement were used. The first two phases of a five-phase NASA program to demonstrate the long-time flight service performance of a selectively reinforced center wing box have been completed. During the first phase of program activity, the advanced development work necessary to support detailed design of a composite-reinforced C-130 center wing box was conducted. Activities included the development of a basis for structural design, selection and verifications of materials and processes, manufacturing and tooling development, and fabrication and test of full-scale portions of the center wing box. Phase I activities have been previously documented in NASA CR-112126, Reference 2.

During Phase II, the basic C-130E aluminum center wing box design was changed by removing aluminum and adding unidirectional boron-epoxy reinforcing laminates bonded to the crown of the hat stiffeners and to the skin under the stiffeners. The laminates were added in a nominal 80/20 area ratio of aluminum to boron-epoxy. Sufficient material was provided to meet ultimate load requirements of the C-130E wing box and the fatigue life of the C-130 B/E wing box[1]. Laminates are tapered out at the rainbow end fittings and access door openings by progressively stopping individual plies of the tape. Fasteners are used at the ends of the laminates to prevent peeling. Adequate bearing surface is provided in fastener penetration areas by titanium doublers integrally bonded into the laminates. Careful design and manufacturing techniques were used to reduce the number of fasteners (particularly blind fasteners) which penetrate the laminates, thus minimizing potential installation and inspection problems. A total of 129 detailed design drawings were prepared for initiation of the production program.

Applied design loads applicable to the Model C-130 B/E extended service life airplane were used to establish internal load distributions for static strength analyses. Surface pressures were obtained by combining surface airloads, fuel inertias, and surface crushing loads due to wing bending. Thermal residual stresses due to adhesive cure techniques and operating temperature extremes were added to the applied internal loads. The composite elements of the upper and lower surfaces were analyzed for combined tension-shear and compression-shear interactions using a specially developed computer program for composite structures. Modes of failure included general instability, local instability, and principal stresses. In all cases, positive margins of safety are shown for the final design.

[1] NOTE: The terminology "C-130 B/E" or "B/E" refers to the existing metallic center wing box which is installed in Model C-130B and C-130E aircraft. This is the metal-reinforced center wing retrofitted to a sizeable part of the C-130 fleet, and is the wing box being used in current production aircraft. In this report, the "B/E" designation always refers to an aircraft model and never means boron-epoxy. Where boron-epoxy is discussed, the words are spelled out.

A fatigue endurance analysis was conducted which demonstrated that the C-130E boron-epoxy reinforced center wing box possesses a fatigue capability equal to or greater than that of the C-130 B/E all-aluminum center wing. The analysis was based on wing box loads encountered in current operational usage and test spectra loads for parametric variation of quality levels from 4.0 through 12.0. ⚠ Ten wing stations on both the upper and lower surfaces were analyzed. The fatigue endurance computed for selected quality levels for a typical wing station is shown in Figure 1. The analysis results show that, at any station, the aluminum alloy stress is lower in the composite-reinforced structure than in the original all-aluminum structure. This factor is the major contributor to improved fatigue performance. It is fully expected that the fatigue performance of the C-130E boron-epoxy reinforced wing box will satisfactorily equal or exceed the required 40,000 simulated flight hours on the Phase IV full-scale center wing fatigue test, and will exceed the Phase V operational requirements.

Flutter analyses were conducted to evaluate the effects of any stiffness changes due to the boron-epoxy reinforced center wing on the airplane flutter characteristics. Wing stiffnesses were found to be essentially unchanged, and calculated flutter margins exceed those required. With normal fuel management, flutter speeds are above $1.15V_L$ (i.e., 1.15 times limit speed) for the composite-reinforced C-130E, satisfying specification requirements. Under abnormal fuel sequencing, the composite-reinforced airplane is subject to the same speed restrictions as those currently imposed on the original C-130E and C-130 B/E aircraft.

Although weight saving was not a major program goal, and was actually subordinated to accomplishment of flight service program goals, it is, nevertheless, an important factor, and a weight saving of 229 kg (506 lbs.) is predicted. This prediction, based on actual calculations from the final production drawings, represents a saving in total box weight of slightly more than 10 percent. The 318 kg (700 lb.) total of boron-epoxy to be used in two wing boxes for the 3-year flight evaluation represents a sizeable exposure of boron-epoxy materials to the service environment encountered over the life of an aircraft.

⚠ The quality level, K_f, is defined as the numerical value of an effective stress concentration factor which yields a Miner's damage of unity. In addition to local geometry, a number of uncontrolled variables are included in the determination of the quality level of a specific area of a complex structure such as a wing box. These variables include:

i Material inconsistencies such as: anisotropy; non-homogeneity; inelasticity; inclusions; voids; variations in physical properties; grain size.

ii Manufacturing variables such as: tolerances causing variations in part size and thickness, surface finish; fastener size; hole size; joint friction; assembly errors.

iii Other variables such as: non-linear slippage of joints; local plastic yielding at points of high stress concentration; complexity and redundancy of load paths; fretting of joints; fretting corrosion; design errors; irregularity of service usage and external loadings.

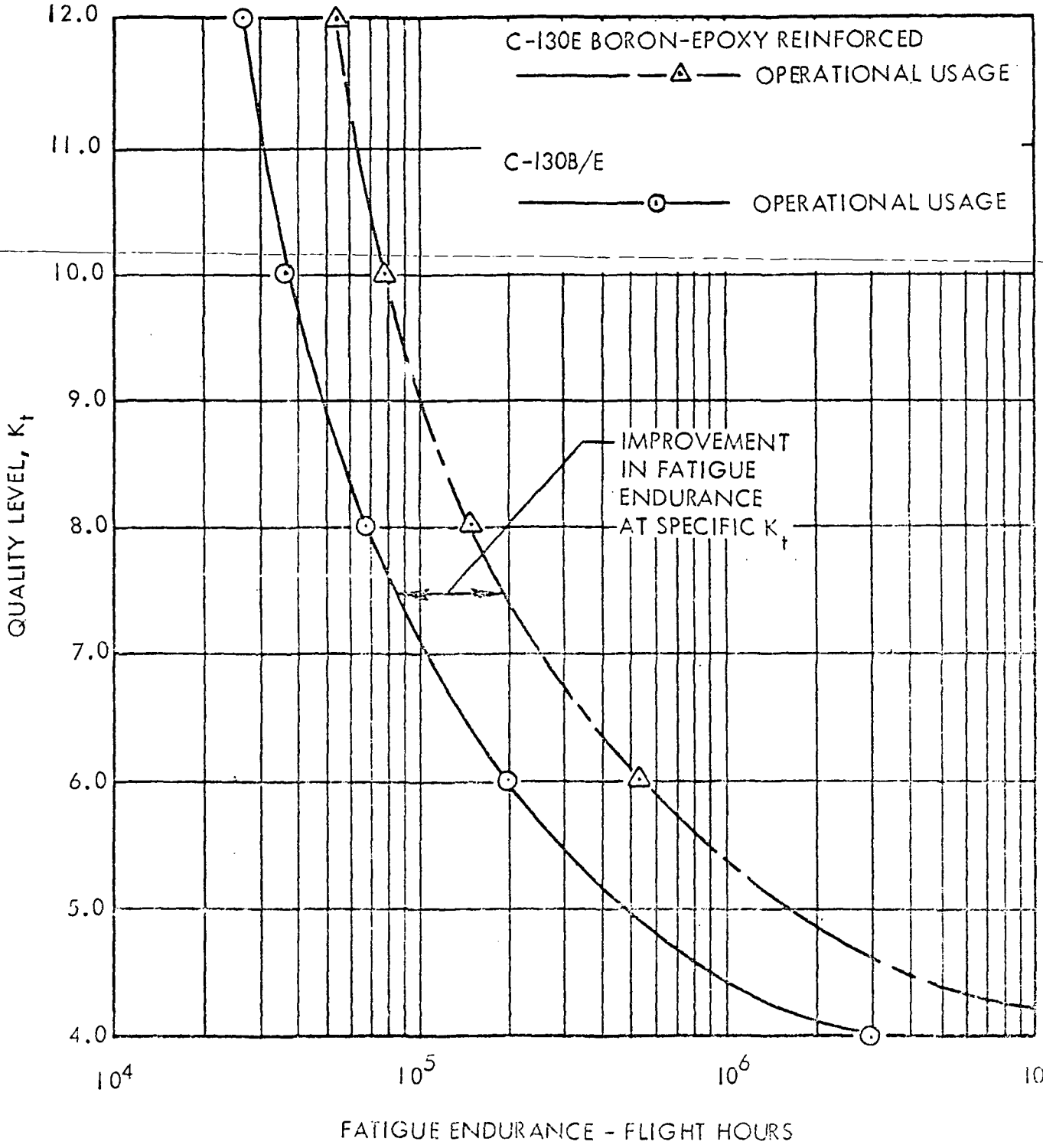

FIGURE 1. - QUALITY LEVEL VERSUS FATIGUE ENDURANCE
W.S. 80 LOWER SURFACE - OPERATIONAL USAGE

Table I summarizes the overall weight of the composite-reinforced center wing box.

TABLE I.-COMPOSITE-REINFORCED CENTER WING BOX STRUCTURE WEIGHT SUMMARY

Center Wing Box Structure	Weight of Metal Structure		Metal Removed		Boron-Epoxy Added		Weight Saved		Weight of Boron-Epoxy Reinforced Structure	
	(kg)	(lb.)	(kg)	(lb.)	(kg)	(lb.)	(kg)	(lb.)	(kg)	(lb.)
Upper Surface	726	1600	227	500	85	187	142	313	584	1287
Lower Surface	671	1480	165	364	74	163	91	201	580	1279
Other (Ribs, spars, bracketry, etc.)	846	1864	4 (Added)	8 (Added)	-	-	-4	-8	850	1872
TOTAL	2243	4944	388	856	159	350	229	506	2014	4438

New material development for this program was limited to adhesives and their processing. The Phase I development work provided a low-temperaturing-curing adhesive system for bonding boron-epoxy laminates to aluminum. The process specification, which defines the laminate to aluminum bonding process, was published during this report period. Minor revisions were made to boron-epoxy material and process specifications to allow a more workable packaging arrangement and slightly less proof testing.

Manufacturing development during Phase II primarily consisted of further evaluation and refinement of the cool tool restraint system for controlling warpage in bonded assemblies. Since the largest specimen fabricated in Phase I was only 366 cm (144 in.) long, Phase II efforts were directed to bonding full-length, 1079 cm (426 in.), boron-epoxy laminates to the aluminum stringers and wing planks. These full-length bonding studies have conclusively shown that, with proper tooling, parts can be bonded to provide a bondline with a low stress at room temperature. The resulting low warpage will allow assembly into a full wing box with a minimum of difficulty. Minor changes were made in the method of generating holes in the boron-epoxy laminates which improve hole quality. A blind fastener installation study determined the amount of aluminum reinforcing material required on the blind laminate surface to contain the swaging action of the blind fastener on installation.

Preliminary cost projects for prediction quantities of C-130 composite-reinforced center wing boxes were made based on test specimen cost data. The total cost increase to add boron-epoxy reinforcement is projected for the 200th production wing box to be $47,840 for labor and materials. The computed cost per pound of weight saved is approximately $95. Changes to the wing box structure are within current C-130 production practices. Special effort was made throughout design development to minimize the producibility impact of the composite-reinforcement addition. Installation of the completed wing box assembly will be the same as for regular production wing boxes.

A reliability and quality assurance program was continued in accordance with the approved program plan. The reliability assessment at the end of Phase II is that a good to high confidence level exists in the final design and the state of readiness for successful fabrication and assembly. Nondestructive inspection methods were refined. There were very few quality discrepancies in test specimens produced during Phase II.

Additional buckling evaluations were conducted during Phase II because of problems encountered in obtaining valid buckling failures in Phase I compression test panels. Applying compressive loads directly to unidirectional boron-epoxy laminates typically causes local stresses at the bearing surface and failure of the epoxy matrix, resulting in unsupported fibers and unloading of the laminate. A technique was developed for encapsulating the element ends in tooling plastic, which provided the laminate fibers with added support during end machining and allowed direct compressive loading. With this load introduction technique, successful compression tests were conducted which included one short crippling specimen, three short buckling panels, and two full-panel buckling specimens. In each test the failure load exceeded the predicted failure load, and good buckling failure modes were observed. The tests confirmed analytical predictions and verified required structural capability.

During Phase I fatigue testing of specimen 130PF-1, minor fatigue cracks were found, originating from cutouts of the stringer crown on some stringers. Although these cracks were traced to a sharp edge remaining after the cutout was made, it appeared that some slight configuration changes might provide a much better cutout design, and specimens were tested to verify the design selection. The tests showed that there was no clear advantage to be gained by a configuration change, and the existing C-130 B/E configuration was retained.

The successful completion of the detailed design work, along with substantiating analyses, tests, and tooling studies, enabled initiation of the fabrication phase of the program. The third phase was started in February 1973.

2.0 INTRODUCTION

Application studies and Advanced Development tests (References 1 and 2), conducted for NASA by Lockheed, have shown that boron-epoxy composite laminates bonded to the skin and stiffeners of the C-130 aircraft center wing box can significantly improve the overall fatigue endurance of the structure, at a lower weight than that possible if metal reinforcements were used to achieve the same endurance levels. These advantages will be demonstrated by designing, fabricating, and testing three boron-epoxy reinforced C-130E center wing boxes, in a five-phase program extending over 5-1/2 years. The program phases and associated schedules are illustrated in Figure 2. Phases I and II have been completed. Documentation of activities is included in this report and in References 1 through 3.

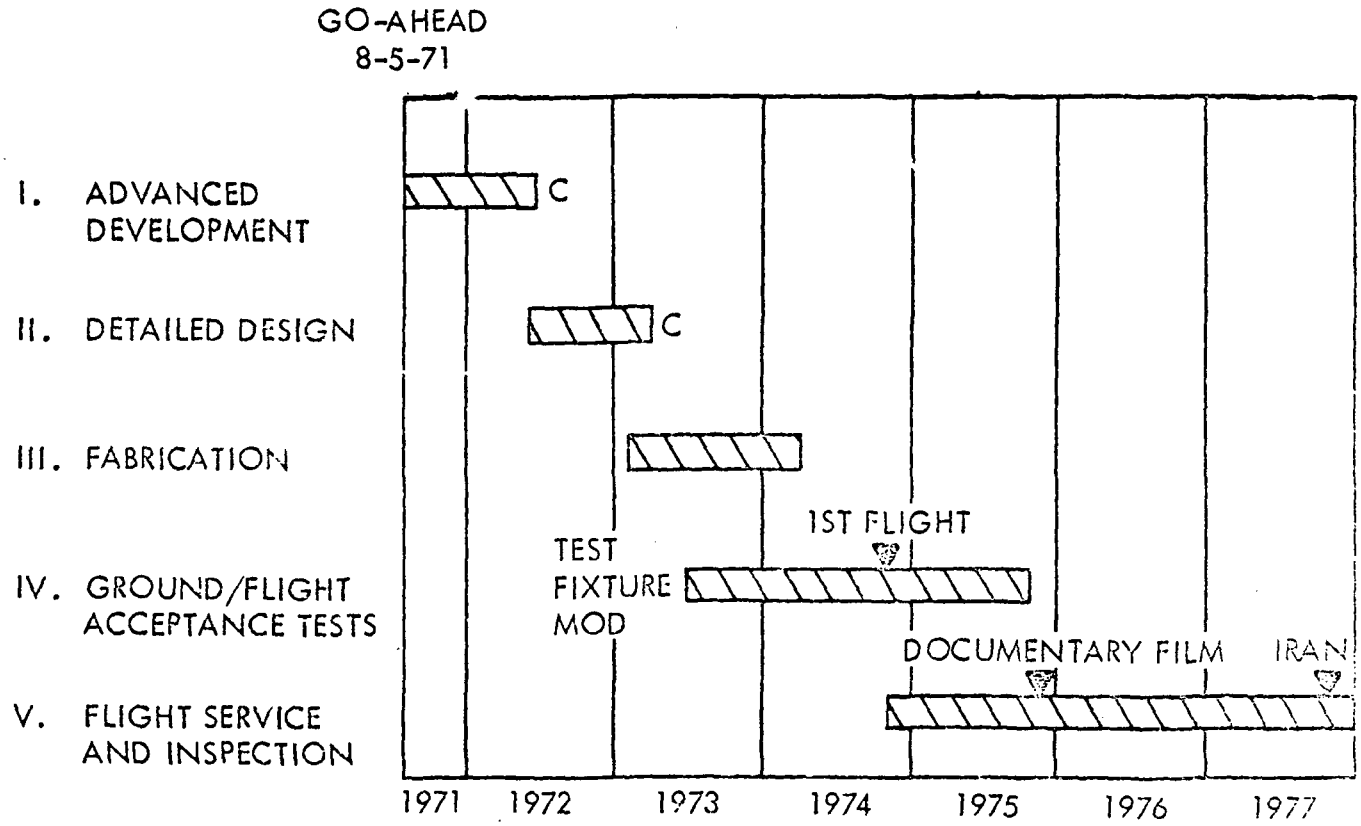

FIGURE 2.-SCHEDULE

The center wing box size and location are illustrated in Figure 3. The box is 11.2m (440 in.) long, 2.03m (80 in.) in chord and, in the all-metal configurations, weighs about 2243 kg (4944 lb.). The all-metal configuration is illustrated in Figure 4.

During Phase I, the advanced development work necessary to support detailed design of a composite reinforced C-130 center wing box was conducted. Activities included the development of a basis for structural design, selection of materials and processes, manufacturing and tooling development, and fabrication and test of full-scale portions of the center wing box. The Phase I results further confirmed that, with boron-epoxy reinforcements as shown in Figure 5, equivalent static strength and fatigue endurance could be provided with a significant weight savings. The aluminum skins and stringers have reduced thicknesses compared with those of the existing metallic center wing box in Model C-130 B/E aircraft. Equivalent strength is provided by the unidirectional composite.

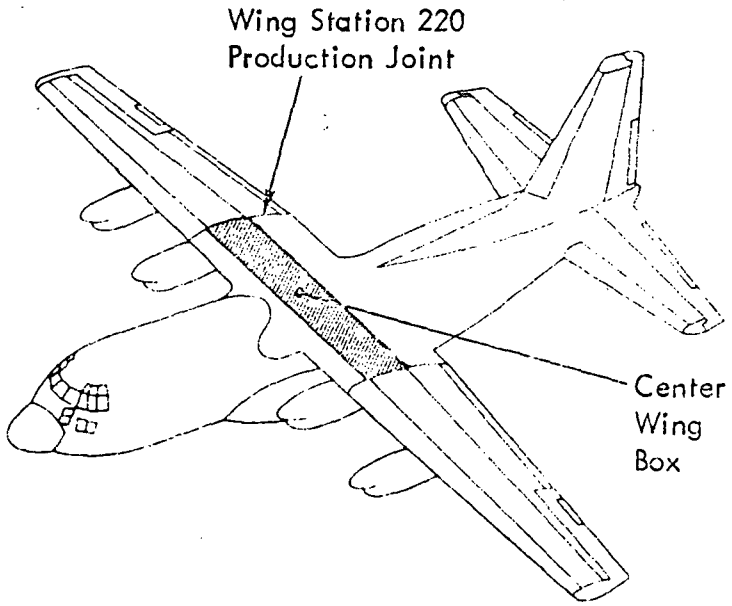

FIGURE 3.-C-130 CENTER WING BOX LOCATION

1. UPPER SURFACE PANELS
2. UPPER SURFACE STRINGERS
3. UPPER SURFACE RAINBOW FITTING
4. LOWER SURFACE PANELS
5. LOWER SURFACE STRINGERS
6. LOWER SURFACE RAINBOW FITTING
7. FRONT BEAM
8. REAR BEAM

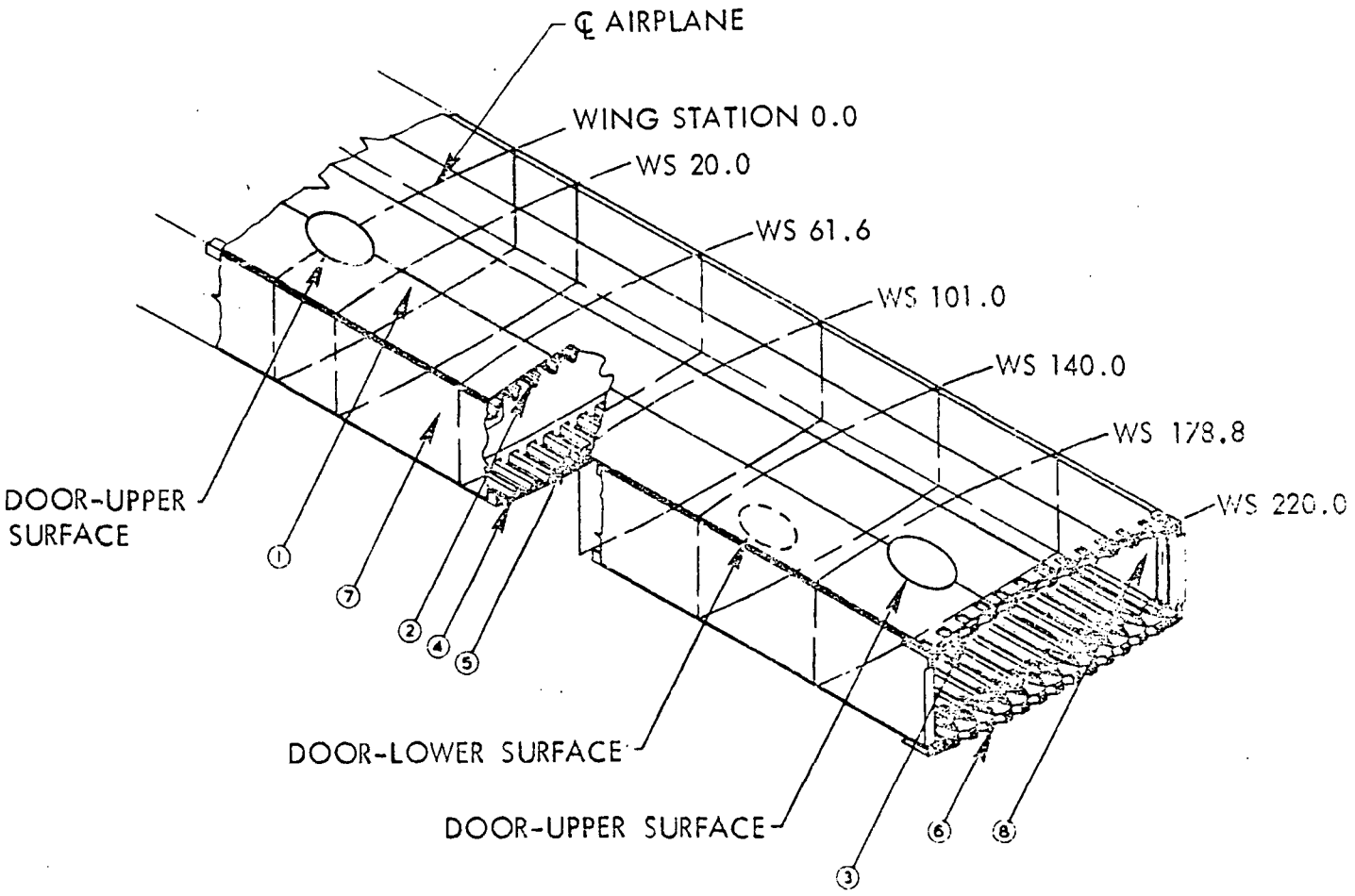

FIGURE 4.-MODEL C-130 B/E CENTER WING BOX

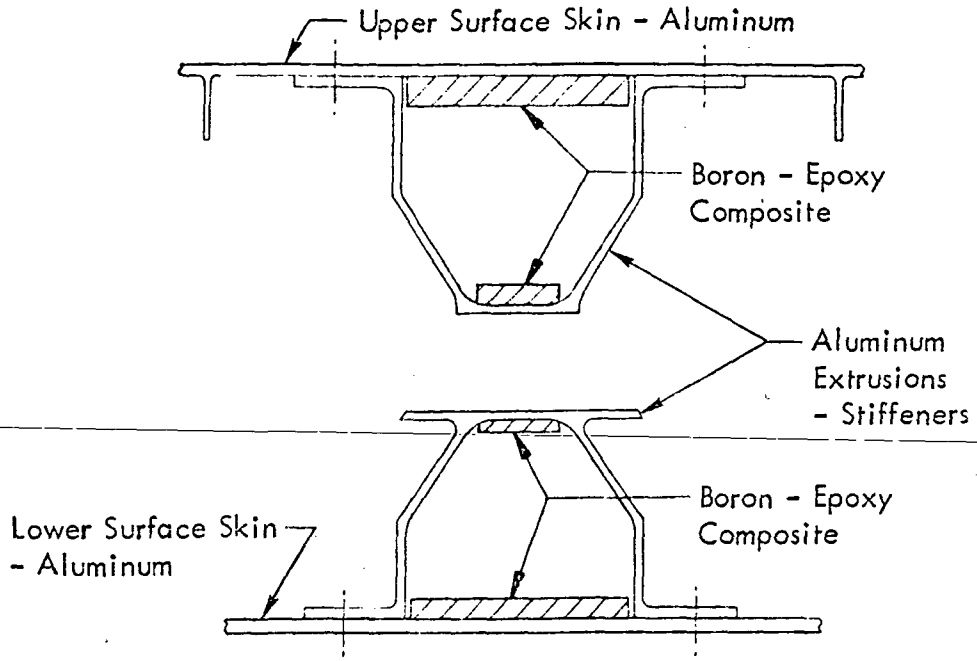

FIGURE 5.-COMPOSITE REINFORCEMENT CONCEPT

Phase II activities described in this report consisted of preparing detailed design drawings and conducting the substantiating static strength, fatigue endurance, flutter, and weight analyses required for proceeding into Phase III wing box fabrication. Some additional component testing was conducted to complete the panel buckling evaluation and to evaluate specific local design concepts. Tooling development activities were continued to further refine the "cool tool" concept and to evaluate residual stresses with full-length skin panels and stringers. The final design configuration is structurally and functionally interchangeable with the production C-130 B/E wing box.

The first composite-reinforced wing box will be static tested to limit load, followed by an endurance test to a fatigue spectrum representative of four aircraft lifetimes. Finally, this box will be tested statically to determine its residual strength. The other two wing boxes, after a complete FACI (First Article Configuration Inspection), will then be installed in two Air Force C-130 E aircraft, and the aircraft will be delivered for operational service. Service experience will be monitored and documented. Detailed inspections of these two wing boxes, including the use of sophisticated non-destructive test techniques, are scheduled to coincide with regularly phased aircraft inspections.

3.0 STRUCTURAL DESIGN

3.1 STRUCTURAL DESIGN PHILOSOPHY

The design philosophy established in Phase I and refined in Phase II retained the basic dimensions of the C-130E configuration and the material of the C-130 B/E wing box. This configuration allowed, as a minimum, the development of 100 percent of the design limit load requirement, without benefit of any composite reinforcement, and provided a degree of fail-safe capability.

The basic aluminum center wing box was reinforced with unidirectional boron-epoxy laminates in the crown of the hat stiffeners and on the skin under the stiffeners. The laminates added were sufficient to allow the center wing box to develop the ultimate load requirements of the C-130E wing box and the fatigue life of the C-130 B/E wing box. Functional and selected structural configurations of the current C-130 B/E model were maintained in the areas of access cutouts, fuselage interface, and joint runouts. Residual thermal stresses induced by joining dissimilar materials were accounted for in the analysis for static and fatigue loading. The detail design gave primary consideration to safety and reliability. Other important considerations included producibility, cost, and maintainability. Although weight saving was of lesser importance, all design decisions were monitored to achieve a minimum practicable weight structure which was consistent with the overall objectives of the flight service program.

3.2 BASIC DESIGN

The center wing box and location of the boron-epoxy composite reinforcement is illustrated in Figure 6. The box is 11.2m (440 in.) long, 2.03m (80 in.) in chord, and in the all-metal configurations weighs approximately 2243 kg (4944 lb.).

Reinforcement of the upper and lower surface assemblies of the wing box is accomplished by designing new skin panels and hat-section stringers and adding boron-epoxy laminates. The cross-sectional area of the aluminum C-130 B/E skin panels and hat-section stringers is reduced to the original C-130E cross-sectional area. Access door areas, wing station 220 joint rainbow fittings, and splice straps are retained in the heavier C-130 B/E configuration. Skin panels and stringers are taper-transitioned to the thinner C-130E configuration inboard of the joint fittings and on each side of the access doors. Outboard of the upper surface outboard access doors, the C-130 B/E configuration is retained because of the close proximity to the W.S. 220 joint. Many of the existing model C-130 B/E components such as ribs, spars, fittings, brackets, and access doors are not changed.

In the final design, laminated strips of boron-epoxy material are to be bonded to the inner surface of the skin panels under each hat-section stringer. Separate laminate strips are bonded to each of the hat-section stringers on the enclosed crown surface. Multiple plies of unidirectional flat boron-epoxy tape are used to fabricate the laminates. The

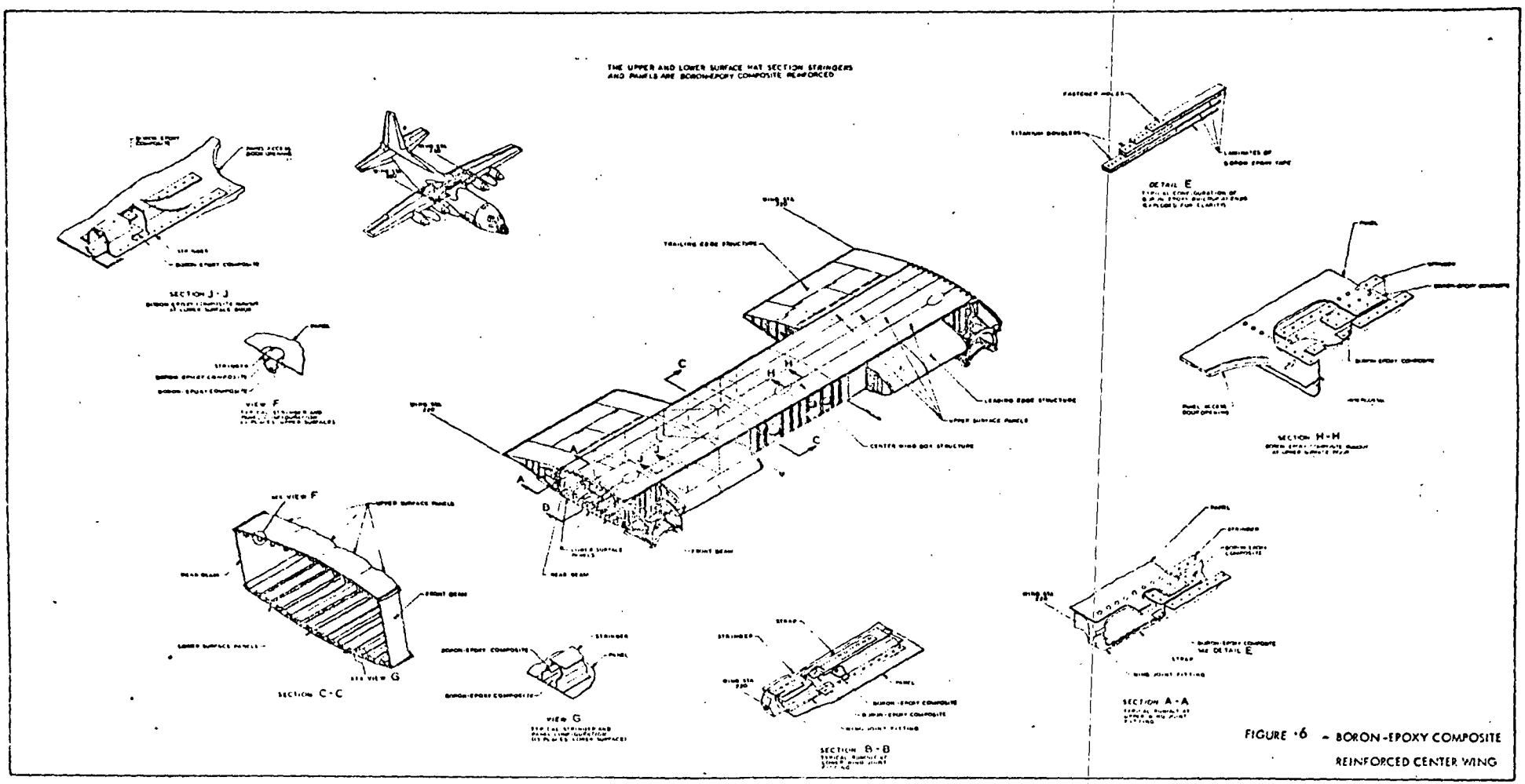

FIGURE 6 - BORON-EPOXY COMPOSITE REINFORCED CENTER WING

laminates are designed to taper out in the panel and stringer taper transition areas. Tapering of the laminates at the rainbow fittings and access door openings is accomplished by progressive stopping of individual plies of tape. Fasteners are used at the ends of the laminates to prevent peeling. Titanium doublers are integrally bonded in the laminate in fastener penetration areas to assure adequate bearing surface.

A total of 129 detailed design drawings were prepared. These are production drawings using Lockheed's standard practice and approval procedures and are now ready for initiation of the production program. Many of these are multiple-sheet drawings and are quite voluminous. They are, therefore, not incorporated into this report, but a listing is provided in Appendix B.

3.3 DESIGN PROBLEMS AND SOLUTIONS

The primary design concern in the use of boron-epoxy laminates is in the added complexity associated with fastener penetration through the laminates. Bonded areas produce no unusual problems, but a concerted design effort was made to minimize the number of fasteners that would penetrate the laminates. In a limited number of locations the structural arrangement and/or required assembly sequence necessitates the use of blind fasteners through the laminate after the stringers are assembled to the skin panels. For all fasteners which penetrate laminates, the following sequence is required to assure proper attachment.

- Titanium doublers are integrally bonded in the laminates at all hole locations.
- Undersized holes are produced in the boron-epoxy laminates during fabrication.
- Upon bonding of laminates to stringers and panels, the undersized holes in laminates are back-drilled through the aluminum stringers or panels.
- The undersized holes through the boron-epoxy and aluminum are then reamed to full size.
- At hole locations where blind fasteners are required on later installations, an aluminum reinforcing plate is bonded to the blind surface of the laminates.
- At other locations, the fasteners are installed from the laminate side of the composite structure.

Careful design and manufacturing techniques were used to reduce the number of locations where blind fasteners were required, precluding potential installation and inspection problems. Some of these potential problem areas, and their solutions, are discussed next.

3.3.1 Brackets and Sub-Structure Attachments

Fasteners which would have penetrated laminates but which could be relocated included attachments for bladder-cell lacing anchors, plumbing support brackets, and other miscellaneous substructure. Design solutions primarily consisted of physical relocation of the component where feasible. For other components, alteration or redesign was specified to eliminate holes which would have penetrated the laminates. Relocation of components was accomplished by designing simple clips and angles which attach through the stringer side flanges rather than the crown areas where the laminates are bonded. (See Figure 7, Detail A.) Some components are relocated to attach directly to the stringer "ears" which are remote from the laminate areas as shown in Figure 7, Detail B. In other instances brackets which bridged pairs of stringers and attached through the stringer crowns were altered or redesigned to bridge the same stringers but attach through the side flanges as shown in Figure 7, Detail C. In all of the above areas, the end item (plumbing, valves, etc.) was kept in its existing location to minimize costs and maintain commonality of functional parts on the FY 73 aircraft.

3.3.2 Nacelle Attach Fitting Attachments

On the new lower surface some of the nacelle attach fitting fasteners would have penetrated skin and skin laminates under the hat sections. These could not be prelocated due to assembly sequence requirements, since the attach fitting is installed after assembly of the stringers to the skin. Design solutions, as illustrated in Figure 8, included elimination of the blind fasteners (which would have penetrated the laminates), increased fastener diameter at adjacent locations and increased skin thickness (local pad to prevent buckling with the new fastener pattern). The nacelle attach angle installation was altered as described above and required other minor changes such as additional shims and sheet-metal clips to permit attachment of the aft nacelles and fairings.

3.3.3 Diagonal Brace Fitting Attachment

A tolerance build-up problem was encountered with the "tee" and fitting attachments at the upper end of diagonal braces. The braces extend from the upper to lower surface hat sections. For current installation, the "tee" fittings extend chordwise across three stringers and are attached by blind fasteners through the horizontal "tee" flange and stringer crown. Prelocation of these fasteners in the upper surface stringer laminates could have caused misalignment of the holes station-wise due to the spanwise tolerance of the holes. This tolerance effect was considered on the individual laminates, in the location of the laminate in relation to the stringer, and finally in the three stringer locations relative to each other.

To overcome the expected difficulties in locating the "tee" members in this area, plates were designed to attach through the stringer crown prior to installation of the stringers to the skin panels as shown in Figure 9. This allowed prelocation of the holes

C

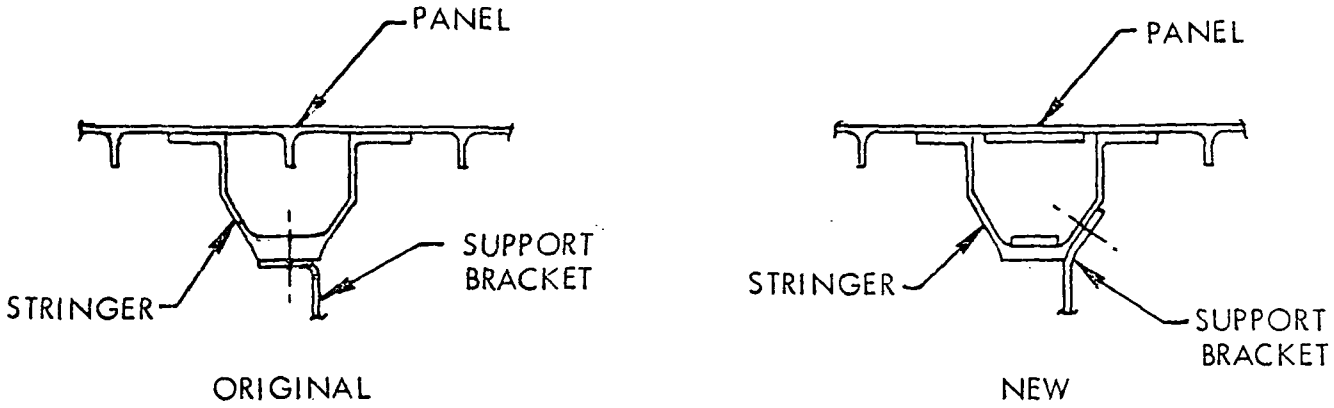

DETAIL A

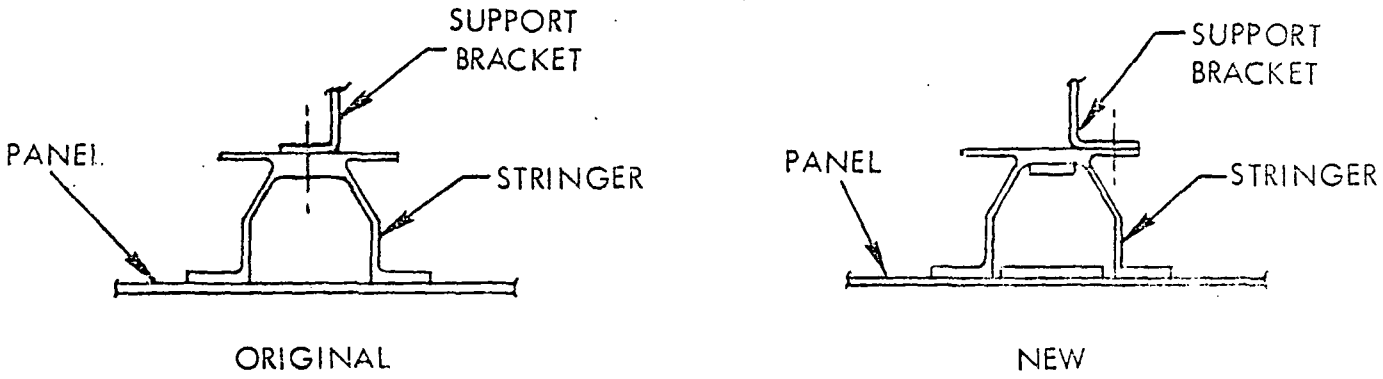

DETAIL B

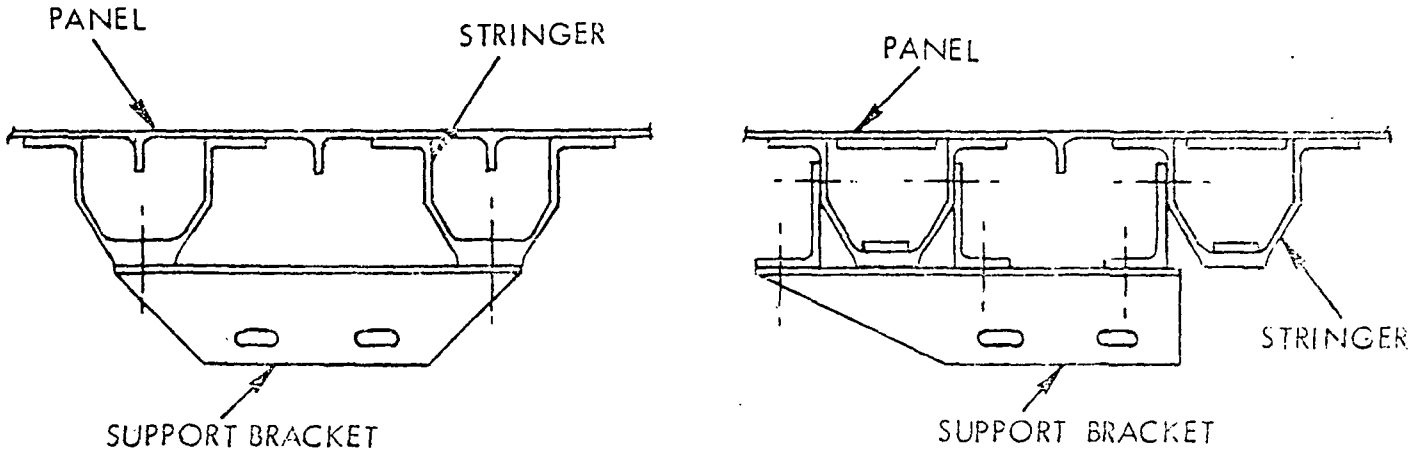

DETAIL C

FIGURE 7.-TYPICAL DESIGN SOLUTION FOR SUPPORT BRACKET

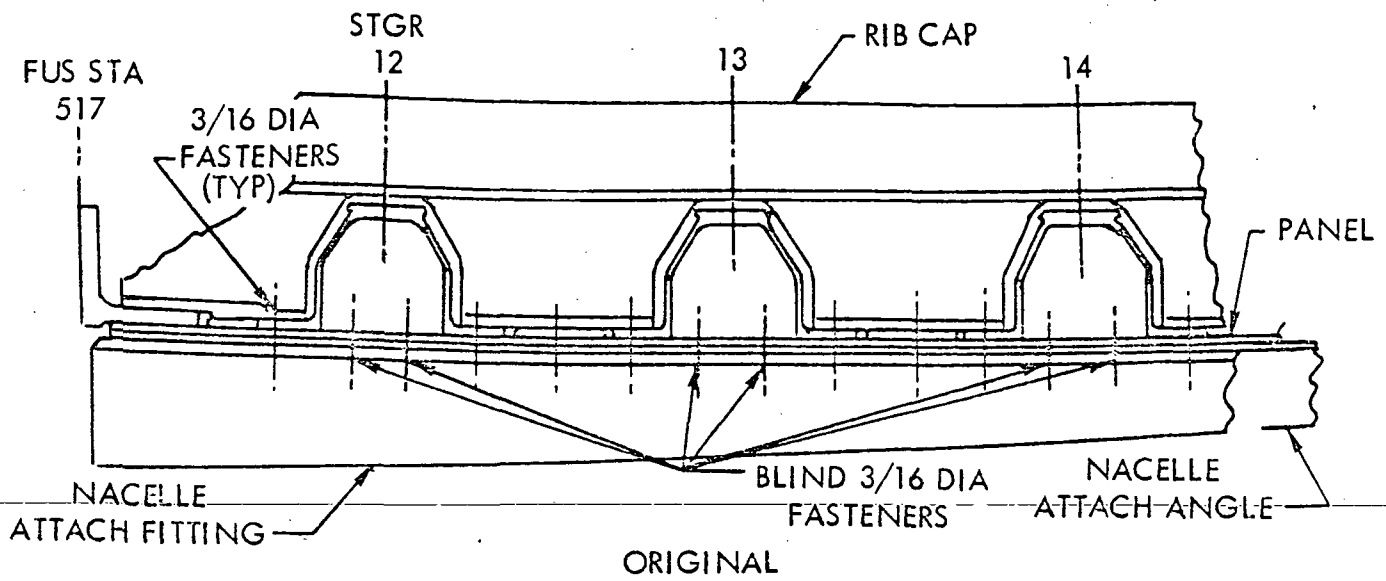

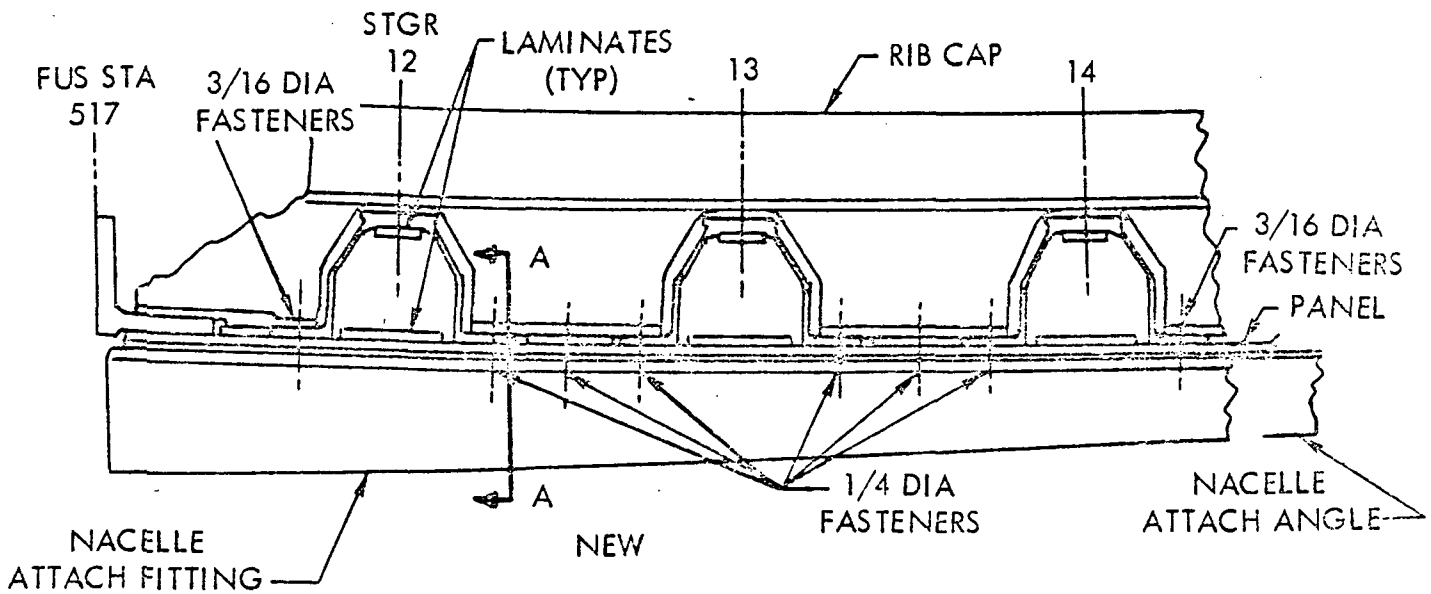

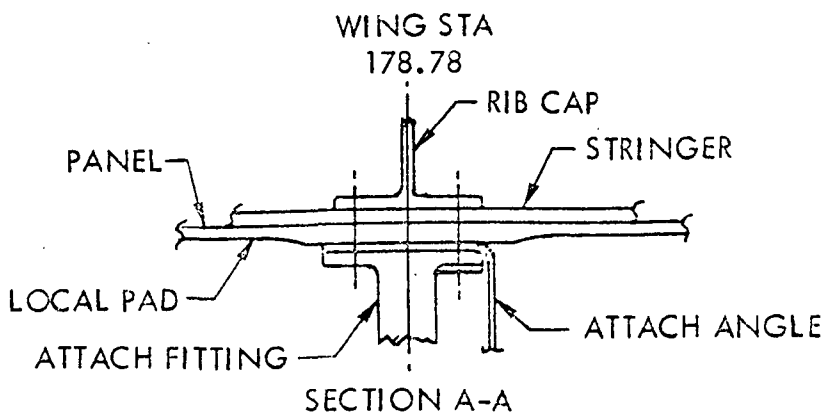

FIGURE 8.-NACELLE ATTACH FITTING ATTACHMENTS

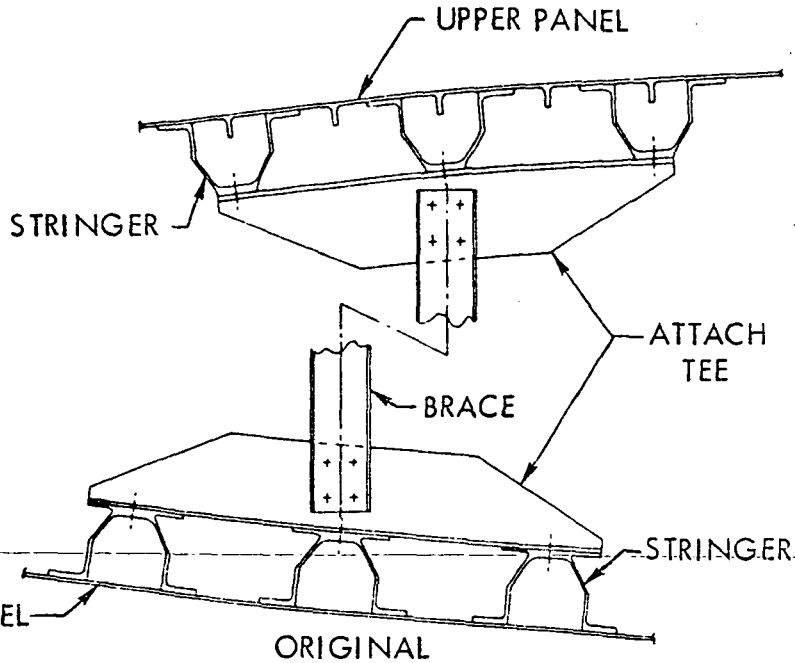

ORIGINAL

VIEW LOOKING INBD AT TYPICAL BRACE FITTING ATTACHMENT

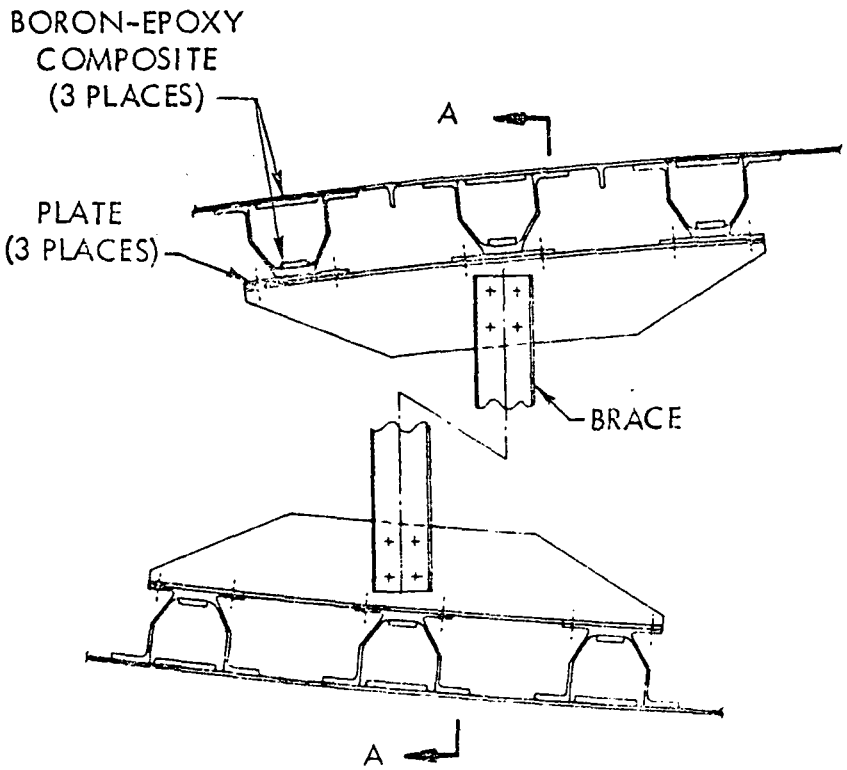

NEW

VIEW LOOKING INBD AT TYPICAL BRACE FITTING ATTACHMENT

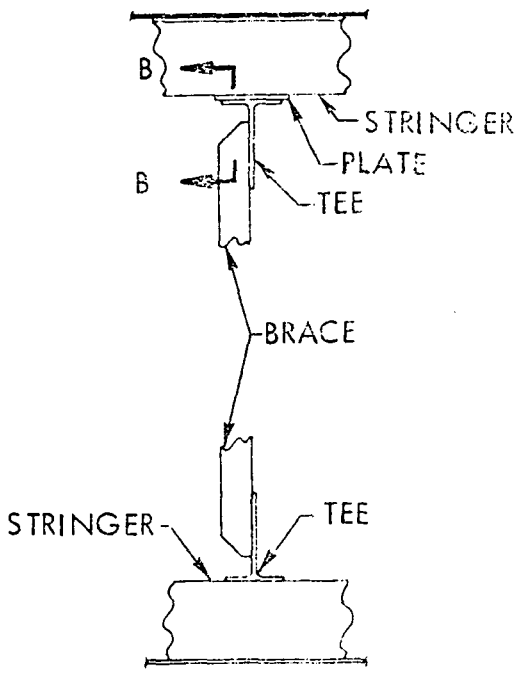

SECTION A-A

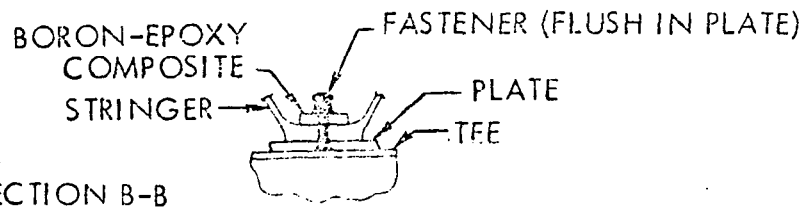

SECTION B-B
(TYP 3 PLACES)

FIGURE 9.-DIAGONAL BRACE FITTING ATTACHMENT

in the laminates and the use of standard fasteners to attach the plates. The plate extends forward and aft of the stringer crown and was made slightly oversize (spanwise-width) to account for adverse tolerances. The "tees" were altered to provide proper fit at the brace attachments with the length controlled to pick up the forward and aft ends of the new plates. Installation of the "tees" is then accomplished by aligning the "tees" station-wise in line with the lower surface fittings, locating and drilling holes through the "tee" horizontal flange and plates, and installing standard fasteners.

4.0 DESIGN SUBSTANTIATION

4.1 STATIC STRENGTH ANALYSIS

The advanced composite-reinforced C-130 center wing box was analyzed in a manner consistent with, and proved by, previous analyses and tests on existing C-130 series airplanes. Wing design loads applicable to the C-130B/E extended-service-life airplane were used to establish the internal load distributions. The internal loads were obtained by a high-speed digital computer program which used the conventional engineering "unit beam" theory of bending. Surface shear distributions were established by determination of the incremental changes in element axial loads and by application of the constant shear-flow torsion theory. Surface pressures, used for local bending analyses, were obtained by combining surface airloads, fuel inertias, and surface crushing loads due to wing bending. Surface pressures due to structural inertia were negligible and were not included. Thermal residual stresses due to adhesive cure techniques and operating temperature extremes of 218°K (-67°F) to 344°K (+160°F) were calculated and added to the applied internal loads.

The structural elements of the upper and lower surfaces were analyzed for both tension-shear and compression-shear interactions by a computer program developed exclusively for the composite reinforced structural configuration used by the C-130 wing. The program included the effects of thermal residual stresses, axial loading, lateral shear, and beam column effects due to the combined action of normal surface pressures and eccentricities of applied axial loading. Modes of failure were established for the individual components of the composite structure and included the analysis of general instability, local instability, and principal stress levels.

Satisfactory strength levels were demonstrated for the front and rear spar webs by the use of conventional diagonal-tension field analyses. The upper and lower surface splices were analyzed for fastener capability using the calculated surface shear distributions. Net section principal stresses were also calculated at skin panel locations with high fastener concentrations, including the effects of thermal residual stresses.

Pertinent results of the composite-reinforced center wing static strength analysis are presented in the following discussion. Torsional and flexural stiffnesses of the wing box are presented in Figures 10 and 11, respectively. For comparison, the previously published stiffnesses of the C-130E and C-130B/E center wings are superimposed on the same figures. Figure 10 shows that the torsional stiffness of the composite-reinforced wing is less than the stiffnesses of the C-130B/E wing but equal to or greater than the stiffness of the C-130E wing. This directly reflects the reduction of surface panel thicknesses from C-130B/E sizes to thicknesses close to those used for the C-130E wing. The boron-epoxy laminates are assumed to provide no contribution to the wing box torsional stiffness. A considerable increase of vertical bending stiffness is illustrated in Figure 11, where the stiffness of the composite reinforced wing is shown to exceed the C-130E and C-130B/E wing stiffnesses. This is due to the substantial contribution of the unidirectional boron-epoxy reinforcement in the spanwise direction.

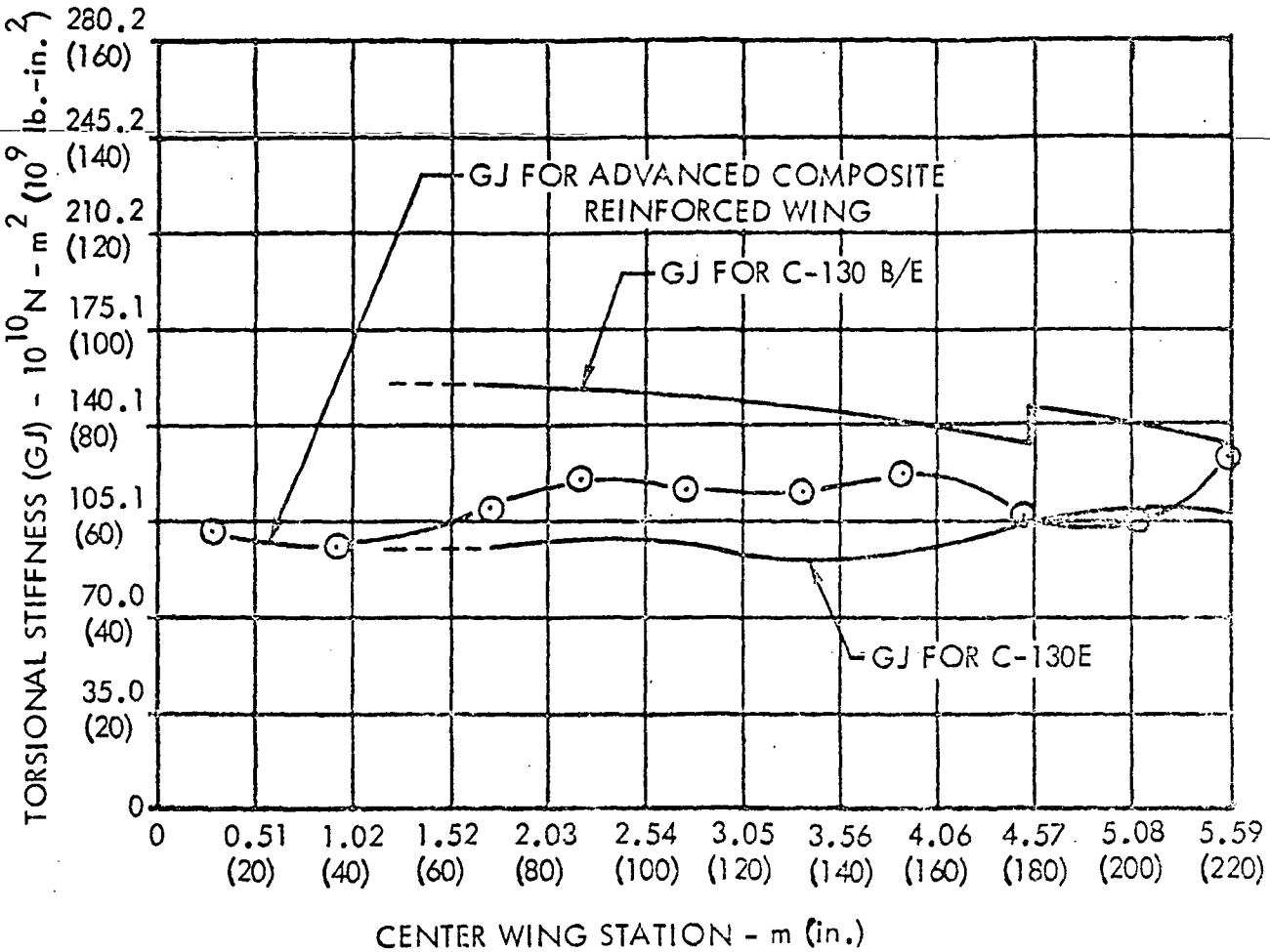

FIGURE 10.- TORSIONAL STIFFNESS (GJ) VERSUS CENTER WING STATION

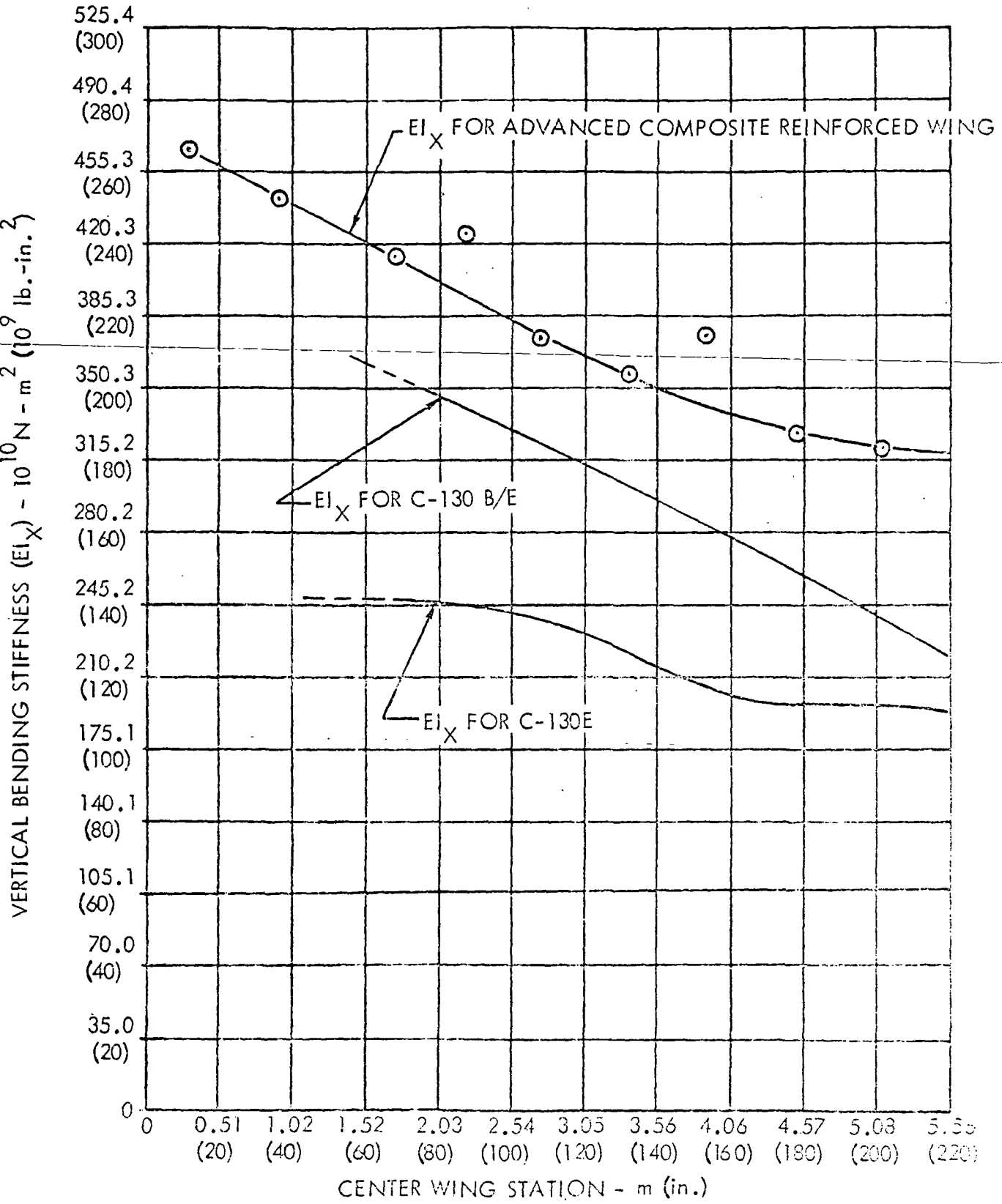

FIGURE 11.- VERTICAL BENDING STIFFNESS (EI_X) VERSUS CENTER WING STATION

Thermal residual stresses for the aluminum and boron-epoxy components, calculated by the method of analysis described in Appendix B of NASA CR-112126 (Reference 2), are presented in Figures 12 and 13. Residual stresses for operating temperatures of 218°K (-67°F), 255°K (0°F), 269°K (25°F), and 344°K (160°F) are presented. In addition, to illustrate the excellent results obtained by the "cool tool" adhesive cure technique, thermal residual stresses for the assumed room temperature of 297°K (75°F) are presented and show the desired low stress magnitudes. For convenience of numerical analysis, thermal residual stresses are plotted versus "aluminum area ratios," which are defined as follows:

$$R = \frac{A_a}{A_a + A_b} \times \frac{100}{1} \qquad \text{(percent)}$$

where R = aluminum area ratio (percent)

A_a = aluminum cross-section area of skin-stringer combination.

A_b = boron-epoxy laminate cross-section area of skin-stringer combination.

To achieve the desired fatigue endurance, the skin-stringer combinations of the composite-reinforced wing were designed nominally for an 80 : 20 distribution of aluminum and boron-epoxy cross-section areas, i.e. R = 80 percent. Variations to the 80 : 20 distribution were made as necessary to achieve desired strength levels and/or to satisfy the taper transition requirements at surface cut-outs and major joints. Typical aluminum area ratios for several representative upper and lower surface skin-stringer components are shown in Figure 14. Using appropriate area ratios and operating temperatures, the thermal residual stresses for the aluminum and boron-epoxy elements may be obtained from Figures 12 and 13, respectively. In accordance with Lockheed policy, and to cover uncertainties in the prediction of thermal strains and resulting stresses, a factor of 1.25 on thermal stresses is used when such a procedure is conservative; i.e., if the thermal residual stress is additive in terms of ultimate load stress (1.5 x limit load stress), the thermal residual stress is multiplied by 1.25 and added to the ultimate load stress.

Conversely, a factor of 1.0 is used if the thermal residual stress is subtractive with regard to ultimate load stress. The thermal residual stress contributions illustrated on Figures 15 and 16 include the appropriate factors.

The maximum axial stress levels for the aluminum and boron-epoxy elements of the composite-reinforced wing are presented on Figures 15 and 16, for upper and lower surfaces, respectively. For comparison purposes, the previously published maximum stresses for the "all aluminum" C-130E and C-130B/E center wings are superimposed on the same figures. Stress levels for the composite-reinforced wing, including the effect of thermal residual stresses, show good agreement with the stress levels of the extended-service-life airplane, model C-130B/E, and indicate that the fatigue endurances of the two airplanes should be similar. The maximum aluminum stress level of approximately 310 MN/m^2 (45 KSI) for the

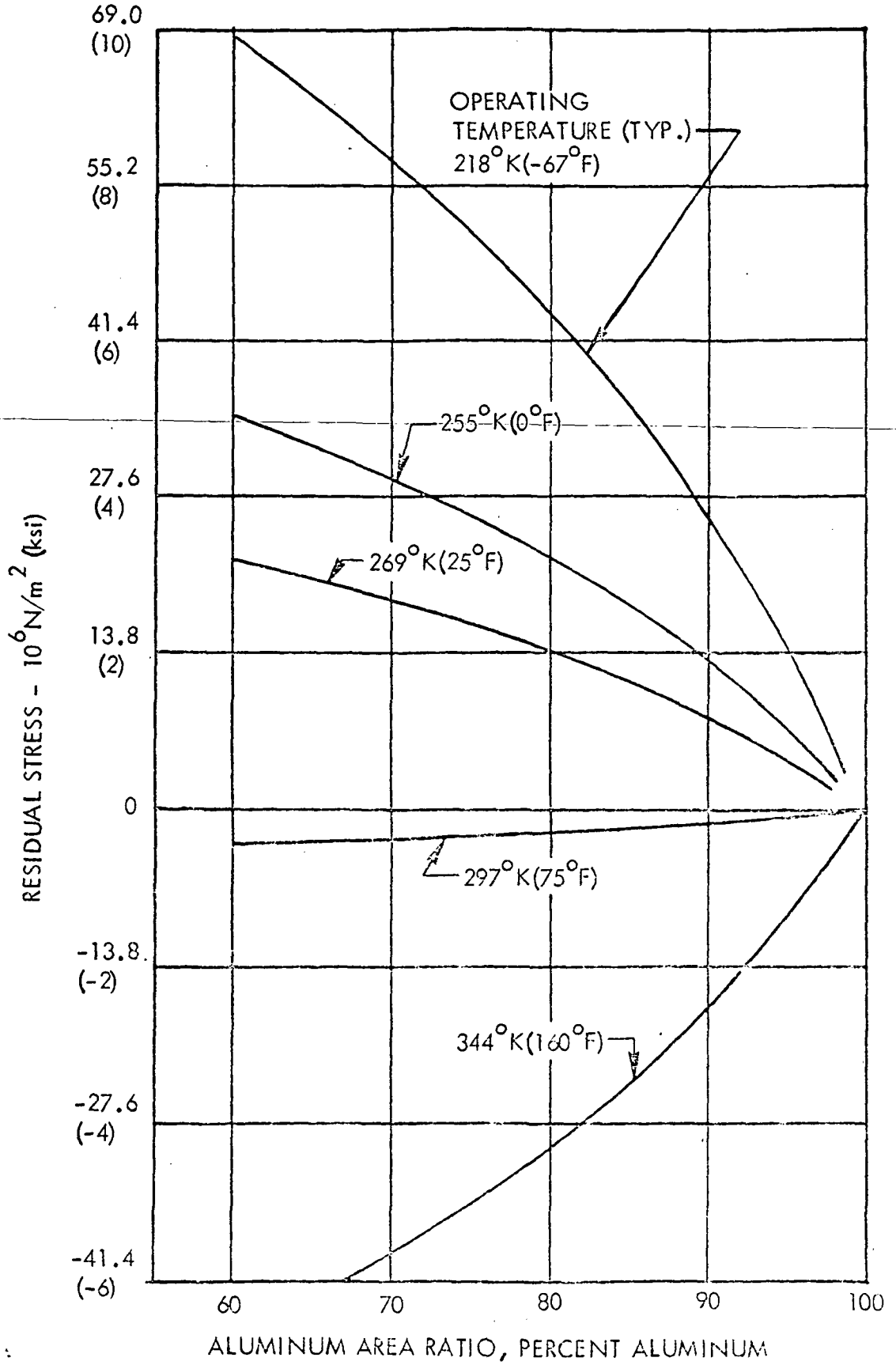

NOTE: COOL TOOL CURE TEMPERATURE 386°K(235°F)

FIGURE 12. - THERMAL RESIDUAL STRESSES FOR ALUMINUM ELEMENTS

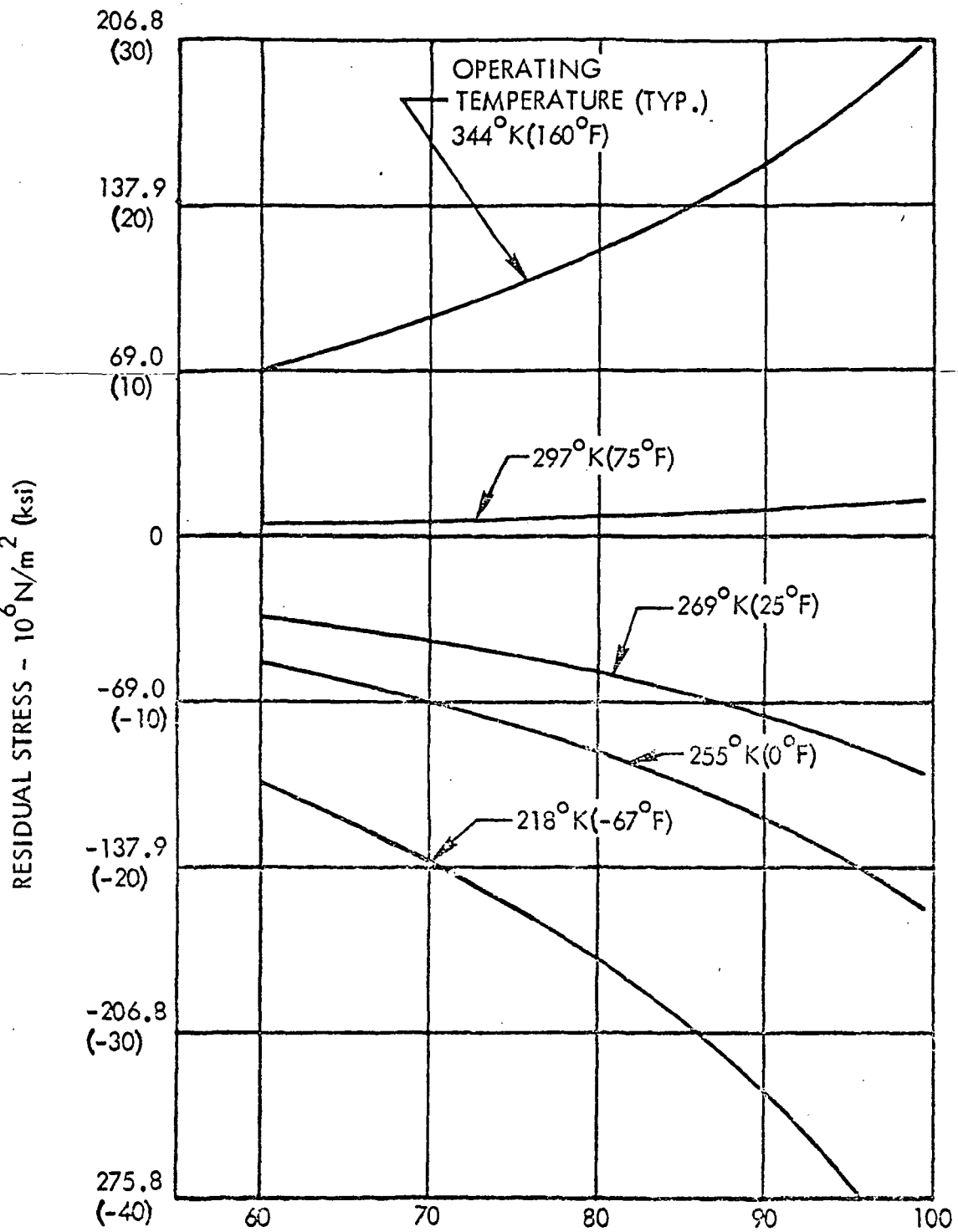

FIGURE 13. - THERMAL RESIDUAL STRESSES FOR BORON-EPOXY ELEMENTS

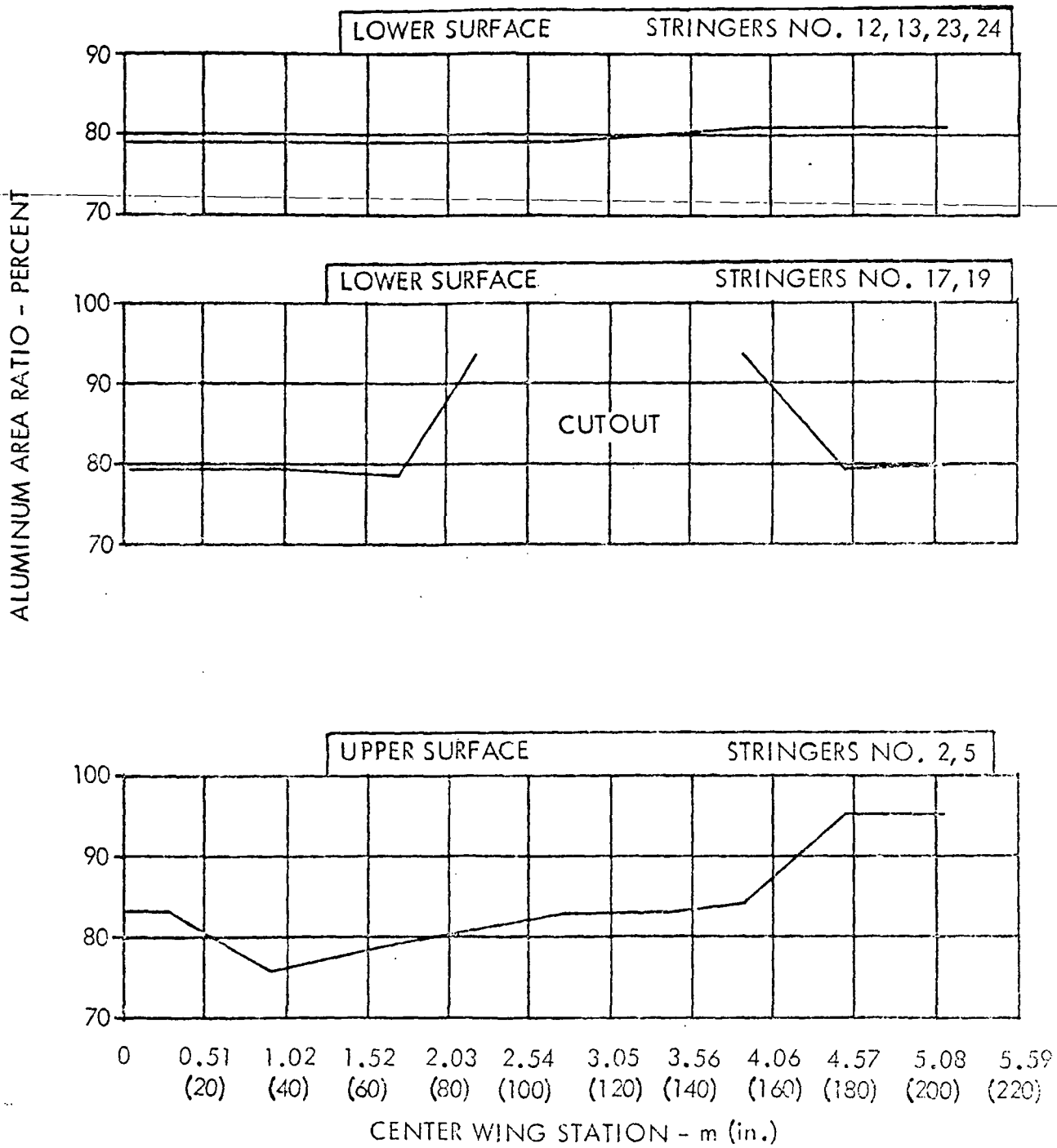

FIGURE 14. TYPICAL STRINGER ALUMINUM AREA RATIOS, PERCENT ALUMINUM VERSUS CENTER WING STATION

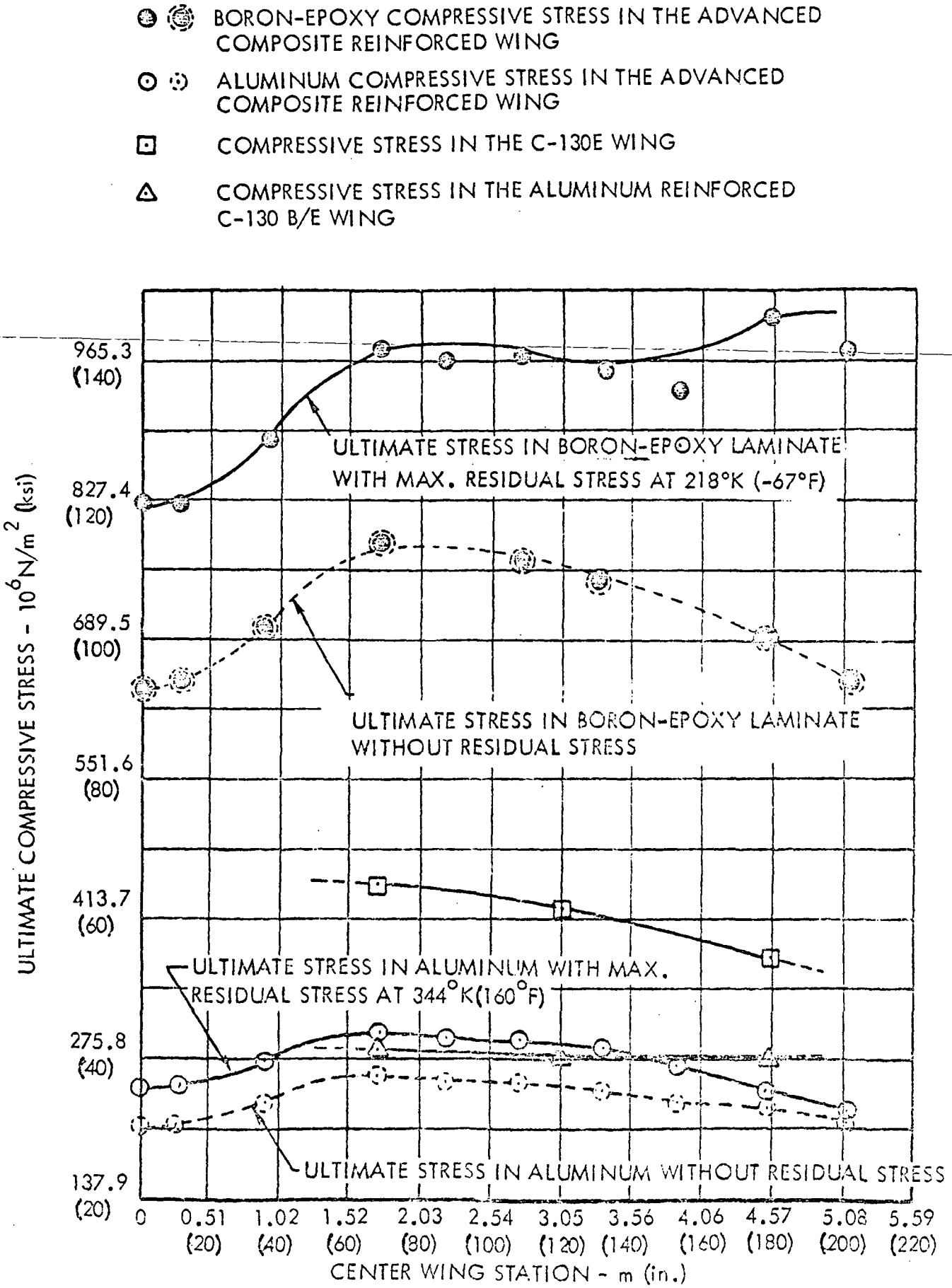

FIGURE 15. ULTIMATE COMPRESSIVE STRESSES FOR UPPER SURFACE STRINGERS VERSUS CENTER WING STATION

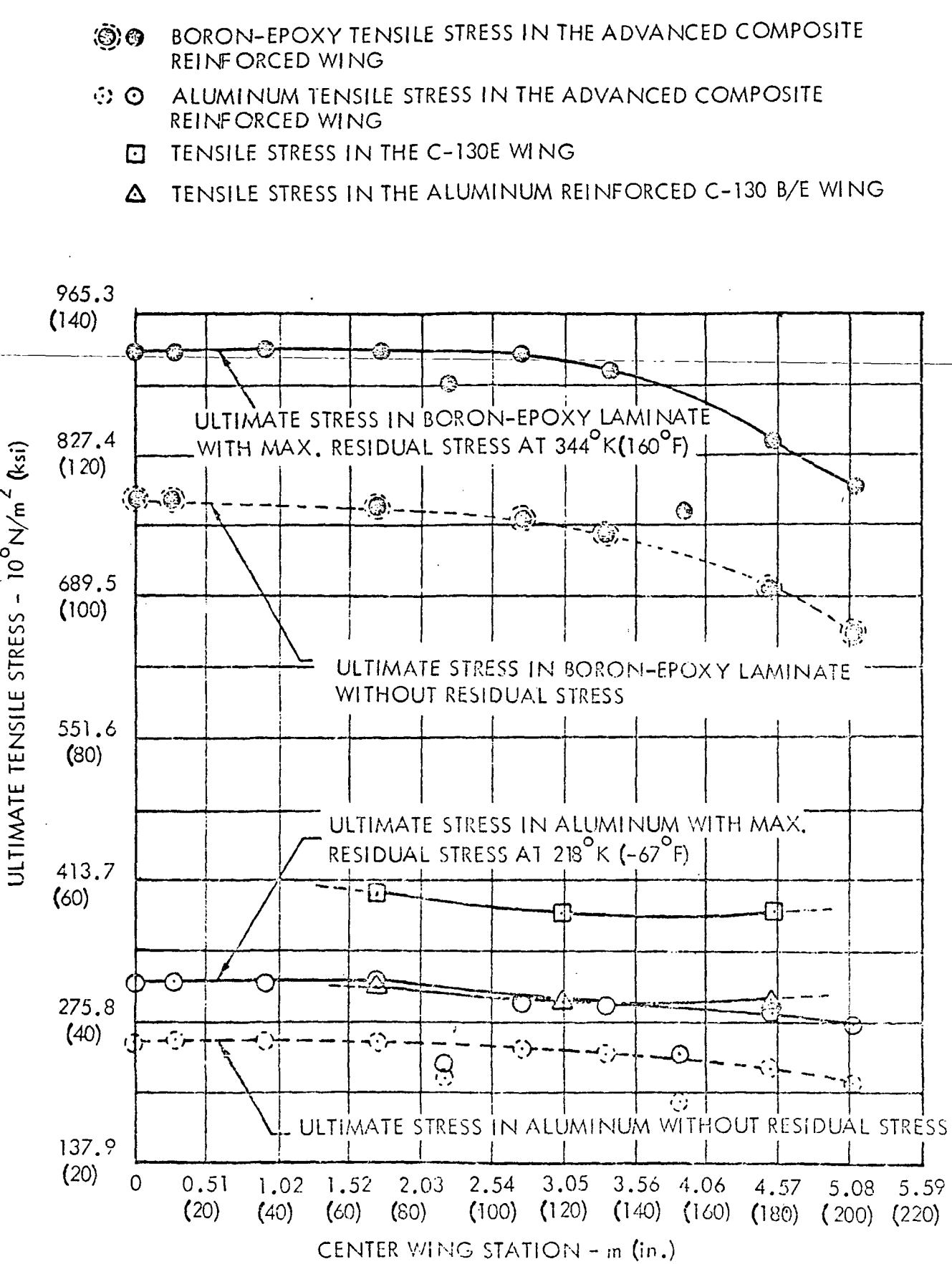

FIGURE 16.-ULTIMATE TENSILE STRESSES FOR LOWER SURFACE STRINGERS VERSUS CENTER WING STATION

composite-reinforced wing is well below the elastic limit of the 7075-T6 and 7075-T73 aluminum alloys being used. The maximum boron-epoxy stress level is compressive and is shown on Figure 15 to be approximately 1007 MN/m^2 (146 KSI). This stress is well below the elastic limit for the material and is below the compressive yield stress of 1517 MN/m^2 (220 KSI) used for structural analysis.

The static analysis of the structural components affected by the composite reinforcement show positive margins of safety for all critical load conditions. Representative margins of safety for the critical components are shown in Table II. In general, the analysis indicates that the boron-epoxy reinforced skin-stringer components are critical for local instability (initial buckling) of the reinforced skin elements located directly under the hat-section stringers. These elements are analyzed using appropriate interactions of axial, shear, and local bending stresses. It should be noted that axial and shear stress interactions are maintained below initial buckling levels due to the uncertainties and lack of data surrounding the behavior of the adhesive bond layer in the post-buckling range. Surface-panel regions with high fastener concentrations, such as spanwise splices and stringer attachments, are critical for the interaction of net shear and axial stresses. Thermal residual stresses are included in the determination of net axial stresses.

The remaining primary structure, including front and rear spar caps, box ribs and W. S. 220 joint details, are identical to the components used on the existing C-130B/E extended service life airplane and have been shown structurally adequate by previously published analyses and test results. Since the internal loads affecting these components do not exceed those previously used, they were not reanalyzed.

TABLE II. - SUMMARY OF MINIMUM MARGINS OF SAFETY

COMPONENT	LOCATION W. S.	LOAD CONDITION	OPERATING TEMP. °K / (°F)	FAILURE MODE	MARGIN OF SAFETY
UPPER SURFACE STRINGER NO. 1	68.0	SYMMETRIC MANEUVER	344/(160)	LOCAL INSTABILITY OF REINFORCED SKIN ELEMENT	.04
UPPER SURFACE STRINGER NO. 2	132.0	SYMMETRIC MANEUVER	344/(160)	LOCAL INSTABILITY OF REINFORCED SKIN ELEMENT	.17
UPPER SURFACE STRINGER NO. 11	201.0	SYMMETRIC MANEUVER	344/(160)	LOCAL INSTABILITY OF REINFORCED SKIN ELEMENT	.12
UPPER SURFACE SPANWISE SPLICE	63.0	SYMMETRIC MANEUVER	344/(160)	NET SHEAR-COMPRESSION FAILURE OF SKIN PANEL	.03
UPPER SURFACE SPANWISE SPLICE	138.0	ACCELERATED AILERON ROLL	218/(-67)	FASTENER BEARING FAILURE IN SKIN PANEL	.01
LOWER SURFACE STRINGER NO. 21	201.0	SYMMETRIC MANEUVER	218/(-67)	LOCAL INSTABILITY OF SKIN ELEMENT BETWEEN STRINGERS	.03
LOWER SURFACE STRINGER NO. 13	87.0	SYMMETRIC MANEUVER	218/(-67)	NET SHEAR-TENSION FAILURE OF SKIN PANEL	.001
LOWER SURFACE STRINGER NO. 14	87.0	SYMMETRIC VERTICAL GUST	218/(-67)	NET SHEAR-TENSION FAILURE OF SKIN PANEL	.02
LOWER SURFACE NACELLE FITTING	178.0	POSITIVE TORQUE SURGE		FASTENER BEARING FAILURE IN SKIN PANEL	.23
FRONT SPAR WEB	70.0	SYMMETRIC MANEUVER		WEB TEAR FAILURE AT FASTENER LINE	.06
REAR SPAR WEB	70.0	SYMMETRIC VERTICAL GUST		WEB TEAR FAILURE AT FASTENER	.15

4.2 FATIGUE ENDURANCE ANALYSIS

An analysis was conducted to compare the fatigue endurance of the boron-epoxy reinforced center wing and the current all-aluminum C-130B/E center wing. In assessing the comparative fatigue endurance, this study demonstrated that the C-130E boron-epoxy reinforced center wing box possesses a fatigue capability equal to or greater than that of the C-130B/E all-aluminum center wing.

4.2.1 Analysis Approach

Demonstration of the fatigue capability of the boron-epoxy center wing was accomplished using both the fatigue test spectra loading currently being used in the C-130B/E fatigue test and a selected mix of the USAF nine mission requirements. The purpose of computing the fatigue endurance by both the test spectra loads and the flight spectra loads was to ascertain the fatigue capability of the boron-epoxy reinforced center wing when it is subjected to the loading of the scheduled full-scale test of Phase IV and the typical flying conditions of Phase V.

Three basic parameters are required to define the fatigue endurance of a structure. These are: (1) the operational usage in terms of mission profiles and utilizations, (2) the design stress level, and (3) the structural quality level[1]. Using these parameters in conjunction with Miner's Therory of Cumulative Damage, relatively reliable fatigue endurances can be determined by analytical procedures.

The parameter, operational usage, when presented in terms of mission profiles and utilizations defines the aircraft configuration in terms of gross weight, fuel, cargo, etc., and the environmental conditions to which it is subjected. Mean load levels (1.0 g loads) are primarily computed on the basis of the operational configuration; variable loads are determined by statistical analysis of the environment. In combination, the mean and variable loads produce the fatigue loads for specific areas of structure.

---

[1] The quality level, K_f, is defined as the numerical value of an effective stress concentration factor which yields a Miner's damage of unity. In addition to local geometry, a number of uncontrolled variables are included in the determination of the quality level of a specific area of a complex structure such as a wing box. These variables include:

i Material inconsistencies such as anisotropy, non-homogeneity, inelasticity, inclusions, voids, variations in physical properties, and grain size.

ii Manufacturing variables such as tolerances causing variations in part size and thickness, surface finish, fastener size, hole size, joint friction, and assembly errors.

iii Other variables such as non-linear slippage of joints, local plastic yielding at points of high stress concentration, complexity and redundancy of load paths, fretting of joints, fretting corrosion, design errors, irregularity of service usage, and external loadings.

The second parameter, the design stress level, is a value equal to the maximum stress to which a particular compenent is subjected under maximum or envelope design load. This maximum stress value, together with the envelope design load, forms a ratio that is used to convert the fatigue loads into usable stress spectra. This is accomplished by multiplying the fatigue loads (loads spectra) by the stress-to-load ratio.

The first two parameters are definable for any given operational use and structural configuration. Due to non-linear notch behavior, the third parameter, quality level, can not be accurately determined by analysis of the local geometry. Comparison of observed fatigue performance of a structural location with the performance of laboratory coupons having nominal (elastic) values of quality level through the application of Miner's cumulative damage theory yields the "test-demonstrated quality level" for the location. The quality level is considered to be a function only of local geometry and provides the parameter by which changes in operational use and/or design stress level may be evaluated. The quality level reflects the fatigue sensitivity of the particular structural configuration and provides the parameter by which changes in operational use and/or design stress level may be evaluated.

4.2.2 Analysis Criteria

Aluminum is the parent material of the composite-reinforced structure. The fatigue analysis of the 80 : 20 aluminum to boron-epoxy cross-sectional area distribution is based on the concept that the aluminum is the more fatigue-susceptible material of the bonded structure. Fail-safe considerations confirm this concept, as loss of the boron-epoxy laminates during operational usage and applied limit load would not result in catastrophic failure.

The fatigue-endurance analysis of the boron-epoxy center wing was based on the following criteria:

- The aluminum material is more fatigue-susceptible than the boron-epoxy or the adhesive bond.

- The computed fatigue endurance of the C-130E boron-epoxy reinforced center wing box is based on the stresses in an aluminum area which has the same extensional rigidity as that of the composite-reinforced section:

  $Ea \cdot A_{equivalent} = Ea \cdot Aa + Eb \cdot Ab$

- When comparing the fatigue endurance of the boron-epoxy reinforced center wing box with that of the C-130B/E structure, the quality level, K_f, is considered to be the same for both structures at each location.

- A mean structural operating temperature of 225°K (0°F) is established for the lower surface. This temperature is selected because most lower surface fatigue damage occurs at altitude when structural temperatures are low.

- A mean structural operating temperature of 269°K (25°F) is established for the upper surface. Fatigue damage on the upper surface is primarily due to ground-air-ground loading cycles.

4.2.3 Fatigue-Susceptible Areas

The C-130E boron-epoxy reinforced center wing and the C-130B/E center wing were analyzed at wing stations 40, 60, 80, 100, 120, 140, 160, 180, 200, and 214 for both the upper and lower surfaces. The stress-to-moment ratios for these locations are plotted versus wing station in Figure 17, and show that at any station the aluminum alloy stress is lower in the composite-reinforced structure than in the original all-aluminum structure. This factor is the major contributor to improved fatigue performance. Variations in the curve shape of the composite-reinforced stress-moment ratio curves which do not appear in the C-130B/E stress-moment ratio curves are due primarily to more rigorous analysis of the composite-reinforced wing box at more locations. Multiplication of the applied wing bending moment (M_x) by the stress- moment ratio yields the tension stress for the surface.

4.2.4 Operational Loads

The fatigue endurance of any aircraft is partly determined by the type and frequency of missions flown. The mission profiles and their utilization rates are the basis for computing mean and variable load levels acting on different components of the aircraft. Mean loads are derived on a single-load-level occurrence basis; variable loads are developed by an exponential distribution form.

Each of the nine mission profiles for the C-130B/E aircraft as used by the USAF is described by a representative mission profile. Mission utilization depends on the base and/or the command to which the aircraft is assigned. A fatigue evaluation can be performed when utilization data are combined with the basic nine mission profiles.

C-130B/E aircraft usage data taken from reported utilization of the USAF fleet were used to determine the combination of the nine mission profiles currently being flown. These data were obtained over the 12-month period from June 1971 to June 1972. The percent utilization of each mission is listed in Table III. This typical operational use is also referred to as "nine-mission utilization."

TABLE III.- C-130 MISSION DISTRIBUTION

Mission	Percent Utilization
1. Proficiency Training	11.7
2. Basic Training	6.5
3. Shuttle	7.5
4. Short Range Logistics	25.3
5. Long Range Logistics	27.7
6. Air Drop	3.8
7. Storm Reconnaissance	0.0
8. Combat Training	11.5
9. Low Level	6.0

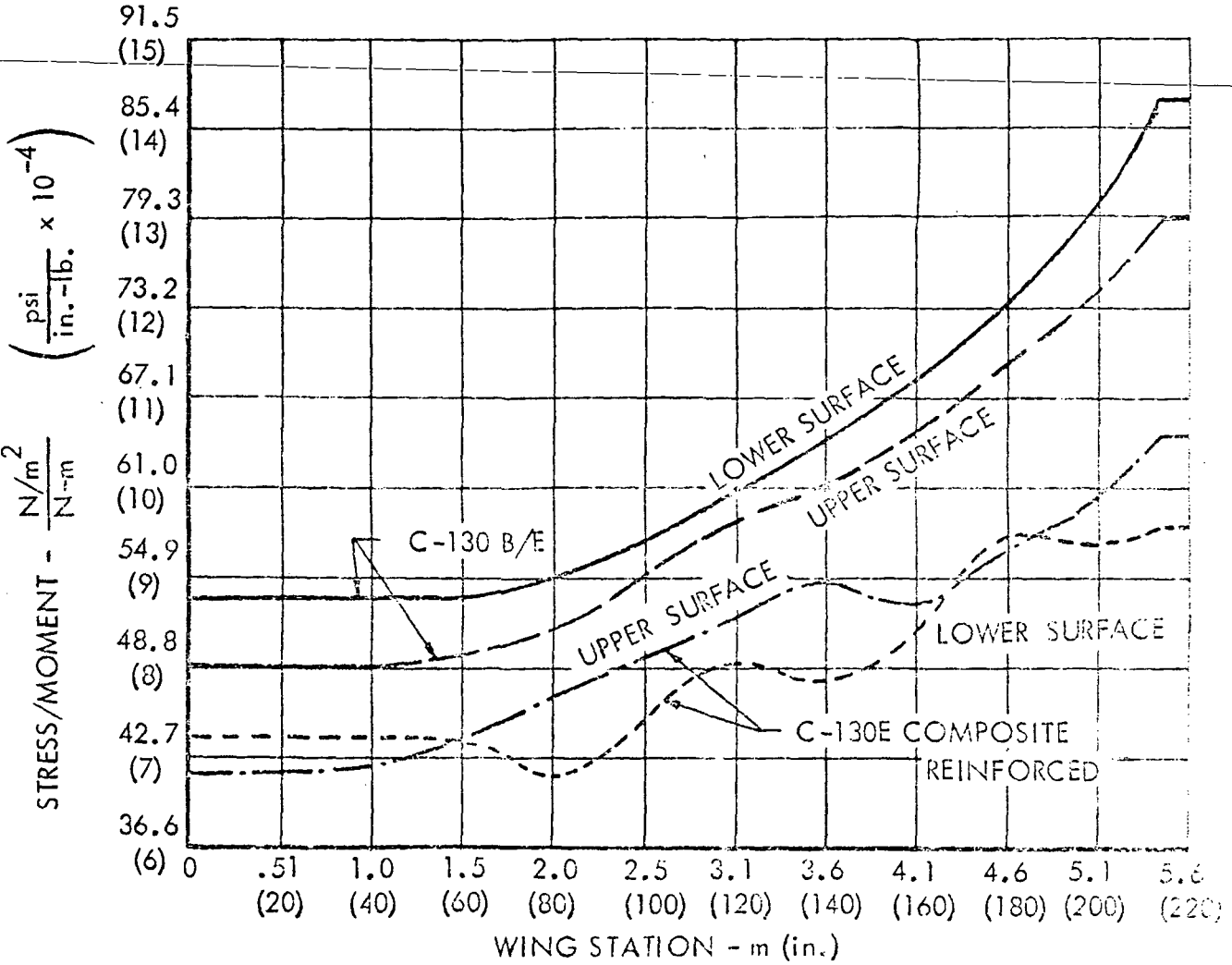

FIGURE 17. - STRESS/MOMENT RATIO - C-130B/E AND C-130E BORON-EPOXY REINFORCED CENTER WING

The Lockheed-Georgia DART (Damage Analysis in Rapid Time) computer program was modified to accept the stress-to-load ratios and the residual stresses in the basic aluminum structure due to bonding. The DART program calculated fatigue endurance using the combination of the nine C-130 mission profiles for each of the fatigue-susceptible locations previously defined in Section 4.2.3. Quality level versus fatigue endurance curves for both the C-130B/E and C-130E boron-epoxy reinforced center wing using the operational loads are presented in Appendix C. Representative quality level versus fatigue endurance curves for typical upper and lower surface locations are presented in Figures 18 and 19. At any particular structured location, the quality level for the composite-reinforced wing box is expected to be the same as that for the C-130B/E wing box. The curves show that, at equivalent quality levels, the endurance of the composite wing box is greater than that of the C-130B/E wing box.

4.2.5 Test Spectra Loading

The large number of load levels presented in the analytical spectrum prohibit its use as a test spectra, since it would not be economically feasible to provide the complex systems and rigs required to apply such loading to a test airframe. Because of this, the analytical spectrum is simplified to a test spectrum of 18 load levels.

The basic rule for test spectrum development states that reasonable simulation of flight loads will be provided when the calculated damage, based on Miner's Theory, is the same at a particular quality level for the same number of damaging cycles of the portion of the analytical fatigue load spectrum being considered. The complexity of the loads spectra, involving a large number of incremental and mean loads, requires a vast number of arithmetic calculations to simplify the spectra to a usable form. Existing computer programs were used to handle the data and perform the necessary calculations. The number of load levels used in the test spectra depends on the variety of mission profiles required. In the C-130B/E wing test, two separate loads spectra (designated Spectra A and Spectra B) had been applied. Therefore, comparative endurances for both spectra were included in the analysis of the composite reinforced structure. Quality level versus fatigue endurance curves for typical upper and lower surface locations are presented in Figures 20 and 21. Curves for all wing stations analyzed are presented in Appendix C. The boron-epoxy reinforced structure shows greater fatigue endurance than the C-130B/E aluminum reinforced structure.

4.2.6 Fatigue Endurance Conclusions

The superior fatigue capability of the C-130E boron-epoxy reinforced center wing is analytically demonstrated by comparison with the endurance of the C-130B/E model at the fatigue-critical areas selected for study. The calculated fatigue endurance of the boron-epoxy reinforced wing is greater than the endurance of the C-130B/E center wing when the wing box is subjected to the loads of current operational usage or the test spectra loads for quality levels of 4.0 to 12.0, inclusively.

The demonstrated quality level is the basis for correlating the Phase I panel fatigue test results to the Phase IV full-scale center wing box testing and the Phase V operational

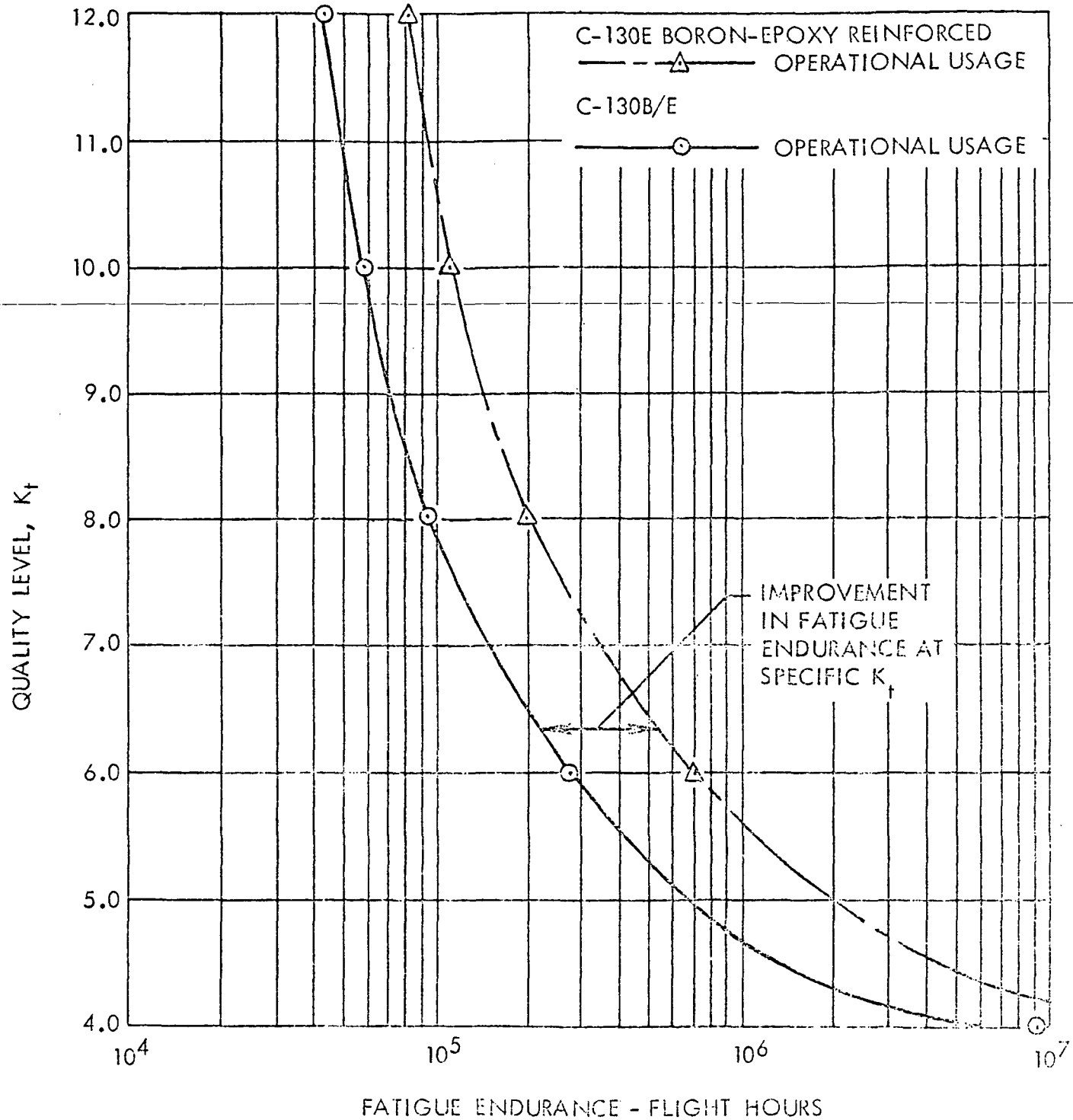

FIGURE 18. - QUALITY LEVEL VERSUS FATIGUE ENDURANCE
W.S. 160 UPPER SURFACE-OPERATIONAL USAGE

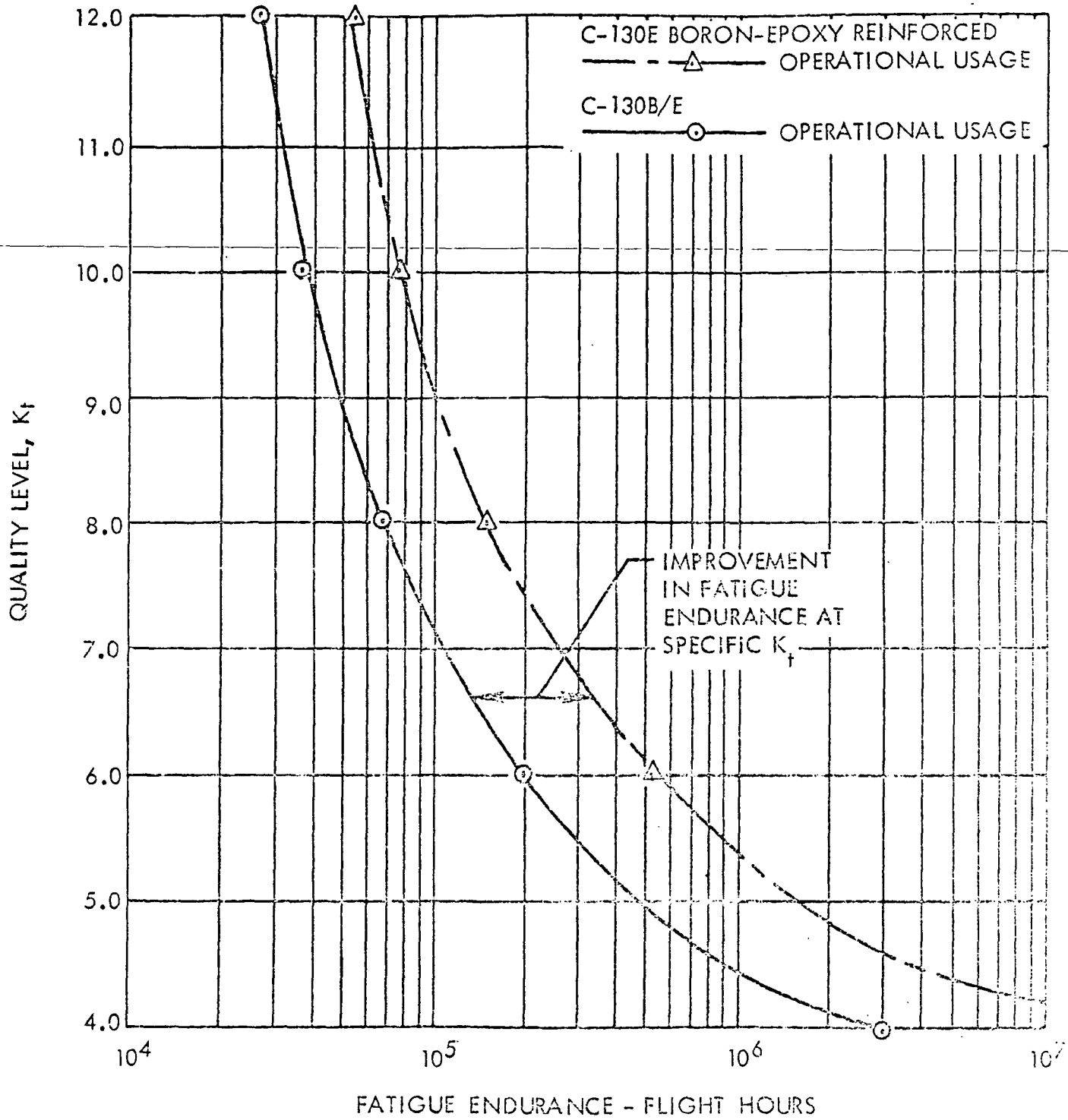

FIGURE 19. - QUALITY LEVEL VERSUS FATIGUE ENDURANCE
W.S. 80 LOWER SURFACE-OPERATIONAL USAGE

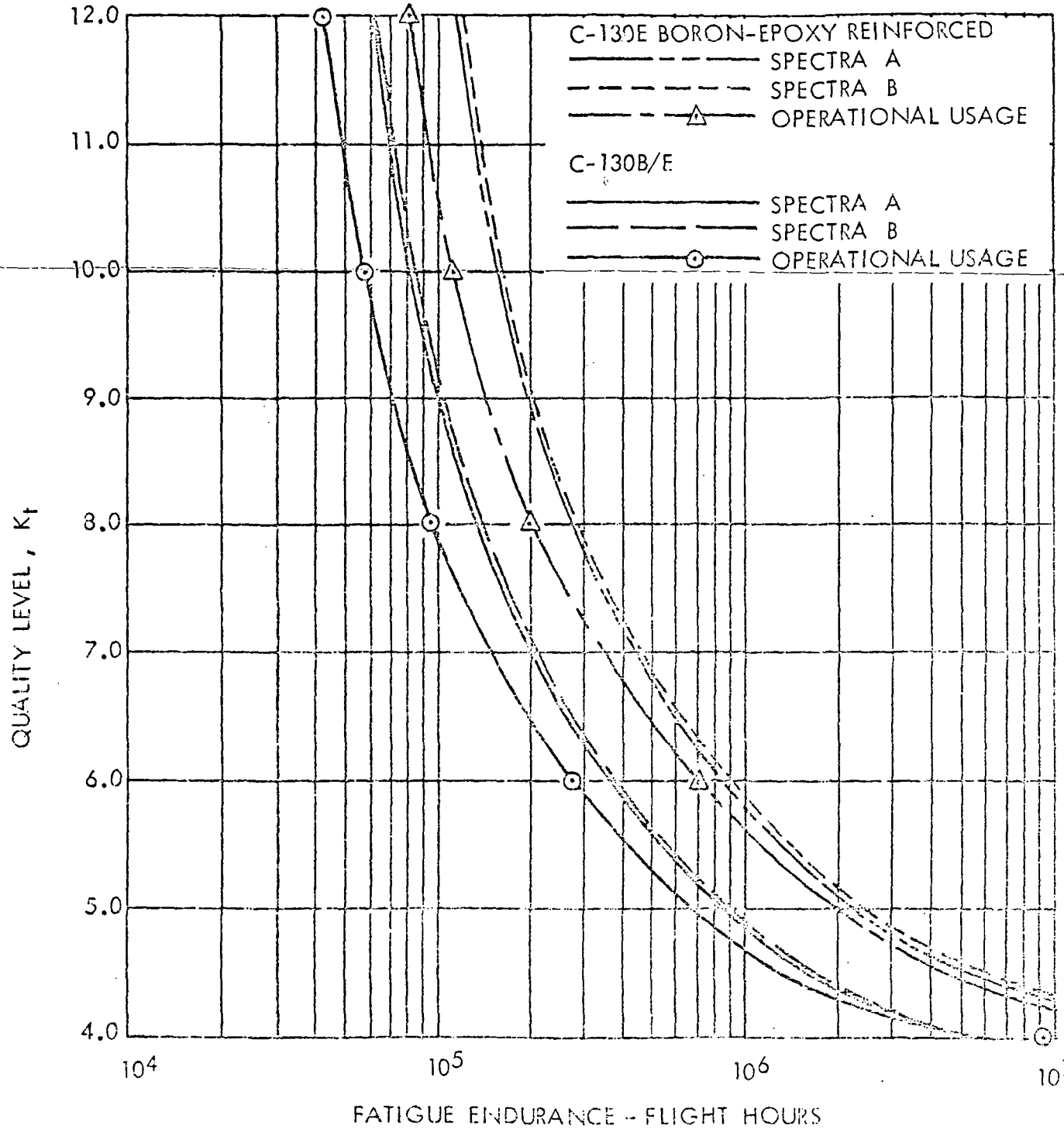

FIGURE 20. - QUALITY LEVEL VERSUS FATIGUE ENDURANCE
W.S. 160 UPPER SURFACE

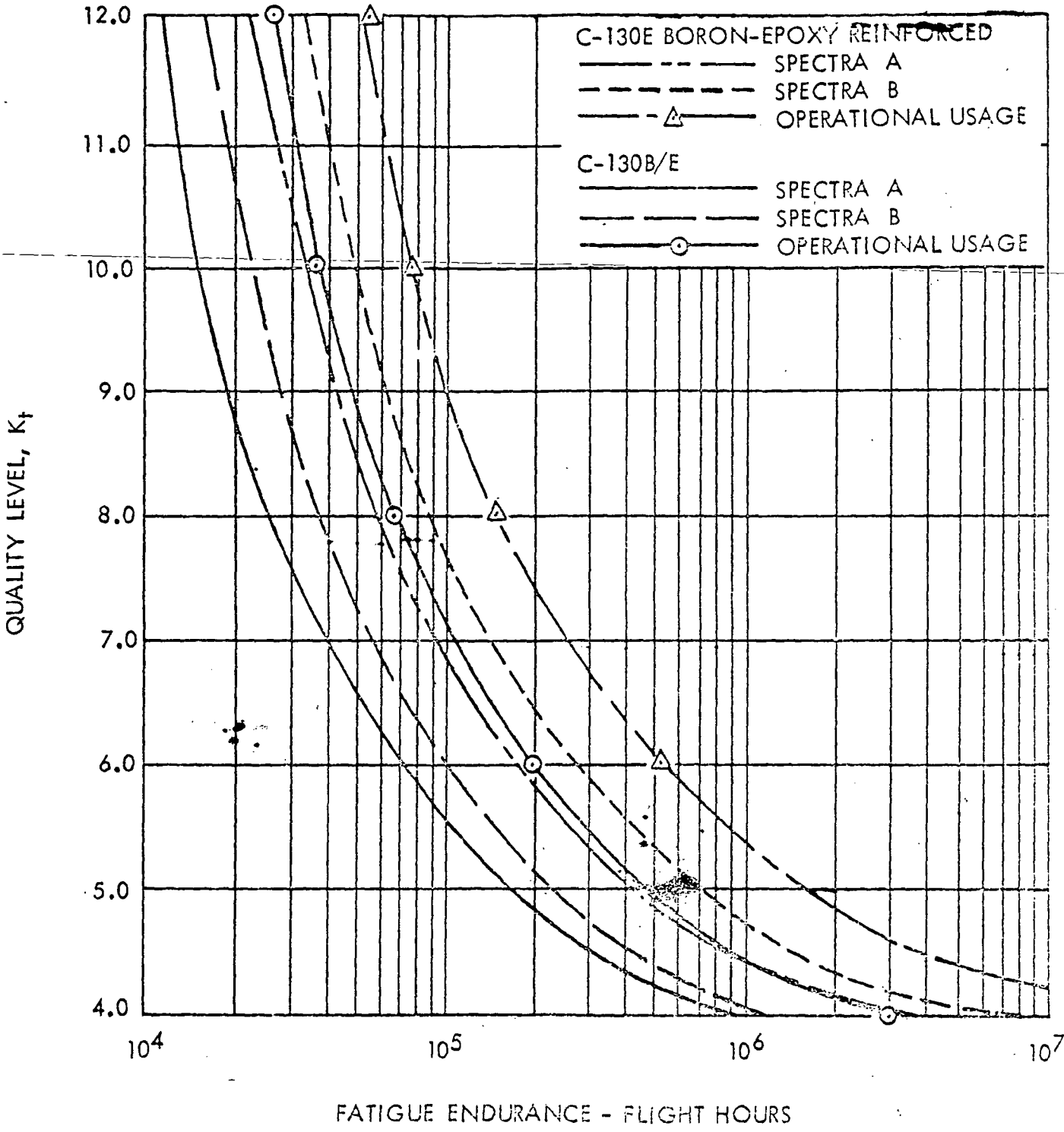

FIGURE 21. - QUALITY LEVEL VERSUS FATIGUE ENDURANCE
W.S. 80 LOWER SURFACE

wing boxes. The quality level as determined by the component testing may be applied to the same structural areas on the full-scale wing box. With the exception of the premature stringer crack on fatigue specimen PF-2 and the "nuisance" crack of the stringer run-out of specimen PF-1, all the component panel specimens exhibited fatigue performance equal to that of the C-130B/E component panels. Table IV lists the quality levels of stations which exhibited fatigue cracking during the Phase I testing.

Typical operational endurance data from Appendix C (nine-mission utilization as specified in Table III) are cross-plotted against wing station for representative values of quality level. Using Phase I test-demonstrated quality level (Table IV), the operational endurance is calculated and superimposed on the curves of Figures 22 and 23. Similarly, available full-scale C-130B/E test-demonstrated quality level operational endurance data are plotted in Figures 22 and 23 at the appropriate wing station.

With regard to the PF-1 stringer runout crack with $K_T > 12$ (Figure 22), it is noted that the cracking resulted from an atypical machining condition. Furthermore, other adjacent stringers with ostensibly identical configuration (hence K_T) concluded 80,000 simulated flight hours of testing without cracking. These two results indicate that an appropriate representative quality level for that location is considerably less than 12. The corresponding C-130B/E component panel test survived 150,000 simulated flight hours without cracking, indicating that the quality level for this location is less than 8.0. This result ($K_T = 8.0$) is also shown in Figure 22.

Based on the quality levels demonstrated by Phase I tests and C-130B/E component panel tests, and those now being demonstrated by the C-130B/E full-scale test, the operational (specified nine-mission) endurance exceeds the 40,000-flight-hour requirement.

TABLE IV. -OBSERVED QUALITY LEVELS IN PHASE I FATIGUE TESTS

SPECIMEN	SPECIMEN DESCRIPTION AND LOCATION	OBSERVED QUALITY LEVEL	LOCATION
130-JE-1	0.315 m (12.4 in.) wide and 0.985m (38.8 in.) long, two-stiffener section of lower surface wing plank to W.S. 220 rainbow joint transition fitting	6.65	W.S. 220
130-JE-4	Identical to 130-JE-1 except for minor changes in laminate configurations and aluminum/ boron-epoxy bond cycle	10.22	W.S. 210
130-PF-1	1.016 m (40.0 in.) wide and 3.658 m (144 in.) long, two plank (six-stiffener) upper surface specimen which includes W.S. 0 door opening	>12.0	W.S. 17
130-PF-2	1.016 m (40.0 in.) wide and 3.20 m (126 in.) long, two plank (six-stiffener) upper surface specimen which includes W.S. 220 rainbow fitting	>12.0	W.S. 209
130-PF-3	0.432 m (17 in.) wide and 1.524 m (60 in.) long, single plank (three-stiffener) lower surface specimen which includes W.S.220 rainbow fitting	9.74	W.S. 217
130-PF-4	Two 0.152 m (6.0 in.) wide and 1.092 m (43.0 in.) long, single stiffener specimens to simulate upper surface W.S. 0 door stringer termination areas	<6.0	W.S. 17

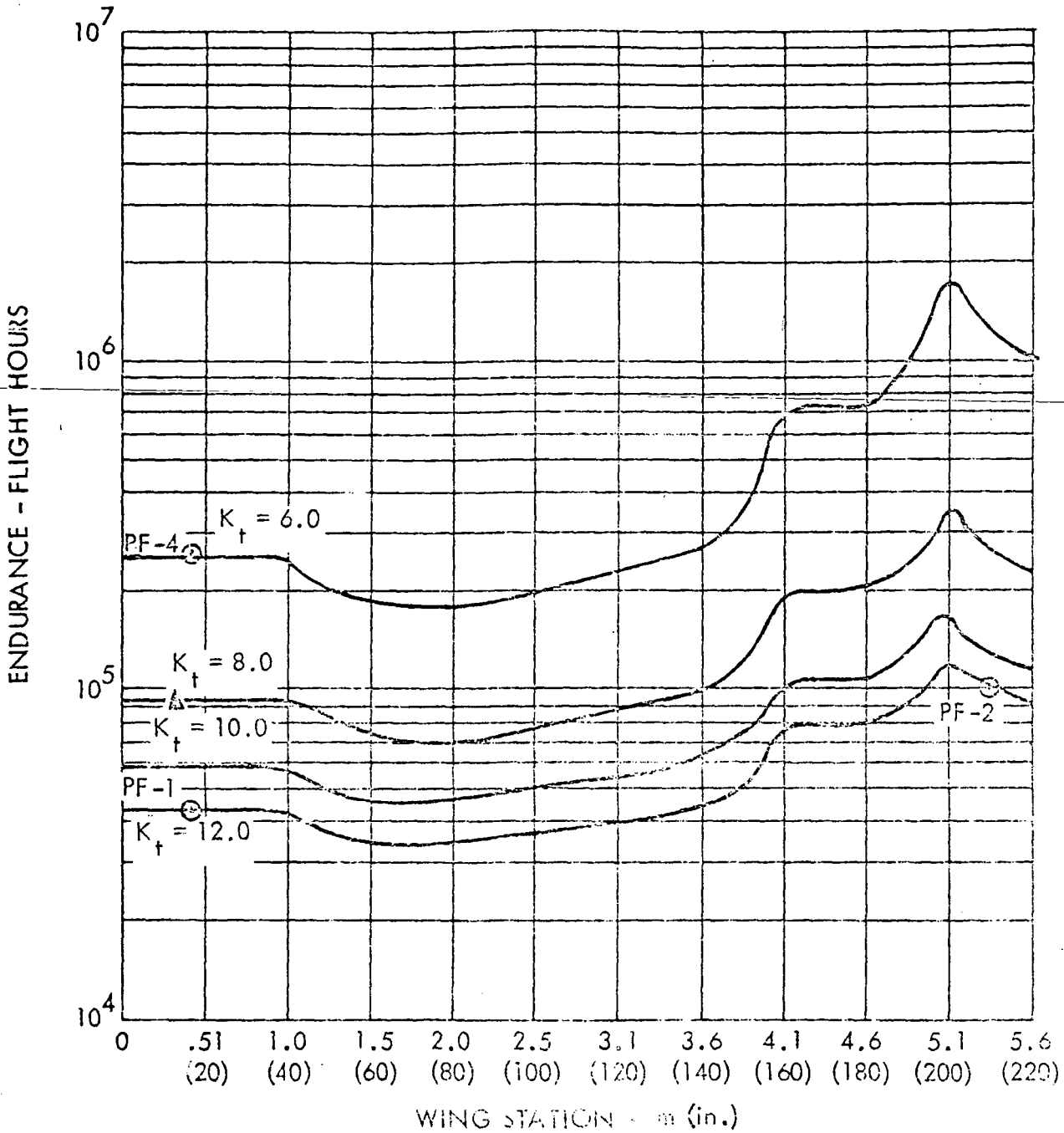

▲ C-130B/E COMPONENT PANEL FATIGUE TEST RESULTS

⊙ PHASE I PANEL FATIGUE TEST RESULTS
NO FULL-SCALE C-130B/E RESULTS AVAILABLE

FIGURE 22. -UPPER SURFACE - FATIGUE ENDURANCE OF THE NINE MISSION PROFILES VERSUS WING STATION

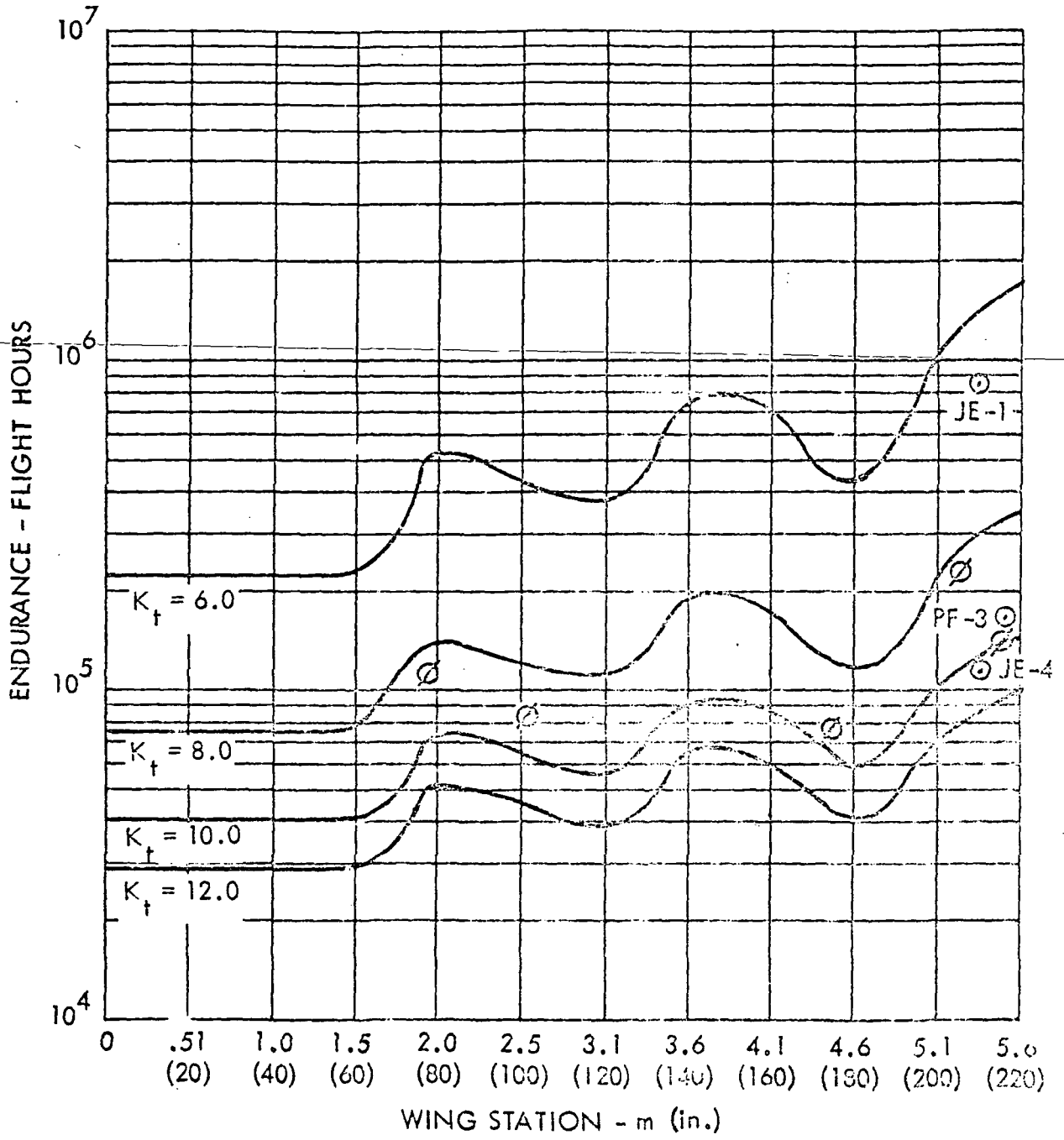

FIGURE 23.- LOWER SURFACE - FATIGUE ENDURANCE OF THE NINE MISSION PROFILES VERSUS WING STATION

E

4.3 FLUTTER ANALYSIS

Flutter analyses were conducted to evaluate the effects of any stiffness changes due to the boron-epoxy reinforced center wing box on the airplane flutter characteristics. The results of these analyses were compared with results of similar analyses of the original C-130E and the C-130B/E with a metal-reinforced center wing box. Previous C-130 flutter analyses and flutter model tests have shown that 22 percent internal wing fuel for normal burning sequence is the most critical internal wing fuel condition. Figure 24 shows typical flutter speed versus percent of internal wing fuel. Under normal fuel management, the external tank is emptied before 22 percent internal wing fuel is reached but the flutter speed is further reduced if the fuel is mismanaged and the external tank contains fuel; therefore, the empty and full external tank conditions with 22 percent internal wing fuel are considered in the C-130B/E flutter analyses.

Uncoupled cantilevered component vibration modes were inertially coupled to obtain free-free airplane vibration modes. Fifteen symmetric free-free elastic modes, rigid body pitch, vertical translation, and fore and aft translation were used in the symmetric flutter analyses. Fifteen antisymmetric free-free elastic modes, rigid body lateral translation, roll, and yaw were used in the antisymmetric flutter analyses.

Oscillatory aerodynamic loads were applied to the wing, vertical stabilizer, and horizontal stabilizer using modified strip-theory aerodynamic coefficients. The flutter analyses were conducted using atmospheric conditions at an altitude of 4267 m (14,000 ft.). Previous C-130 analyses have shown this altitude to be the most critical from the flutter viewpoint.

As in previous analyses, symmetric flutter speeds are considerably higher than the corresponding antisymmetric flutter speeds; therefore, only the more critical antisymmetric flutter speeds are presented. The results obtained are summarized in Figure 25.

The results show the flutter characteristics obtained using the original C-130E, metal-reinforced center wing, and boron-epoxy reinforced center wing stiffnesses are essentially identical. For these analyses, the boron-epoxy reinforced center wing torsional stiffness was considered to be the same as the original C-130E center wing torsional stiffness, and the boron-epoxy reinforced center wing vertical bending stiffness was considered to be the same as the metal-reinforced center wing vertical bending stiffness. Variations in the wing vertical bending stiffness above and below the assumed values of the boron-epoxy reinforced center wing do not cause any appreciable reduction in the flutter speed.

With normal fuel management, flutter speeds are above 1.15 V_L (i.e. 1.15 times limit speed) for the C-130E with the boron-epoxy reinforced center wing box. This satisfies applicable Military Specification requirements. Under abnormal fuel sequence, the aircraft with the composite-reinforced center wing box is subject to the same speed restrictions as those imposed on the original C-130E and the C-130B/E metal-reinforced center wing airplanes.

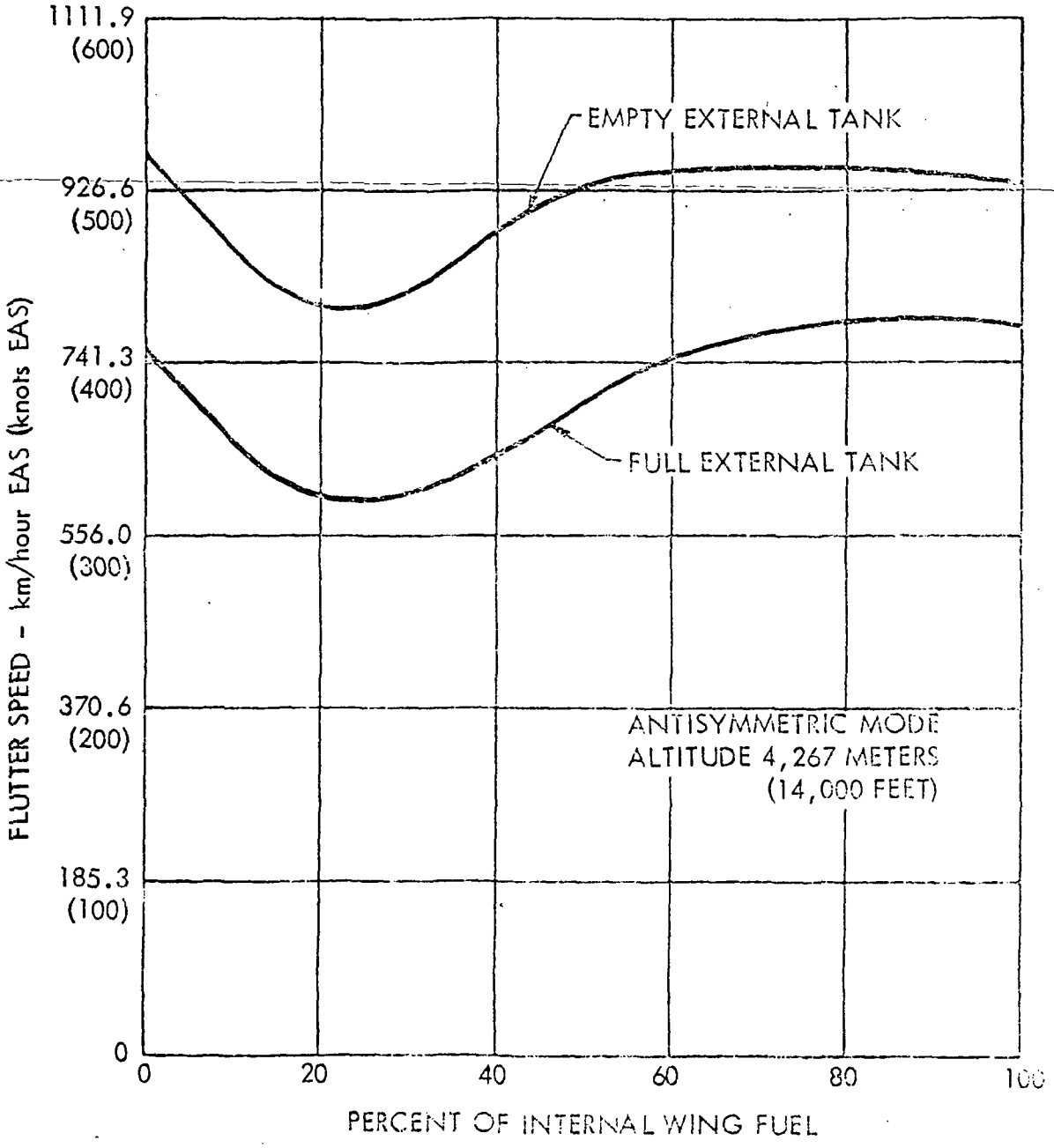

FIGURE 24. - C-130E FLUTTER SPEED VERSUS INTERNAL WING FUEL

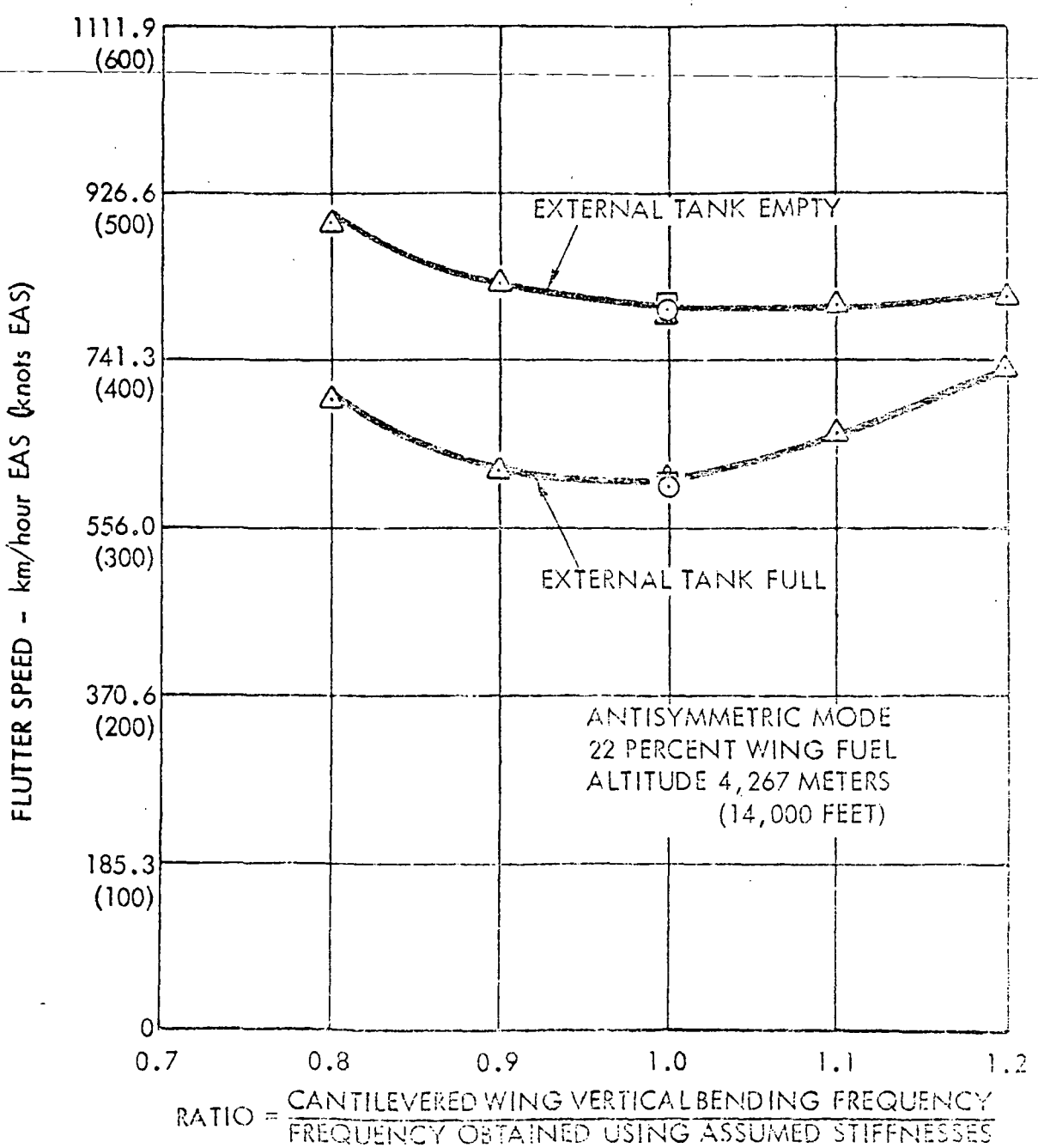

FIGURE 25. - EFFECTS OF WING STIFFNESSES ON FLUTTER SPEED

4.4 WEIGHT PREDICTION

Although weight saving was not a major program goal and was actually subordinate to accomplishment of flight service program goals, it is an important factor, and a weight saving of 229 kg (506 lbs.) is predicted. This prediction is based on actual calculations from the final production drawings listed in Appendix B and represents a saving in total box structural weight of slightly more than 10 percent. For the upper and lower surface panels, which were the only areas modified with composite reinforcement, the percentage of weight saved is actually much higher, 16.4 percent.

The weight saved on the upper surface is 142 kg (313 lbs.) out of 726 kg (1600 lbs.) or 19.5 percent of the stringer and panel weight. The boron-epoxy laminate added to achieve this reduction is 85 kg (187 lbs.). The weight savings on the lower surface is 91 kg (201 lbs.) out of 671 kg (1480 lbs.), or 13.6 percent of the stringer and panel weight. The boron-epoxy laminate added to achieve this reduction is 74 kg (163 lbs.).

Table V summarizes the overall weight of the composite-reinforced center wing box structure based on the predicted saving and a basic all-metal box weight of 2243 kg (4944 lbs.).

It is of interest to note that, in the areas where reinforcement was added, a metal removed/composite added ratio between 2.2 and 2.7 was achieved. This indicates a high potential for weight saving in future composite-reinforced metal designs where less conservative criteria may be established than those used for this particular design.

TABLE V. - SUMMARY OF OVERALL WEIGHT OF COMPOSITE-REINFORCED CENTER WING BOX STRUCTURE

Center Wing Box Structure	Weight of Metal Structure		Metal Removed		Boron-Epoxy Added		Weight Saved		Weight of Boron-Epoxy Reinforced Structure	
	(kg)	(lb.)	(kg)	(lb.)	(kg)	(lb.)	(kg)	(lb.)	(kg)	(lb.)
Upper Surface	726	1600	227	500	85	187	142	313	584	1287
Lower Surface	671	1480	165	364	74	163	91	201	580	1279
Other (Ribs, spars, bracketry, etc.)	846	1864	4 Added	8 Added	----	----	-4	-8	850	1872
TOTAL	2243	4944	388	856	159	350	229	506	2014	4438

5.0 MATERIALS AND PROCESSES

5.1 MATERIALS

New material development for this program was minimal and was limited to adhesives and their processing. This development work, conducted during Phase I, provided a low-temperature curing adhesive system for bonding boron-epoxy laminates to aluminum. Other materials such as boron-epoxy preimpregnated tape, aluminum, sealants, finishes, titanium, and fasteners were procured and/or processed to the requirements of existing Lockheed specifications.

5.2 PROCESSES

Difficulties in manufacturing boron-epoxy reinforced aluminum structures are created by the differences in coefficients of thermal expansion for the two adherends. These differences cause residual stresses in the bonded structure at temperatures other than the cure temperature. Process development effort was directed to minimization of this problem and culminated in the "cool tool" restrain. process. This process has been previously discussed in detail in the Phase I final report (NASA CR-112126) and is not repeated herein. Other processing relative to boron-epoxy lamination and surface preparation was accomplished in accordance with existing Lockheed specifications.

5.3 SPECIFICATIONS

Three material and process specifications were revised or prepared and published during Phase II. The boron-epoxy material and process specifications (STM22-450 and STP60-202, respectively) were revised to eliminate minor packaging problems and to reduce the amount of acceptance testing for receiving inspection. Only one of the specification mechanical property requirements was changed. The material specification (STM22-450) average flexural modulus property requirement was reduced to 190. GN/m^2 (27.5×10^6 psi), which is the value most commonly required throughout the industry. The changes do not compromise either program requirements or material quality but allow a more workable p: kaging arrangement and slightly less proof testing. These changes have been made and the documents published. The mechanical property requirements contained in the material specification STM22-450 are listed in Table VI.

A process specification, STP60-205, which defines the bonding of cured boron-epoxy laminates to aluminum was prepared and published during this reporting period. This document provides the usual processing requirements relative to surface preparation, material control, environmental control, process control and inspection requirements. However, in addition to these normal bonding specification requirements, additional requirements are imposed to achieve a bondline which is low in stress at room temperature. Also, authorization for a low-temperature [386 ± 8.3°K (235 ± 15°F)] adhesive cure cycle is included.

TABLE VI. - ROOM TEMPERATURE MECHANICAL PROPERTY REQUIREMENTS

PROPERTY	UNIT	REQUIRED AVERAGE	MINIMUM INDIVIDUAL
0° Flexure Strength	GN/m^2 (10^3psi)	1.65(240.0)	1.55(225.0)
0° Flexure Modulus	GN/m^2 (10^6psi)	190.(27.5)	179.(26.0)
90° Flexure Strength	MN/m^2 (10^3psi)	89.6(13.0)	75.8(11.0)
0° Horizontal Shear Strength	MN/m^2 (10^3psi)	89.6(13.0)	75.8(11.0)
0° Tensile Strength	GN/m^2 (10^3psi)	Not Specified	1.24(180.0)
0° Tensile Modulus	GN/m^2 (10^6psi)	207.(30.0)	193.(28.0)
90° Tensile Strength	MN/m^2 (10^3psi)	75.8(11.0)	62.1(9.0)
90° Tensile Modulus	GN/m^2 (10^6psi)	20.0(2.9)	18.6(2.7)
0° Tensile Strain	$\mu m/m$ (10^{-6}in./in.)	6000(6000)	Not Specified
90° Tensile Strain	$\mu m/m$ ($^{10-6}$in./in.)	4100(4100)	4000(4000)

6.0 MANUFACTURING DEVELOPMENT

6.1 BONDING STUDIES

Under the Advanced Development portion of this program, considerable advances were made in the bonding of boron-epoxy laminates to aluminum components. The high coefficient of thermal expansion for aluminum and the low coefficient for boron-epoxy creates extreme warpage when the two elements are bonded together at elevated temperatures. A process was developed in which a steel tool was used for restraining the aluminum at elevated temperatures while keeping the steel tool at room temperature with the use of insulation between the aluminum and steel. The pressure for bonding is applied using a pressure hose restrained in a channel over the boron-epoxy strip to be bonded. The channel is mechanically secured to the steel tool. During the Development Phase, this technique was used for bonding all specimens fabricated. Since the largest specimen fabricated was only 3.66 m (144 in.) long, additional efforts in Phase II were directed to bonding full length, 10.8 m (426 in.), boron-epoxy laminates to the aluminum stringers and wing planks.

6.1.1 Laminate Preparation

Boron-epoxy laminates were prepared which were representative of the laminates to be used in the C-130 composite-reinforced center wing box. Standard lay-up and bagging techniques were used in the preparation of these laminates. Included in the study was the measurement of the hole spacing for the tooling pin holes used in the assembly of the stringers to the wing plank. These holes were measured after lay-up in the uncured laminate, after curing the laminate and after bonding. Although there was a measurable movement between the holes for each of the cure cycles, the movement was within the tolerance required for matching these tooling holes in the assembly fixture. The cured laminate strips are shown in Figure 26 .

6.1.2 Tooling for Bonding Cycle

For these studies a special steel frame was mounted on top of an existing long, flat, aluminum bonding tool. The frame was made with steel channel welded into a rectangular box shape. The ends of the aluminum skin or stringer component are butted against the ends of the steel frame to provide restraint during bonding. Figure 27 shows the frame on the tool with the 2.54 cm (1.0 in.) Marinite insulating board positioned and the technician installing the Nichrome heater blanket on top of the insulation. All other parts, including heater and insulation, were the same type as used in Phase I and documented in NASA CR-112126. The steel bars, pressure hose, and hose containment were fabricated for the full-length tool and assembled as shown in Figure 28 .

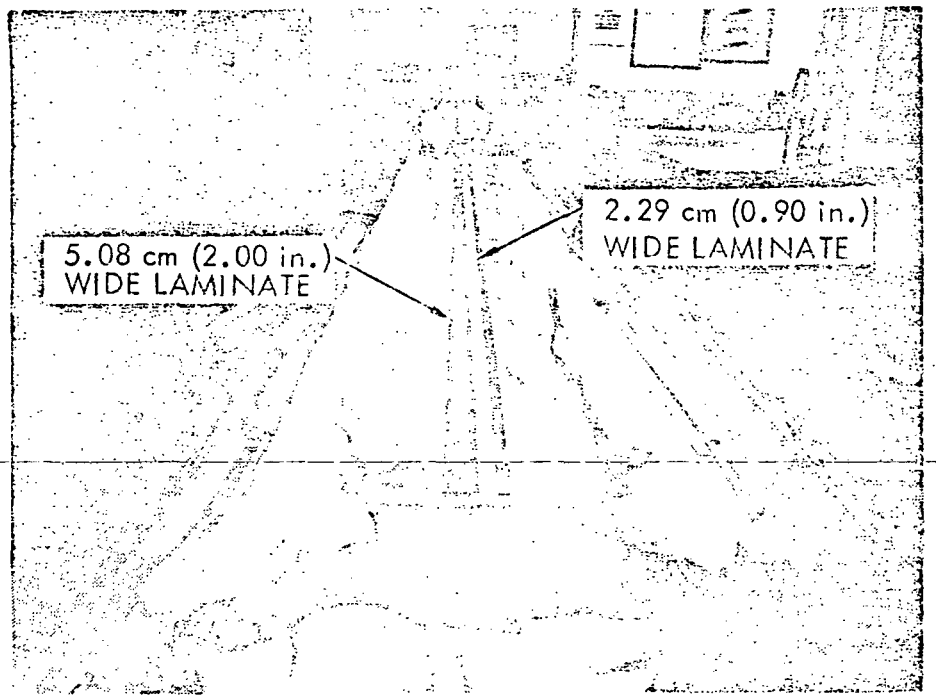

FIGURE 26. - BORON-EPOXY LAMINATES FOR FULL SCALE BONDING TEST

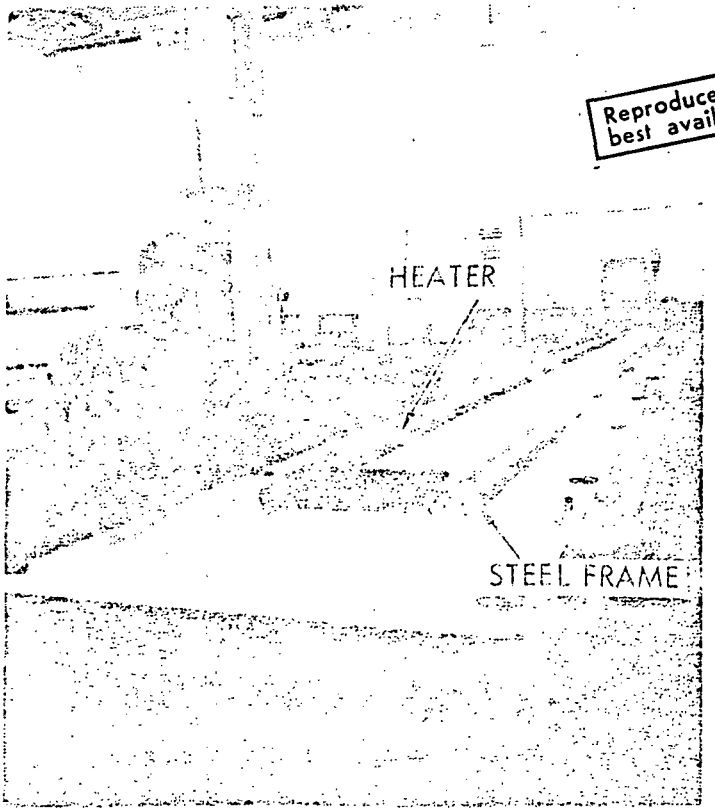

FIGURE 27. - EXPERIMENTAL TOOL, HEATER INSTALLATION

Heating elements were fabricated in four separate zones and were powered and manually controlled using the panels shown in Figure 29 . Each heating zone was controlled by a separate temperature controller with the control temperature feedback being made with a thermocouple circuit measuring the temperature of the Nichrome ribbon in the center of the heating element.

To help maintain more uniform temperature distribution, insulating blankets were placed over the assembly during the bonding cycle.

6.1.3 Laminate-to-Stringer Bond

A full length stringer was obtained from the C-130 production line after it had been rejected by Inspection for being out of machining tolerance. The stringer was then remachined to the C-130E configuration and the sulphuric acid anodizing was stripped from the surfaces. After hand-cleaning the bonding surface, the stringer was locked in the tool with the ends restrained within the steel frame.

Since the metal stringer (as received) had a bow in two directions (vertical and horizontal), it was straightened with clamps and hand pressure in the tool. The adhesive was applied to the stringer and the boron-epoxy strip positioned using a pin to align the hole in the laminate to the fixed hole in one end of the stringer. Only one end of the laminate was fixed so that it could freely expand around the hole during the cure cycle. The standard bond cycle established for the program was used.

After bonding, the stringer was actually straighter than it had been prior to installation in the tool. The completed part is shown in Figure 30 . Assessment indicates that the composite-reinforced stringer will be straight and acceptable for production use.

6.1.4 Laminate-to-Wing Plank Bond

As in the case of the stringer, a scrapped wing plank which had been rejected for use in C-130 production was obtained for the study. The plank was a middle, lower surface, C-130 wing plank which has two access openings and consequently has a large variation in cross-sectional area. The plank was sawed lengthwise into strips which were representative of the width to be reinforced by one boron-epoxy strip. After being cleaned and prepared for bonding, the plank was positioned in the tool and restrained at the ends. Standard "cool tool" bonding procedures were followed in making the laminate-to-aluminum bond. In the first attempt, a failure in the temporary tooling occurred which essentially allowed the bond to be completed without restraint to the aluminum. As shown in Figure 31 , the resulting bonded assembly was severaly warped. The resulting bow to length ratio was about 1 to 7.

The tool problem was corrected and the bond cycle was repeated with good results as shown in Figures 32 and 33 . Some warpage was still evident. The bow was sinusoidal with reverse bows occurring in the thin sections of the plank. Figure 34 illustrates the ease of straightening out the bows in this plank with only hand pressure being applied.

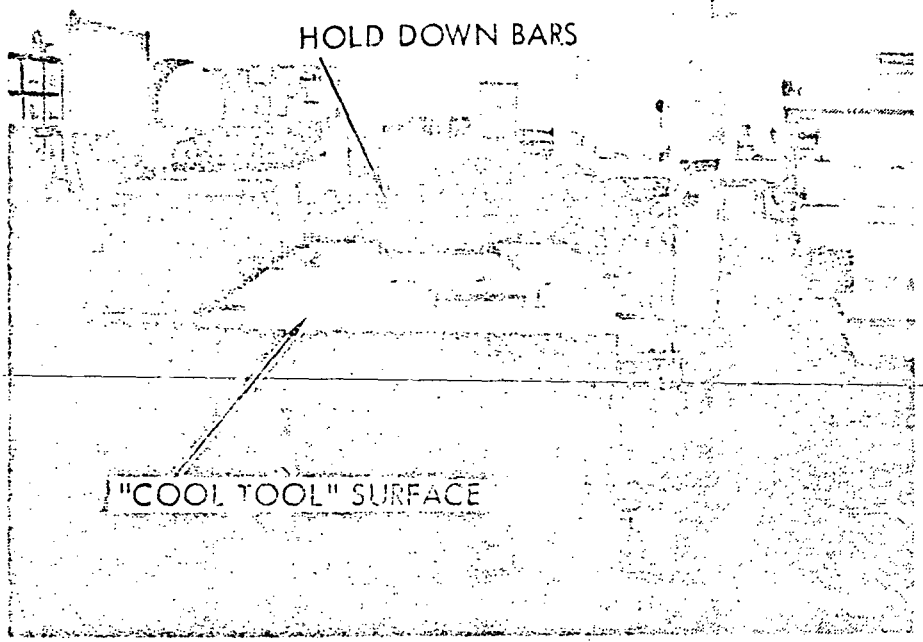

FIGURE 28. - ASSEMBLED COOL TOOL

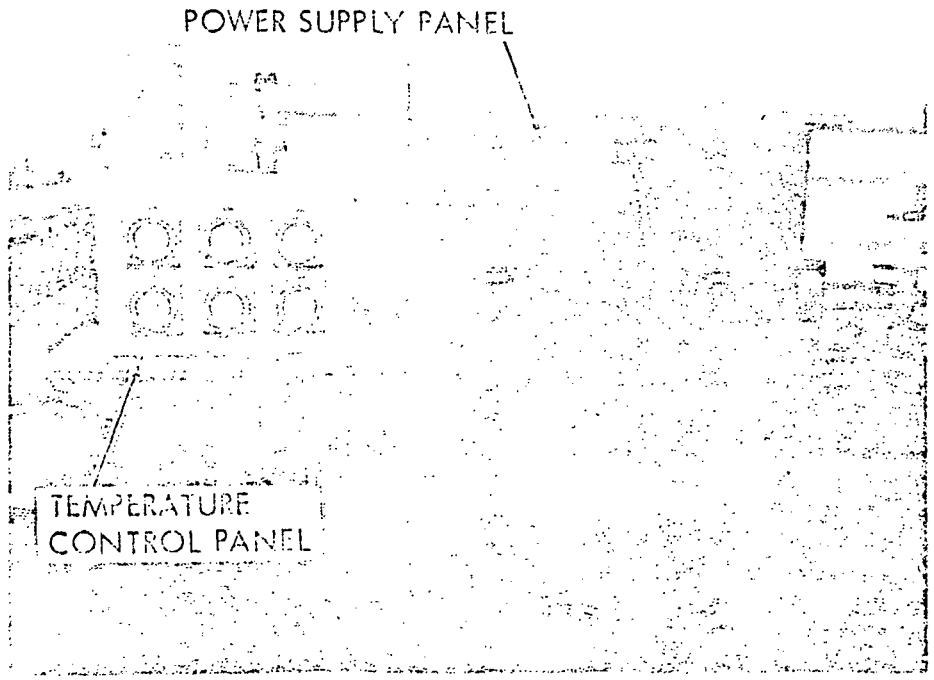

FIGURE 29. - ELECTRICAL PANEL AND
TEMPERATURE CONTROLLERS

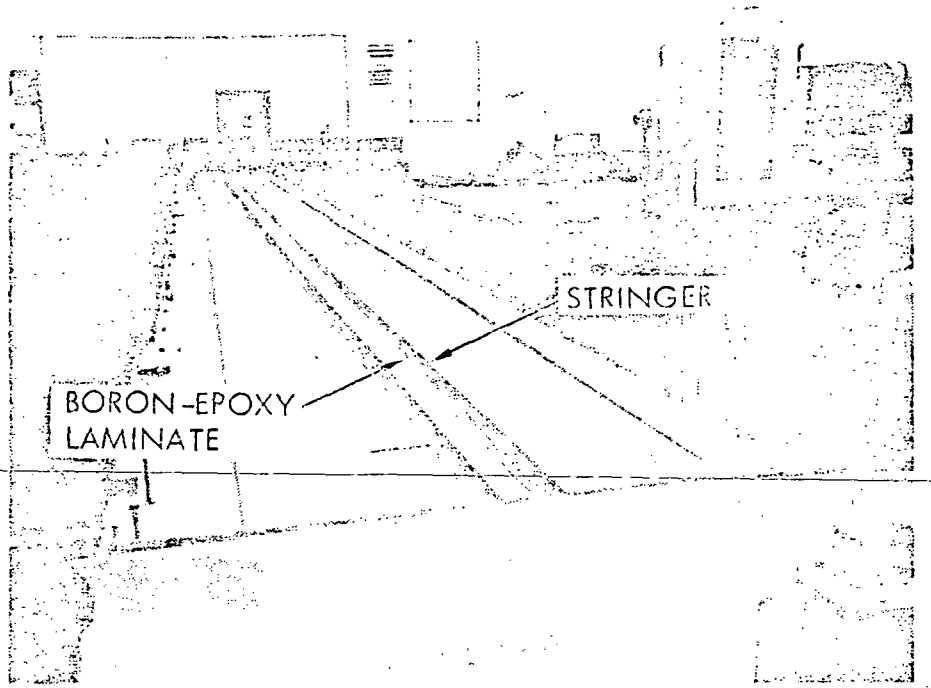

FIGURE 30. - C-130 STRINGER REINFORCED WITH BORON-EPOXY

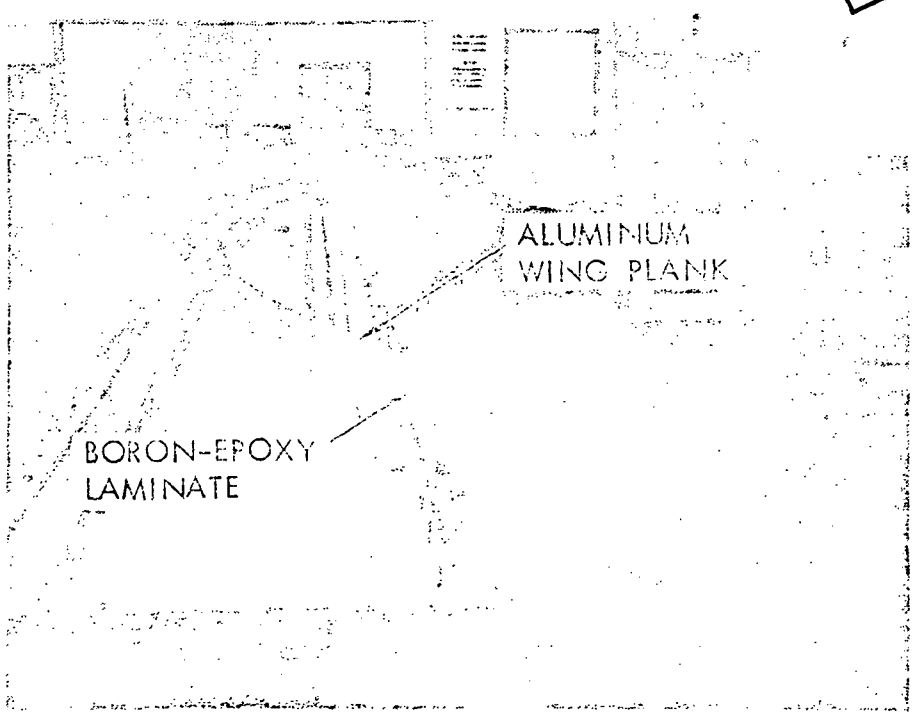

FIGURE 31. - BONDED ALUMINUM/BORON-EPOXY PLANK WITHOUT RESTRAINT

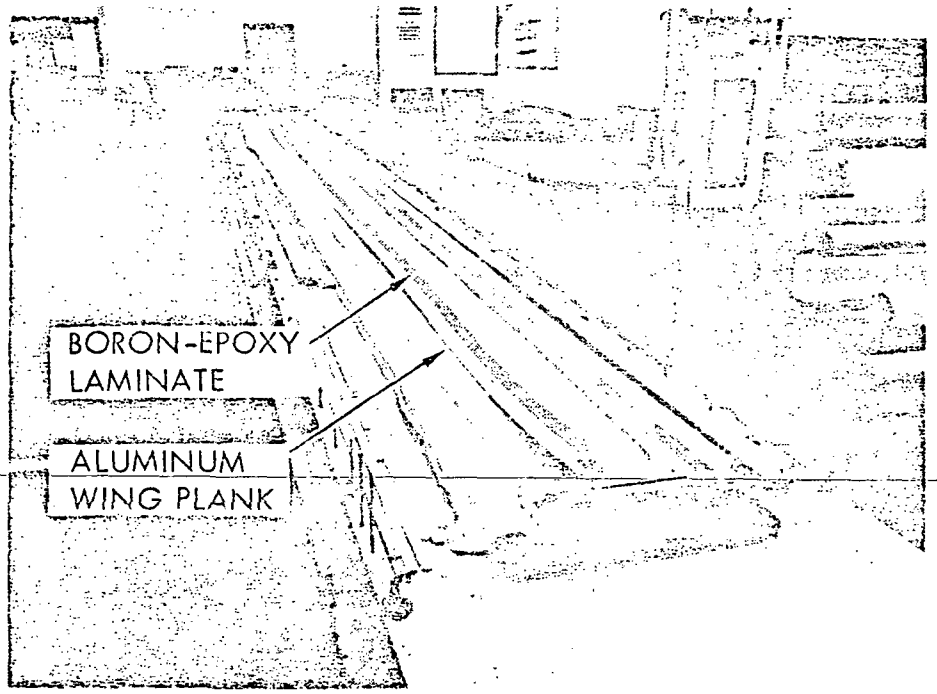

FIGURE 32. - ALUMINUM/BORON-EPOXY PLANK BONDED WITH END RESTRAINT (SHOWN LAYING FLAT)

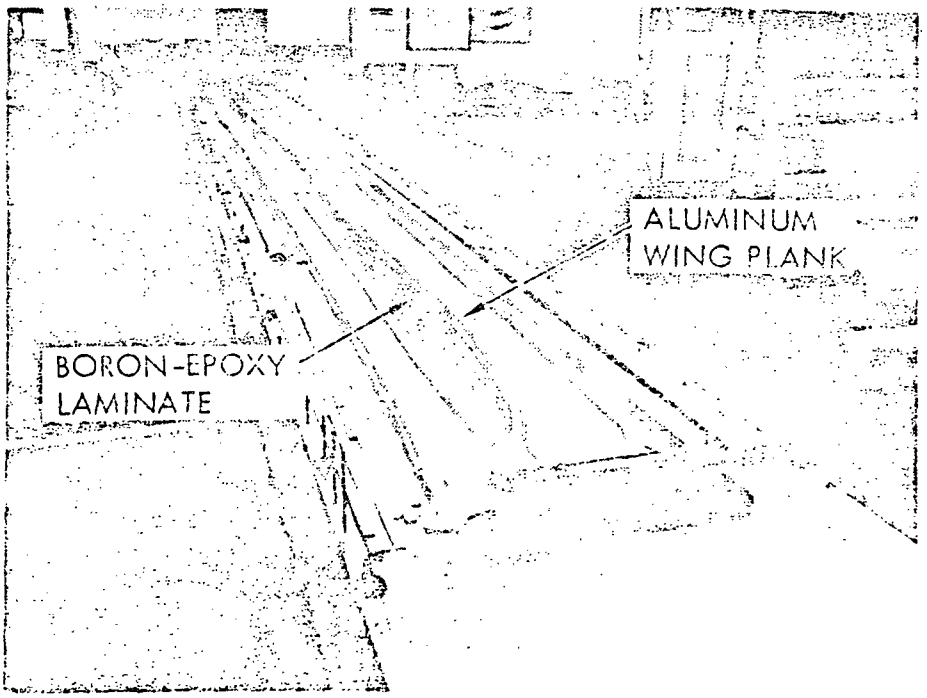

FIGURE 33. - ALUMINUM/BORON-EPOXY PLANK BONDED WITH END RESTRAINT (SHOWN ON EDGE)

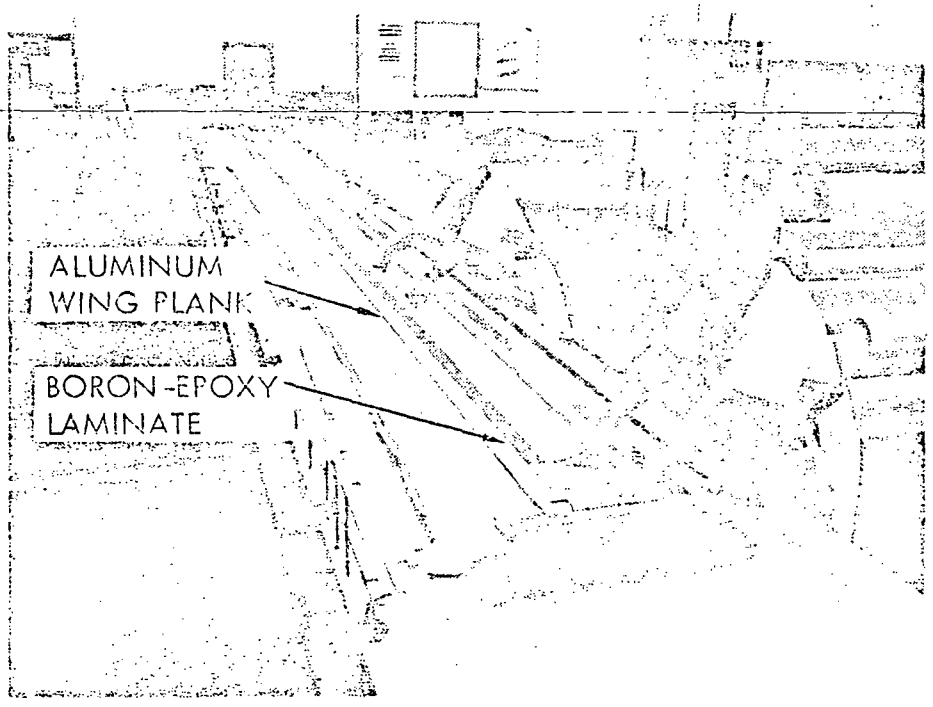

FIGURE 34. - STRAIGHTENING ALUMINUM/BORON-EPOXY PLANK WITH HAND PRESSURE

In addition to this hand-straightening operation, the wing plank and stiffener were clamped together with C-clamps. Spacing of the clamps left short areas where gaps were present between the plank and stringer. Figure 35 shows these gaps being removed with finger pressure.

The full-length bonding studies have thus conclusively shown that, with proper tooling, parts can be bonded to provide a bondline with a low stress at room temperature. The resulting low warpage will allow assembly into a full wing box with a minimum of difficulty.

6.2 HOLE GENERATION

A successful method for generating holes in boron-epoxy laminates reinforced with titanium was developed during Phase I and is fully described in NASA CR-112126. Efforts were continued during Phase II to improve hole quality. In punching holes in the uncured boron-epoxy laminate, the punch would sometimes strike the edge of a predrilled hole in the titanium doubler. This problem is related to properly positioning the titanium doublers and holding this position during the punching operation. To alleviate the problem, the holes in the titanium were slightly enlarged and the punch diameter was reduced.

As a secondary check of the effect of hole quality on assembly strength, the rainbow strap area of Phase I fatigue test specimen 130 PF-2 was cut out of one stringer and tested. This specimen had several holes which were relatively low quality. All holes were pulled in double shear on the fasteners (twice the load experienced in single shear for the actual assembly); in all holes tested, the fastener failed. There was no failure in the boron-epoxy reinforced aluminum, which indicates that adequate strength can exist even in relatively poor holes. The procedural changes noted above, however, are allowing production of much improved hole quality and will be used.

6.3 BLIND FASTENER INSTALLATION STUDY

During the Phase I fabrication of fatigue test specimen 130 PF-2, two delaminations occurred during installation of blind fasteners. A study was initiated, therefore, to determine how much back-up was required to contain the swaging action of the blind fastener on installation.

A 35-ply unidirectional laminate of boron-epoxy was available and was bonded to a piece of 7.950 mm (0.313 in.) thick aluminum. Three different thicknesses of 7075-T6 aluminum, 0.508 mm (0.020 in.), 1.016 mm (0.040 in.), and 1.524 mm (0.060 in.), were bonded to the back side of the boron-epoxy laminate using a room-temperature-curing epoxy adhesive.

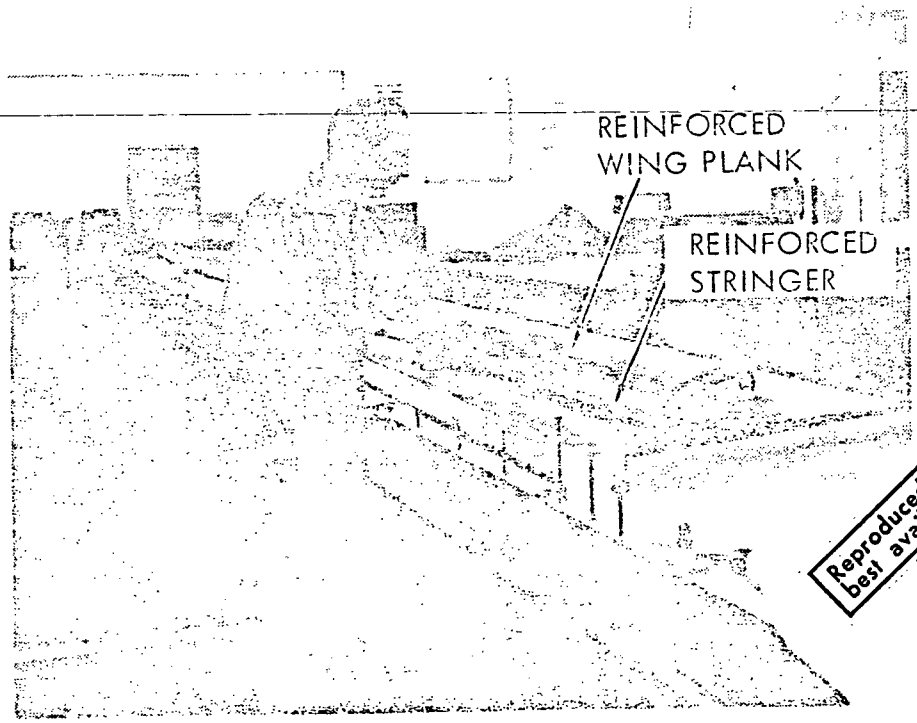

FIGURE 35. - PLANK/STRINGER ASSEMBLY
WITH CLAMP PRESSURE

Holes were drilled through the aluminum/boron-epoxy sandwich using a step drilling process to a diameter one drill size less than the diameter of the required hole. The hole was then reamed to full diameter for the fastener. The resulting hole had a burr on the break out side in all three of the aluminum thicknesses being checked. This burr was removed before installation of the fastener.

After installation of the blind fasteners, the specimens were sliced through the fasteners. It appeared that the 0.508 mm (0.020 in.) thick material showed some swaging action into the boron-epoxy laminate. Both the 1.016 mm (0.040 in.) and 1.524 mm (0.060 in.) thick back-up plates were satisfactory. Figure 36 shows the cutaway view of the three thicknesses.

As a result of this study, the design drawings specify that a 1.016 mm (0.040 in.) thick 7075-T6 aluminum reinforcing plate be bonded to the blind surface of the laminate at blind fastener hole locations.

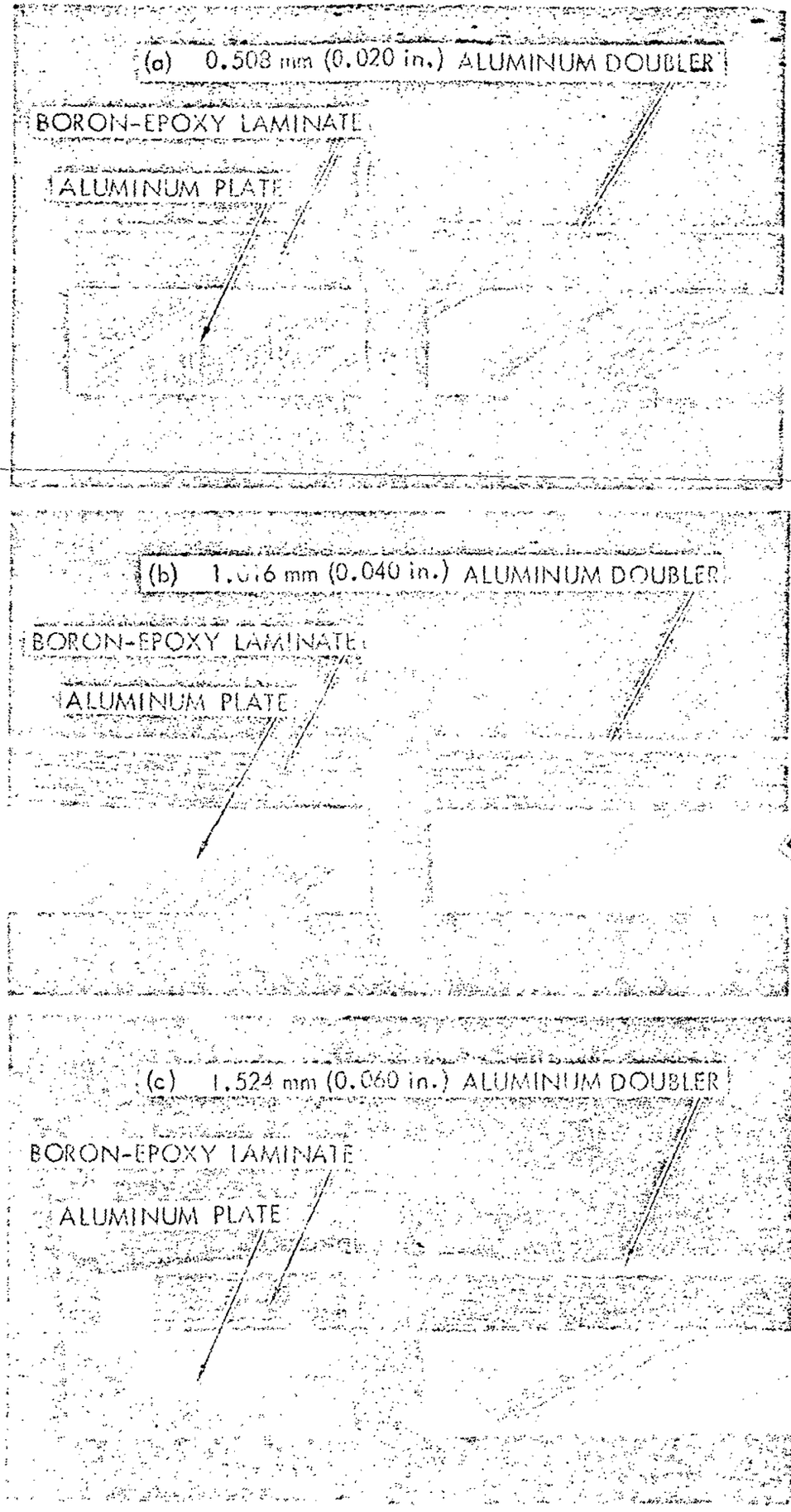

FIGURE 36. - CUTAWAY VIEW OF BLIND FASTENER TEST INSTALLATIONS IN BONDED ALUMINUM/BORON-EPOXY

7.0 COST/PRODUCIBILITY DEVELOPMENT

7.1 COST ESTIMATES

7.1.1 Labor Cost Estimates

Preliminary cost projections for production quantities of C-130 center wing boxes reinforced with boron-epoxy have been made based on the cost data developed during the Phase I fabrication of the three fatigue test components. These manufacturing manhours were projected to a full-size C-130 center wing box for all of the composite-related work. No cost changes in the aluminum structure occurred during the Phase II design effort. Consequently, all costs shown are cost increments to the aluminum baseline.

Table VII shows the distribution of basic manhours for each area of manufacturing operations. These manhours are for composite fabrication and assembly operations at the 200th center wing box unit.

Figure 37 shows the manhours required to reinforce the C-130 center wing box with boron-epoxy for increasing quantities of production units.

7.1.2 Material Cost Estimates

The C-130 center wing assembly used 159 kg (350 lb.) of boron-epoxy preimpregnated tape; 85 kg (187 lb.) in the upper surface and 74 kg (163 lb.) in the lower surface. At a material usage rate of 1.1 and an assumed cost for boron-epoxy tape of $221/kilogram ($100/pound), a material cost of $38,500 per center wing results. Additional materials such as adhesive and titanium shim stock might add another $1000 for a total material cost increase of $39,500 for a boron-epoxy reinforced center wing box.

7.1.3 Summary of Estimated Incremental Costs

The total cost increase to add boron-epoxy reinforcement to the C-130E center wing box is projected for the 200th production unit as follows:

Labor

695 manhours x $12.00/manhour = $8,340

Material

$38,500 (boron-epoxy tape) + $1,000 (adhesive, etc.) = $39,500

Total Cost Increase (200th unit)

Labor + Material = $47,840

TABLE VII. - PROJECTED MANHOUR DISTRIBUTION FOR COMPOSITE FABRICATION AND ASSEMBLY OPERATIONS AT THE 200th PRODUCTION UNIT

	Titanium Fabrication	Boron-Epoxy Lay Up	Cure Laminate and Bond Panels	Produce Holes	Total
Man Hours	106	80	459	50	695
Percent	15.2	11.5	66.0	7.3	100.0

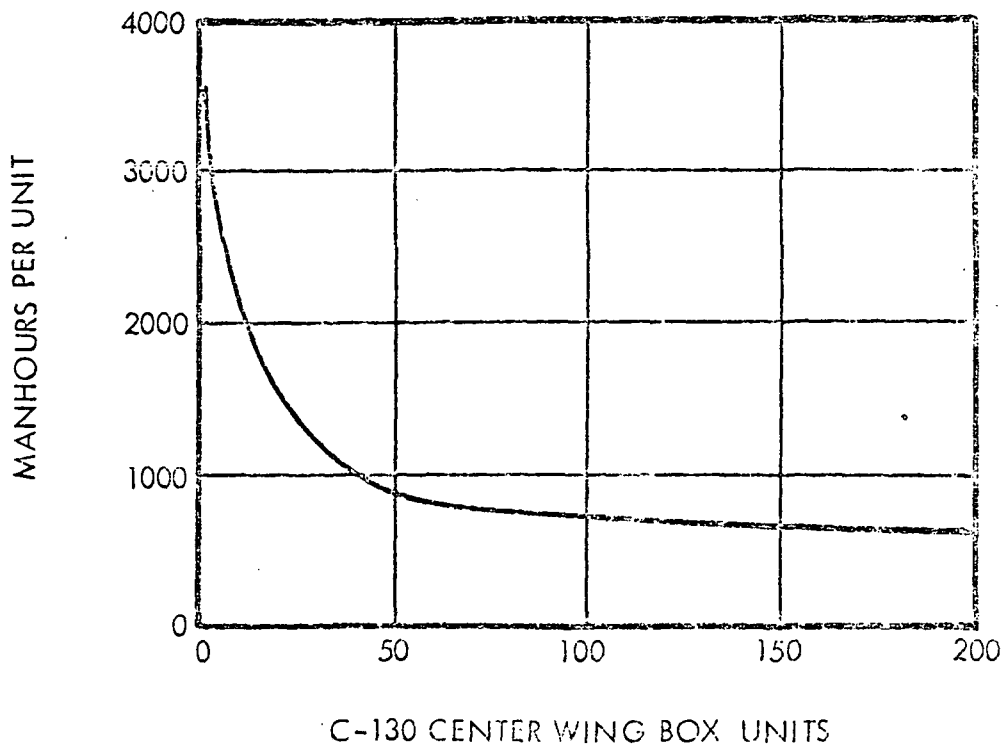

FIGURE 37. - COMPOSITE FABRICATION AND ASSEMBLY MANHOURS VERSUS C-130 CENTER WING BOX UNITS PRODUCED (ESTIMATED DATA)

At a total weight saving of 229 kg (506 lb.), the computed value per unit of weight saved is:

$47,840 ÷ 229 kilograms = $208.91/kilogram

$47,840 ÷ 506 pounds = $94.55/pound

7.2 PRODUCIBILITY

The aluminum structure of the boron-epoxy reinforced C-130 center wing box is essentially unchanged from a production standpoint. All changes made to the box structure are in the surface panel assemblies and are within current C-130 production practices. Machining practices are unchanged. Changes involving finishing, sealing, and assembly are within basic C-130 wing box manufacturing practices.

Boron-epoxy reinforcement fabrication practices and concepts were developed during Phase I. These same concepts have been translated into the full-scale center wing box design. Special effort was made throughout design development to reduce or eliminate the impact of the addition of boron-epoxy reinforcement.

Installation of the completed reinforced center wing box will be the same as for regular production center wing boxes.

8.0 RELIABILITY AND QUALITY ASSURANCE

A reliability and quality assurance program was continued in accordance with a NASA-approved program plan. The plan, which complies with required elements of NASA specifications NHB 5300.4 (1A and 1B), was revised during Phase II to incorporate program changes in the subsequent production and test phases.

8.1 RELIABILITY PROGRAM

The objective of the C-130 composite-reinforced wing box reliability program is to attain a high level of inherent reliability in system design; to assure that this level of reliability is not degraded throughout the production, test, and operational phases; and to provide to NASA the assurance and visibility that specified reliability requirements are achieved. During Phase II, reliability program activities were primarily concerned with detail design and manufacturing development. A continuing program of informal reviews, biweekly status meetings, and quarterly program reviews was used to assess progress and identify and resolve problems.

8.1.1 Reliability Progress

As detail design progresses, drawings were reviewed for reliability adequacy. The number of fasteners which penetrate the boron-epoxy has been minimized by redesigning plumbing brackets and revising fastener hole patterns. Several potential manufacturing problems were thereby successfully avoided. Formal static strength, fatigue endurance, and flutter analyses have been completed which show the final design to be suitable for the intended application.

Favorable results were obtained in the single stringer and short panel compression tests as well as in the buckling evaluation tests. Thus, the questions arising from the Phase I buckling tests have been resolved and the adequacy of the buckling analysis has been demonstrated.

Work on material and process specifications was satisfactorily completed. Each specification was reviewed for reliability adequacy. Several changes were incorporated in process specification STP 60-205 to strengthen and clarify the requirements for bonding cured boron-epoxy laminates to aluminum.

Significant manufacturing development progress was made in Phase II. The cool-tool concept was refined to obtain better control of warpage in a skin panel of changing cross-section. Valuable experience was gained from the bonding of full-length stringer and skin panel specimens. Several skin panel failures during bonding identified the degree of tooling support required in thin panel sections and will result in better production tooling. The amount of warpage in the long stringer and skin panels appears

to be quite acceptable from a stress and assembly viewpoint. Although the ability to hold location tolerances between holes on the full-length parts was demonstrated, this is an area where special attention may be required in production. Hole quality in the boron-epoxy laminates and titanium shims was improved by a slight increase in titanium shim hole size, which reduces the chance of damage while punching the hole in the boron-epoxy.

Manufacturing and inspection planning was initiated on a pilot basis to identify and eliminate any potential barriers to effective communication of fabrication, assembly, and inspection sequences. These are areas where a high degree of detail must be transmitted to enhance achievement of high quality in the full-scale wing boxes. Planning efforts included making provisions for material batch and age control, as well as the recording of critical parameters such as time, temperature, and pressure during the layup and bonding processes.

8.1.2 Reliability Assessment

Qualitative assessments were made of the confidence level for achievement of reliability objectives with the current state of technology in the areas of design, analysis, materials and processes, manufacturing, inspection, and testing. Each assessment was based on a detailed review of the many factors involved in each area. Consideration was given to the degree to which theoretical concepts are developed and proved, extent and type of experience data available, number of critical steps or sequences, number of relative unknowns, complexity of methodology, skill levels required, and schedule restraints.

A high confidence level continues in the area of design. The design configuration is based on the proved C-130 wing box design, Phase I and Phase II test results, and thorough static strength and fatigue analyses. Several specific design changes were incorporated to avoid potential manufacturing problems.

In the area of static strength and fatigue analysis, the confidence level ranges from good to high. Computerized analysis data along with compression test results have improved the Phase II reliability confidence level.

The materials and processes confidence level remains good. A significant contribution to reliability achievement was the development of process specification STP 60-205, defining the bonding of cured boron-epoxy laminates to aluminum.

A notable improvement in a good reliability confidence level was made in manufacturing development. Contributing to this improvement was the added experience with, and refinement of, the cool-tool concept, successful bonding of full-length stringer and skin panels, and demonstrated ability to control warpage and meet hole quality and location tolerance requirements.

Confidence in inspection capabilities is rated good. State-of-the-art non-destructive inspection equipment and methods are being applied. The design configuration will use considerable reliance on established material and process controls to assure adequate bonding.

Wing box testing remains a high confidence area because of the similarity to previous C-130 static and fatigue test programs. Successful component testing during Phase II reinforced this high reliability confidence rating.

The consolidated reliability assessment is that a good to high confidence level exists at the end of Phase II in the composite-reinforced wing box design and in the state of readiness for successful fabrication and assembly.

8.2 QUALITY ASSURANCE PROGRAM

Quality Assurance effort during the Detailed Design Phase consisted primarily of reviewing design drawings for inspectability, formalizing of nondestructive test methods and techniques, and inspection support of Phase II test specimen fabrication.

8.2.1 Design Support

Detail design drawings were reviewed to define potential inspectability problems. The most significant inspection problem encountered related to the inboard engine drag angle attachment where the assembly sequence required that holes be drilled through the laminate-reinforced lower surface skin during final wing box assembly. This design was not acceptable for inspection because of the risk of delamination when drilling from the metal side without back-up support to the laminate. The possibility of detecting damage and the difficulty of repairing it in the limited access area under the hat-section stringers dictated the need for redesign. As a result, an alternative design was devised which eliminated the blind hole and fastener requirement. This alternative has been previously described in Section 3.0 of this report. In general, the use of blind fasteners through boron-epoxy laminates was discouraged. When blind fasteners were unavoidable, suitable bearing plates were provided to protect the laminate from the head or tail end of the fasteners.

8.2.2 Non-Destructive Inspection

Ultrasonic inspection procedures were finalized for checking the quality of the boron-epoxy laminates and the laminate-to-aluminum bond. Thru-transmission and pulse-echo inspection techniques are applied using the following equipment:

- o Reflectoscope, Sperry UM-715
- o Transducer, 5.0 mHz, 1/4-inch diameter, Longitudinal Wave, Sperry P/N 57A2214
- o Cable, 6 foot, Microdot/UHF Connector, Sperry P/N 57A2270
- o Video Plug-in Module, 10 N, Sperry P/N 50E533
- o Couplant (water is typically used)
- o Calibration Standard [1]
- o Aluminum Block, Polished to Mirror Finish, 3.81 cm (1.5 in.) wide x 5.08 cm (2.0 in.) deep x 15.24 cm (6.0 in.) long

8.2.2.1 Laminate Inspection

Laminate quality is determined using thru-transmission ultrasonic techniques where loss of sound transmission indicates a void area. Sound is transmitted through the laminate to an ultrasonic mirror, then back through the laminate to a receiver, as illustrated in Figure 38. A water couplant is used to couple the transducer to the laminate strip and the strip to the ultrasonic mirror block. With the transducer placed on the laminate, the reflectoscope gain is adjusted to obtain a back-reflection from the mirror block as illustrated for a good laminate in Figure 38. The mirror is then removed to simulate a delamination, and the reflectoscope display is as illustrated for a delaminated area in Figure 38. Thus the laminate itself is used as a calibration standard, since the presence or absence of a signal indicates good or delaminated areas, respectively. After calibration, the laminate strip is inspected with the mirror block water coupled to one side of the laminate strip and the coupled transducer scanning the opposite side. If no defects are detected, the mirror block is moved to another area until the entire laminate is inspected. All of the laminates produced in Phases I and II were 100% inspected, and no delaminations were found.

8.2.2.2 Bondline Inspection

The bondline between the laminate and the aluminum skin or stringer is inspected using pulse-echo ultrasonic techniques. If the inspection is made from the boron-epoxy side, the technique is similar to that used for laminate inspection with the aluminum skin acting as the mirror. An inspection from the aluminum side requires calibration with a known standard, as illustrated in Figure 39. The pulse-echo method detects

[1] The term "standard" does not refer to a specification or military standard. It is, instead, a piece of calibration equipment, representative of the part to be inspected, which contains intentionally included defects as well as "good" areas. The use of this standard is described in subsequent sections of this report.

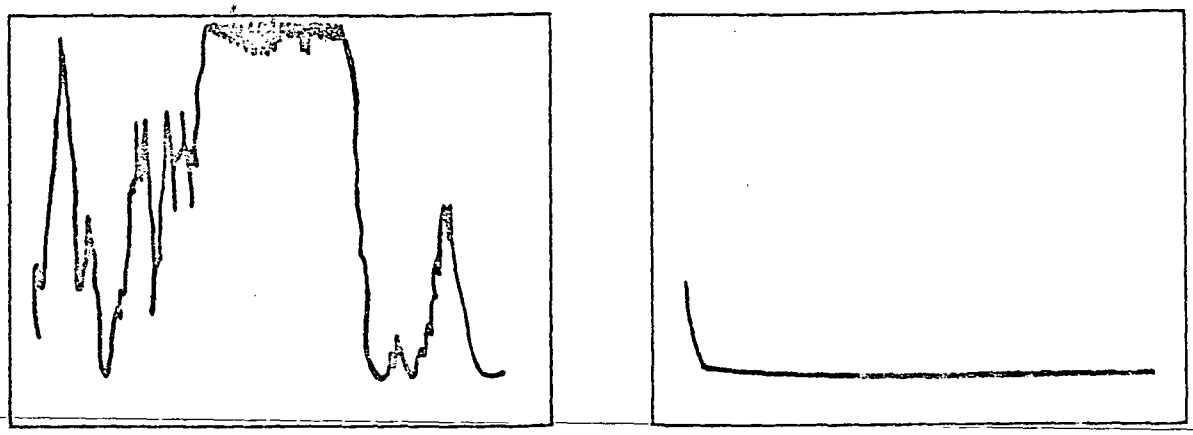

GOOD LAMINATE SIGNAL

VOID OR DELAMINATION SIGNAL

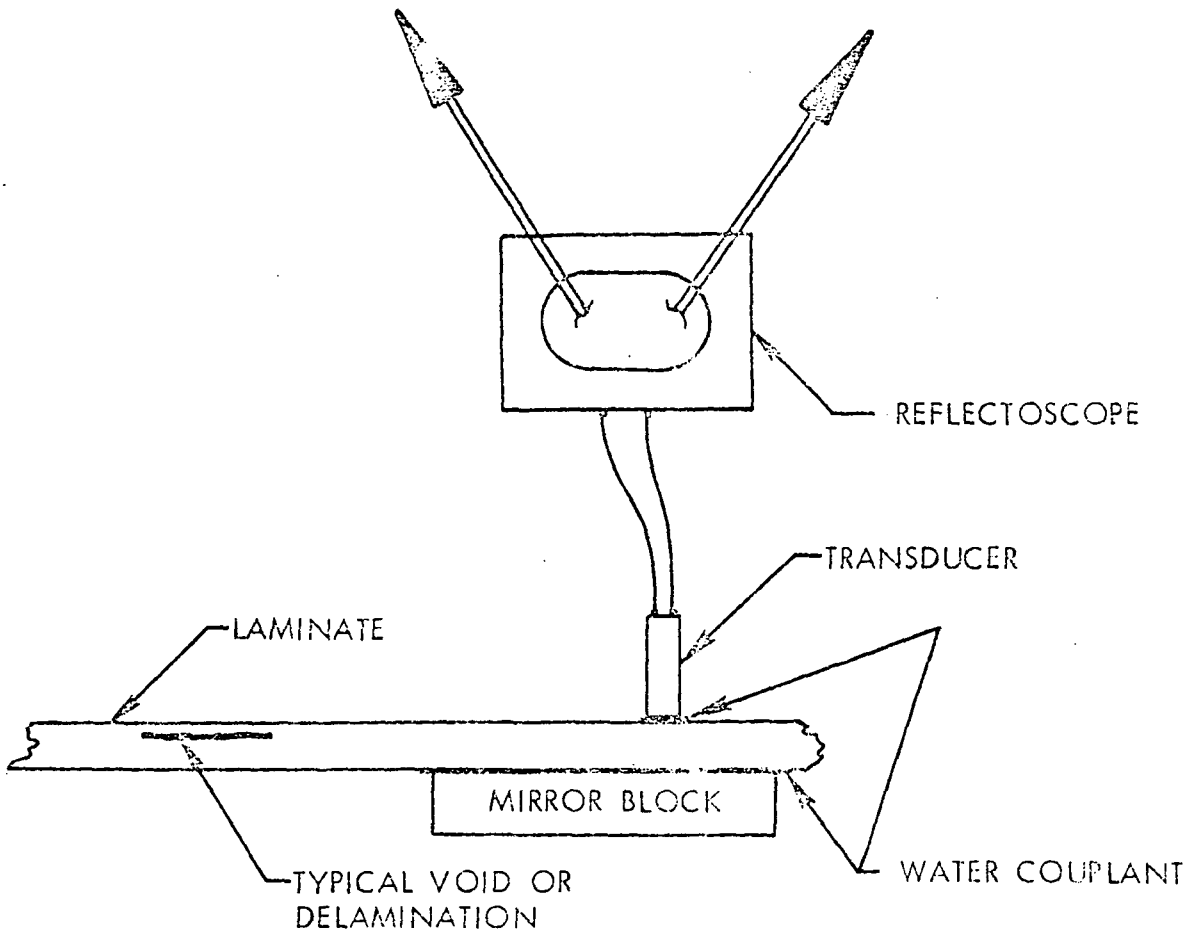

FIGURE 38. - ULTRASONIC INSPECTION OF BORON-EPOXY LAMINATES

A. NEARSIDE DISBOND - FROM SKIN
B. FARSIDE DISBOND - FROM SKIN

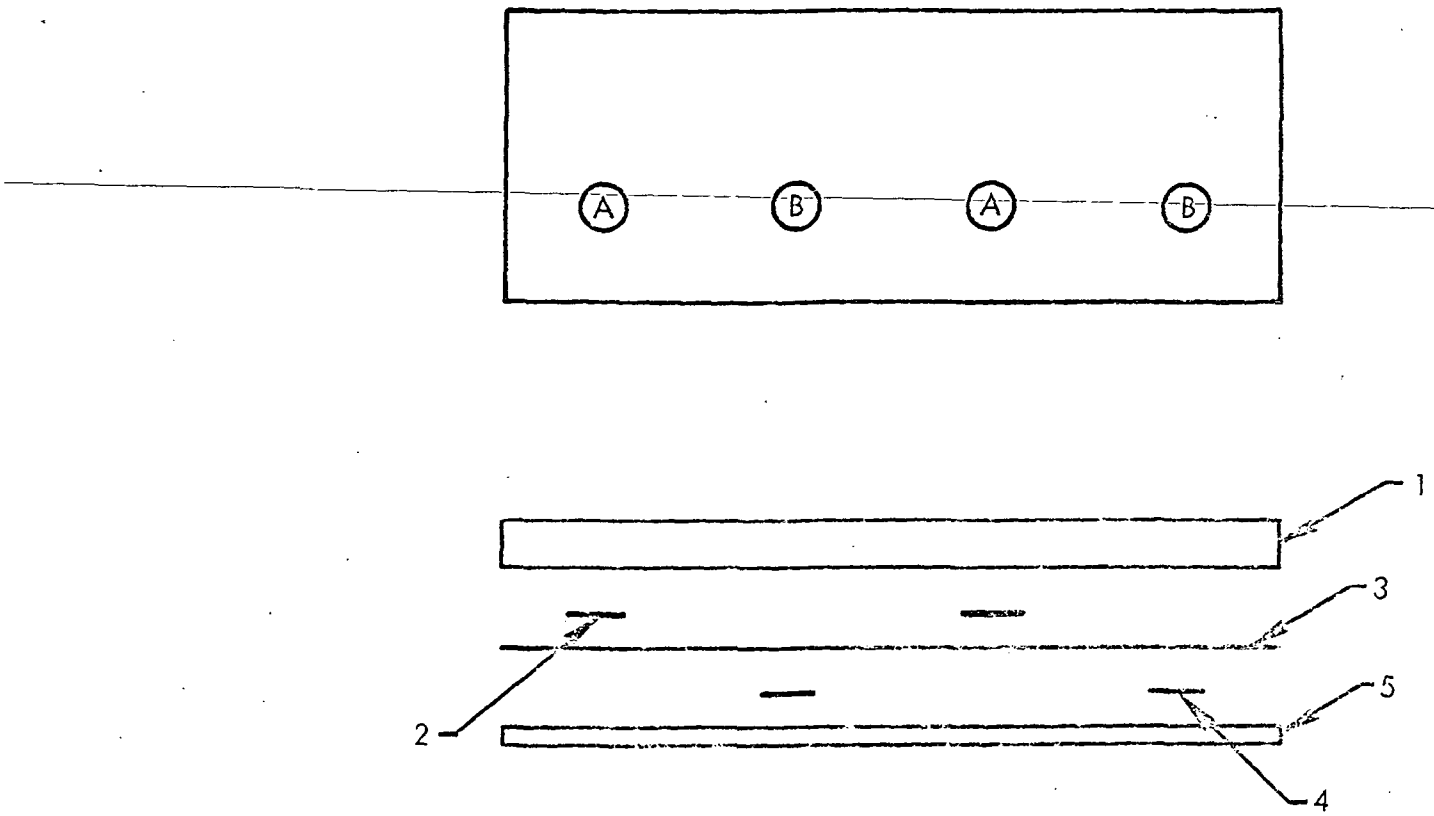

1. ALUMINUM SKIN
2. SIMULATED DISBOND BETWEEN ADHESIVE AND ALUMINUM SKIN
3. ADHESIVE
4. SIMULATED DISBOND BETWEEN ADHESIVE AND LAMINATE
5. BORON-EPOXY COMPOSITE LAMINATE

FIGURE 39. - TYPICAL BONDLINE CALIBRATION STANDARD

voids by differentiating between high sound dampening areas and no sound dampening. In the nearside void case, the sound energy continues to echo in the aluminum component and is indicated by a saturation signal on the reflectoscope. The instrument is calibrated by coupling the transducer to a good bond location on the calibration standard. The sweep is then adjusted to cause a signal display similar to the good bond signal illustrated in Figure 40. By sliding the transducer over each simulated disbond in the standard, the characteristic signal for each type of disbond is observed. Typical delamination or disbond signals are also illustrated in Figure 40. Nearside disbonds or disbonds between the aluminum and the adhesive are readily detectable. Farside disbonds or disbonds between the adhesive and the laminate are more difficult to detect from the aluminum side. The sound dampening characteristics of farside disbonds often produce a reflectoscope display which is between a good bond signal and an ideal farside disbond signal. Although some signal is returned, it is weaker than that returned for the clearly "good" display. This signal can be interpreted by experienced technicians using calibration standards which closely simulate actual defects. Such interpretation, however, requires a high level of expertise, and work is continuing to simplify the procedure. Partially delaminated buckling and fatigue test specimens are being used in this work.

Assembled wing planks are inspected for bond integrity by scanning the aluminum surface with the water coupled transducer and observing the display for signal characteristics indicating a probable disbond. Normally, ultrasonic inspection will not pick up shallow disbonds along the edge of a part. Voids or disbonds up to about 3.175 mm (0.125 in.) from the edge of the part must be detected visually or mechanically.

A method for real-time monitoring of adhesive cure during composite bonding was explored using an Audrey II dielectrometer and analog computer system. Inputs to the analog computer are temperature, bondline conductivity, bondline capacitance, bond pressure, and elapsed time. By developing a parameter sensing program which characterizes the AF127-3 adhesive, an effort is being made to produce a running estimate of final bond strength with high correlation to lap shear values. This work is expected to allow use of the dielectrometer/computer system in conjunction with standard process controls during fabrication of full-scale bonded assemblies.

8.2.3 Fabrication Inspection

Nondestructive evaluations were conducted on test specimens fabricated during Phase II. The composite strips were ultrasonically evaluated prior to bonding. The bondlines were evaluated for voids and porosity after bonding. A discrepancy was noted in test panel 130PB4-7-1 and documented on DR 877632. There was a void at the edge of the bondline about one inch long, starting one inch from the end of the part. The void, less than 3.175 mm (0.125 in.) wide, was not detectable with ultrasonics since it was on the edge of the part. The defect was repaired by injecting EA 9309-1 room-temperature-cure adhesive into the void area.

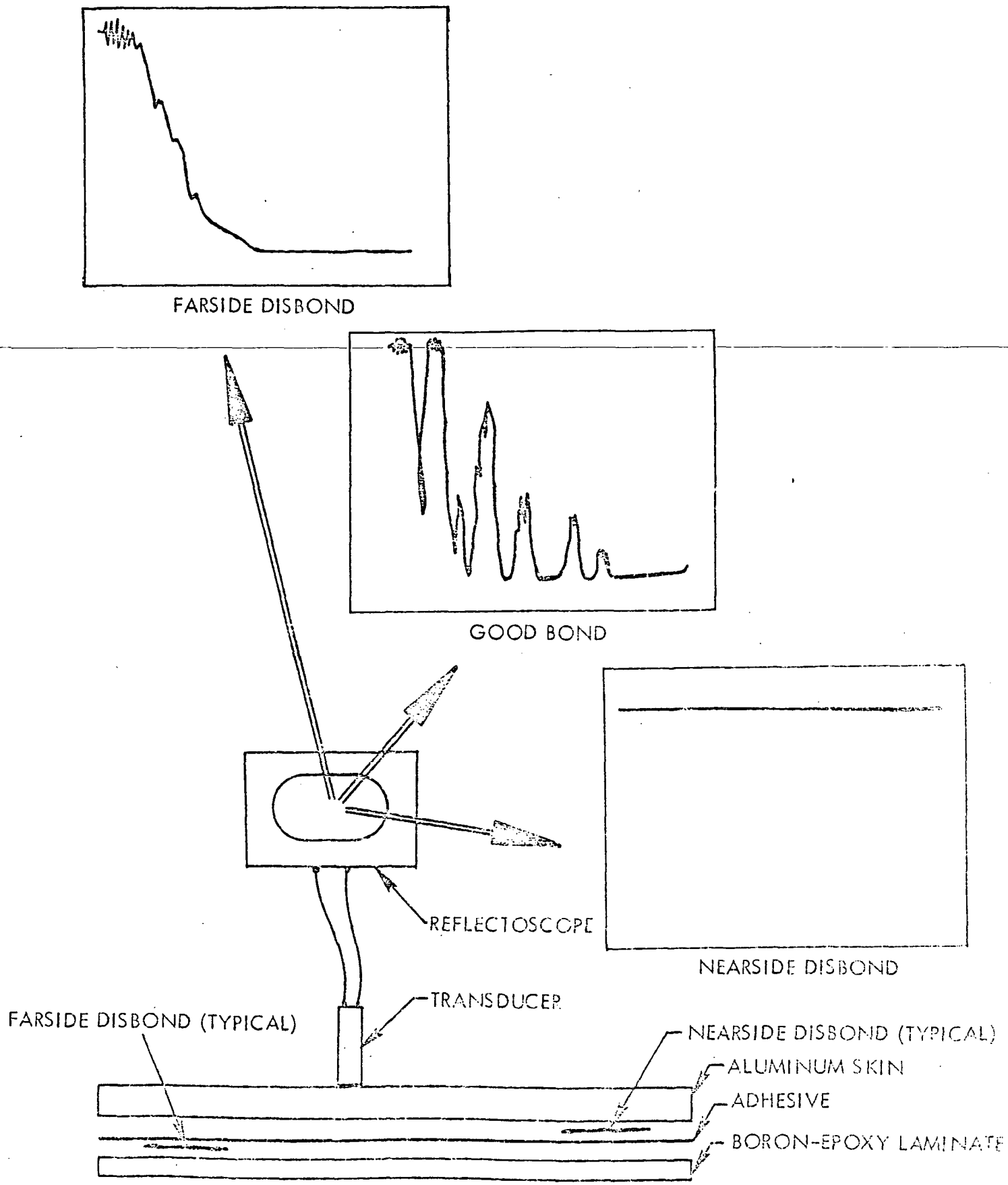

FIGURE 40. - ULTRASONIC INSPECTION OF BONDED ASSEMBLY

G

All specimen parts were inspected for dimensional conformity and workmanship, and only two discrepancies were noted. Two test panels, 130-PF-401-17 and -19, were withheld on DR 25505 for "holes not to print." There was some distortion of the titanium shims at the holes and 0.381 to 0.635 mm (0.015 to 0.025 in.) positive cones around the holes on the laminate side. Parts were accepted "as is" for the test. As a result of this discrepancy, a program was initiated to improve the quality of holes in the boron-epoxy laminates. An improved hole-generation technique, described in Section 6.0, resulted from this work.

9.0 EXPERIMENTAL STUDIES

During the component tests, conducted in Phase I, two areas were identified where some additional testing was necessary. The more important of these was related to the compression tests performed in Phase I, where some problems were encountered in obtaining valid buckling failures in the panel tests. These problems were associated with terminating the boron-epoxy laminates at the specimen ends to allow final machining and uniform introduction of compressive loads. On past programs, difficulty has been experienced in applying compressive loads directly to unidirectional boron-epoxy laminates. Local stresses at the bearing surface caused failure of the epoxy matrix, resulting in unsupported fibers. The unsupported fibers "broom" and unload the laminate. Difficulties are also encountered in machining boron-epoxy with conventional cutters. For these reasons, boron-epoxy laminates for the Phase I buckling specimens were staged out with titanium inlays at the specimen ends. A short titanium plate was placed over the termination, and mechanical fasteners were installed through the plate, laminate termination, and aluminum structure. This scheme, however, resulted in sufficient local eccentricy to precipitate failures near the specimen ends, and prevented determination of the true buckling capabilities of the specimens. Because of these problems, additional buckling evaluations were performed during Phase II.

The second area related to detail design selection in the radius of a stringer cutout. During PF-I fatigue tests, minor fatigue cracks were found originating from cutouts of the stringer crown on some stringers terminating at the W.S. 0.00 access door. Although these particular cracks were traced to a sharp edge remaining after the cutout was made, it appeared that some slight configuration changes might provide a much better cutout design, and specimens were tested to verify the design selection.

The testing conducted in these two areas is discussed in the following subsections.

9.1 PRELIMINARY CRIPPLING TEST

Prior to initiating the Phase II buckling studies, preliminary evaluations were conducted to improve the specimen end configuration. A crippling-type specimen was selected for the preliminary evaluation. If satisfactory performance could be obtained at strain levels required for crippling, satisfactory performance would be assured at strain levels required to produce a buckling failure in the test panel.

9.1.1 Description of Crippling Specimen

Rather than constructing a crippling specimen, a short single-element section was cut from fatigue specimen 130-PF-2 which was tested during Phase I. The element had an extruded skin of 7075-T73511 aluminum alloy and a hat-shaped stiffener of 7075-T6511 aluminum alloy. The inside crown of the stiffener had a 2.29 cm (0.9 in.) wide boron-epoxy laminate containing 33 unidirectional plies, and the skin had a 5.08 cm (2 in.) wide laminate of the same thickness. The stiffener was attached to the skin with TL-100 Taper-lok fasteners of alloy steel. Configuration of the finished specimen is shown in Figure 41.

9.1.2 Fabrication of Crippling Specimen

The spanwise edges of the element were machined to produce a symmetrical specimen. Two 3.8 cm (1.5 in.) long rings were cut from a 152.4 cm (6.0 in.) diameter steel pipe. A ring was placed on Teflon film and nearly filled with a mixture of five parts Magnabond 69-9A to one part Magnabond 69-9B. One end of the test element was placed in the mixture, which was then allowed to cure. When the first end was cured, the other end was prepared in the same manner. Magnabond is a filled epoxy tooling plastic which has low shrinkage upon curing. As an epoxy it also has adhesion. The purpose was to completely encapsulate the element ends, especially the cavity between the skin and stringer. Encapsulation plus adhesion to the boron-epoxy and aluminum parts was expected to provide sufficient support to prevent damage to the laminate upon subsequent machining. Also it was hoped that sufficient lateral support and containment would be provided to allow direct compressive loading of the laminate without experiencing brooming at the bearing surface. The element ends were then machined flat, parallel, and normal to the span. A shell-type milling cutter was used, and it was necessary to sharpen the cutter after making about five passes. No damage was caused by the machining. A view of a machined end is shown in Figure 42. The boron-epoxy is practically invisible since its color blends with that of the Magnabond.

The element was instrumented with electrical resistance strain gages at the locations shown in Figure 43. All gages were of the axial type with their grids aligned in the spanwise direction. Two gages, on the boron-epoxy laminates, were installed prior to casting the ends in Magnabond, and were installed as close to the spanwise centerline of the element as possible without disassembly. Lead wires for these two gages were routed through a small hole drilled in the upstanding leg of the stiffener. The hole was approximately 5 cm (2 in.) from one end and on the approximate centroid of the element.

9.1.3 Crippling Test

The test specimen was placed in the compression bay of a 17.79×10^5 N (400,000 lb.) capacity Baldwin Universal Testing Machine. Load was applied through ground steel plates, sized so that load was not applied to the steel ring surrounding the Magnabond. The maximum load range was used, and load was applied in 4.45×10^4 N (10,000 lb.) increments until specimen failure. Load was held constant at each increment long enough to collect strain data using a Baldwin Strain Indicator along with a switching and balancing box. Specimen failure occurred at a load of 7.78×10^5 N (175,000 lb.).

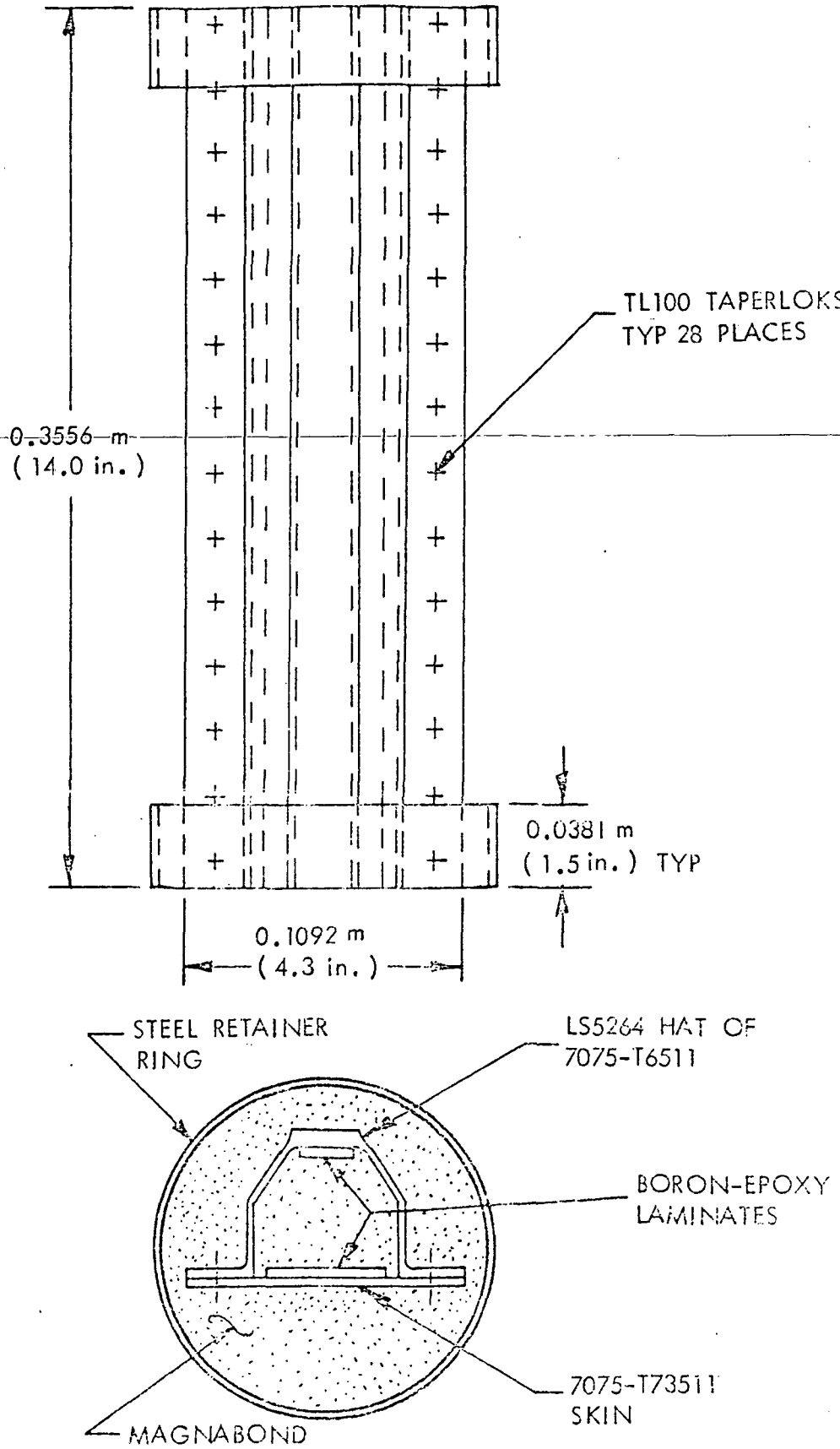

FIGURE 41. - GENERAL CONFIGURATION OF PRELIMINARY CRIPPLING SPECIMEN CUT FROM 130-PF-2

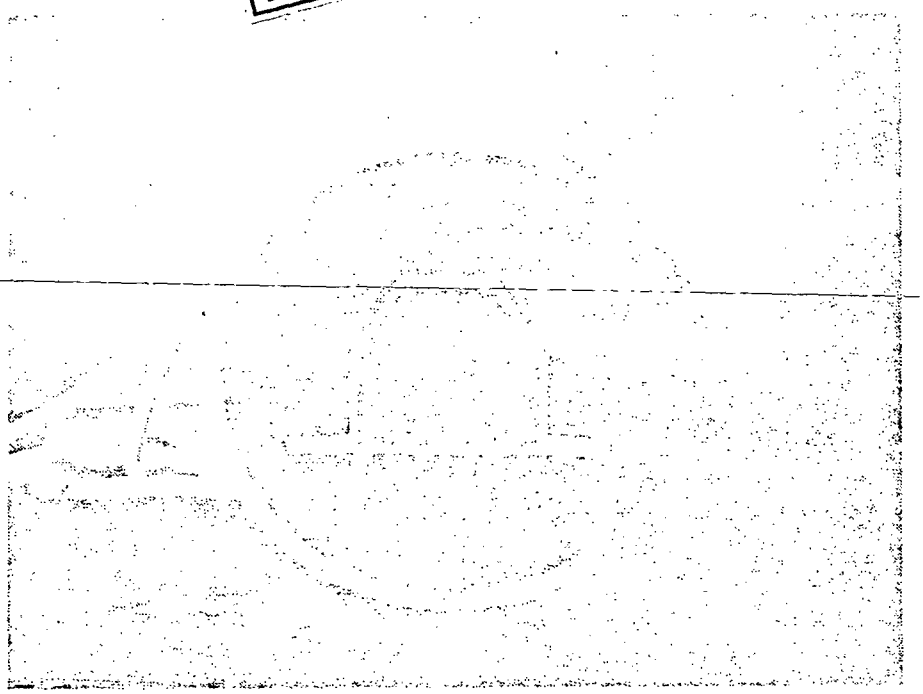

FIGURE 42. - PHOTOGRAPH SHOWING MACHINED END OF PRELIMINARY CRIPPLING SPECIMEN

9.1.4 Evaluation of Crippling Test

Test specimen failure at a load of 7.78×10^5 N (175,000 lb.) occurred in the test section, and there was no evidence of end effects. Photographs of the failed specimen are contained in Figure 44. Load-strain data were collected for all nine strain gage locations. Typical load-strain data are presented in Figures 45, 46, and 47.

Observation of the strain data showed that the boron-epoxy laminates sustained maximum strains comparable with those obtained for basic compression sandwich beam tests for boron-epoxy laminates. The valid failure, coupled with the high strain level sustained, provided confidence that this method of end preparation could successfully be used on the Phase II buckling evaluation.

In this test, and in all other tests conducted, the specimens were sectioned after testing, and were dimensionally checked. All parts were within design tolerances.

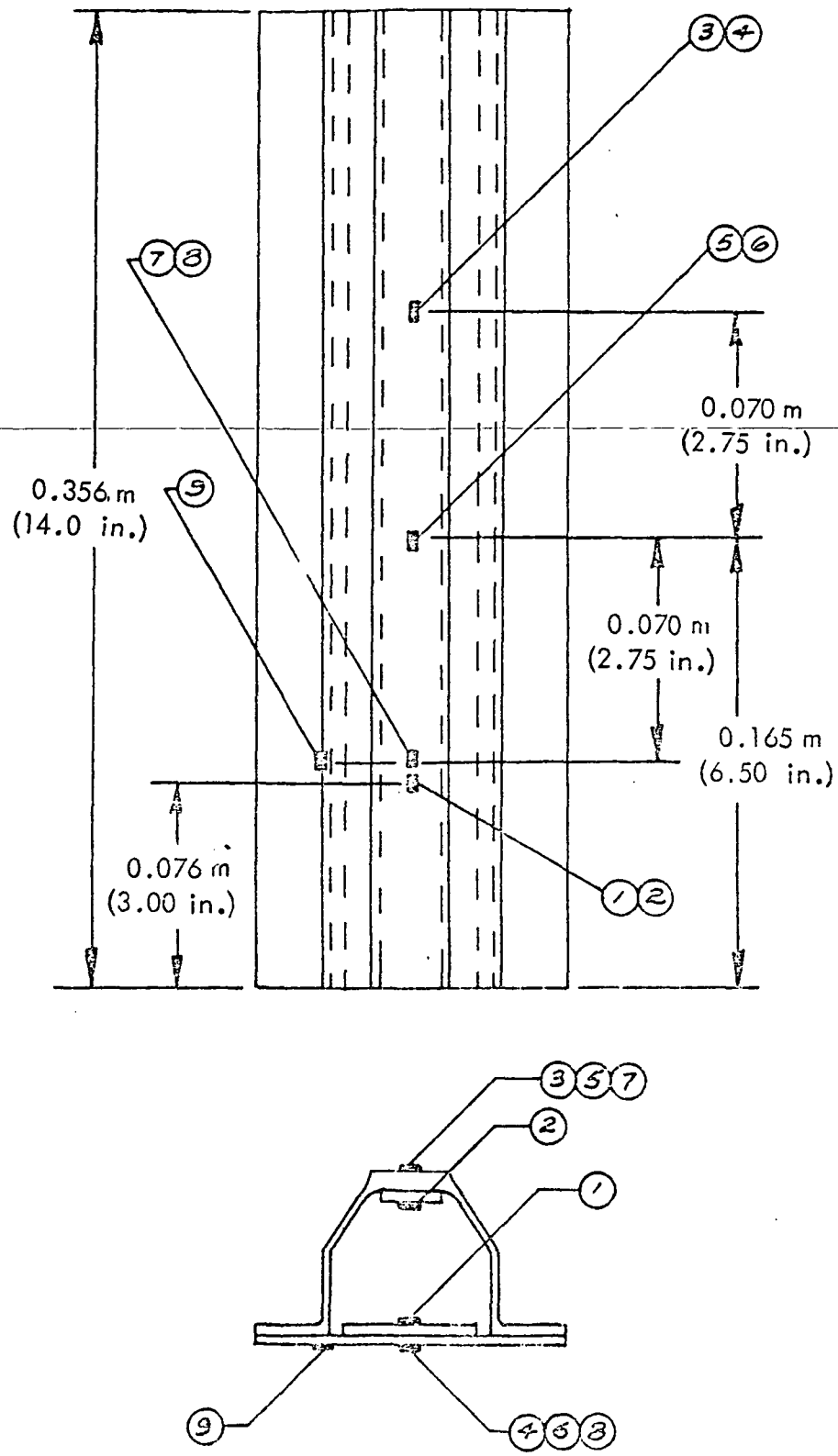

FIGURE 43. - PRELIMINARY CRIPPLING SPECIMEN - STRAIN GAGE LOCATIONS

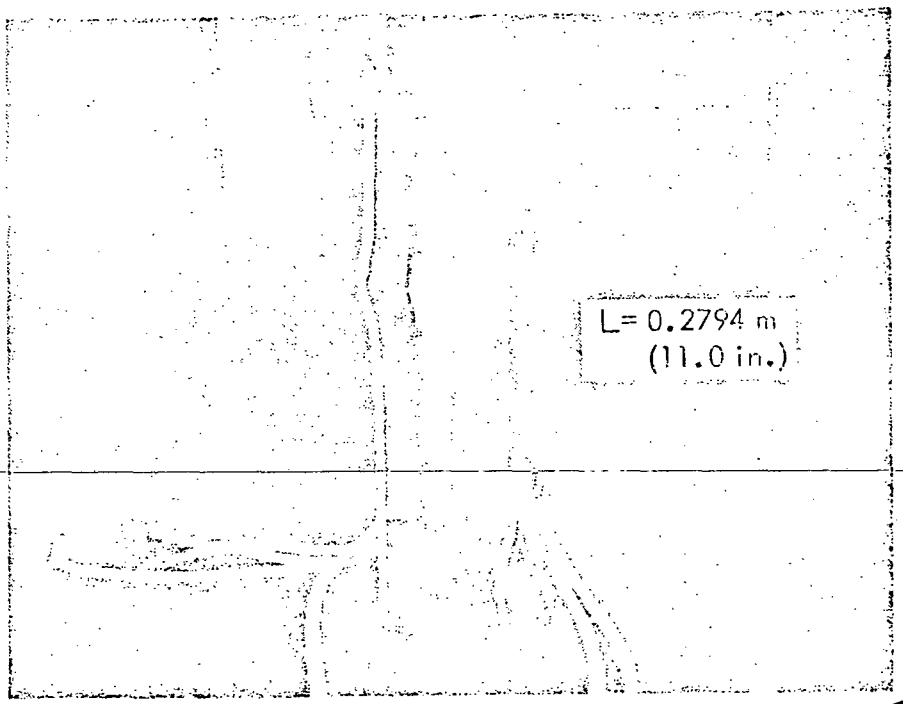

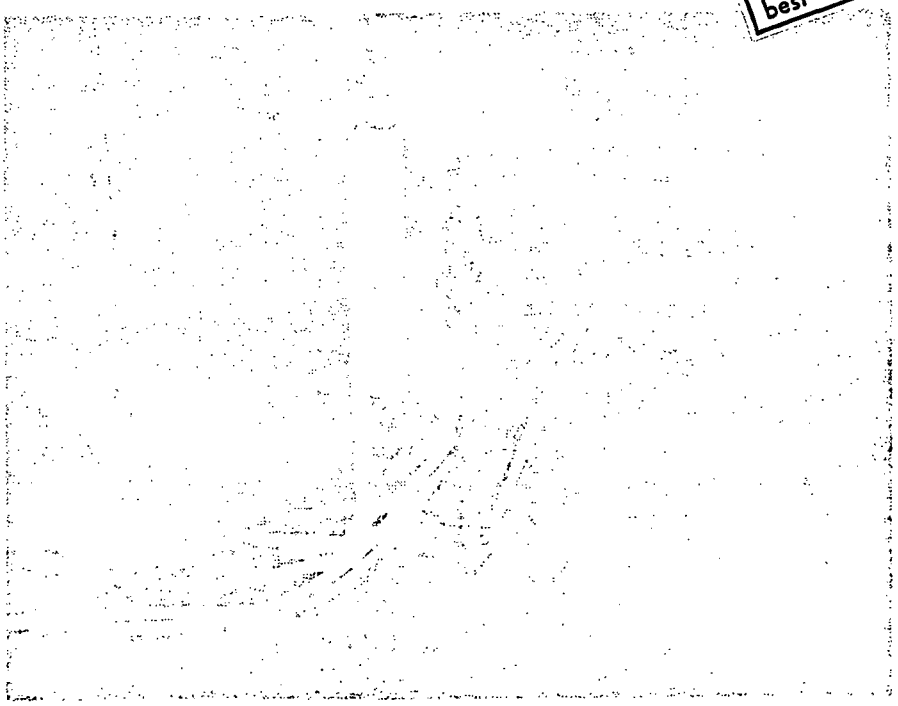

FIGURE 44. - PHOTOGRAPHS SHOWING PRELIMINARY CRIPPLING SPECIMEN AFTER FAILURE

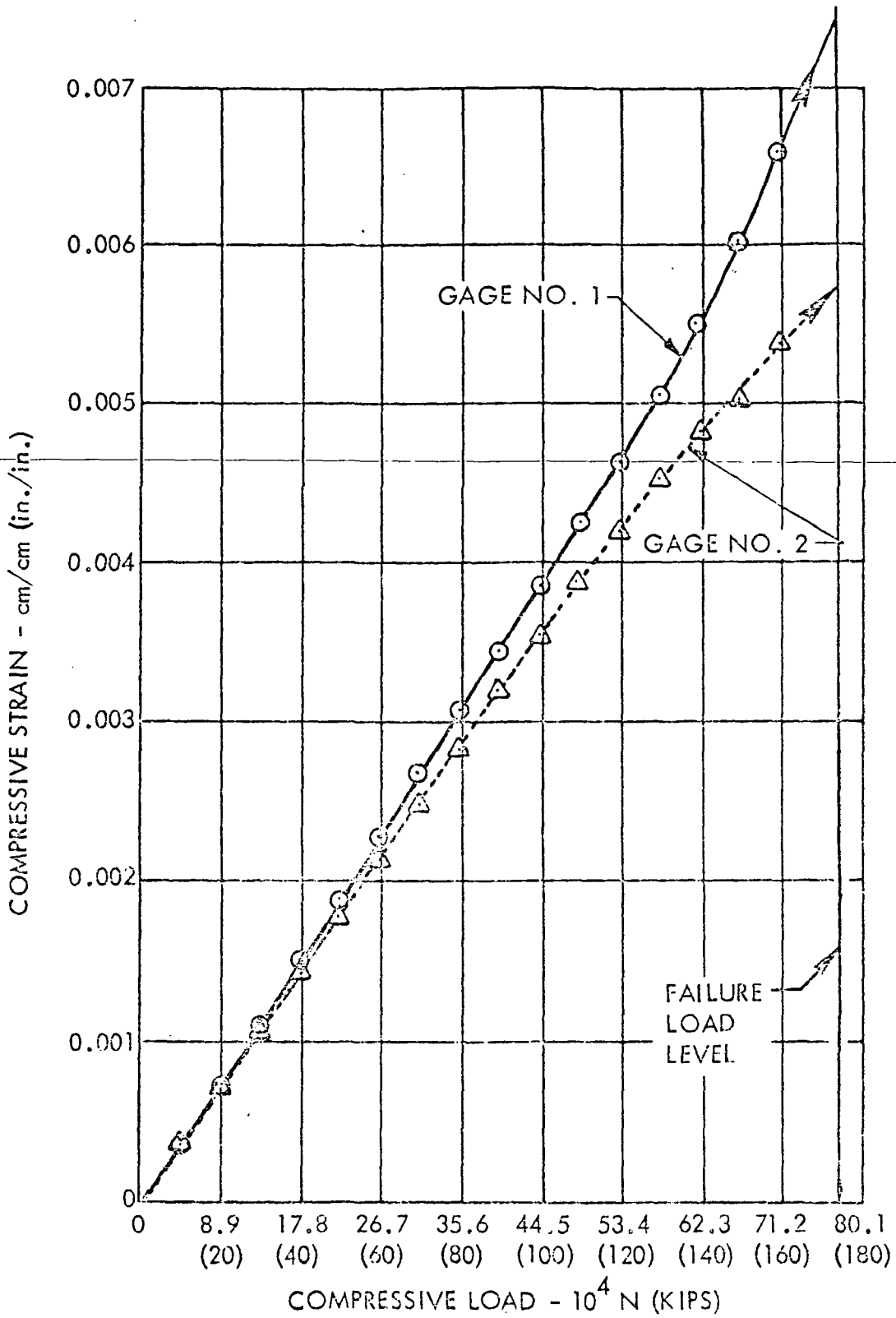

FIGURE 45. -COMPRESSIVE LOAD VERSUS STRAIN
PRELIMINARY CRIPPLING SPECIMEN - GAGES 1 AND 2

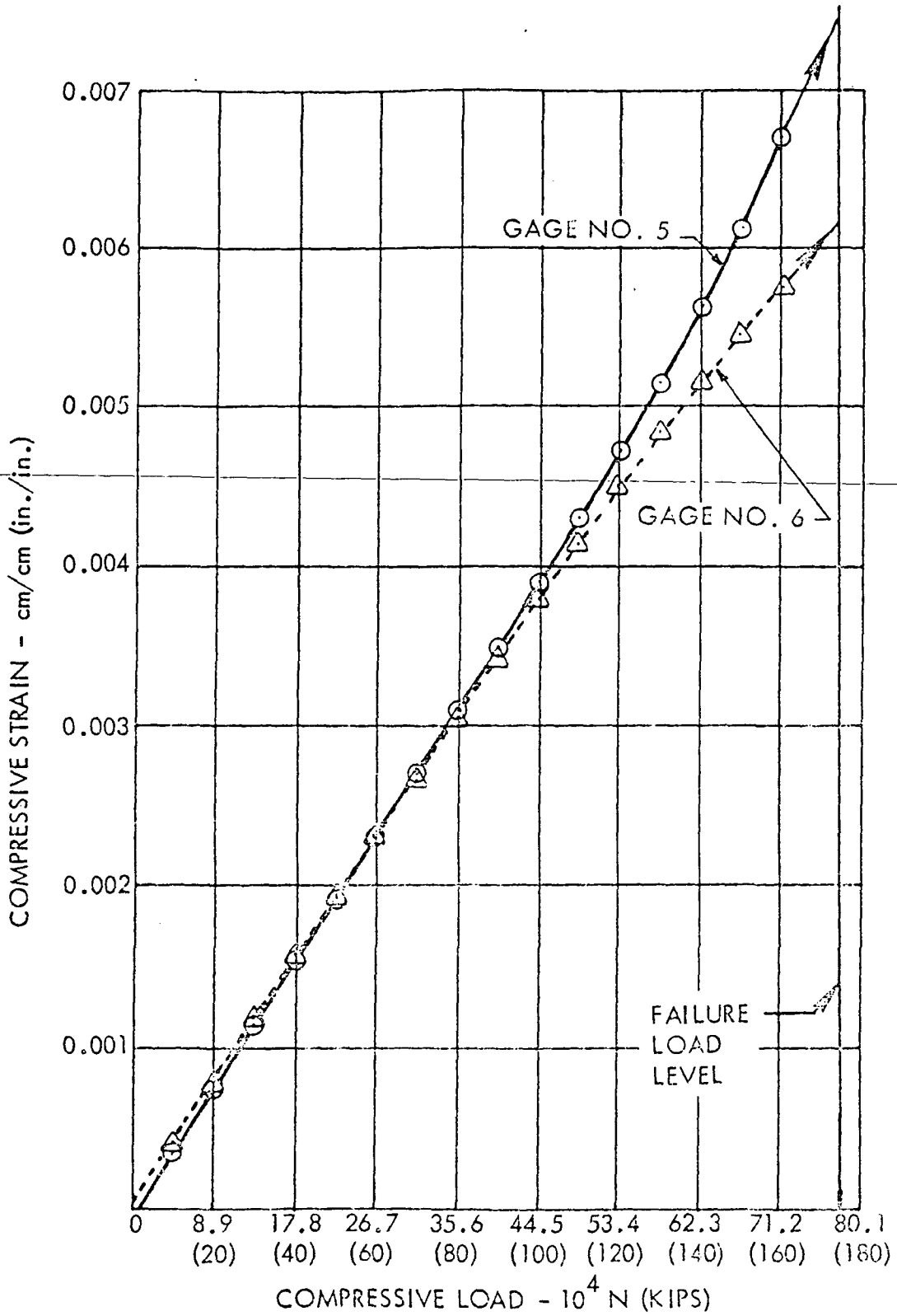

FIGURE 46. - COMPRESSIVE LOAD VERSUS STRAIN
PRELIMINARY CRIPPLING SPECIMEN - GAGES 5 AND 6

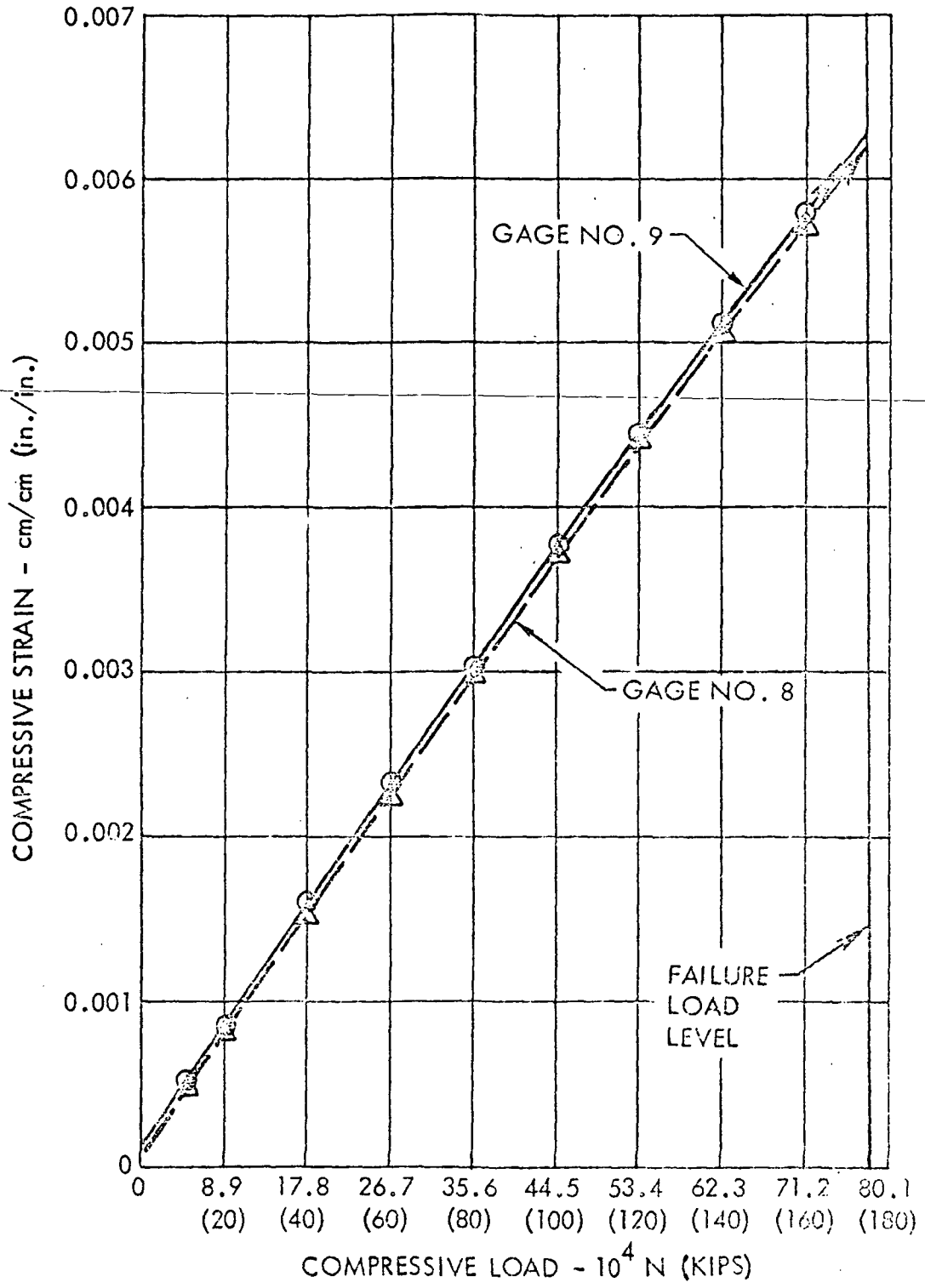

FIGURE 47. - COMPRESSIVE LOAD VERSUS STRAIN
PRELIMINARY CRIPPLING SPECIMEN - GAGES 8 AND 9

9.2 SHORT PANEL COMPRESSION TESTS

After the single-stringer compression test had shown load introduction end effects could be successfully minimized, three short panel compression tests were conducted to evaluate the improved load introduction and to provide better compressive strength data. These short panels were cut from part of an unused buckling panel, fabricated in Phase I but untested because of the load introduction problems. The short panels were representative of the upper wing surface between wing stations 20 and 61.

9.2.1 Description of Short Panels

Three short panel compression specimens (130-PB-3A-1A, 130-PB-3A-3A, and 130-PB-3A-5A) were obtained by cutting the remaining Phase I 130-PB-3 buckling panel. Figure 48 shows the general configuration of specimen 130-PB-3A-1A, while the configuration of specimen 130-PB-3A-3A and 130-PB-3A-5A is shown in Figure 49. The difference in configurations lies in the fastener system used where some steel fasteners were used in the -3A and -5A specimens and aluminum rivets were used in the center of the -1A specimen. Fastener systems are described in detail below.

9.2.2 Fabrication of Short Panels

Figure 50 illustrates the manner in which the specimens were cut from the remaining 130-PB-3 buckling specimen. The short specimens were each 0.457 m (18 in.) long and three stiffeners wide. The heavy titanium blocks in the laminate ends of the PB-3 panel were removed and discarded. The remaining portion of the component was then cut into 0.457 m (18.00 in.) lengths, which were essentially identical to each other except for some variation in fasteners. The 130-PB-3A-1A specimen had steel Hi-loks attaching the stiffeners to the skin near the ends, but retained aluminum rivets in the test section as shown in Figure 48. In the 130-PB-3A-3A and -5A specimens, which were identical, the aluminum rivets originally in the 130-PB-3 panel were replaced with steel Hi-loks as shown in Figure 49.

All specimen ends were cast in Magnabond using a method similar to that used for the preliminary crippling test specimen as reported in Section 9.1. Steel end frames were fabricated and were used as molds for the epoxy that encapsulated the ends of each specimen. After the epoxy had cured for 24 hours at room temperature, the ends were machined flat, parallel, and normal to the span. Final machining was carried out with a grinding wheel attached to the drive shaft of a Lucas horizontal boring mill. This process provided an end flatness within $\pm$ 0.0254 mm ($\pm$ 0.001 in.).

Each test specimen was instrumented with electrical resistance strain gages. Generally, Dentronics gages, Type 204C13, were used on aluminum surfaces, and B.L.H. gages, Type FAE-25-1256, were used on boron-epoxy laminate surfaces. All gages were of the axial type with their grids aligned in the spanwise direction. Since all the rivets had to be removed from the 130-PB-3A-3A and -5A specimens, it was convenient to remove

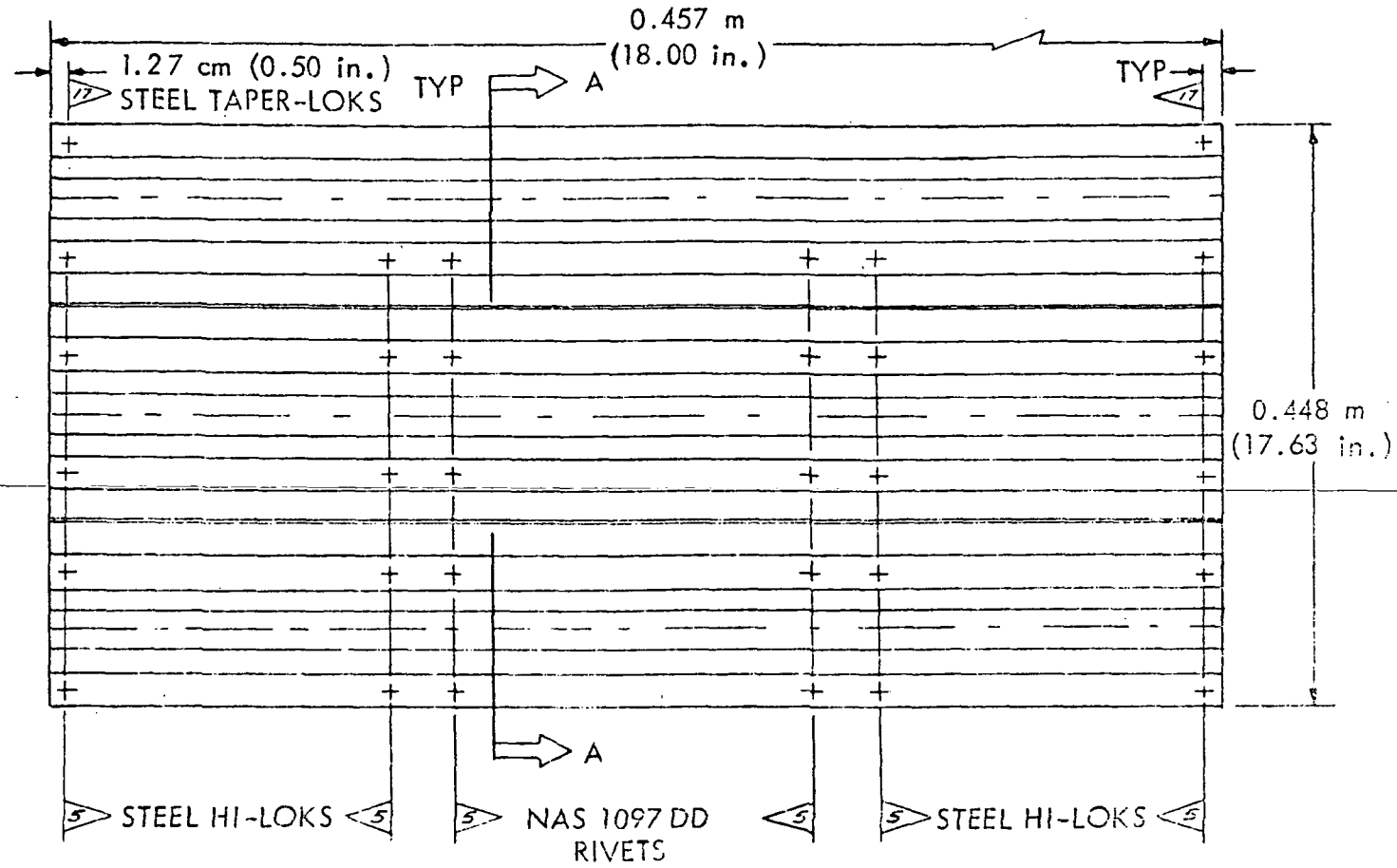

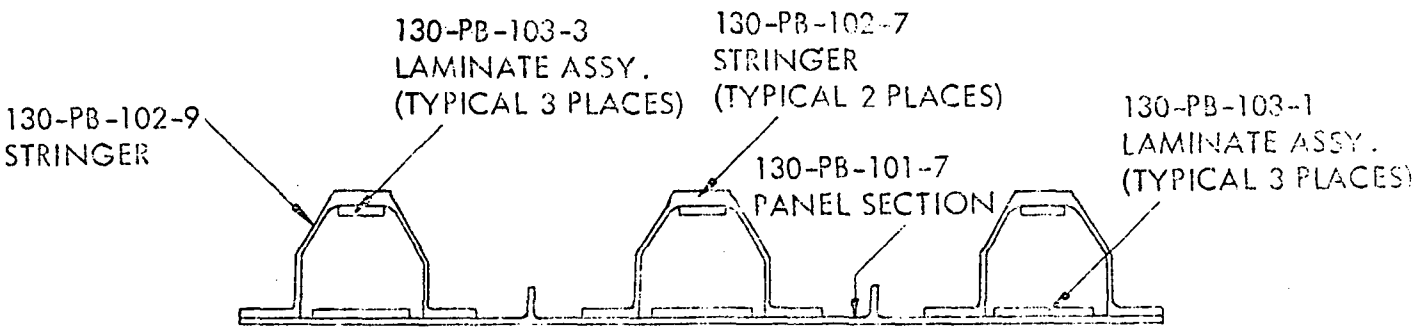

SECTION A-A

FIGURE 48. - GENERAL CONFIGURATION OF SPECIMEN 130-PB-3A-1A

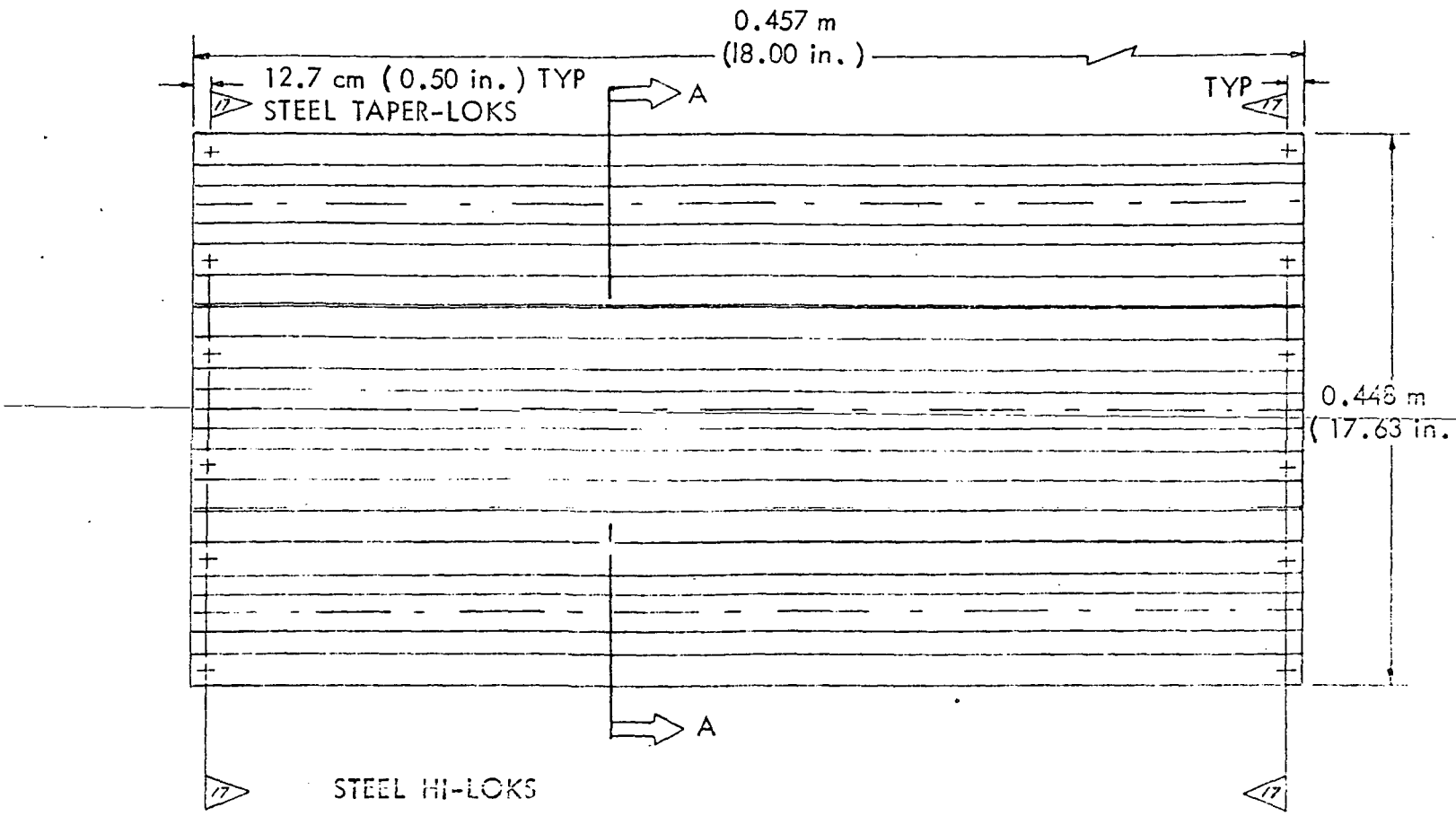

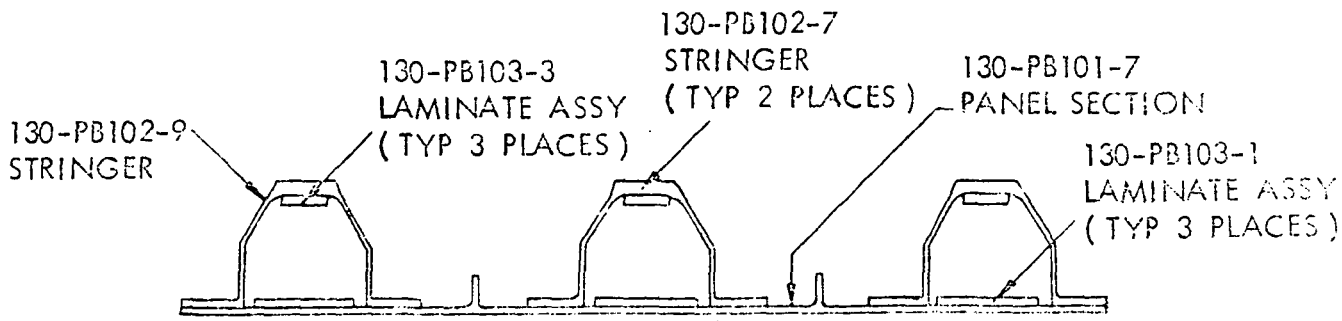

SECTION A-A

FIGURE 49. - GENERAL CONFIGURATION OF SPECIMENS 130-PB3A-3A AND 130-PB3A-5A

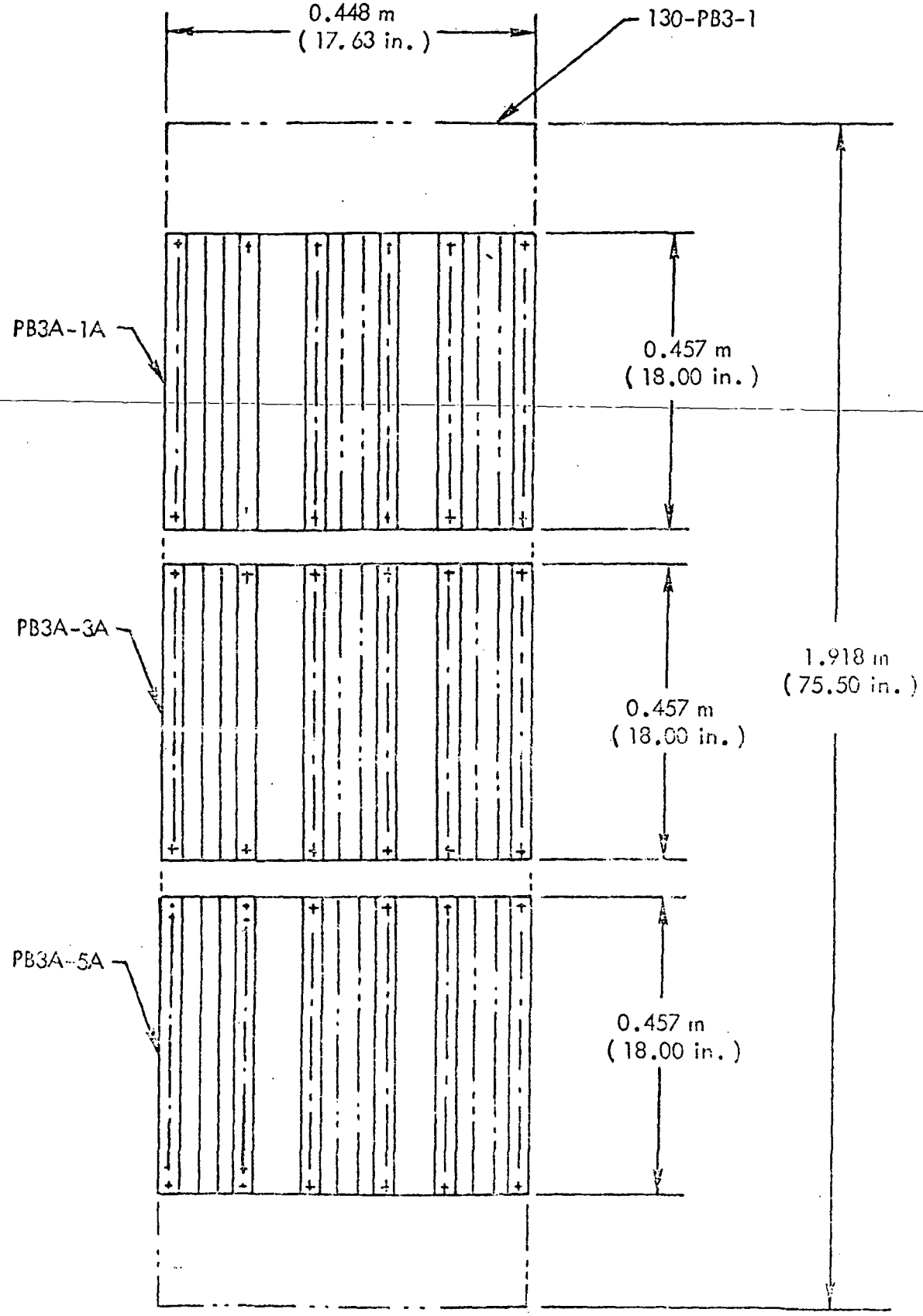

FIGURE 50. - 130-PB3-A BUCKLING SPECIMENS

C2

the stiffeners and install gages on the boron-epoxy laminates prior to reassembly. This was not so for the 130-PB-3A-1A specimen; therefore, the only gages that were located on the boron-epoxy laminates in that specimen were those that had been installed prior to assembly of the large 130-PB-3 panel. Strain-gage locations for the specimens are presented in Figure 51 and 52.

9.2.3 Short Panel Tests

All tests were conducted in a 5.34×10^6 N (1,200,000 lb.) capacity universal testing machine. The 2.67×10^6 N (600,000 lb.) load range was used, and the machine had an accuracy of 0.1 percent of load range or 0.5 percent of indicated load, whichever was greater. A typical test arrangement is shown in Figure 53 . Initially, a small compressive load was applied to the specimen, and strain measurements were recorded. A B&F digital strain data acquisition system was used for collecting all strain data.

Based on these strains, loading alignment was adjusted using the alignment mechanism which is an integral part of the testing machine compressive loading head. Strains were again measured and examined for uniformity. This process was repeated until acceptable uniformity in strain distribution was achieved. During this process, the load magnitude was limited to approximately 25 percent of the predicted failing load.

Specimen 130-PB-3A-1A was loaded in 2.22×10^5 N (50,000 lb.) increments up to 13.34×10^5 N (300,000 lb.), and each incremental load was held constant long enough to record strain data. The load was then reduced to 2.22×10^5 N (50,000 lb.) and strain data were again recorded. Load was subsequently increased to 13.34×10^5 N (300,000 lb.) and the strain data were compared with those obtained previously for the first application of this load level to check for permanent set. Loading was then continued in 2.22×10^5 N (50,000 lb.) increments until failure occurred at 26.69×10^5 N (600,000 lb.). A similar procedure was used for specimens 130-PB-3A-3A and 130-PB-3A-5A, except that the permanent set check was omitted, and the incremental loading was progressively applied to failure. Specimen 130-PB-3A-3A failed at 26.20×10^5 N (589,000 lb.) and 130-PB-3A-5A failed at 25.53×10^5 N (574,000 lb.).

9.2.4 Evaluation of Short Panel Tests

Failure loads of 26.69×10^5 N (600,000 lb.), 26.20×10^5 N (589,000 lb.), and 25.53×10^5 N (574,000 lb.) for specimens 130-PB-3A-1A, -3A, and -5A, respectively, exceeded the predicted failure load of 25.0×10^5 N (562,000 lb.) for all three specimens and provided a comfortable margin of safety. All panel failures occurred in the test section with no evidence of end effects. In these specimens, no noticeable differences could be attributed to the difference in fastener systems. All specimens failed within a narrow scatter band and all tests resulted in good crippling failure modes as typified by the failure mode shown in Figure 54.

Typical test load-strain data are shown in Figures 55, 56, 57, and 58. Data from the strain gages showed that boron-epoxy laminates of all three test specimens sustained strains prior to specimen failure comparable with strains obtainable from compression sandwich beam tests.

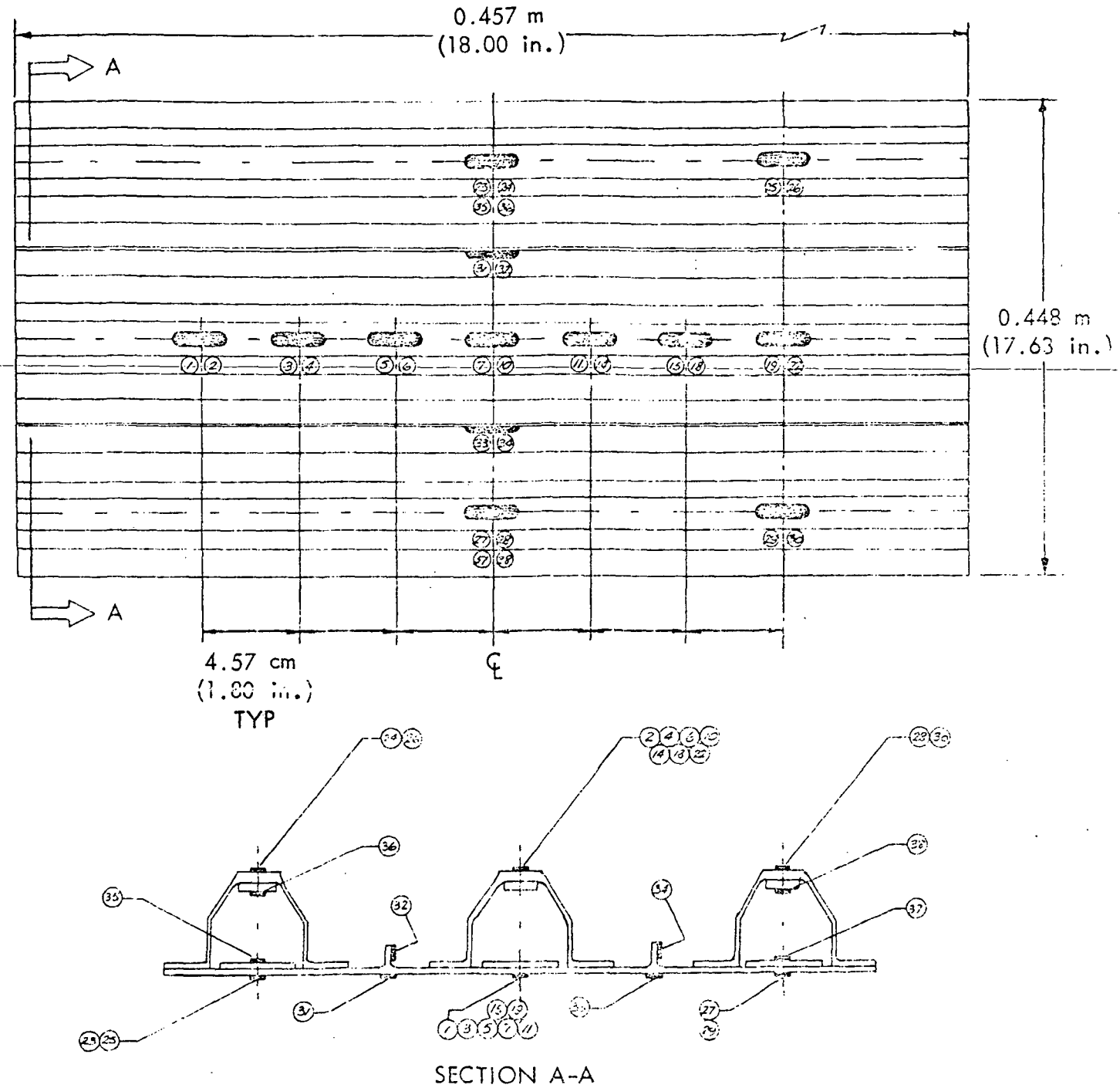

FIGURE 51. - STRAIN GAGE LOCATIONS FOR SPECIMEN 130-PB-3A-1A

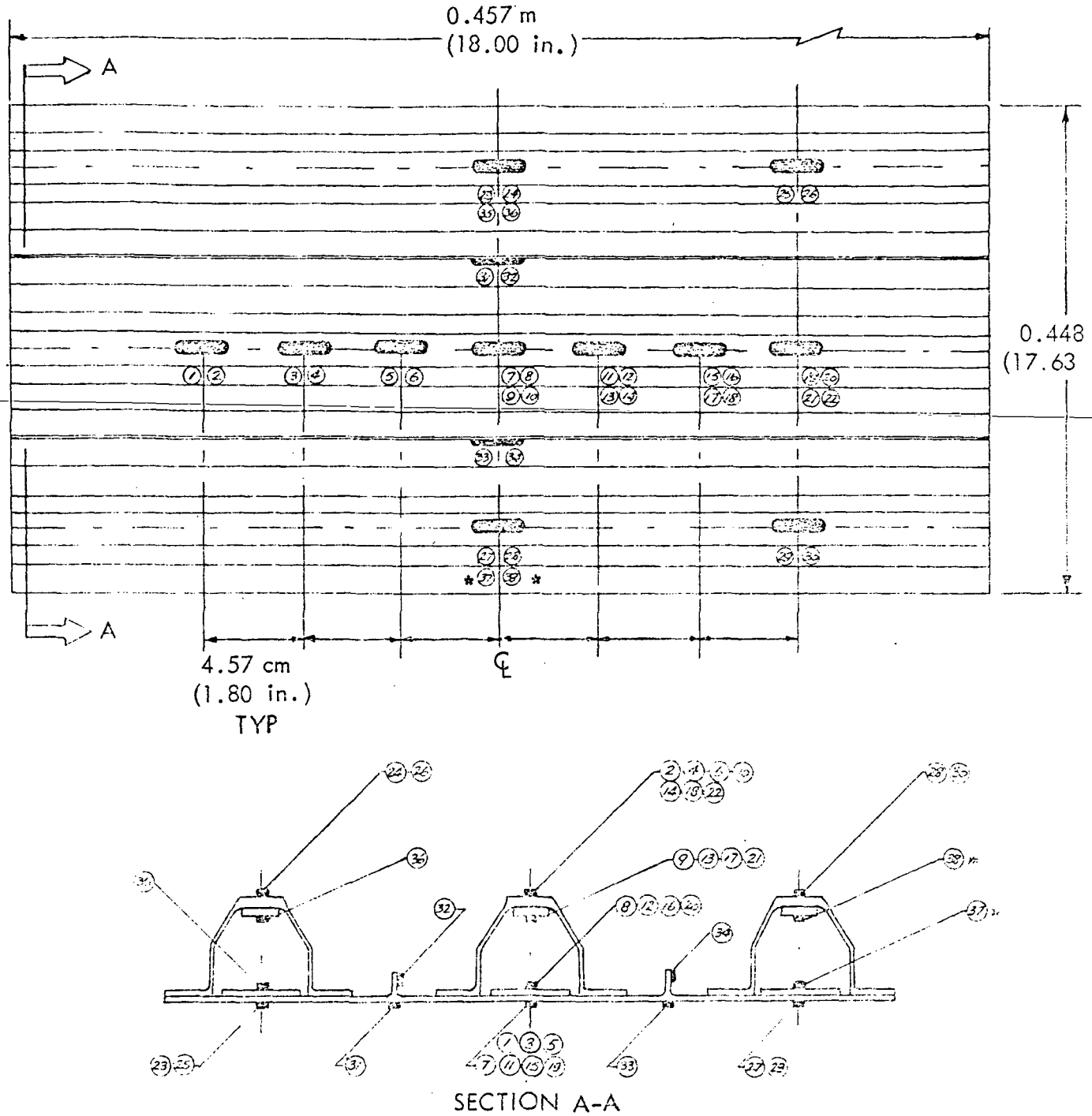

*ON SPECIMEN 130-PB-3A-5A THESE GAGES WERE LOCATED ADJACENT TO GAGES 29 AND 30

FIGURE 52. - STRAIN GAGE LOCATIONS FOR SPECIMENS 130-PB-3A-3A AND 130-PB-3A-5A

FIGURE 53. - TYPICAL TEST ARRANGEMENT FOR SHORT PANEL COMPRESSION TESTS

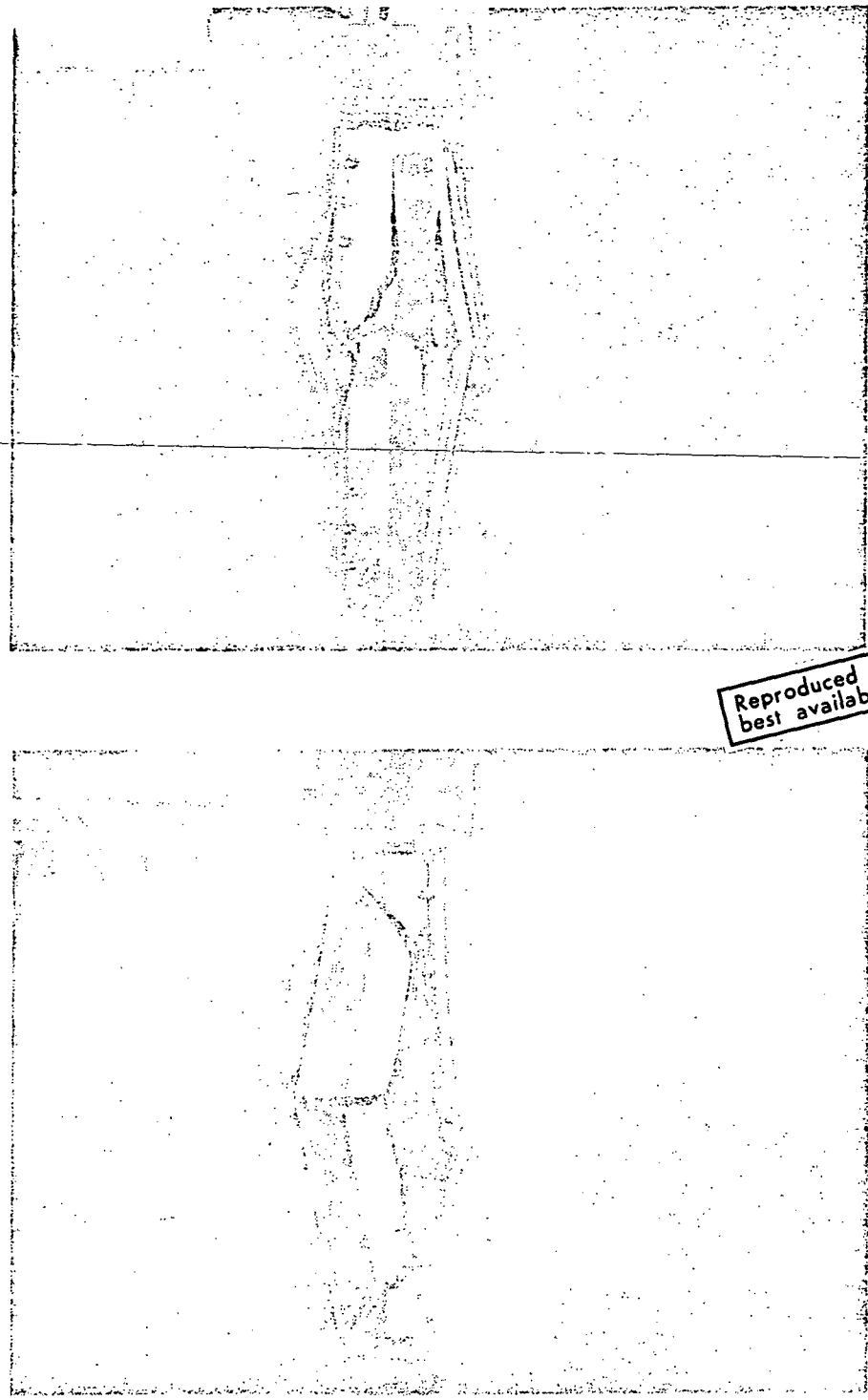

FIGURE 54. - TYPICAL FAILURE MODE FOR SHORT PANEL COMPRESSION TESTS

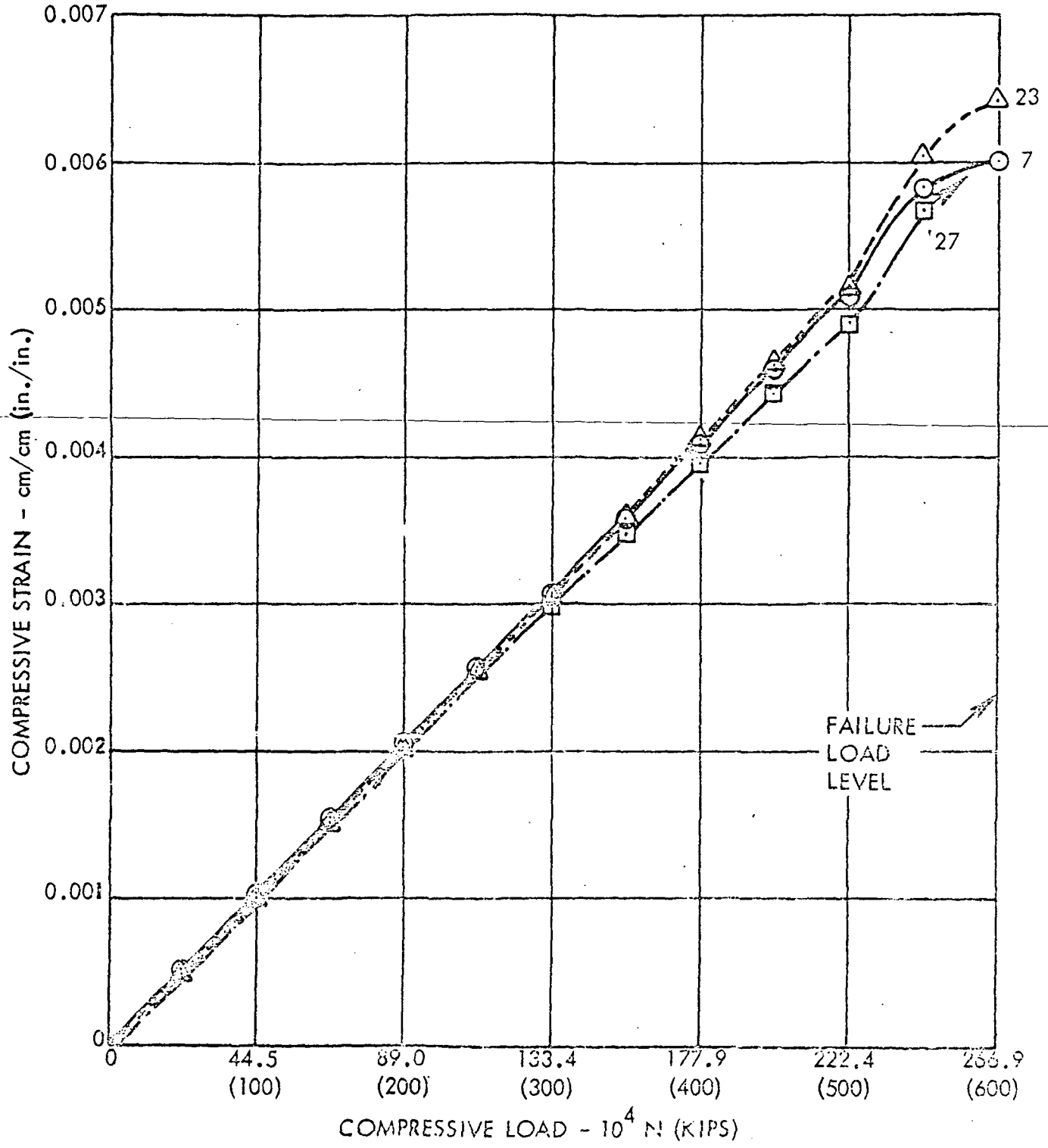

FIGURE 55. -COMPRESSIVE LOAD VERSUS STRAIN
SHORT PANEL COMPRESSION SPECIMEN 130-PB-3A-1A
GAGES NO. 7, 23, AND 27

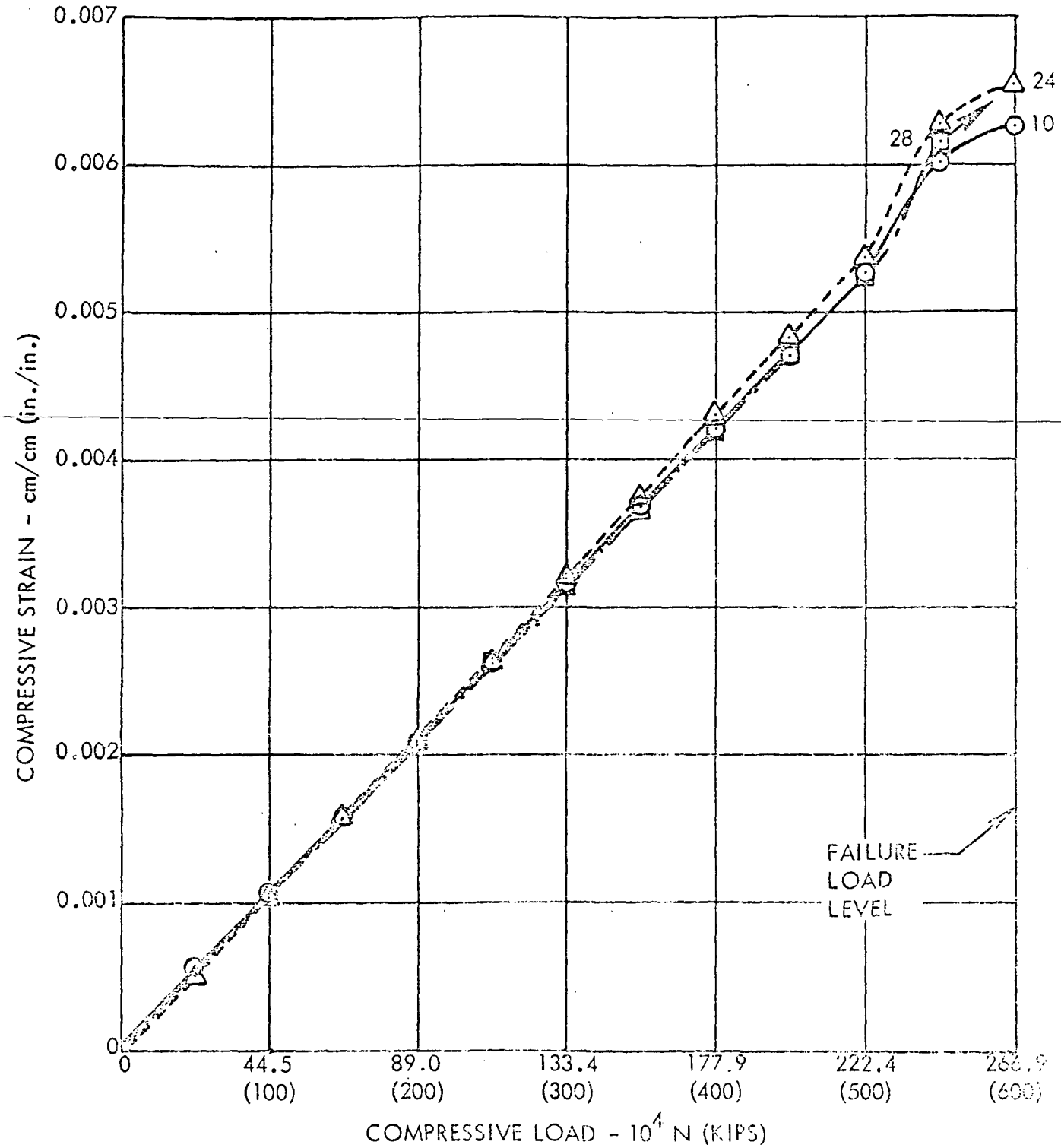

FIGURE 56. - COMPRESSIVE LOAD VERSUS STRAIN
SHORT PANEL COMPRESSION SPECIMEN 130-PB-3A-1A
GAGES NO. 10, 24, AND 28

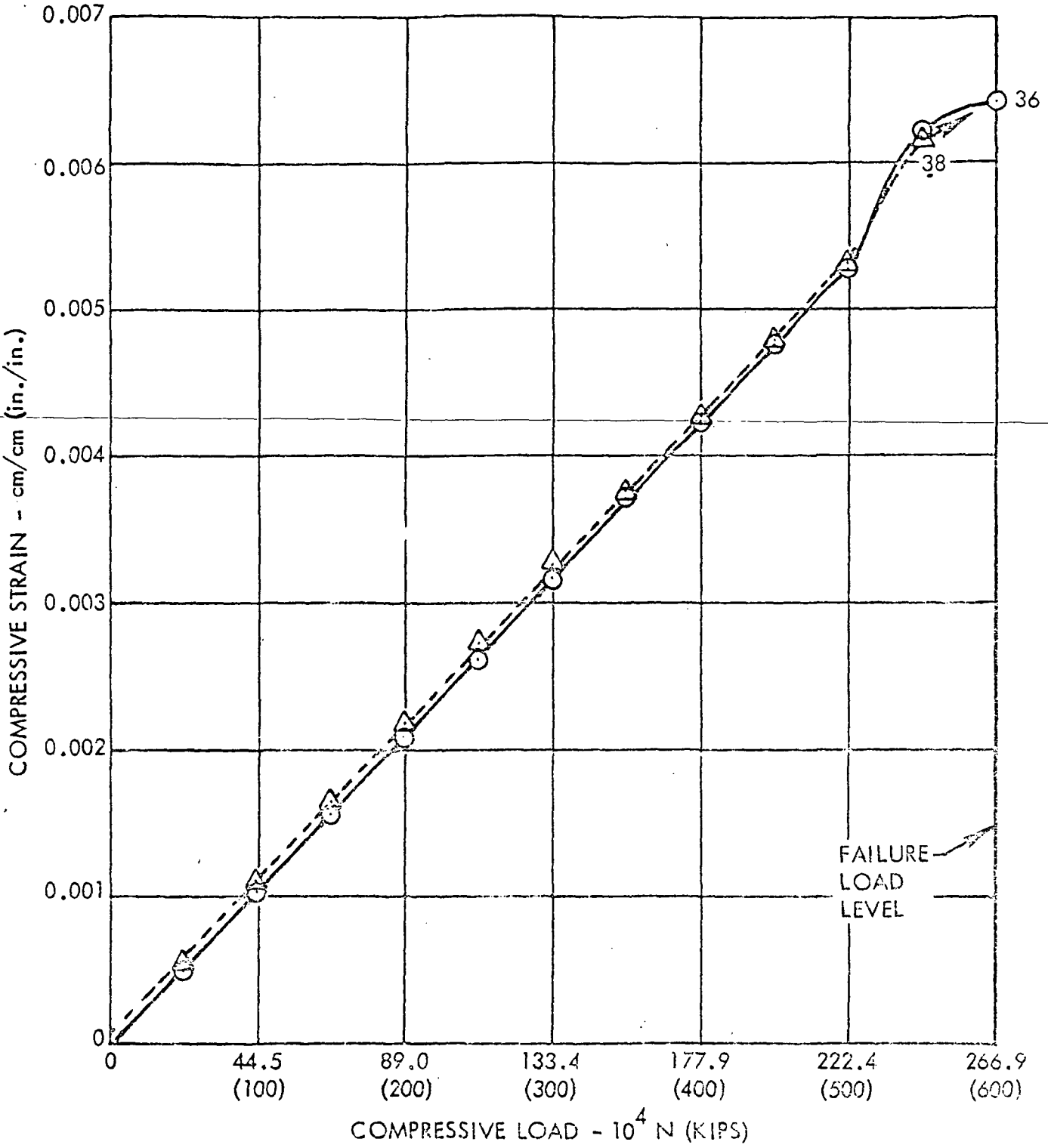

FIGURE 57. - COMPRESSIVE LOAD VERSUS STRAIN
SHORT PANEL COMPRESSION SPECIMEN 130-PB-3A-1A
GAGES NO. 36 AND 38

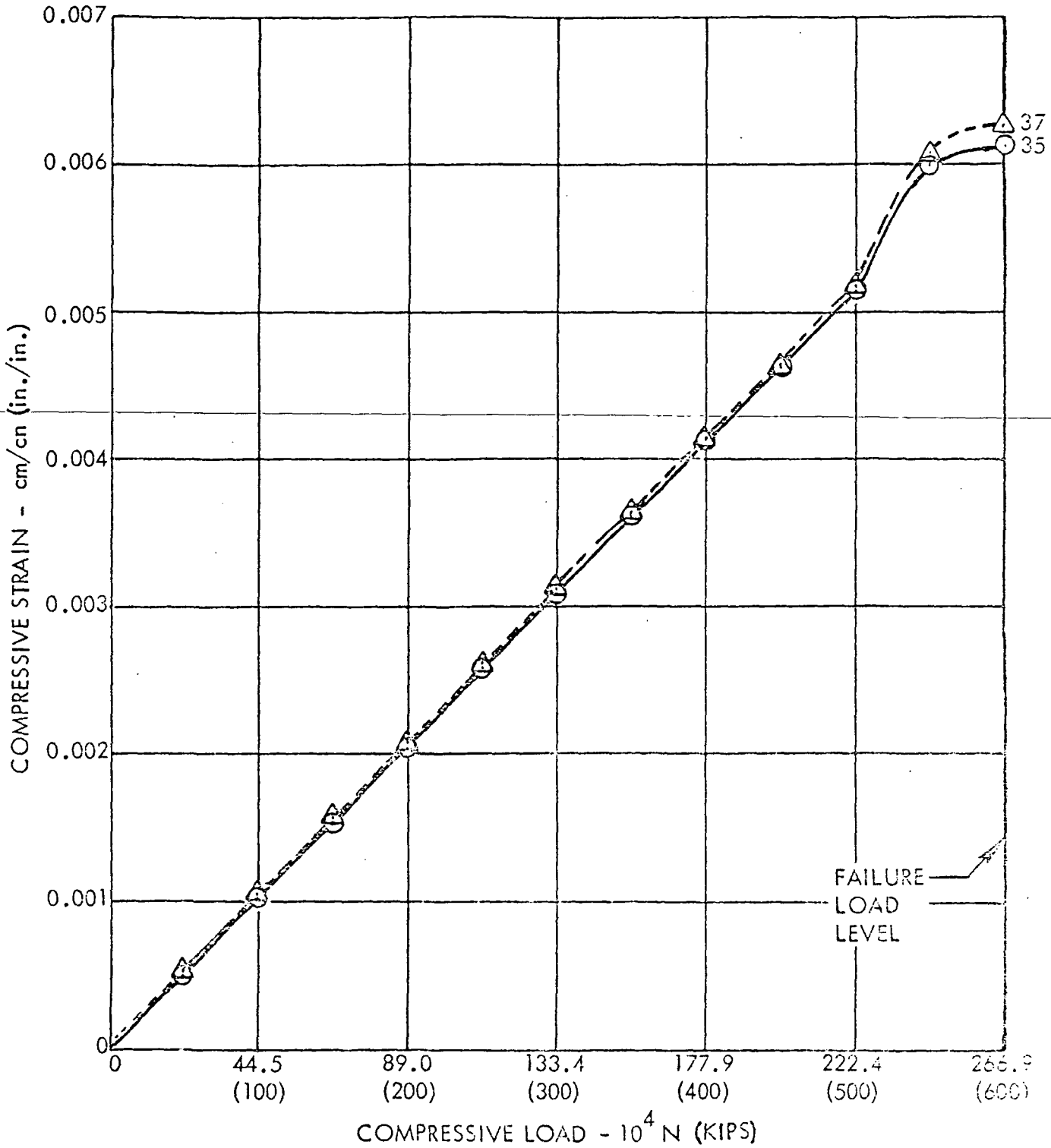

FIGURE 58. - COMPRESSIVE LOAD VERSUS STRAIN
SHORT PANEL COMPRESSION SPECIMEN 130-PB-3A-1A
GAGES NO. 35 AND 37

9.3 FULL PANEL BUCKLING TESTS

Following successful completion of the preliminary crippling tests (Section 9.1) and the short panel compression tests (Section 9.2), two buckling specimens were fabricated which were similar in configuration to Phase I specimen 130-PB-1. Both specimens were comprised of wing skin panels having hat shaped stiffeners, and the skins and stiffeners had adhesive bonded strips of unidirectional boron-epoxy laminates. The two large buckling test specimens were fabricated and successfully tested with no evidence of end condition influence on the test results.

9.3.1 Description of Buckling Panels

The specimens, 130-PB4-1 and 130-PB4-3, were nominally configured to the design of the single-plank upper surface specimen 130-PB-1 with three hat stiffeners. The nominal length and width of the specimens were 1.905 m (75 in.) and 0.457 m (18 in.),respectively. General configuration of the two specimens is shown in Figure 59. Both specimens were identical in configuration except for the crown thickness of the aluminum alloy stringers. For specimen 130-PB4-1 the crown thickness was 7.620 mm (0.300 in.) and the thickness was 4.572 mm (0.180 in.) for specimen 130-PB4-3.

9.3.2 Fabrication of Buckling Panels

All aluminum alloy parts were machined and passed required Quality Assurance inspections, including penetrant inspection. The two specimens were fabricated with the cool tool technique. Previous tests had shown that the warpage might be decreased by additionally heating the boron-epoxy laminate to assure full expansion at the bonding temperature. This method was used. The boron-epoxy strips were maintained at a temperature approximately 260.9° K (10°F) above that of the aluminum. The resulting skin warpage was less than 0.00267 mm/mm (in./in.) throughout the length of the constant section skins. The hat sections, however, had a very slight reverse bow. Both finished specimens were flat and well within the C-130 center wing box tolerance requirements. The specimens passed all inspections items and were documented on standard shop orders.

The skins had two integral stiffeners and were machined from standard 7075-T7351 aluminum alloy extrusion. Stringers for both specimens were hat-shaped and were machined from 7075-T651 aluminum alloy extrusions. The hat-section reinforcing laminates were 2.29 cm (0.9 in.) wide and contained 46 plies of unidirectional boron-epoxy oriented in the 1.905 m (75 in.) length direction. The skin assembly for each specimen was comprised of three laminates bonded to a 130-PB4-5 skin. These skin reinforcing laminates were 5.08 cm (2.0 in.) wide and contained 46 plies. The stringer assemblies were attached to the skin assemblies with alloy steel Taper-lok fasteners, TL100. One of the finished specimens is shown in Figure 60. Magnabond was cast on the specimen ends, and final machining performed in the manner previously described for the short panel compression tests (Section 9.2). Figure 61 shows a specimen end after casting in Magnabond.

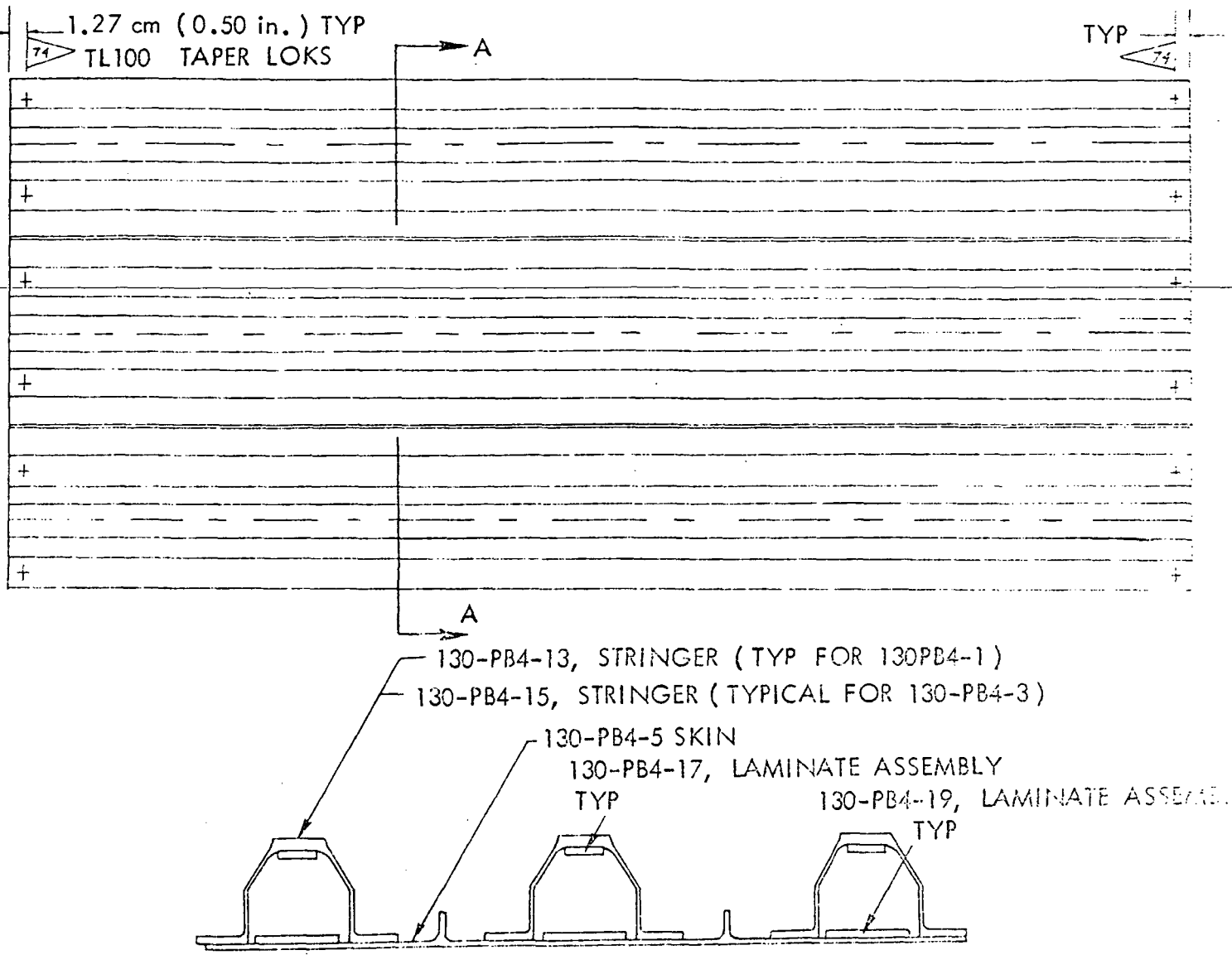

SECTION A-A

FIGURE 59. - GENERAL CONFIGURATION OF SPECIMENS
130-PB4-1 AND 130-PB4-3

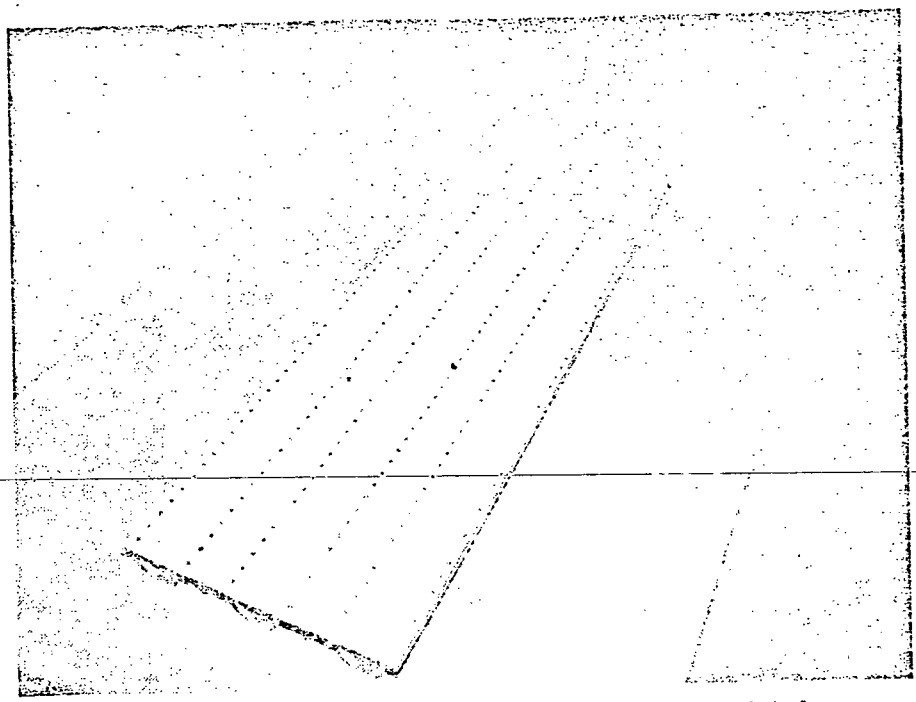

FIGURE 60. - BUCKLING SPECIMEN 130-PB4-1 AFTER ASSEMBLY (SKIN SIDE)

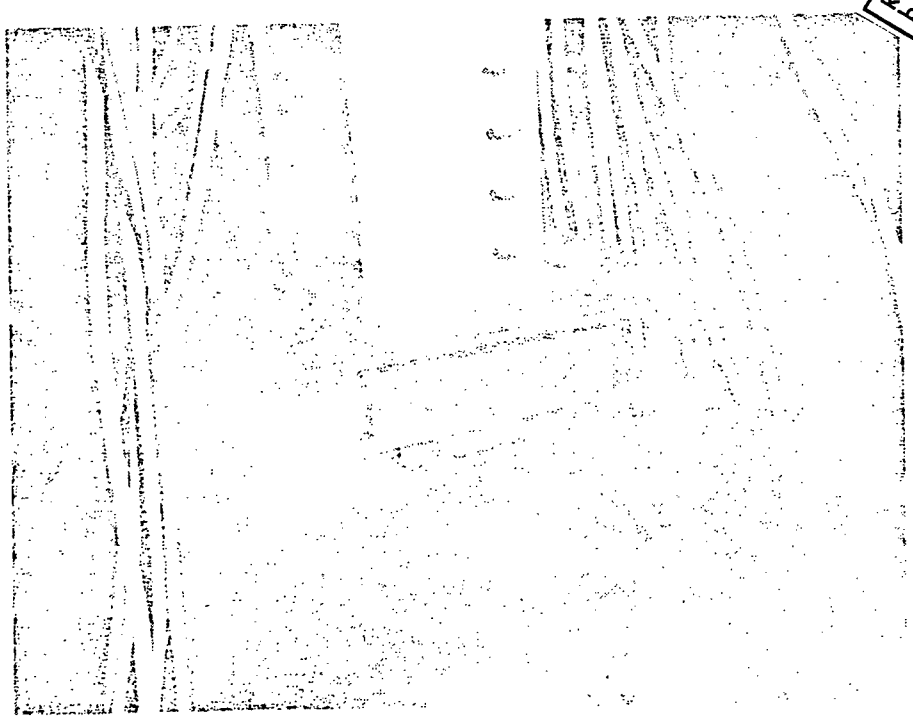

FIGURE 61. - SPECIMEN END CAST IN MAGNABOND

After assembly and final machining, measured dimensions of 130PB4-1 were 1.908 m (75.1 in.) long by 0.451 m (17.75 in.) wide. The assembled panel was determined to be flat within + 0.25 mm (+ 0.010 in.). For 130PB4-3, measured length and width were 1.905 m (75.0 in.) and 0.452 m (17.80 in.), respectively. This specimen deviated from flatness by 1.27 mm (0.050 in.) in both the spanwise and chordwise directions. The flatness deviation produced a concavity in the skin, which was accounted for in comparative analyses.

Each of the two specimens was instrumented with electrical resistance-type strain gages at locations where strain data were desired to guide specimen alignment prior to test as well as to monitor specimen strain state during testing. Gages were located on the aluminum alloy elements as well as on the boron-epoxy laminates. Gages on the laminate surfaces were installed prior to completing the specimen assembly. Lead wires were attached to the gages and were routed spanwise so that all leads extended from the same end of each specimen. During final assembly of the specimen, a 4.57 mm (3/16-in.) diameter hole was drilled in one vertical leg of each stringer and the lead wires were threaded through these holes to the outside. The holes were drilled 11.43 cm (4.5 in.) from the specimen ends and approximately on the centroid of the skin-stringer element. Gages were applied to the metal elements on the outside surfaces of the specimens. Baldwin Type FAE-25-1256 gages were applied to the boron-epoxy surfaces, and Dentronics Type 204C13 gages were applied to the aluminum surfaces. All gages were of the axial type and were aligned parallel to the spanwise direction. Specimen 130PB4-1 had 48 gages. Thirty-eight gages were installed on specimen 130PB4-3. Gage locations are shown in Figures 62 and 63.

During manufacture of the Phase I panel buckling specimens, pieces of the skin and stringer extrusions used were collected to determine tensile and compressive properties of the specimen materials. The same piece of extrusion was used for the 130PB4-1 and 130PB4-3 skins, consequently, mechanical properties of the skins were common to these two specimens. The hat-shaped stiffeners were procured especially for this program and all extrusions of a given type were from the same production batch. Consequently, mechanical properties were determined from one piece of material for each different type stiffener. Since the same basic extrusion was used for the stringers of both specimens, mechanical properties of these were also common to both specimens. All property data for the skin and stringer extrusions were within the allowable specification tolerances.

9.3.3 Buckling Panel Tests

The specimens were tested in the compression bay of a 53.38×10^5 N (1,200,000 lb.) capacity Baldwin Universal Testing Machine. A beam with ground faces was centered on the testing machine platen, and a specimen was placed on the beam. A ground plate was sandwiched between the other end of the specimen and the machine cross-head. Dial indicators, attached to an external frame, were used to measure lateral deflections at several spanwise and chordwise positions on the specimens. Figure 64 shows the dial indicator positions for the specimens. Dial indicators used had a sensitivity of 0.025 mm (0.001 in.). Strain-gage leads were connected to a B&F Model SY 156 data acquisition system with 200-channel capacity and digital output at a maximum print rate of 20 channels per

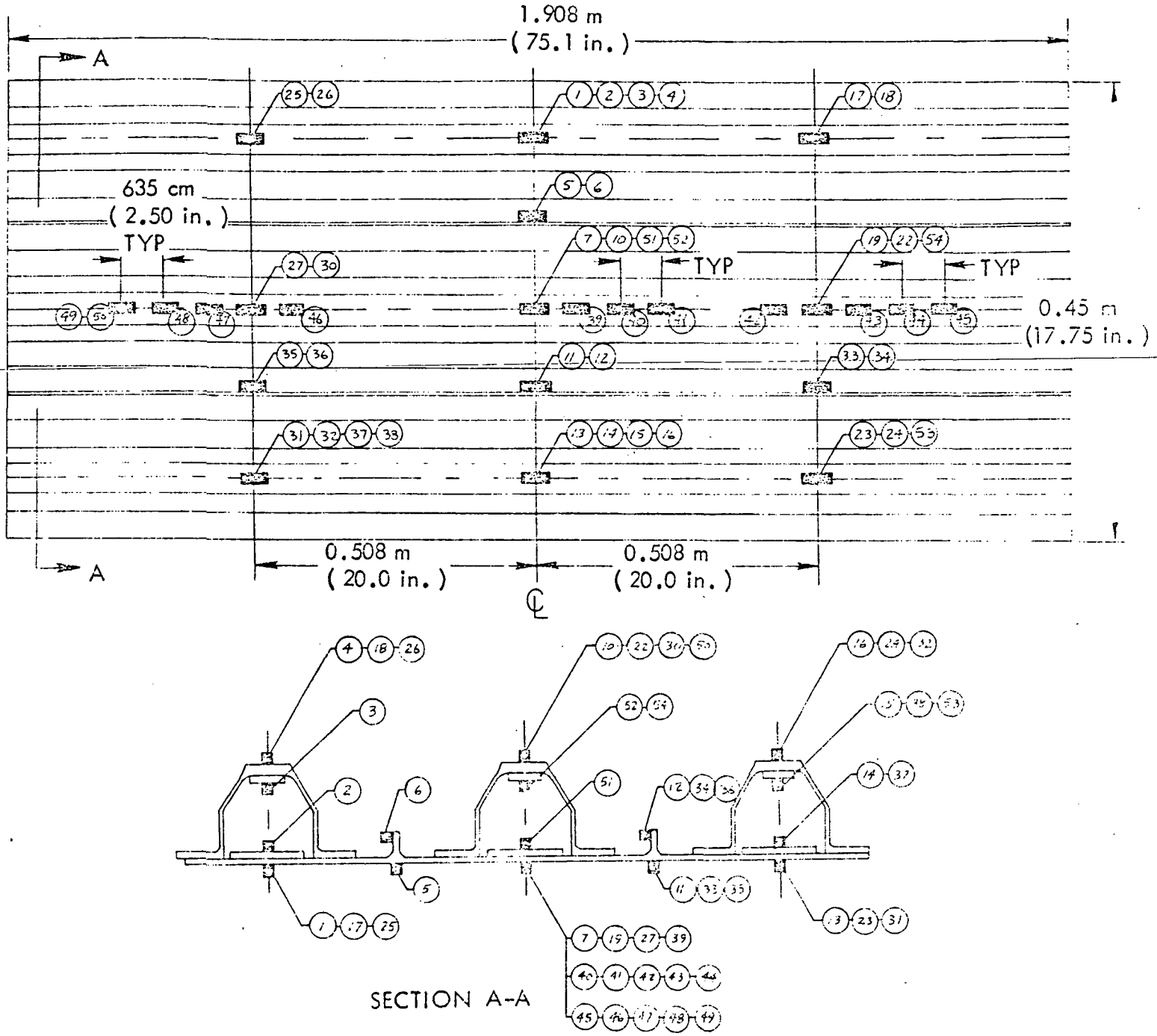

FIGURE 62. - STRAIN GAGE LOCATIONS FOR SPECIMEN SPECIMEN 130-PB4-1

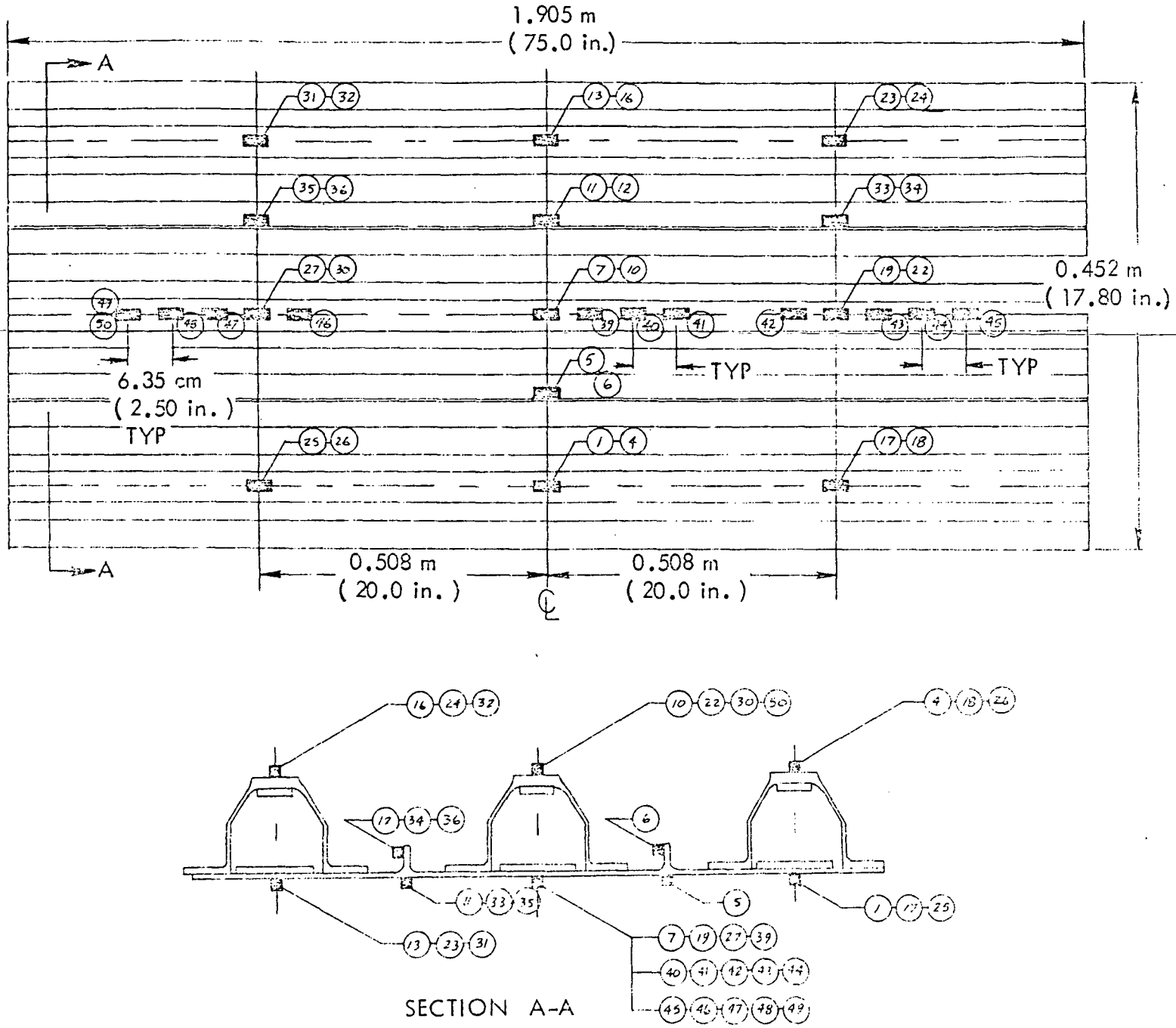

FIGURE 63. – STRAIN GAGE LOCATIONS FOR SPECIMEN 130-PB4-3

second. The test arrangement for both buckling specimens is illustrated by Figure 65. After the specimen was arranged in the testing machine a small compressive load was applied and strain measurements were recorded. Based on these strains, the loading alignment was adjusted and strains were again measured and examined for uniformity. This process was repeated until acceptable uniformity in strain distribution was achieved. During alignment, load magnitudes were limited to 20 percent of the expected buckling load for the specimen.

The 26.69×10^5 N (600,000 lb.) load range was used for testing both specimens. Load was applied to the specimens in 2.22×10^5 N (50,000 lb.) increments up to 13.34×10^5 N (300,000 lb.) for 130PB4-1 and up to 11.12×10^5 N (250,000 lb.) for 130PB4-3. Load was held at each increment long enough to record strain and deflection data. The load was then reduced to 2.22×10^5 N (50,000 lb.) at which strain and deflection data were again recorded. At this time the dial indicator support frame was moved away from the specimen to prevent damage upon specimen failure. Load was then increased to the previous maximum load and strains were again recorded. The load was then increased in 2.22×10^5 N (50,000 lb.) increments to failure and strains were recorded at each increment.

9.3.4 Evaluation of Buckling Tests

Failure of 130PB4-1 occurred while stabilizing load at 22.24×10^5 N (500,000 lb.) as compared to a calculated load of 22.15×10^5 N (498,000 lb.). The panel exhibited a permanent set as shown in Figure 66, but there was no evidence of local buckling for the aluminum alloy parts. One stringer was then removed to allow inspection of the boron-epoxy laminates. The laminate bonded to the skin had sustained little damage; however, the stringer laminate had a chordwise fracture at mid-span. It was also failed over the entire span by failure of the matrix between the scrim and first ply of boron on the adhesive bonded side. Typical strain and deflection data for specimen 130PB4-1 are presented in Figures 67, 68, 69, 70, and 71. These data show excellent strain/load linearity beyond two thirds of the failure load and uniform load distribution within the specimen. Dial gages show that lateral deflections were minimal and did not significantly affect the test results.

Specimen 130PB4-3 failed at a load of 19.82×10^5 N (445,500 lb.) compared to a predicted value of 17.79×10^5 N (400,000 lb.). Unlike 130PB4-1, the specimen failed by local instability of the aluminum alloy parts as well as exhibiting boron-epoxy failures. However, damage to the stringer laminate was minimal while the skin laminate exhibited fractures, spanwise splitting, and failures of the matrix between the scrim and first ply of boron on the adhesive bonded side. Figure 72 shows the failed specimen. Typical strain and deflection data for specimen 130PB4-3 are presented in Figures 73, 74, 75, and 76. These data show excellent strain/load linearity beyond two-thirds of the failure load and uniform load distribution within the specimen. Dial gages show that the lateral deflections were minimal and did not significantly affect the test results.

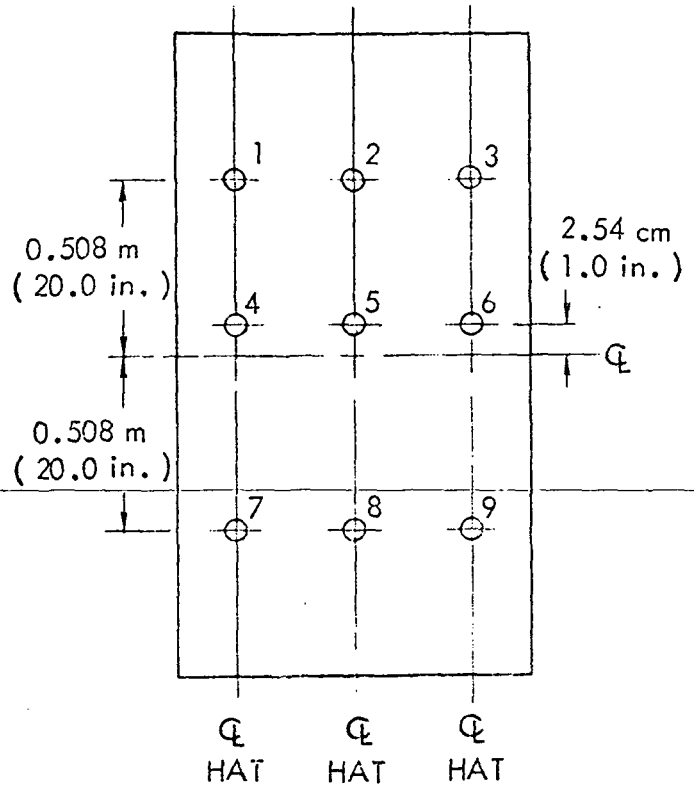

FIGURE 64. - DIAL INDICATOR LOCATIONS FOR SPECIMENS 130-PB4-1 AND 130-PB4-3

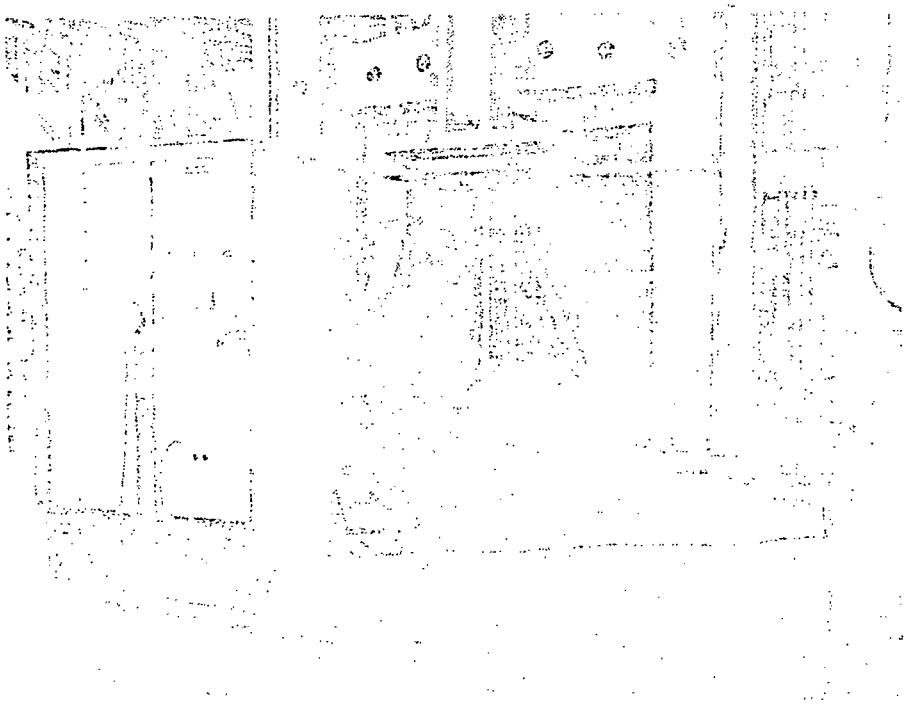

FIGURE 65. - GENERAL TEST ARRANGEMENT FOR SPECIMENS 130-PB4-1 AND 130-PB4-3

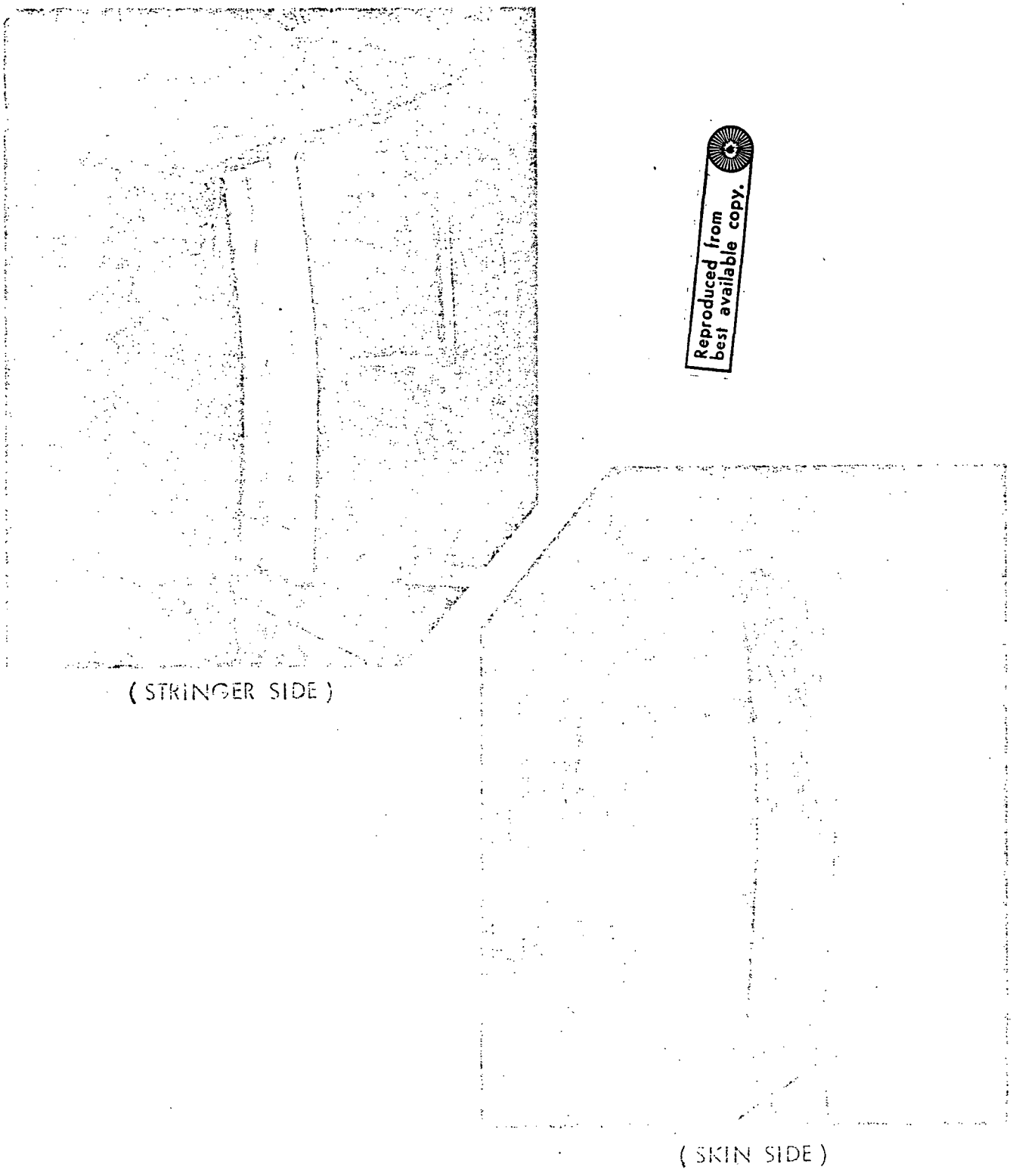

FIGURE 66. - SPECIMEN 130PB4-1 AFTER TEST

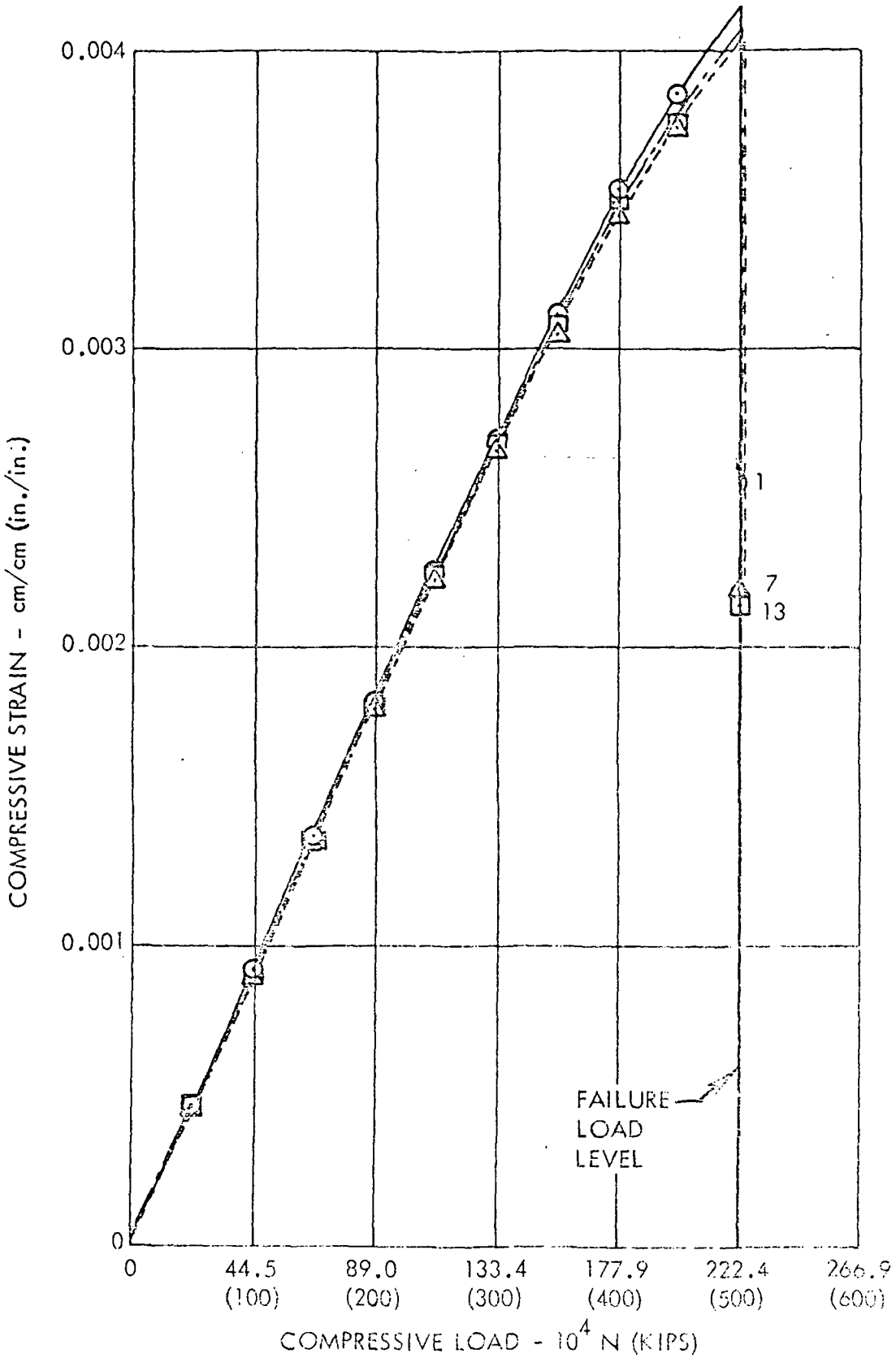

FIGURE 67. - COMPRESSIVE LOAD VERSUS STRAIN
PANEL BUCKLING SPECIMEN 130PB4-1
STRAIN GAGES NO. 1, 7, AND 13

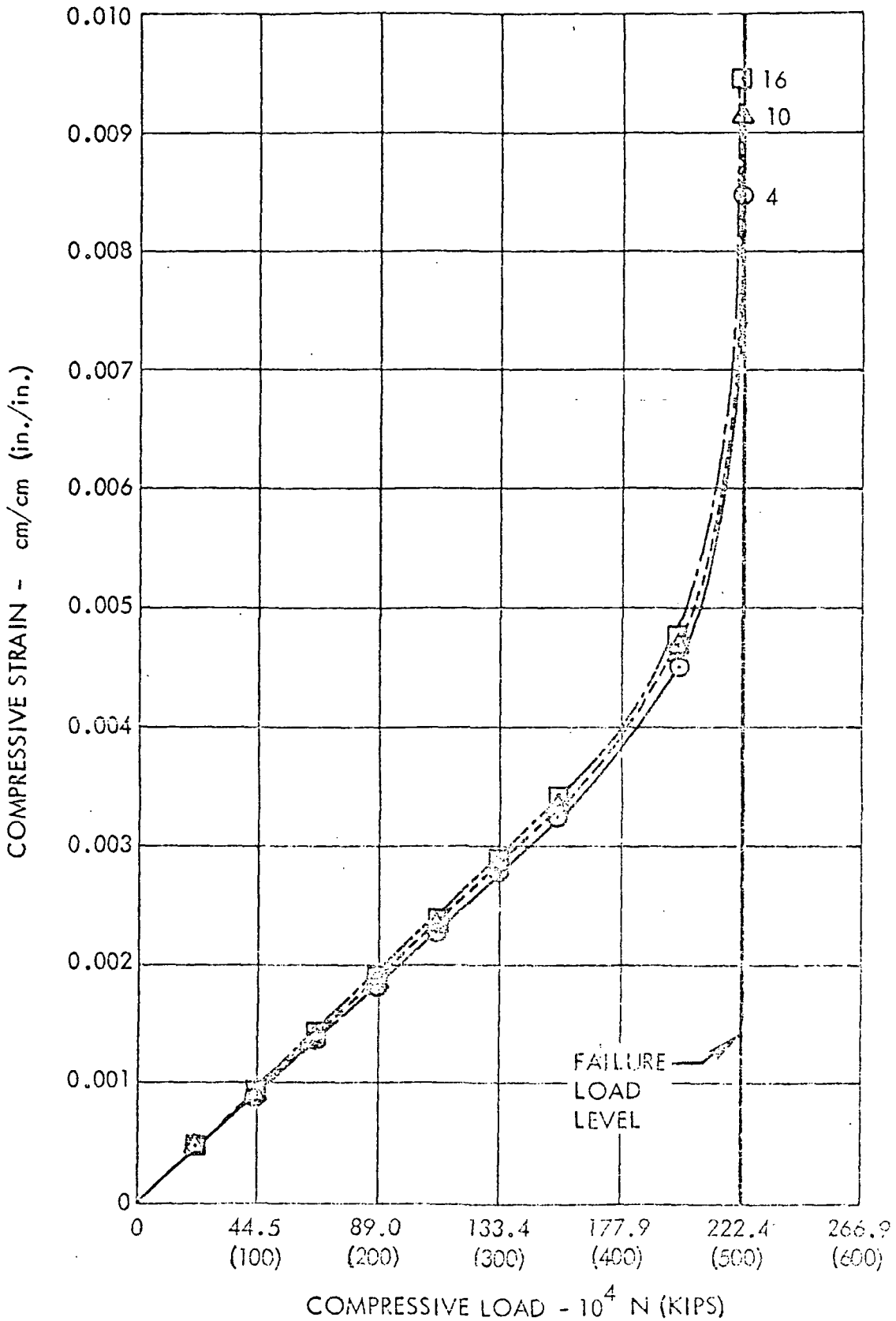

FIGURE 68. - COMPRESSIVE LOAD VERSUS STRAIN
PANEL BUCKLING SPECIMEN 130PB4-1
STRAIN GAGES NO. 4, 10, AND 16

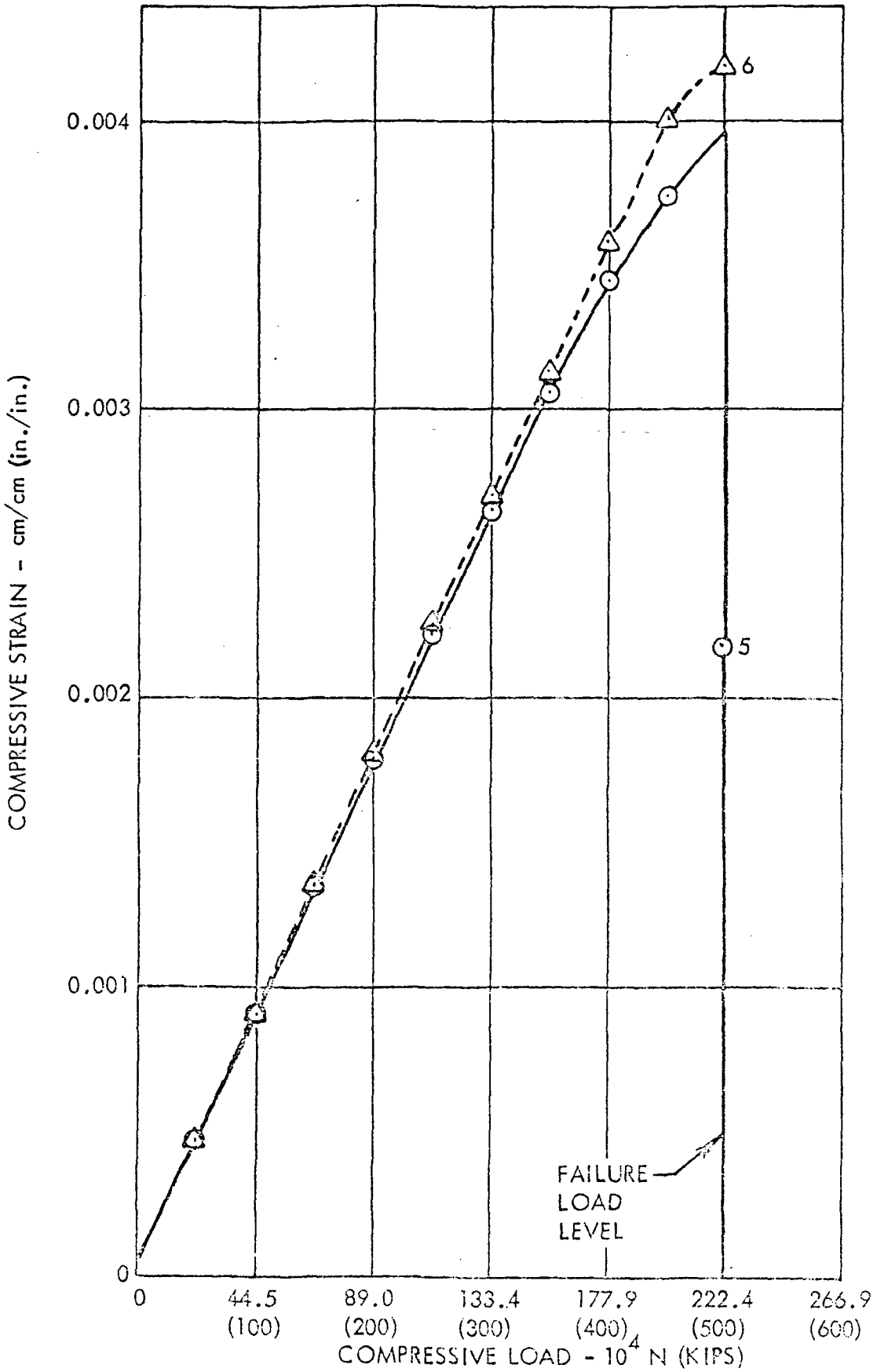

FIGURE 69. - COMPRESSIVE LOAD VERSUS STRAIN
PANEL BUCKLING SPECIMEN 130PB4-1
STRAIN GAGES NO. 5 AND 6

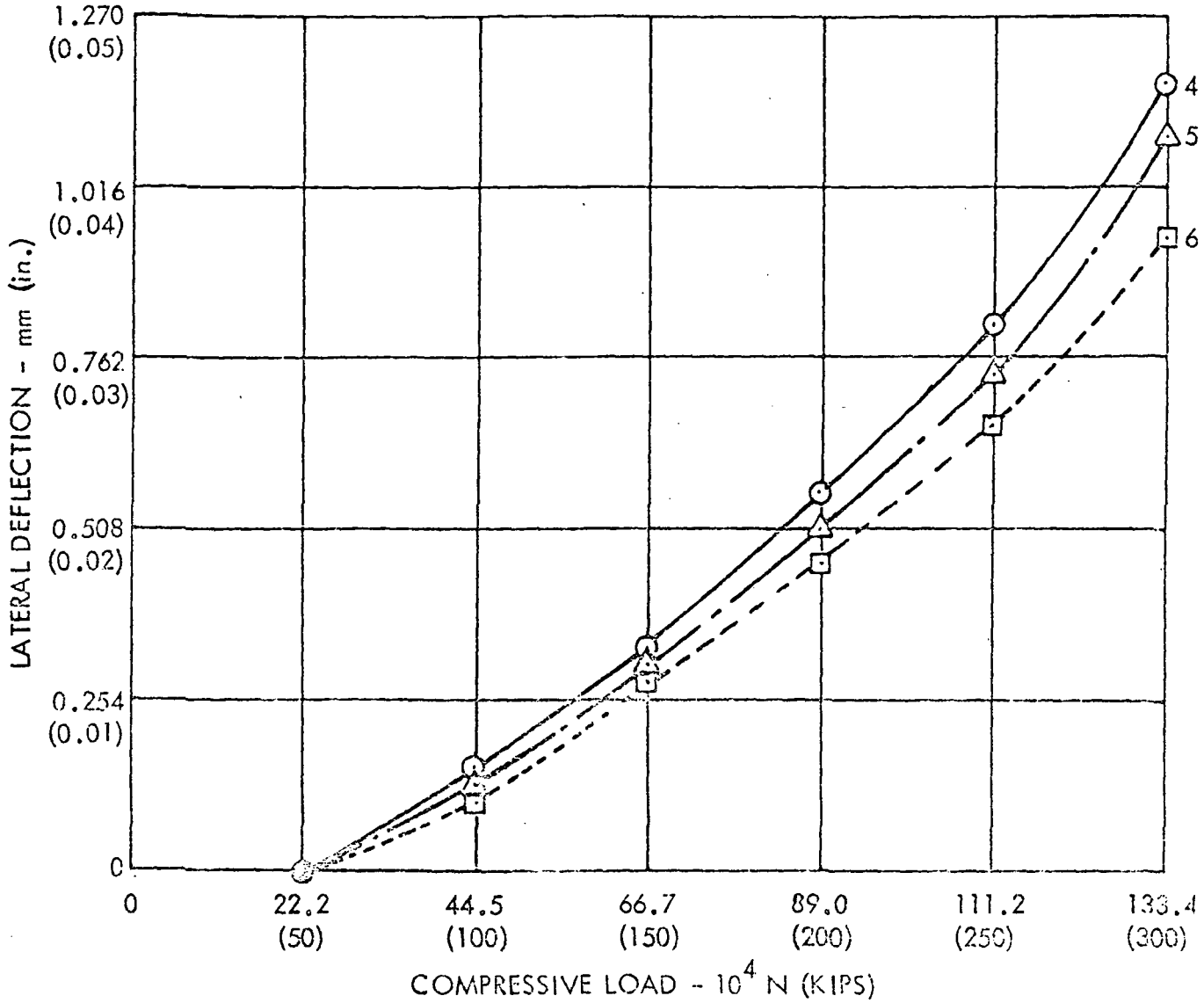

FIGURE 70. - COMPRESSIVE LOAD VERSUS LATERAL DEFLECTION
PANEL BUCKLING SPECIMEN 130PB4-1
DIAL GAGES NO. 4, 5, AND 6

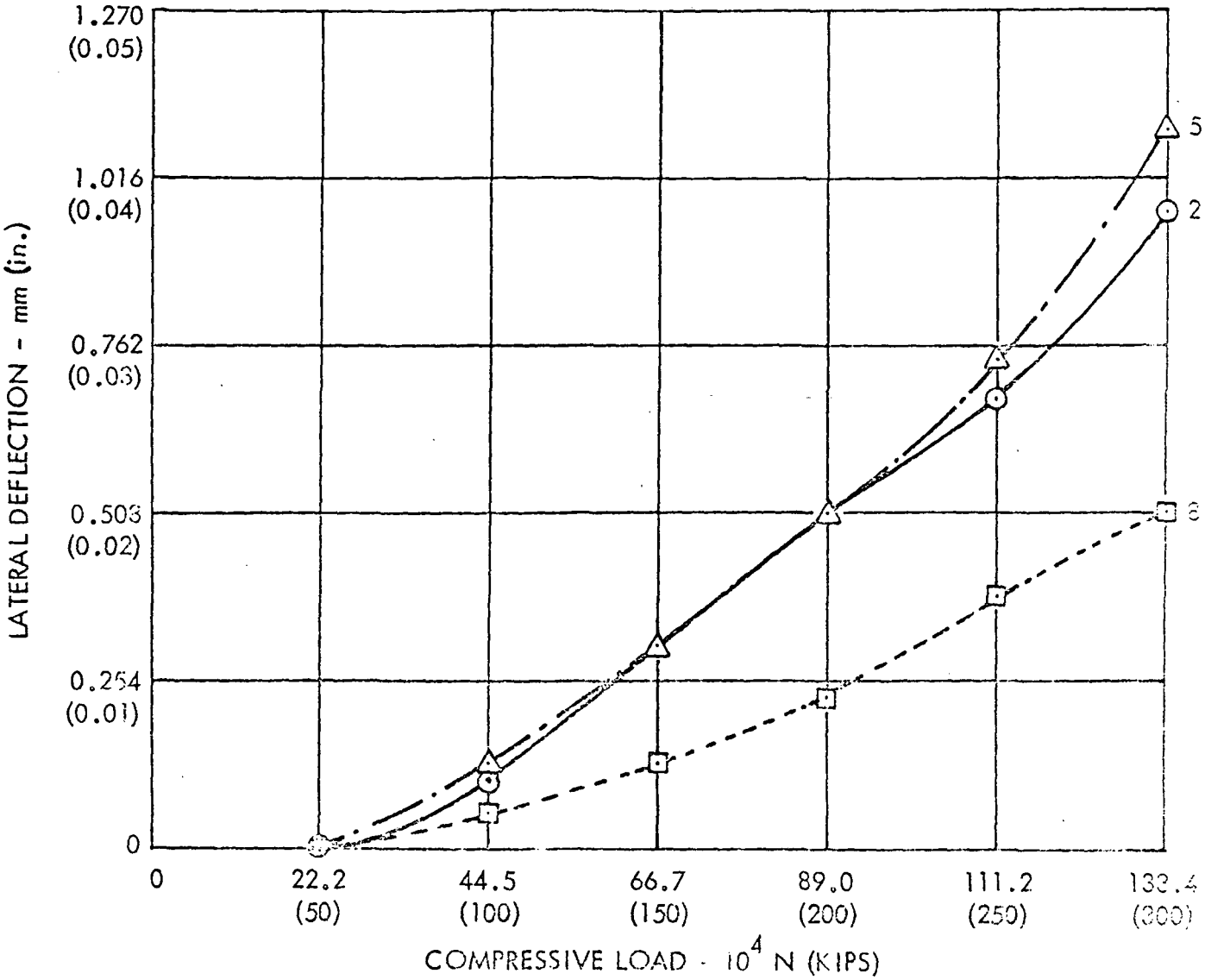

FIGURE 71. - COMPRESSIVE LOAD VERSUS LATERAL DEFLECTION
PANEL BUCKLING SPECIMEN 130PB4-1
DIAL GAGES NO. 2, 5, AND 8

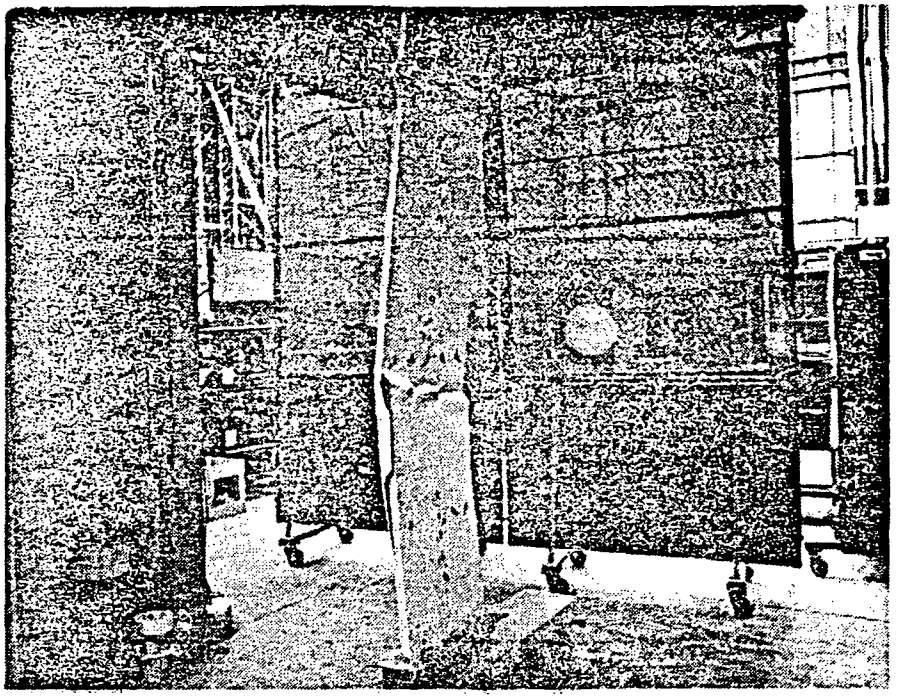

(SKIN SIDE)

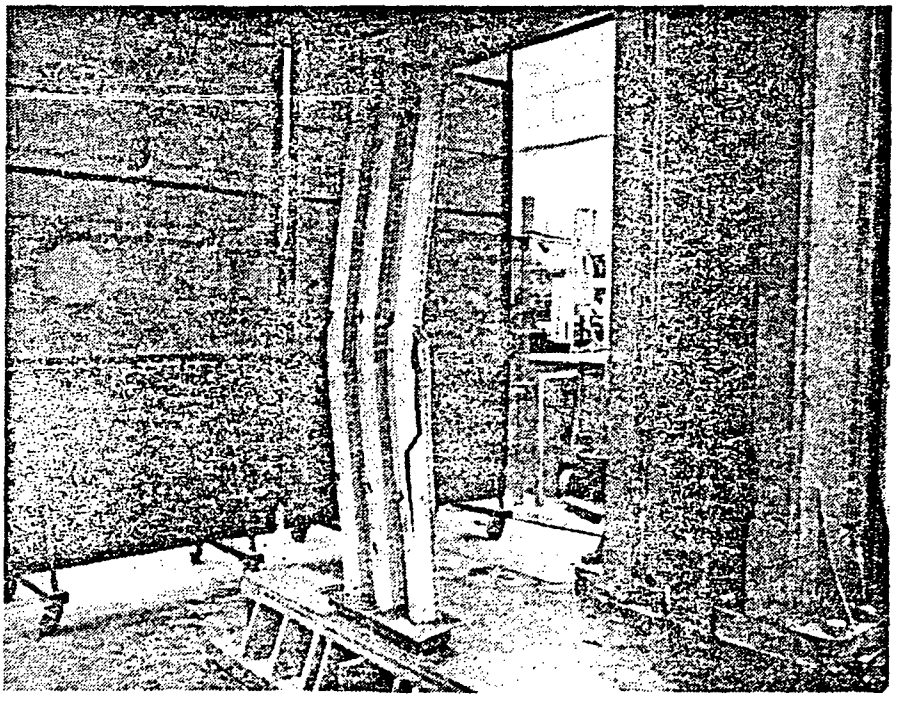

(STRINGER SIDE)

FIGURE 72. - SPECIMEN 130PB4-3 AFTER TEST

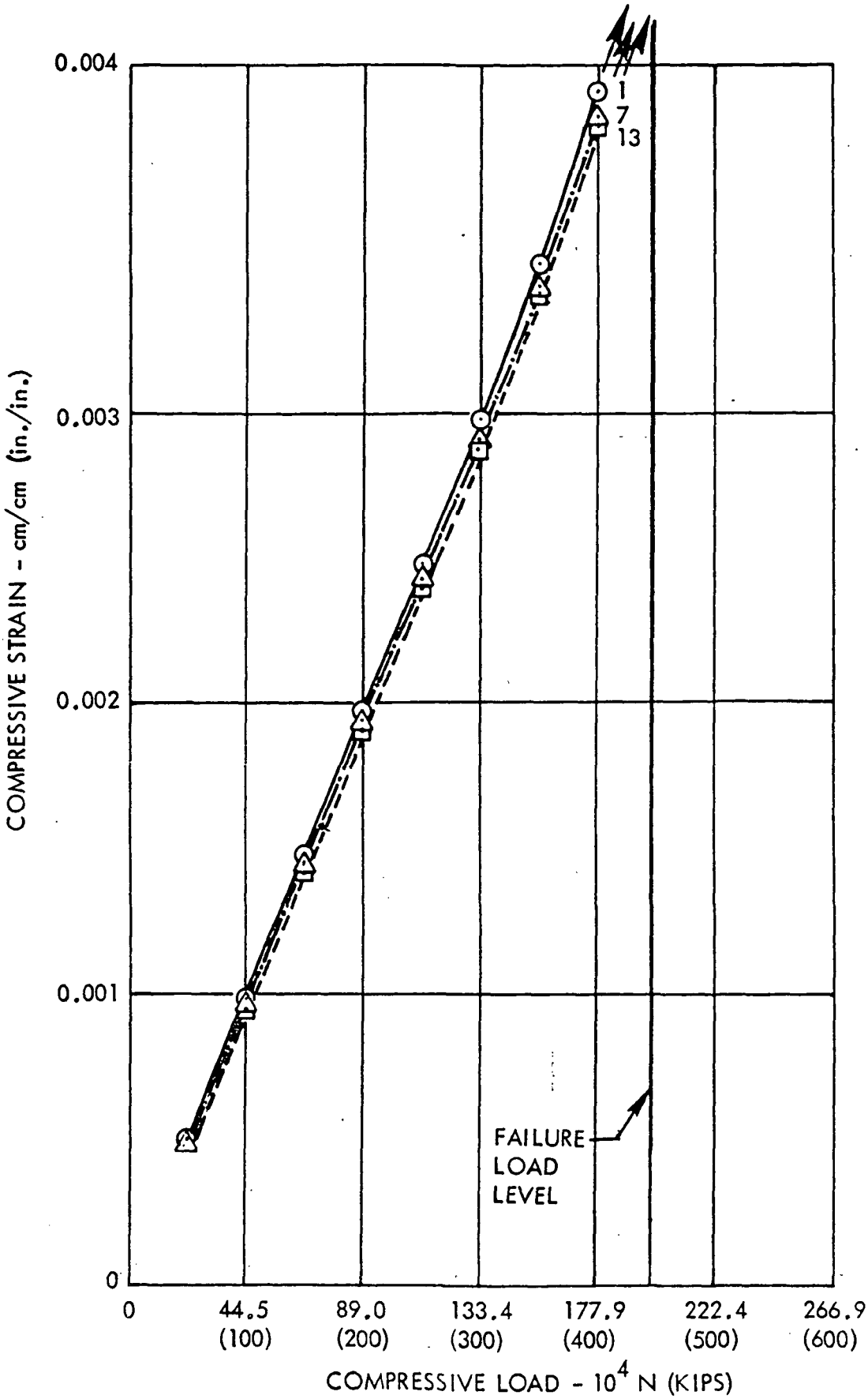

FIGURE 73. - COMPRESSIVE LOAD VERSUS STRAIN
PANEL BUCKLING SPECIMEN 130PB4-3
STRAIN GAGES NO. 1, 7, AND 13

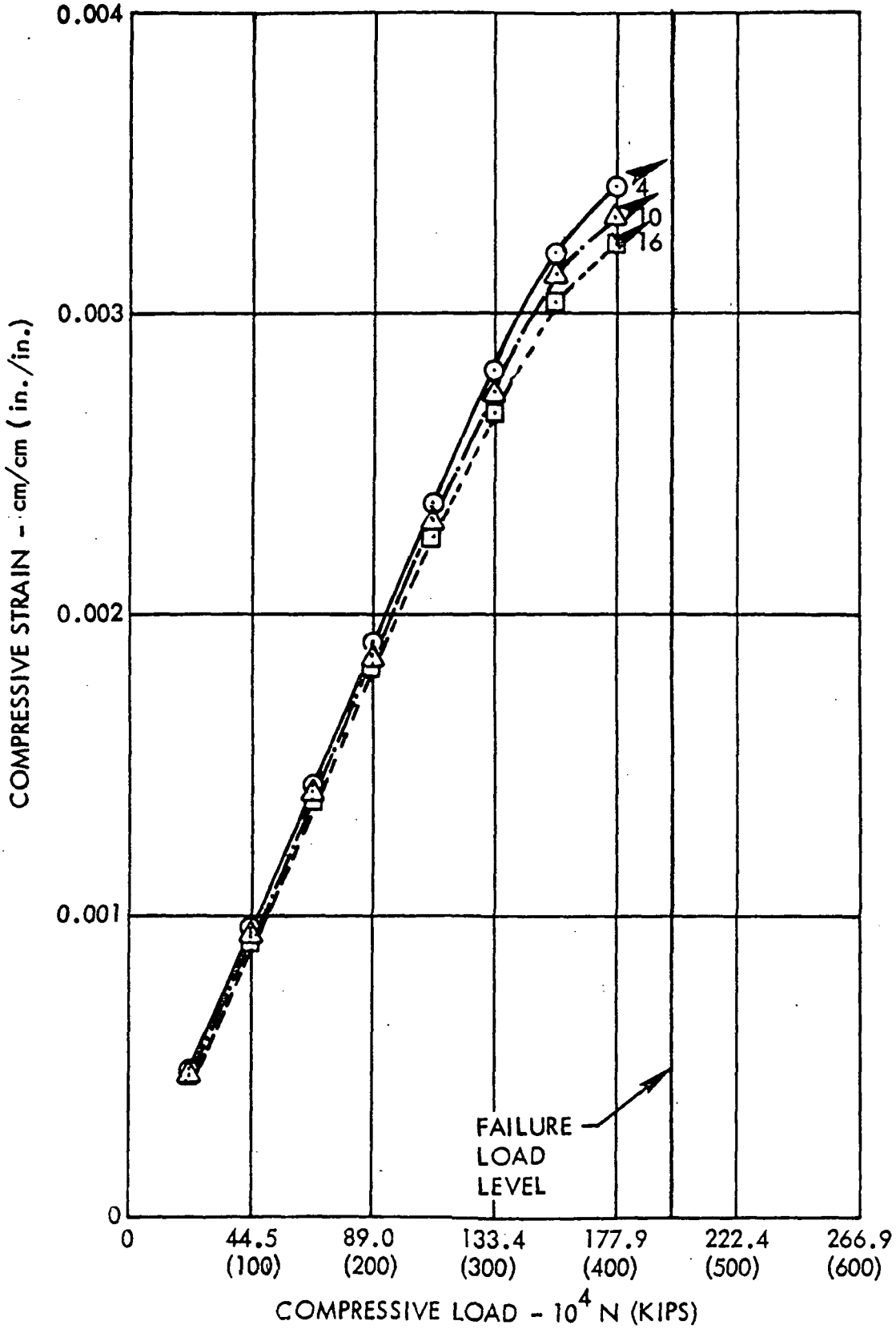

FIGURE 74. - COMPRESSIVE LOAD VERSUS STRAIN
PANEL BUCKLING SPECIMEN 130PB4-3
STRAIN GAGES NO. 4, 10, AND 16

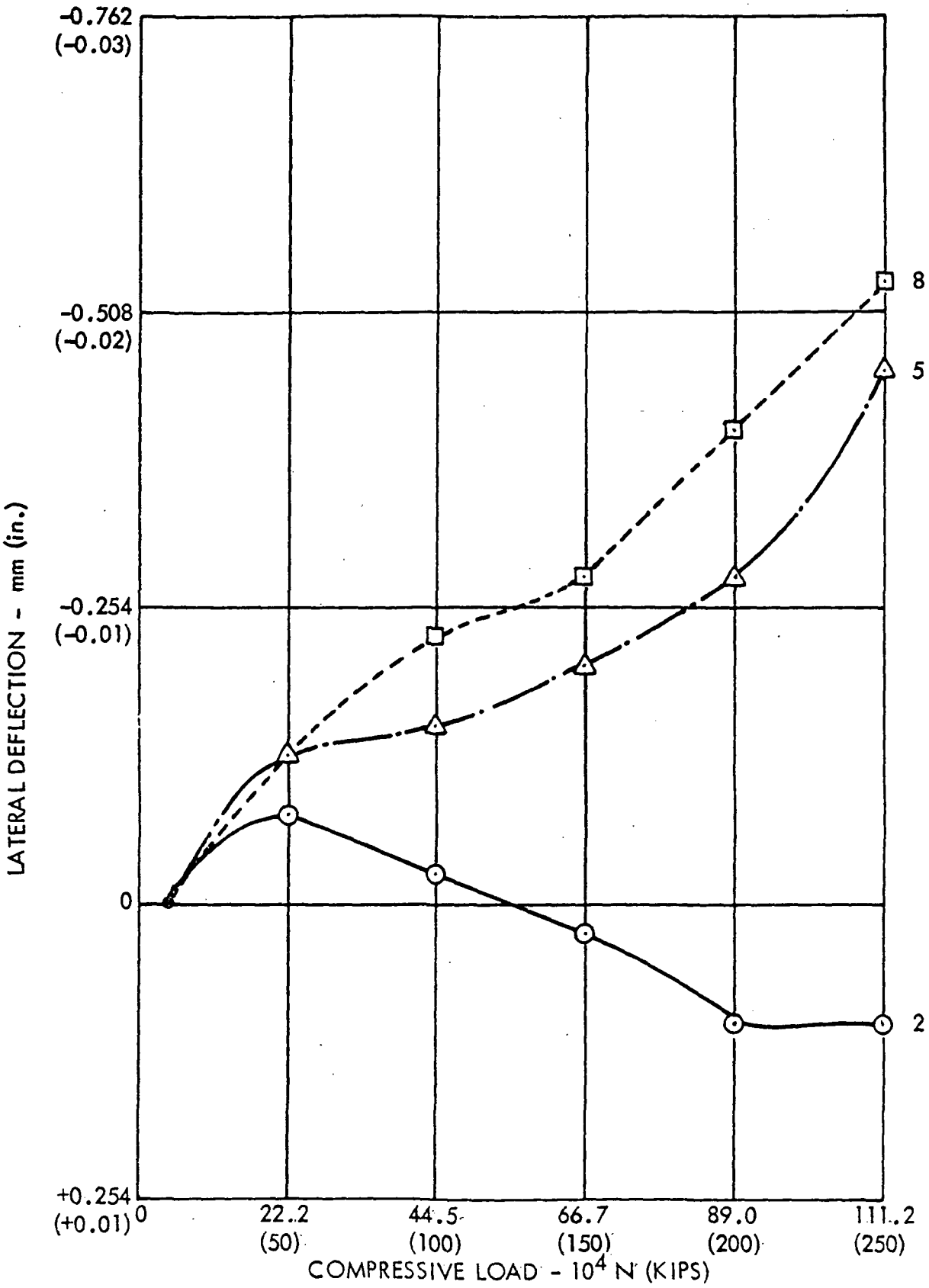

FIGURE 75. - COMPRESSIVE LOAD VERSUS LATERAL DEFLECTION
PANEL BUCKLING SPECIMEN 130PB4-3
DIAL GAGES NO. 2, 5, AND 8

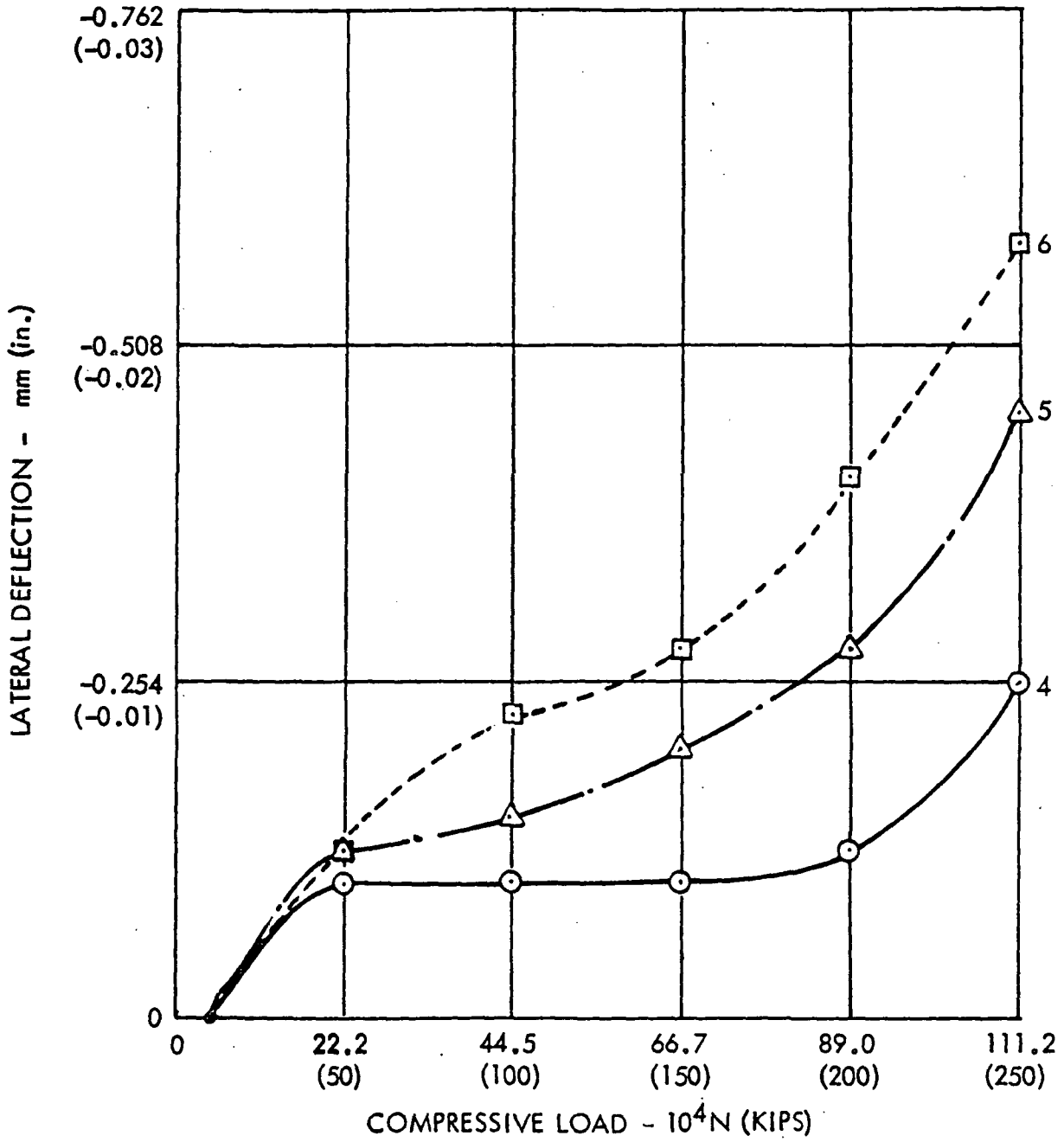

FIGURE 76. - COMPRESSIVE LOAD VERSUS LATERAL DEFLECTION
PANEL BUCKLING SPECIMEN 130PB4-3
DIAL GAGES 4, 5, AND 6

There was no evidence that end conditions influenced results for the 130PB4 specimens. The tests were very satisfactory, confirming analytical predictions and verifying required structural capability.

9.4 STRINGER CUTOUT TESTS

As noted earlier, some minor fatigue "nuisance" cracks were found in stringer cutout areas during Phase I tests of specimen PF-1. To see if this cutout area could be improved, two fatigue specimens reflecting current and selected stringer cutout configurations were designed, fabricated, and tested. All of the tested configurations exceeded minimum requirements by a sizeable margin, verifying earlier conclusions that the cracks were caused by a sharp edge which should have been chamfered. Fatigue loads taken from the specimen applied to the PF-1 panel specimen were used in the test.

9.4.1 Description of Stringer Cutout Specimens

Each specimen was 1.092 m (43.00 in.) long and 0.152 m (6 in.) wide. The 130PF4-1 specimen represented the existing C-130 B/E configuration which was tested in Phase I on the 130PF-1 panel and provided baseline data. The second specimen 130PF4-3 had two different runout configurations ("A" and "B") as shown in Figure 77. Both specimens had the same boron-epoxy reinforcement in the stringer crown and skin plank as that tested on the 130PF-1 fatigue test. As noted, the two specimens were identical except for the profile of the stringer terminations near the specimen center.

9.4.2 Fabrication of Stringer Cutout Specimens

The stringer cutout specimens, 130PF4-1 and 130PF4-3 were fabricated using established techniques for lay-up of boron-epoxy reinforcements and for "cool tool" bonding. The bond was completed with no appreciable warpage,and the assembled panels were within the straightness requirements for the C-130 center wing box. All fabrication operations for these specimens were documented and inspection procedures were followed as established for the program. The completed 130PF4-3 specimen is shown in Figure 78 .

9.4.3 Stringer Cutout Specimen Tests

Both specimens were tested in axial load fatigue by a 6.67×10^5 N (150,000 lb.) capacity electrohydraulic servo-controlled test system. Specimen 130PF4-1, assembled in the test system, is shown in Figure 79. Lateral restraint was applied to the specimen by a Teflon-coated rub block attached to one vertical column of the testing machine. This arrangement provided support in only one direction, and the test arrangement was similar for both specimens. The 2.22×10^5 N (50,000 lb.) load range was used to apply

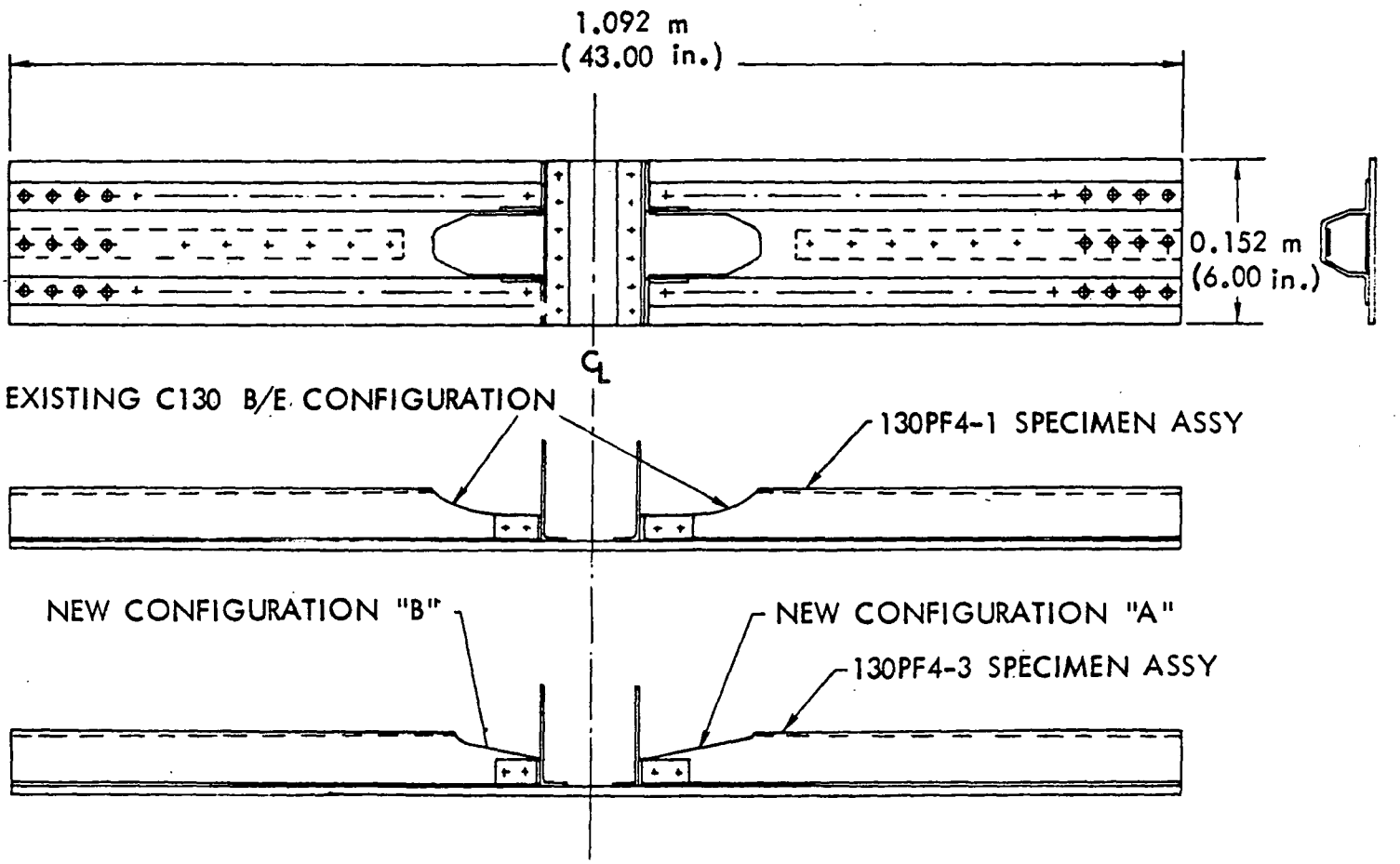

FIGURE 77. - 130-PF-4 STRINGER RUNOUT FATIGUE SPECIMENS

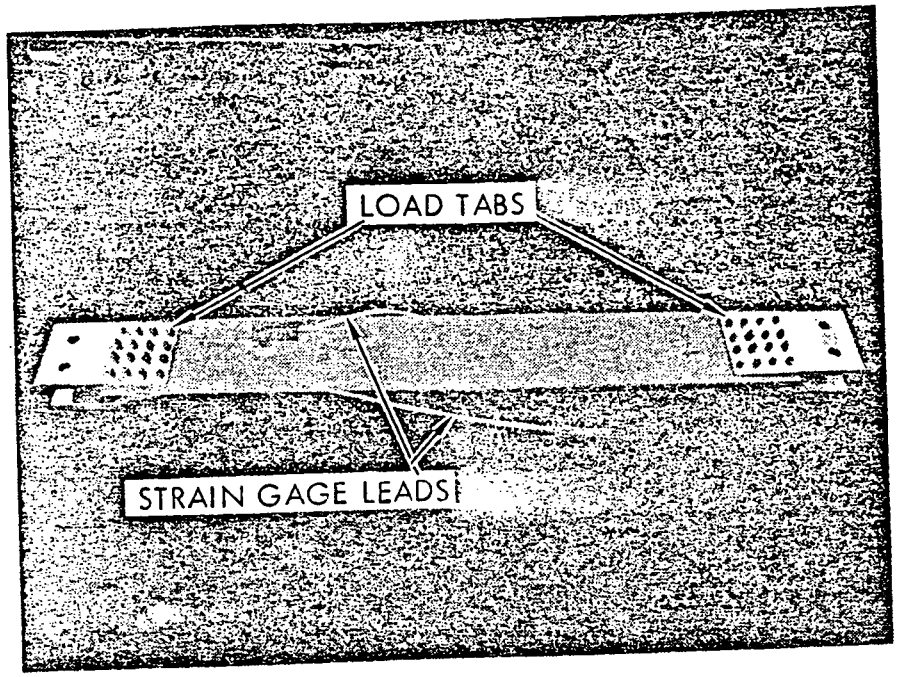

(SKIN SIDE)

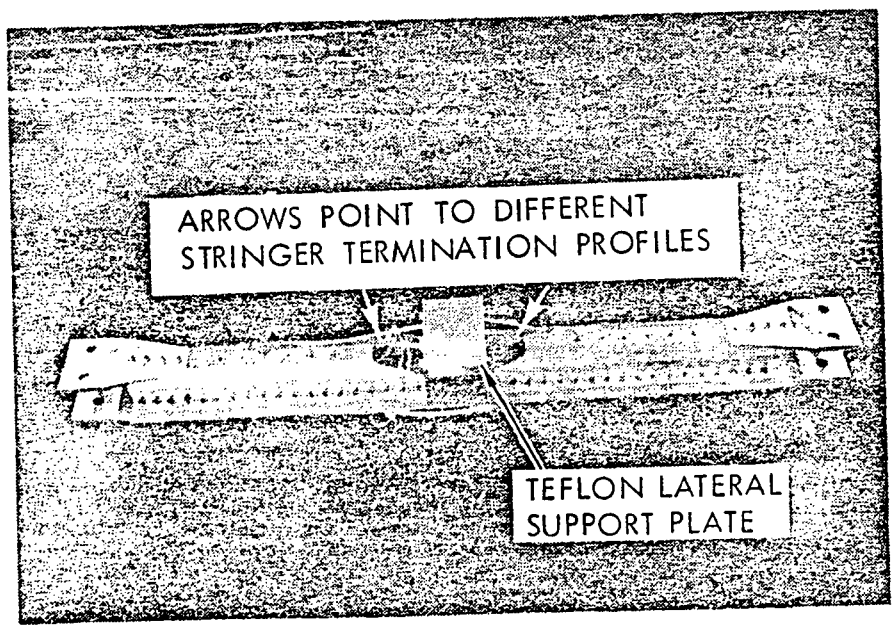

(STRINGER SIDE)

FIGURE 78. - STRINGER CUTOUT CONFIGURATION SPECIMEN

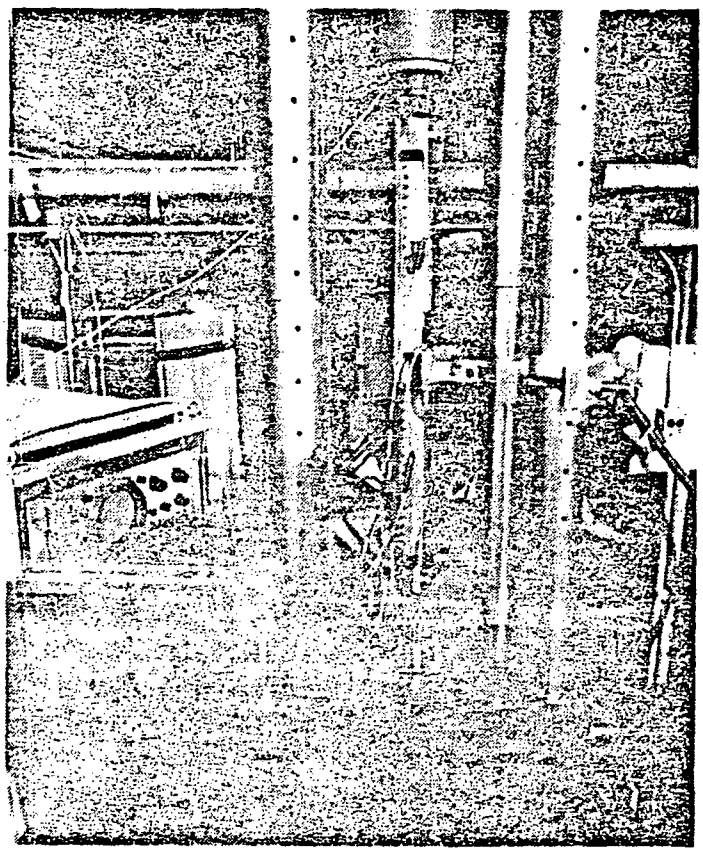

FIGURE 79. - FATIGUE TEST ARRANGEMENT FOR STRINGER CUTOUT SPECIMENS

constant-amplitude sinusoidal fatigue cycles at 18 cycles per second. Maximum and minimum loads of 1.28×10^5 N (28,900 lb.) and 0.49×10^5 N (11,100 lb.), respectively, were used for both specimens. No failures were obtained in the test area.

9.4.4 Evaluation of Stringer Cutout Tests

Specimen 130PF4-1 sustained 400,680 cycles before a fatigue crack was found in one stringer crown beside the first fastener attaching the end fitting. This specimen was of the existing model C-130 B/E configuration. Examination of the test section portion of the specimen revealed no cracks. Since the test section had sustained far more fatigue cycles than required, testing was discontinued at 400,680 cycles.

Specimen 130PF4-3 (the "improved" configuration) sustained 514,740 cycles before a fatigue crack was found in one stringer crown beside the fastener attaching the boron-epoxy laminate to the stringer crown near the end fitting. Examination of the test-section portion of the specimen revealed no cracks. Testing was terminated at 514,740 cycles.

Stringer runout specimens were tested to loads taken from the same fatigue test spectrum as that previously applied to component panel test specimen PF-1. Both specimens exhibited superior fatigue performance before fatigue failure occurred in the hat section away from the runout area. Failure locations are shown in Figure 80. The expected fatigue endurance in the runout area of the existing C-130B/E configuration was calculated to be 68,000 cycles for $K_t = 12$. Both specimens demonstrated a quality level better than 6.0, and any of these configurations selected for incorporation into the full scale wing box should meet the required fatigue life. Since there was no clear advantage to be gained by a configuration change, the existing C-130B/E configuration will be retained.

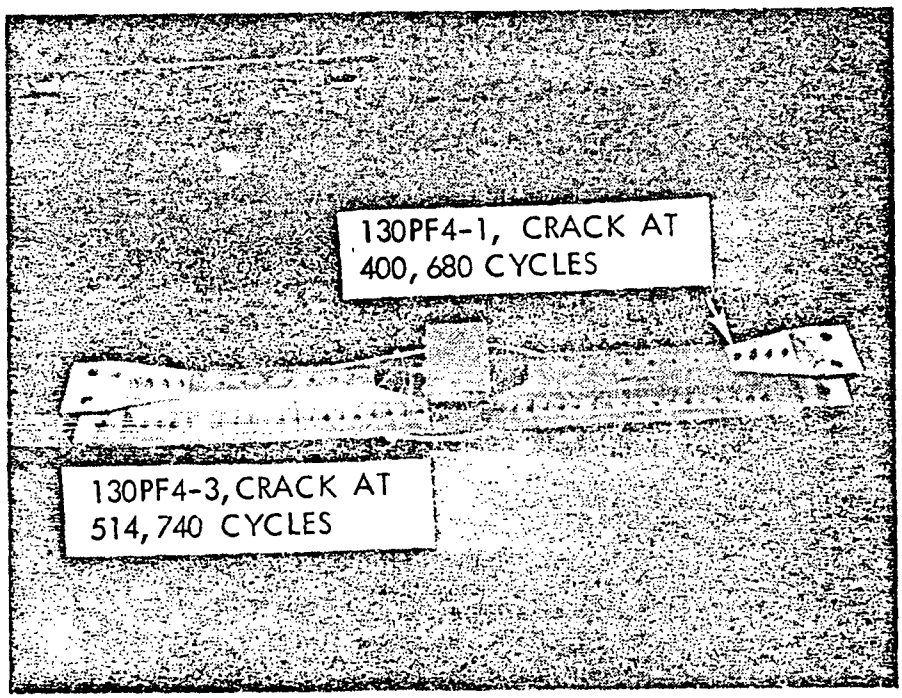

FIGURE 80. - LOCATION OF FATIGUE FAILURES IN STRINGER RUNOUT FATIGUE SPECIMENS

REFERENCES

1. Petit, P. H., "An Application Study of Advanced Composite Materials to the C-130 Center Wing Box," NASA CR 66979, Lockheed-Georgia Company, June 1970.

2. Harvill, W. E., et al., "Program for Establishing Long-Time Flight Service Performance of Composite Materials in the Center Wing Structure of C-130 Aircraft: Phase I - Advanced Development," NASA CR-112126, Lockheed-Georgia Company, November 1972.

3. Staff, Quarterly Progress Reports for NAS 1-11100 Contract, "Advanced Composite Reinforcement of C-130 Center Wing Box," Lockheed-Georgia Company:

    - First QPR: Phase I - Advanced Development, November, 1971
    - Second QPR: Phase I - Advanced Development, February, 1972
    - Third QPR: Phase II - Detailed Design, August, 1972
    - Fourth QPR: Phase II - Detailed Design, November, 1972
    - Fifth QPR: Phase II - Detailed Design, February, 1973

APPENDIX A

RELATIONSHIP BETWEEN SI UNITS AND U.S. CUSTOMARY UNITS

BASIC SI UNITS		
Physical Concept	Measurement	Abbreviation
Length	meter	m
Mass	kilogram	kg
Time	second	s
Force	Newton	N
Thermodynamic Temperature	degree Kelvin	^{o}K
Density	kilograms/meter^3	kg/m^3

PREFIXES		
Factor By Which Unit Is Multiplied	Prefix	Symbol
10^9	giga	G
10^6	mega	M
10^3	kilo	k
10^2	hecto	h
10	deca	da
10^{-1}	deci	d
10^{-2}	centi	c
10^{-3}	milli	m
10^{-6}	micro	μ

CONVERSION FACTORS		
To Convert From	To	Multiply By
Celsius (temp.)	kelvin	$t_K = t_c + 273.15$
Fahrenheit (temp.)	kelvin	$t_K = (5/9)(t_F + 459.67)$
foot	meter	3.048×10^{-1}
inch	meter	2.54×10^{-2}
pound mass (lbm avoirdupois)	kilogram	4.536×10^{-1}
pound mass force (lbf)	newton	4.44822
$lbm/inch^3$	$kilogram/meter^3$	2.768×10^4
psi	$newton/meter^2$	6.895×10^3

APPENDIX B

LISTING OF ALL DRAWINGS PREPARED FOR THE COMPOSITE REINFORCED CENTER WING

LRC DWG.NO.	LOCKHEED DWG. NO.	DWG. TITLE
LX939398	3307615	Boron Laminate - C. Wing Lower Surface, Stringer Crown, Assy Of.
LX939399	3307570	
LX939400	3307571	
LX939401	3307572	
LX939402	3307573	
LX939403	3307574	
LX939404	3307575	
LD939405	3307583	Boron Laminate - C. Wing Lower Surface, Stringer Crown, Assy Of.
LX939406	3307607	Stringer-No. 12,13,14,22,23 & 24, Lower Surface
LX939407	3307608	Stringer-No. 15 & 21, Lower Surface
LX939408	3307609	Stringer-No. 16 & 20, Lower Surface
LX939409	3307565	Stringer-No. 17 & 19, Lower Surface, Inboard
LX939410	3307566	Stringer-No. 17 & 19, Lower Surface, Outboard
LX939411	3307567	Stringer-No. 18, Lower Surface, Inboard
LX939412	3307610	Stringer-No. 18, Lower Surface, Outboard
LX939413	3307576	Stringer-No. 12,13,14,22,23 & 24, Lower Surface Composite Reinforced, Assy Of.
LX939414	3307577	Stringer-No. 15 & 21 Lower Surface, Composite Reinforced Assy Of.
LX939415	3307578	Stringer-No. 16 & 20, Lower Surface, Composite Reinforced, Assy Of.
LX939416	3307579	Stringer-No. 17 & 19, Lower Surface, Inboard, Composite Reinforced, Assy Of.
LX939417	3307580	Stringer-No. 17 & 19, Lower Surface, Outboard Composite Reinforced, Assy Of.
LX939418	3307581	Stringer-No. 18, Lower Surface, Inboard, Composite Reinforced, Assy Of.
LX939419	3307582	Stringer-No. 18, Lower Surface, Outboard, Composite Reinforced, Assy Of.
LC939420	3307613	Plate-Stringer Laminate, Lower Surface
LX939421	3307595	Boron Laminate-C. Wing Upper Surface Stringer Crown, Assy Of.
LX939422	3307596	
LX939423	3307597	
LX939424	3307599	
LX939425	3307600	Boron Laminate-C. Wing Upper Surface Stringer Crown, Assy Of.

LRC DWG. NO.	LOCKHEED DWG. NO.	DWG. TITLE
LD939426	3307601	Doubler-Boron Laminate Upper Surface Stringer
LX939427	3307584	Stringer-No. 7,8,10 & 11 Upper Surface
LX939428	3307585	Stringer-No. 3, Inboard, Upper Surface
LX939429	3307586	Stringer-No. 4, Upper Surface
LX939430	3307587	Stringer-No. 6, Upper Surface
LX939431	3307588	Stringer-No. 2 & 5, Upper Surface
LX939432	3307589	Stringer-No. 1, Upper Surface, Composite Reinforced, Assy Of.
LX939433	3307590	Stringer-No. 2 & 5 Upper Surface, Composite Reinforced, Assy Of.
LX939434	3307591	Stringer-No. 3 & 4, Inboard, Upper Surface, Composite Reinforced, Assy Of.
LX939435	3307592	Stringer-No. 6, Upper Surface, Composite Reinforced, Assy Of.
LX939436	3307593	Stringer-No. 7,9 & 10, Upper Surface, Composite Reinforced, Assy Of.
LX939437	3307594	Stringer-No. 8 & 11, Upper Surface, Composite Reinforced, Assy Of.
LX939438	3307602	Stringer-No. 1, Upper Surface
LX939439	3307603	Stringer-No. 9, Upper Surface
LX939440	3307614	Support-Stringer Attachment, Upper Surface
LD939441	3307620	Doubler-Boron Laminate, Skin Panels, Upper & Lower
LX939442	3307621	Boron Laminate-C. Wing, Lower Surface, Skin Panel, Assy Of.
LX939443	3307622	
LX939444	3307623	
LX939445	3307624	
LX939446	3307625	
LX939447	3307626	
LX939448	3307627	
LX939449	3307616	
LX939450	3307617	
LX939451	3307618	
LX939452	3307619	Boron Laminate-C. Wing, Lower Surface, Skin Panel, Assy Of.
LX939453	3307555	Panel-Upper Surface, C.W., No. 1, Composite Reinforced, Assy Of.
LX939454	3307556	Panel-Upper Surface, C.W., No. 2, Composite Reinforced, Assy Of.

LRC DWG. NO.	LOCKHEED DWG. NO.	DWG. TITLE
LX939455	3307557	Panel-Upper Surface, C.W., No. 3, Composite Reinforced, Assy Of.
LX939456	3307558	Panel-Upper Surface, C.W., No. 4, Composite Reinforced, Assy Of.
LX939457	3307604	Panel, Lower Surface, C.W., Forward, Composite Reinforced, Assy Of.
LX939458	3307605	Panel, Lower Surface, C.W., Middle, Composite Reinforced, Assy Of.
LX939459	3307606	Panel, Lower Surface, C.W., Aft, Composite Reinforced, Assy Of.
LD939460	3307628	Mounting Bracket-Pylon Tank Press. Switch, Inbd Dry Bay, Assy Of.
LD939461	3307629	Bracket-Refuel & Cross Feed, C.W.S. 58L/R
LD939462	3307630	Clip-Tube Support, Fuel
LD939463	3307631	Bracket-Fire Extinguisher Directional Valve, No. 3 Dry Bay.
LD939464	3307632	Bracket-Bladder Cell Fuel Press. Switch & Takoff Tee Support, Inbd, Dry Bay.
LD939465	3307633	Bracket-Bladder Cell Fuel "Y" Support, Inbd., Dry Bay.
LX939466	3307635(Sh. 1)	Support Instl-Plumbing, Ctr Dry Bay
LX939467	3307635(Sh.2)	Support Instl-Plumbing, Ctr Dry Bay
LX939468	3307635(Sh.3)	Support Instl-Plumbing, Ctr Dry Bay
LX939469	3307636	Support Instl-Plumbing NAC. No. 2 Dry Bay
LX939470	3307637	Support Instl-Plumbing NAC. No. 3 Dry Bay
LD939471	3307644	Bracket-Tube Support, Cross Feed
LD939472	3307645	Bracket-Shut-Off Valve Support
LC939473	3307646	Bracket-Fuel Tee Support, Assy Of.
LD939474	3307647	Bracket-Tube Support, W.S. 57L & 57R
LC939475	3307648	Support-Check Valve, Assy Of.
LC939476	3307649	Support Angle-Refuel Tube, Left Hand Auxiliary Tank, Horizontal
LD939477	3307598	Fitting-Attach, Spt to Stiff, C.W.S. 39.5R & 41L, Upper.
LD939478	3307611	Fitting-Attach, Spt to Stiff, C.W.S. 39.5R & 41.5L, Lower.
LX939479	3307612	Support Instl - Stiff., C.W.S. 39.5R & 41.5L
LX939480	3307638	Support Instl.-Stiff., Ctr Wing Sta. 0
LX939481	3307639	Fitting-Attach, Support to Stiffener, Ctr Wing Sta. 0, Upper, Assy Of.

LRC DWG. NO.	LOCKHEED DWG. NO.	DWG. TITLE
LX939482	3307641	Former Instl-Center Wing Sta. 108.125
LX939483	3307642	Former Instl-Center Wing Sta. 192.125
LX939484	3307643	Support Instl - Brackets, Upr Stanchion & Litter Strap
LX939485	3307552	Test Article-C-130 C.W. Box, Composite Reinforced
LD939486	3307550	Wing Mod Index-Fy 73 A/C, Composite Reinforced C.W.
LX939487	3308050	C.W. Assy-Spares, Mod.
LX939488	3308051	C.W. T.E. Assy-Spares, Mod.
LX939489	3308053(Sh. 1)	Upper Surface Instl-C.W.
LX939490	3308053(Sh.2)	Upper Surface Instl-C.W.
LD939491	3308054	Abchor-Instl-Fuel Cell, C.Wing, Upper Surface
LX939492	3307553(Sh. 1)	Upper Surface-C.W., Composite Reinforced, Assy Of.
LX939493	3307553(Sh.2)	
LX939494	3307553(Sh.3)	
LX939495	3307553(Sh.4)	
LX939496	3307553(Sh.5)	
LX939497	3307553(Sh.6)	
LX939498	3307553(Sh.7)	
LX939499	3307553(Sh.8)	
LX939500	3307553(Sh.9)	
LX939501	3307553(Sh.10)	Upper Surface-C.W., Composite Reinforced, Assy Of.
LD939502	3308058	Reinforcing Doubler-Center Wing Lower Surface Sta. 56.37
LD939503	3308059	Shim-Drain Trough, Lower Surface, C.W.
LX939504	3308060	Trough-Dry Bay Drain, C.W., LWR Surface, Sta. 56.37, Assy Of.
LX939505	3308056	Attach Angle-Wing to Fus.,C.W.Sta. 61.625, Assy Of.
LX939506	3308057	Attach Angle Instl to Fus.,C.W. Sta. 61.625, Assy Of.
LD939507	3308055	Support Angle-C.W. Sta. 61.625
LX939508	3307554(Sh. 1)	Lower Surface-C.W. Composite Reinforced, Assy Of.
LX939509	3307554(Sh.2)	
LX939510	3307554(Sh.3)	
LX939511	3307554(Sh.4)	
LX939512	3307554(Sh.5)	
LX939513	3307554(Sh.6)	
LX939514	3307554(Sh.7)	
LX939515	3307554(Sh.8)	Lower Surface-C.W. Composite Reinforced, Assy Of.
LX939516	3307640(Sh. 1)	Door Structure Instl-Access, Nacelle Dry Bay, C.W.
LX939517	3307640(Sh.2)	
LX939518	3307640(Sh.3)	Door Structure Instl-Access, Nacelle Dry Bay, C.W.

LRC DWG. NO.	LOCKHEED DWG. NO.	DWG. TITLE
LX939519	3308061	Attach Angle-Aft Nacelle, Lower Surface, C.W., Assy Of.
LD939520	3308062	Filler-Nacelle Attach Angle, Lower Surface, C.W.
LX939521	3308052(Sh. 1)	Lower Surface Instl - C. W.
LX939522	3308052(Sh.2)	Lower Surface Instl - C. W.
LX939523	3307551(Sh. 1)	Center Wing Structure-Composite Reinforced, Assy Of.
LX939524	3307551(Sh.2)	Center Wing Structure-Composite Reinforced, Assy Of.
LD939525	3307634	Support Angle-Plumbing, Ctr Dry Bay
LD939526	3308063	Strap-Splice, Skin Panel No.2 & 3, Outboard, Upper Surface, C.W.
LX939527	3308064	Splice Plate-External, Lower Surface, C.W.

APPENDIX C

PRINCIPLES OF FATIGUE ANALYSIS AND ENDURANCE DATA

This appendix consists of two sections:

- o Principles of Fatigue Analysis: a general discussion of fatigue from which the methods of analysis of Section 4.2 may be derived.
- o Endurance Data: a compendium of endurance as a function of quality level graphs for Section 4.2.

C.1 PRINCIPLES OF FATIGUE ANALYSIS

Fatigue is the description for a material failure process in which cracks develop in a structural member due to repeated application of stresses below the ultimate strength of the material. Fatigue failure is the certain result of irreversible (plastic) deformation at a surface. The accumulation of plastic deformation becomes a micro-crack when its long dimension (generally transverse to principal tension stress) approximates grain size, and a macro-crack when its dimension is similar to the minimum dimension of the part. The accumulation is generated by repeated stress characterized by the number of cycles and either mean and variable stress or maximum stress and stress ratio, as defined in Figure C-1.

It is hypothesized that the number of cycles to the generation of a macro-crack at a specified stress - or conversely, the stress required to generate a macro-crack in a specified number of cycles - is a material property in the same sense as ultimate strength, yield strength etc. ⚠ However, the true stress at the location of crack nucleation concentrated by geometric and microscopic stress risers is not known due primarily to plasticity. Geometric stress concentration factors can be derived, presuming linearly elastic isotropic material, relating the stress at the notch root to the nominal gross section stress as a function of notch geometry. But tests are required to determine the fatigue sensitivity to be associated with the geometric stress concentration factor. Typical test results are explained in the next section.

⚠ Note that fatigue is a strain process; it is assumed in this analysis that the stress-strain relationships are known (static and cyclic).

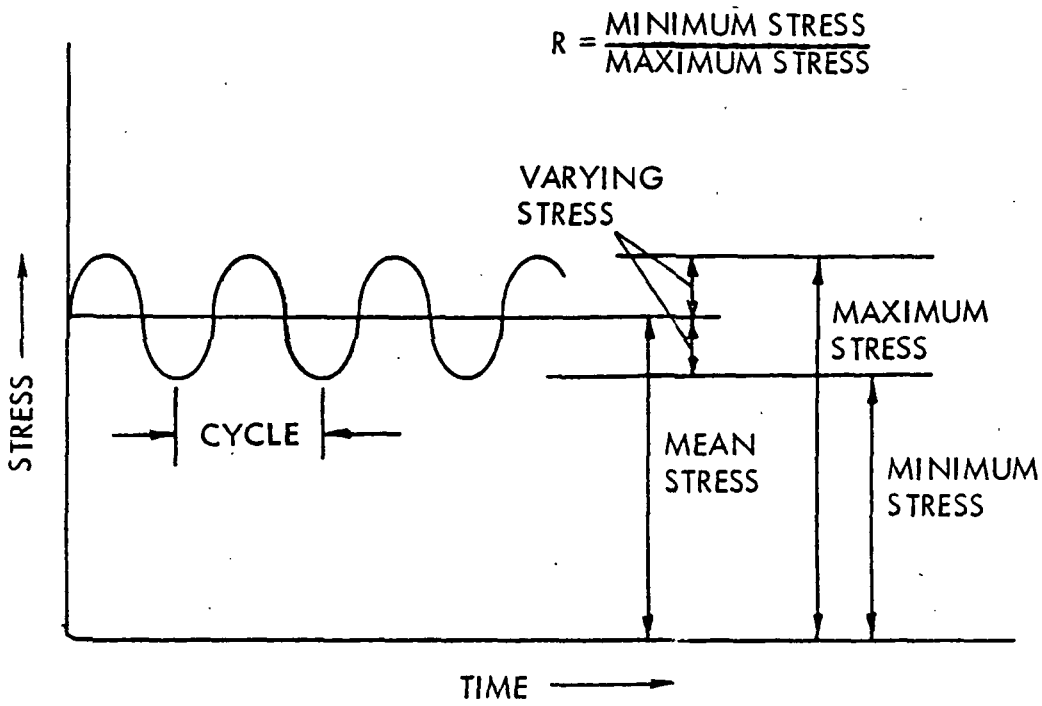

FIGURE C-1. - CHARACTERIZATION OF APPLIED REPEATED STRESS

C.1.1 S-N Curves

To measure the material property cyclic endurance, N, (number of cycles to macro-crack generation for a specified stress condition, σ_m, $\sigma_{var.}$) sets of laboratory specimens are cycled to failure at a particular stress condition - constant amplitude testing - for particular values of elastic stress concentration factors. The results are parametric S-N curves such as those sketched in Figure C-2a. For the compact specimen shape used in such tests, the number of cycles from the formation of a macro-crack to failure is very short compared with the number required to generate the crack. Hence, the cyclic endurance to failure for the specimen is a measure of cycles to "fatigue crack initiation" for more crack-tolerant structural configurations.

Since the stress concentration factor does not account for the reduction in cyclic endurance (due primarily to inherent plasticity); the nominal stress concentration factors are relabeled "quality levels" (unfortunately retaining the symbol K_T in practice). The endurance limit is the variable stress below which the part (at a particular K_T and mean stress) does not fail in fatigue; that is, no plastic deformation at the most severe stress riser. Hence, the S-N curve has a horizontal asymptote at a variable stress which is called the "endurance limit." For aluminum alloys, the S-N curve has a negative slope for all values of N; i.e., the endurance limit does not exist. For comparative purposes, the endurance limit for aluminum is selected as that variable stress yielding an endurance of 10^7 cycles.

C.1.2 Palmgren - Miner Hypothesis

The material property, N, is considered an "allowable" in the same manner as other material properties, such as ultimate strength. If a number of cycles, n_i ($n_i < N_i$), are applied to the specimen at stress state, σ_{vi}, σ_{mi}, the portion of endurance used, n_i/N_i, is termed analytical damage, D_i. If cycles, n_k, at another stress state (2), σ_{vk}, σ_{mk} are applied, the analytical damage is presumed to accumulate from the end state of the previous condition. Hence, the total analytical damage at any number of stress states, P, is

$$D = \sum_{i=1}^{P} n_i/N_i$$

and the allowable endurance curve is reached when total analytical damage is D = 1.0, at which time failure is expected to occur. This hypethesis is the Palmgren - Miner Theory of Linearly Cumulative Damage, or simply Miner's Theory (see Figure C-2b).

If any applied stress spectrum is divided into a sequence of stress conditions and the quality level of the part is known, failure is predicted at the cumulative number of cycles at which time Miner's Theory predicts D = 1.0.

---

(2) The second or third stess state may be the same as a previous state.

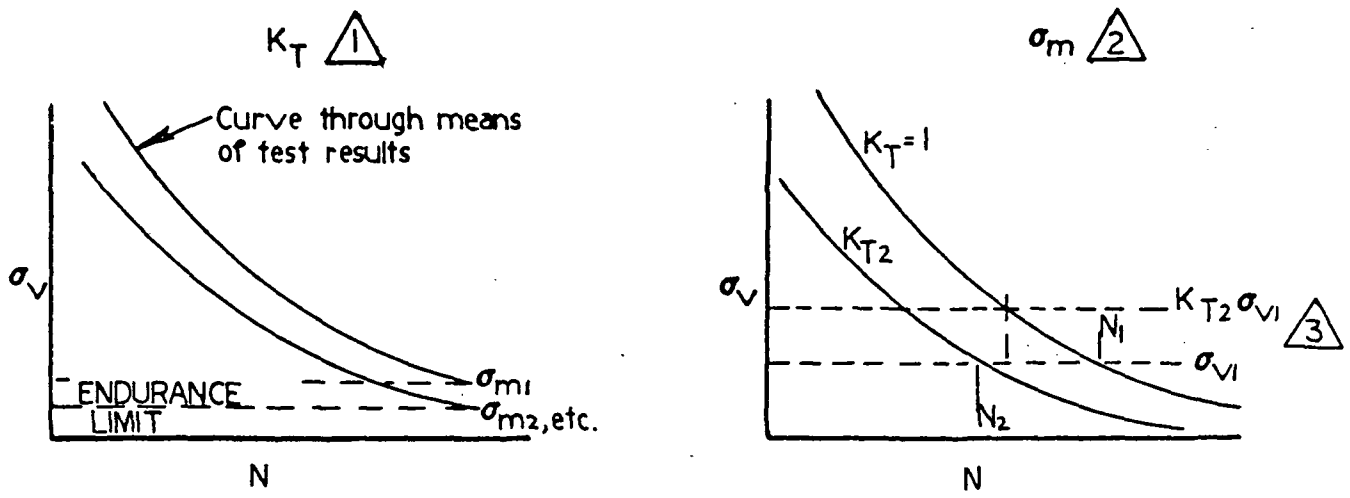

1 FAMILIES OF CURVES FOR PARAMETRIC VALUES OF K_T

2 CROSS PLOT FOR PARAMETRIC VALUES OF σ_m

3 MULTIPLYING STRESS BY K_T DOES NOT ACCOUNT FOR REDUCTION IN CYCLES TO FAILURE BECAUSE OF PLASTICITY.

(a) TYPICAL CONSTANT AMPLITUDE S-N CURVES

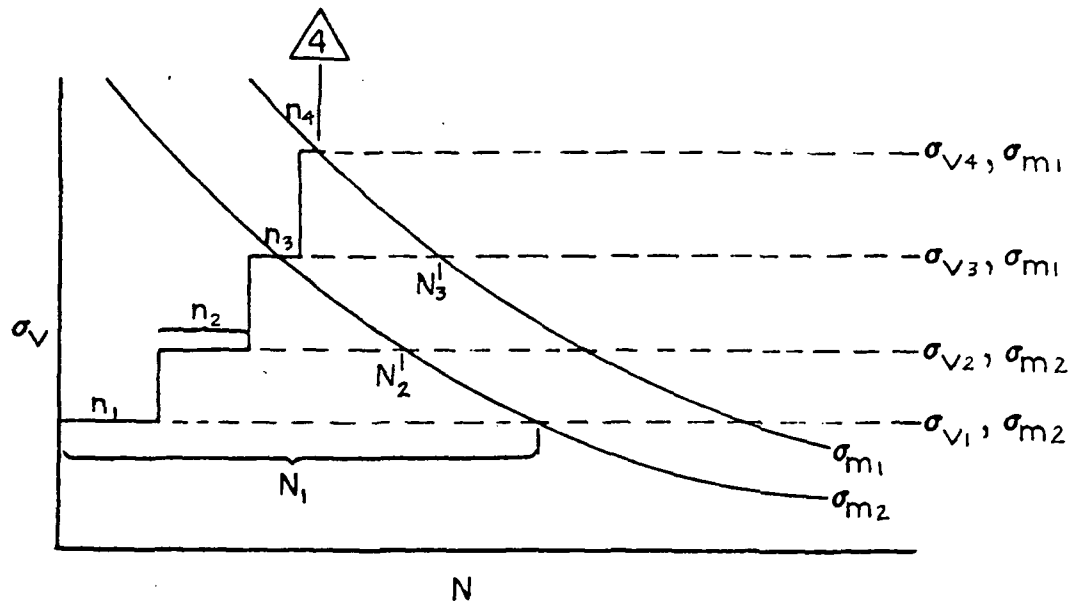

4 FAILURE EXPECTED TO OCCUR WHEN "ALLOWABLE" CURVE ENCOUNTERED:
$D = n_1/N_1 + n_2/N_2 + n_3/N_3 + n_4/N_4$, FAILURE AT $D = 1.0$
WHEN THE CUMULATIVE NUMBER OF CYCLES IS Σn_i

(b) PALMGREN-MINER HYPOTHESIS

FIGURE C-2.-CONSTANT AMPLITUDE S-N CURVES

C.1.3 Ascertaining the Applied Stress Cycles (n_i)

o World-wide surveys provide gust intensity data as a function of geographic location, season, time of day, etc. (VGH data). Runway and taxiway roughness data are also surveyed (TAG data). These data are represented by power spectral density relations.

o The external applied loads at any point in the structure are functions of the dynamic response of the airframe to the spectral relations specifying the loading environment.

o Given a particular airframe structure (stiffness, inertial response, etc.) operated within prescribed bounds (standard operating procedures - flaps and control surfaces deflections, fuel management, etc.) for each event (cruise, climb, take-off, maneuver, etc.), the dynamic response transfer functions may be derived in terms of mission-dependent parameters: flight operations - event type, altitude, airspeed, cargo weight, fuel weight; ground operations - event type, cargo weight, fuel weight, and runway/taxiway condition.

o Hence, operation of the aircraft for a period (mission segment) during which the mission-dependent parameters may be considered to be constant defines the cumulative number of accelerations (incremental load factors) encountered via the transfer functions. These data are presented as families of curves similar to Figure C-3.

o Specifying the duration of each segment then defines the total number of variable load cycles of each magnitude. The event type, along with the other mission dependent parameters, specifies the mean load factor, hence the mean load.

o Fatigue analysis is often simplified by computing the transfer functions, etc., for representative locations such as the wing root. Loads at other locations are specified by multiplying the loads at the representative locations by a load shape factor derived from the load distribution for a limit (or ultimate) load case for which the analysis has been more complete.

o The maximum nominal (gross, or net section at cutouts) stress is computed by multiplying the applied load at a location by the stress-load ratio derived from the stress distribution for a limit (or ultimate) load case for which the stress analysis has been more complete.

o The result is that, for operation of the airplane in a segment for a specified time, the applied stress spectrum is defined in terms of mean stress and number of cycles of variable stress.

o Describing the operation of the aircraft by a series of segments therefore defines the applied stress spectrum. The series of segments can be observed (as in the USAF fatigue life monitoring program) or prescribed for analyses purposes.

o For certain fatigue anlayses, a set of nine prescribed missions has been developed. Each mission is divided into a series of segments so that by the foregoing analysis the applied stress spectrum for each mission (or for, say, 1000 hours of operation in each mission) is derived.

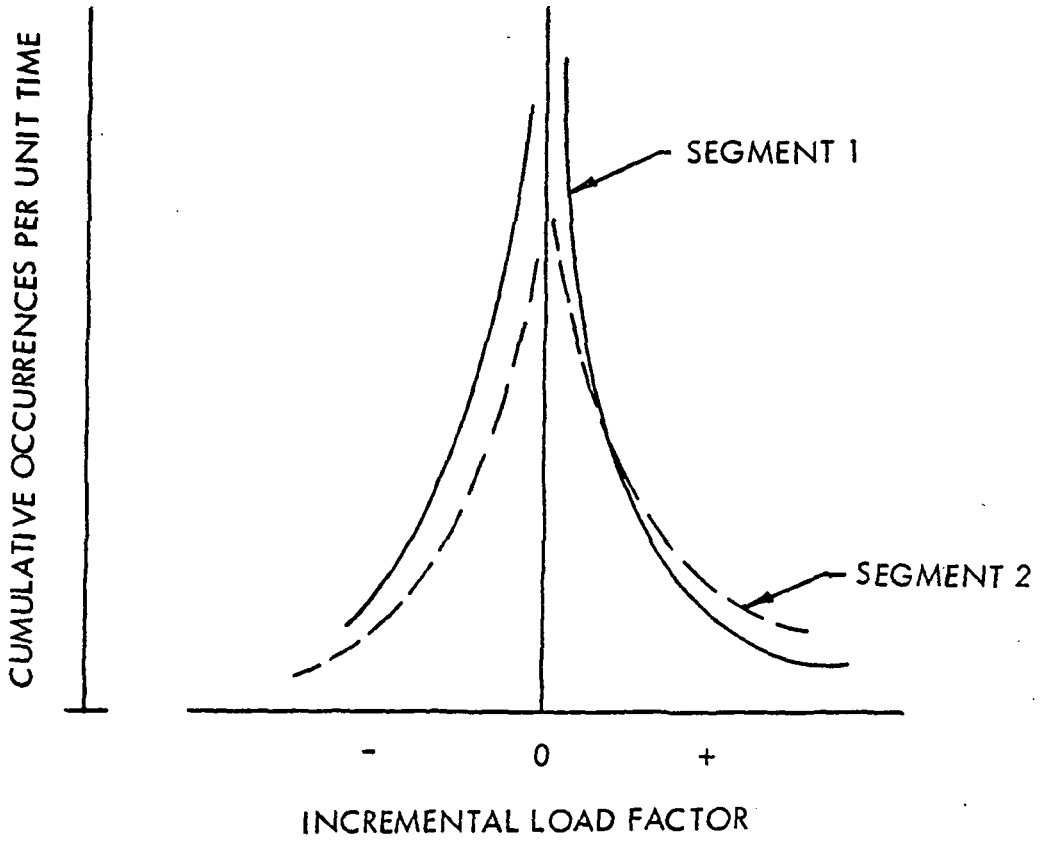

FIGURE C-3. - REPRESENTATION OF INCREMENTAL LOAD FACTORS

o By specifying (or observing) the portion of total airframe hours spent in each of the nine missions, a composite utilization is derived; applying the foregoing analysis, overall utilization is reduced to a single applied stress spectrum.

C.1.4 Analytical Damage, Damage Rate, and Endurance

Having an applied stress spectrum for a mission segment, a mission, or a mission mix, one can apply the Palmgren - Miner hypothesis and derive the analytical damage for the applied spectrum, providing the quality level is known. The applied spectrum is related to a specific flight time via the spectrum derivation process. Therefore, the analytical damage is related to a specific flight time period, e.g., damage for 1000 flight hours with a specified mission mix. This "damage rate" then establishes the "endurance" in terms of a meaningful reference parameter: flight hours.

C.1.5 The Stress-Load Ratio and Quality Level

As outlined in section C.1.3, obtaining the applied loads spectra for reference locations is a very complex process, comprising the major task of aircraft fatigue analyses. The load shape factor, derived from more complete ultimate load analysis, relates the applied loads at other locations to the reference location loads.

At specific locations on the airframe, selected because of suspected, or test-demonstrated, relative fatigue susceptibility, ultimate stress analysis provides the stress-load ratio which translates the applied load spectrum to the applied stress spectrum. If the exact location of fatigue cracking has not been analyzed, or if multiple locations of ostensibly identical fatigue susceptibility exist, or the exact location is not known (for example, in pre-test design phases), a nominal stress is calculated - usually the maximum gross structural cross-section stress. "Gross" is used in the sense that fastener holes, etc., are not deducted; however, door cutouts, etc., affecting the stress distribution are accounted for. Stresses at other locations in the structural cross-section are related to the nominal stress by the parametric stress factor derived from more rigorous ultimate stress analysis accounting for local cutouts, eccentricities, etc. The additional concentration due to fastener holes, notches, etc., is accounted for by the quality level, typically $2 \leq K_T \leq 6$. If the parametric stress factor is not used, the notch stress is related to the nominal stress by the quality level alone, typically $4 \leq K_T \leq 12$. The two approaches are not quite equivalent due to nonlinearities. Utilizing the parametric stress factor is more accurate.

The quality level of a particular structural location may be approximated by calculating the nominal elastic stress concentration factor and by comparison with similar structure. Another alternative is to test the structure to obtain the test-demonstrated quality level. Running a constant-amplitude test would allow interpolation in basic data graphs, such as those sketched in Figure C-2. Experience with laboratory specimens (coupons, components, etc.) has shown that interpretation of spectrum fatigue performance using Miner's Theory and constant-amplitude S-N data leads to large scatter due to

neglected stress-change interactions, fretting corrosion in components, etc. Testing to a spectrum simulating the anticipated in-service conditions alleviates this situation. To compute the quality level from a spectrum test, a curve such as that shown in Figure C-6 (a) is generated by computing the endurance (1.0/damage rate; damage rate = $\Sigma n/N$ for specified period) for assumed values of K_T. The test-demonstrated quality level is that value on the curve corresponding to the observed test endurance. Therefore, for a particular structural location the test demonstrated quality level from a component test (or full scale test) should be the same despite variations in the applied stress spectra. Furthermore, since the quality level is a property of the particular geometry, it can be used to establish endurance for any applied stress spectrum, including a typical operational spectrum, even though the spectra are different and hence yielding different endurance for the same quality level (see Figure C-4 (b)) in terms of flight hours (or simulated flight hours), depending on the severity of the spectrum.

C.1.6 Comparison of Structural Elements

To evaluate the fatigue performance of different locations, it is necessary to know the load shape factor, the stress load ratio, (the parametric stress ratio), quality level, and material S-N data. Comparison on the basis of any one of the parameters can lead to erroneous conclusions if the change in that parameter is accompanied by a change in another, which happens frequently.

In section 4.2.2 it is asserted that, for the 80:20 area distribution of aluminum to boron-epoxy composite, the aluminum is more fatigue-susceptible than either the boron-epoxy composite or the bond. This observation is based upon comparison of stress levels, S-N data, and anticipated quality levels due to fasteners, thickness changes, etc. For example, computer analysis of a boron-epoxy laminate runout shows the peak shear stress in the bond to be approximately 1/14 of the gross aluminum stress. Furthermore, bonded joint tests show that the peak bond shear stress is about 2-1/2 times the nominal bond shear stress. S-N data for the joint tests are given in terms of the nominal shear stress. Using these ratios (similar to parametric stress factor and quality level) at a composite reinforcement run-out (such as WS 214) yields stresses sufficiently low to preclude fatigue failure (less than the endurance limit) for all load levels of the C-130B/E test spectrum B. If a straight line (on a semi-logarithmic plot) is conservatively fit to the data (no endurance limit), all endurances are in excess of 10^9 cycles. Conservatively using $N = 10^9$ cycles for each stress level, the 25,000 cycles per 1000 hours of the C-130B/E test spectrum B yields a damage rate of 2.5×10^{-5} per 1000 hrs., i.e., the endurance is greater than 4×10^7 simulated flight hours. For the aluminum to have an endurance of 4×10^7 simulated flight hours (spectrum B), the associated quality level must be less than 4.25 (see Figure C-24). Phase I tests (JE-1, JE-4, PF-3) show that the quality level is expected to be greater than 6.0 at this location, (see Table IV, Sec. 4.2). Hence the aluminum is more fatigue-susceptible than the bond, even with the conservative assumptions applied.

In comparing the composite reinforced wing with the C-130B/E wing, location for location, the modification of the structure to accommodate the boron-epoxy reinforcement

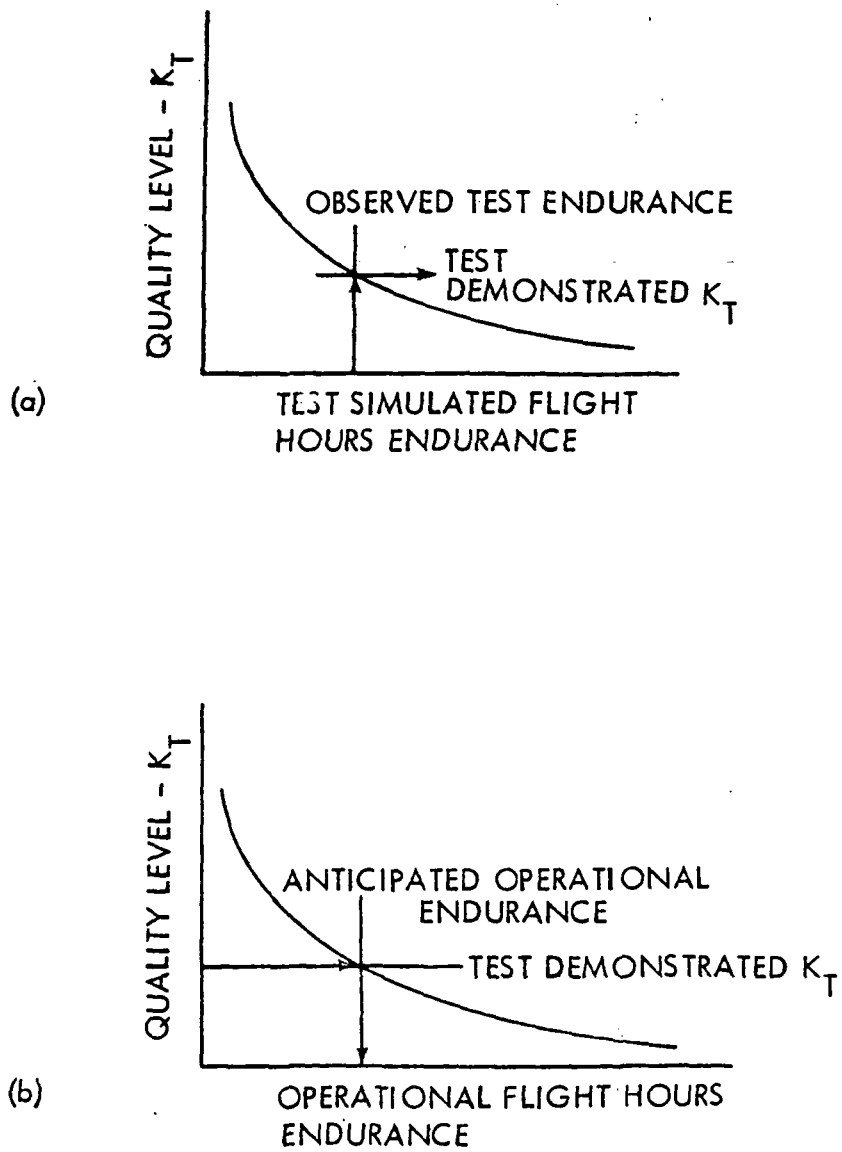

FIGURE C-4. - ENDURANCE AS A FUNCTION OF QUALITY LEVEL

is made in such a fashion that the local strain gradients are about the same (or less severe) as in the corresponding location on the C-130B/E wing. Hence, as asserted in section 4.2.2, the quality level at any location of the composite-reinforced wing is the same as (or less than) that of the corresponding location on the C-130B/E wing. Furthermore, at many locations on the wing which might be expected to be fatigue-critical (door cutouts, rainbow fitting, etc.), the design was not changed.

C.2 ENDURANCE DATA

The methods and analyses described in section 4.2 and C.1 were applied to 20 locations (10 upper surface, 10 lower surface) identified by wing station numbers (inches from aircraft centerline) 40, 60, 80, 100, 120, 140, 160, 180, 200, and 214. Three spectra were used for the analysis: typical operational spectrum (9-mission mix specified in Table III, Sec. 4.2), C-130B/E test spectrum A, and C-130B/E test spectrum B. The endurance (flight hours for operational, simulated flight hours for test) as a function of quality level are presented in Figures C.5 through C.24.

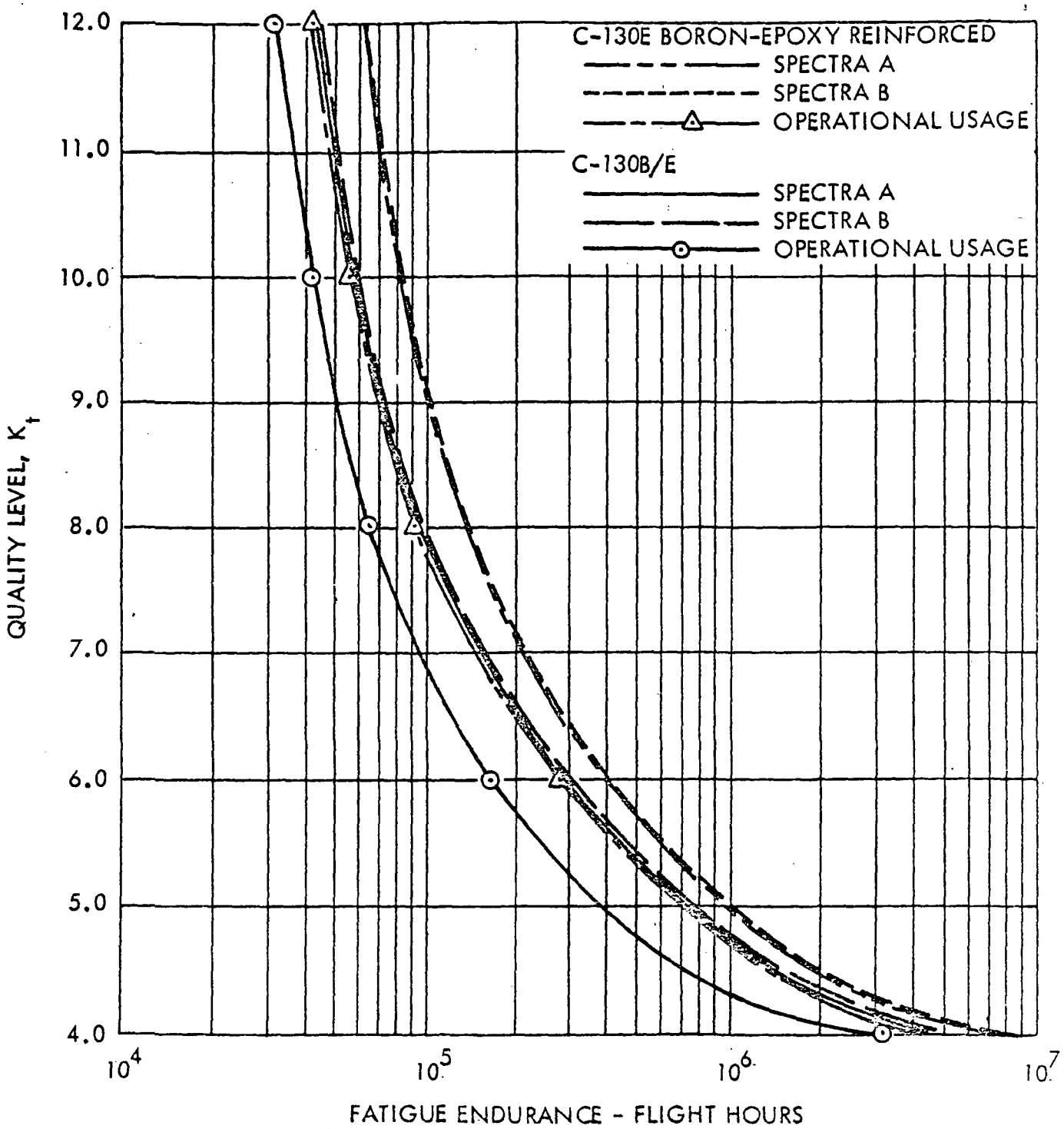

FIGURE C-5. - QUALITY LEVEL VERSUS FATIGUE ENDURANCE
W.S. 40 UPPER SURFACE

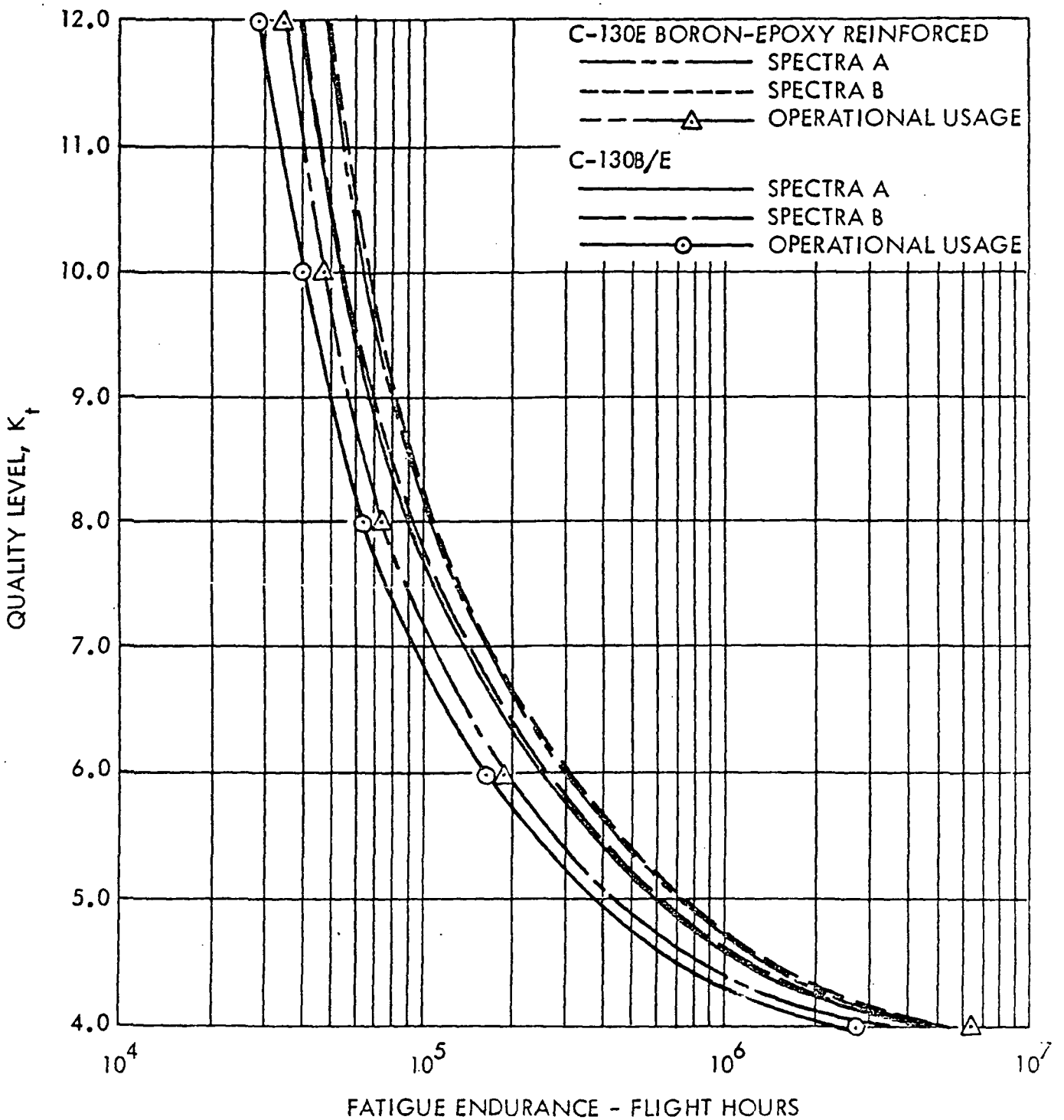

FIGURE C-6. - QUALITY LEVEL VERSUS FATIGUE ENDURANCE
W.S. 60 UPPER SURFACE

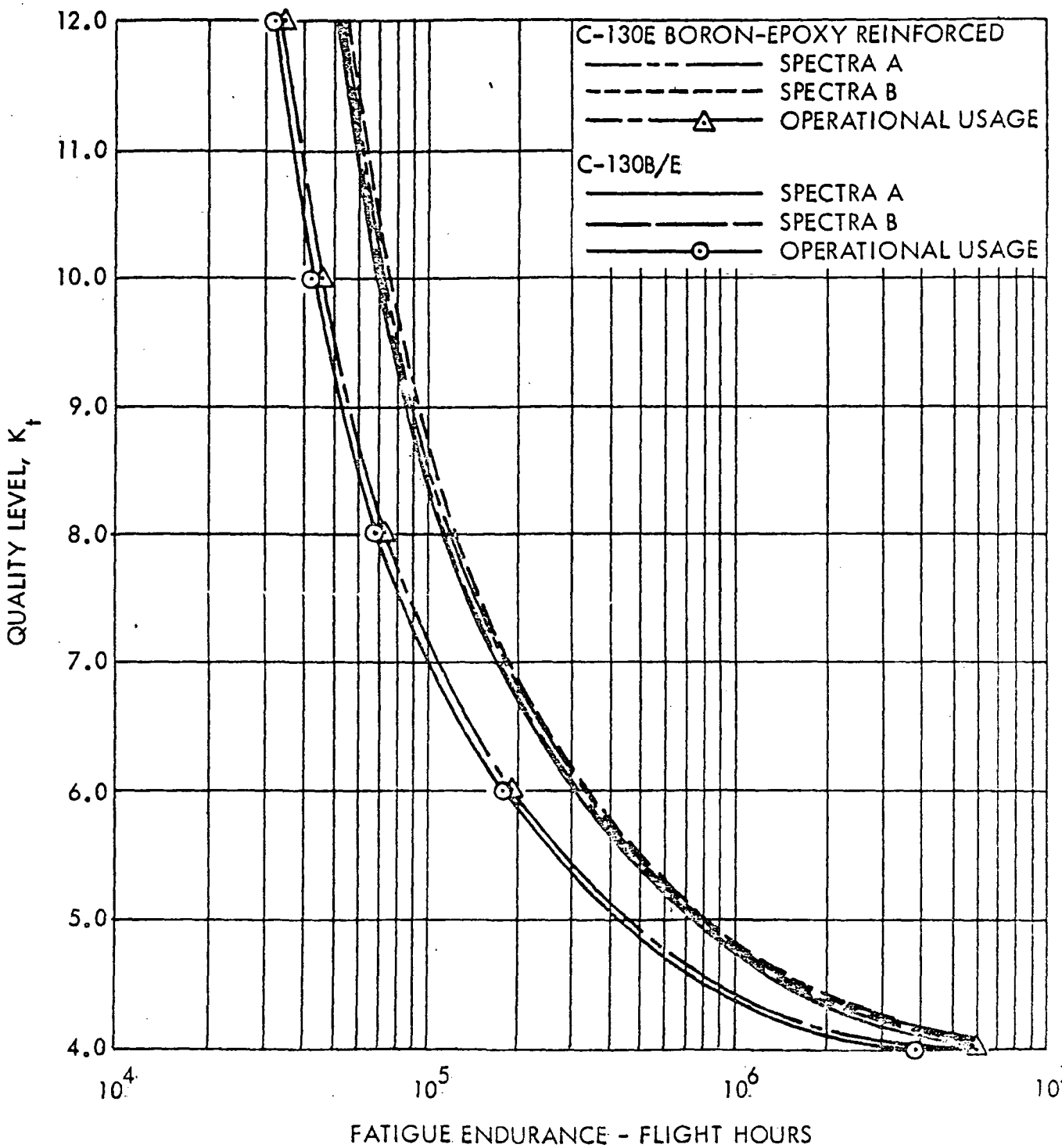

FIGURE C-7. - QUALITY LEVEL VERSUS FATIGUE ENDURANCE
W.S. 80 UPPER SURFACE

E

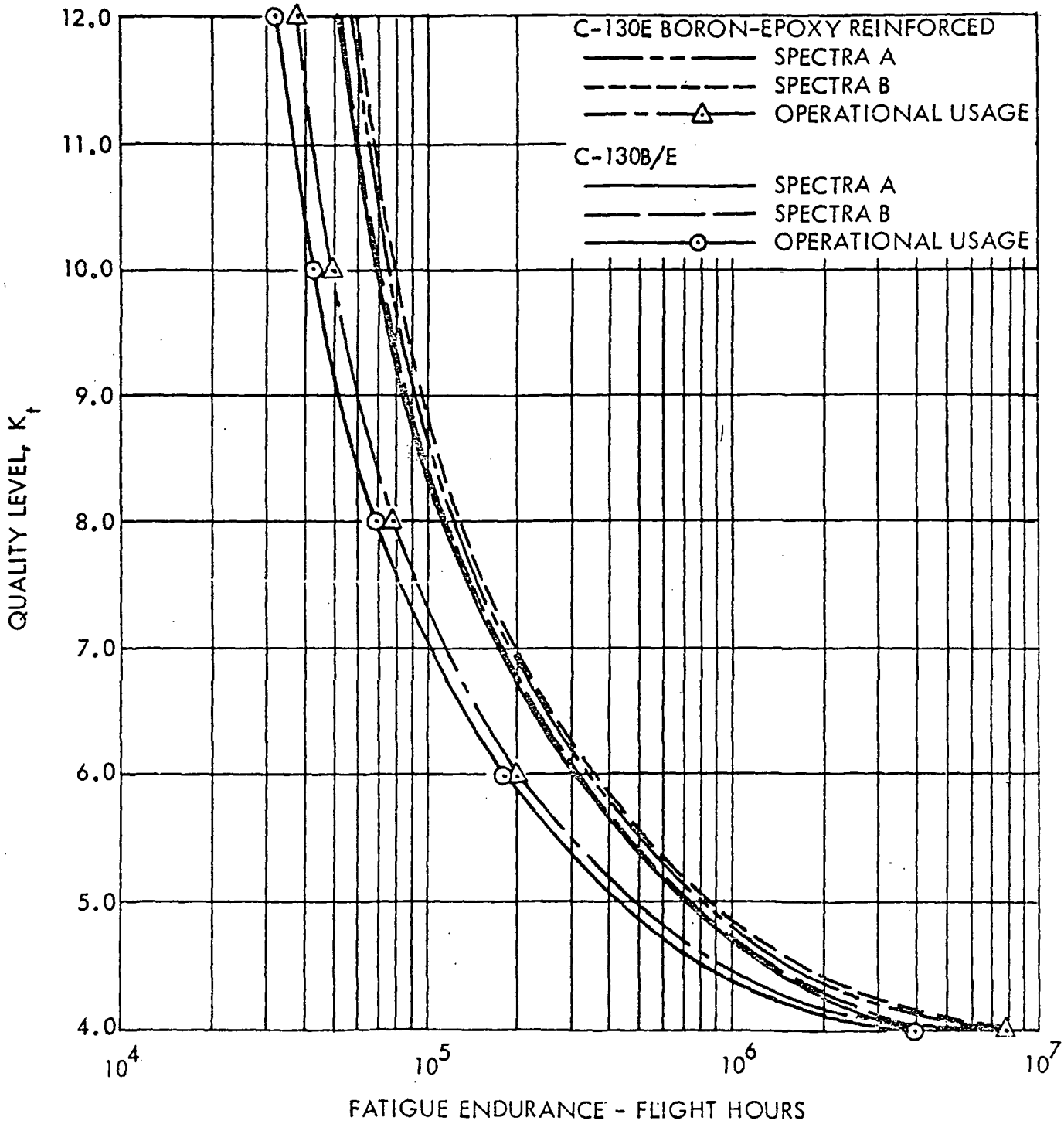

FIGURE C-8. - QUALITY LEVEL VERSUS FATIGUE ENDURANCE
W.S. 100 UPPER SURFACE

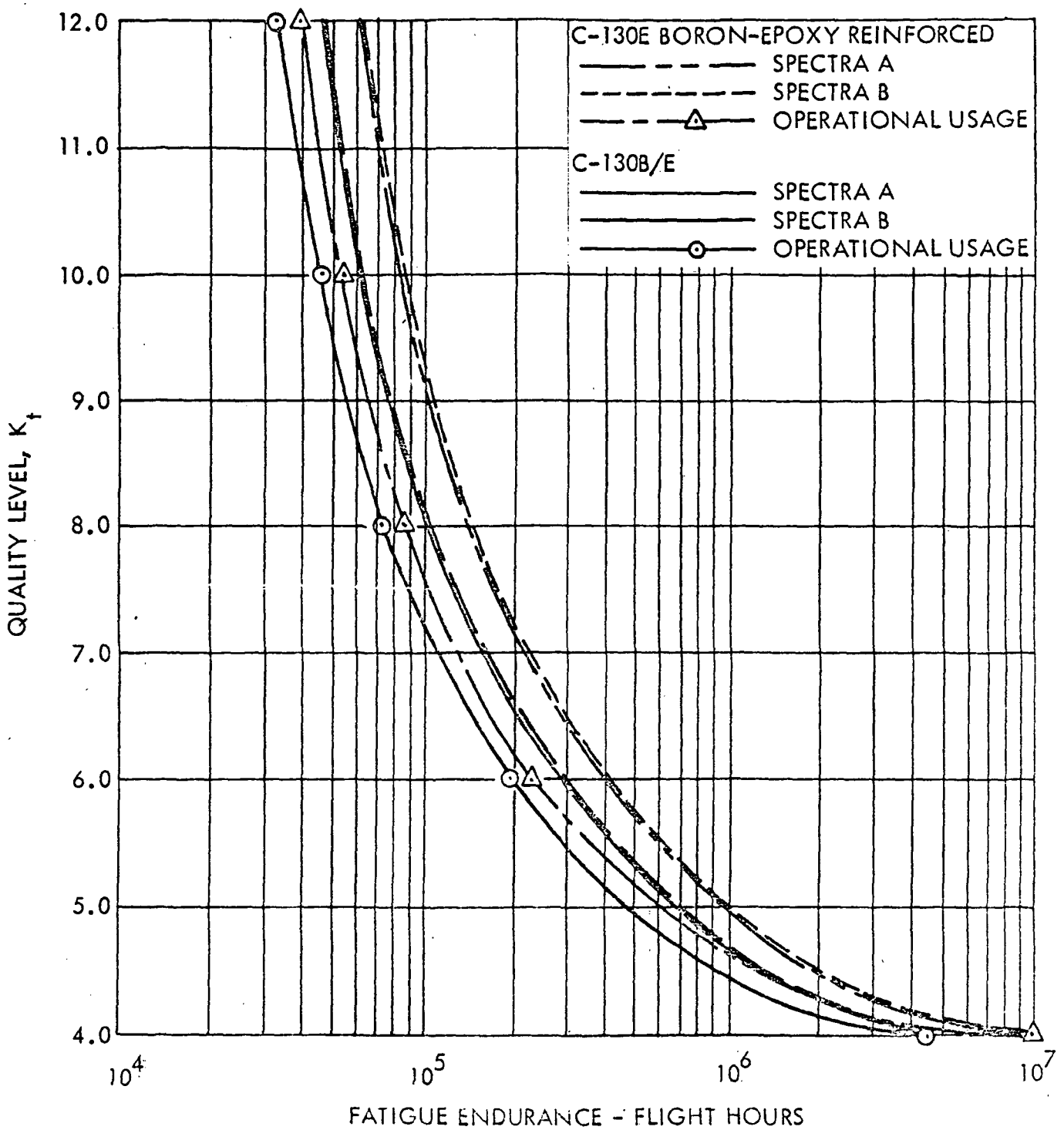

FIGURE C-9. - QUALITY LEVEL VERSUS FATIGUE ENDURANCE
W.S. 120 UPPER SURFACE

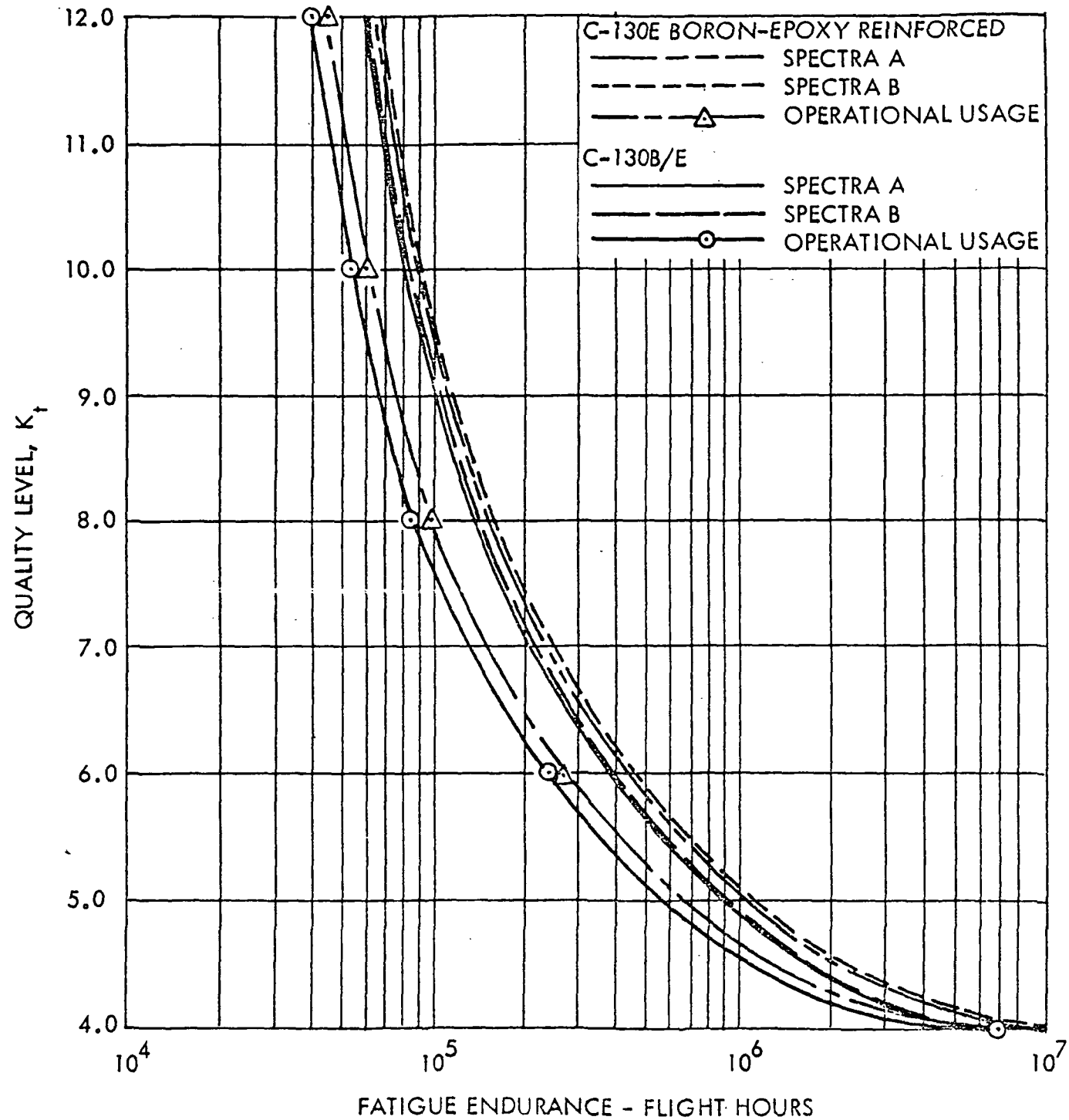

FIGURE C-10. - QUALITY LEVEL VERSUS FATIGUE ENDURANCE
W.S. 140 UPPER SURFACE

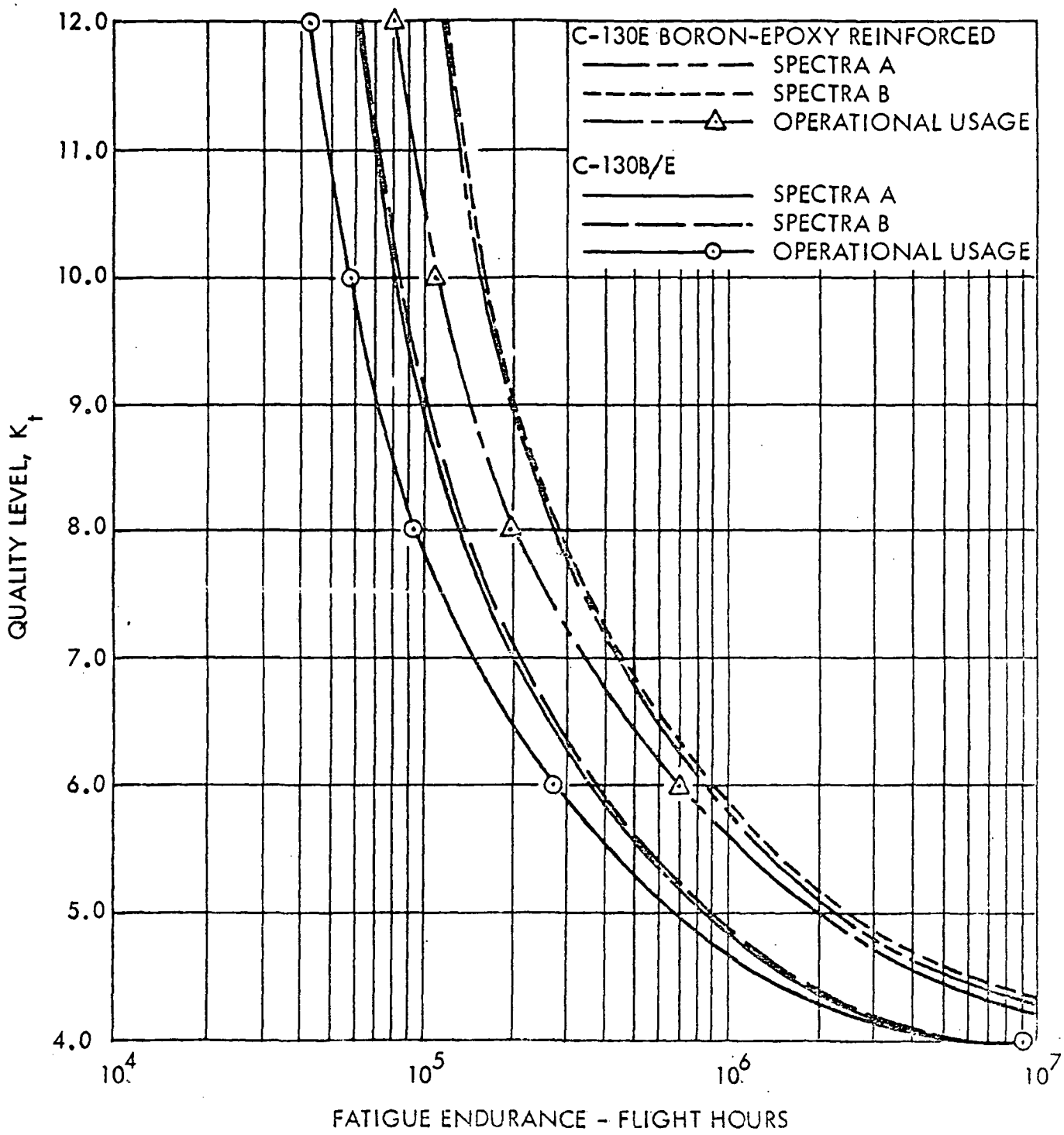

FIGURE C-11. - QUALITY LEVEL VERSUS FATIGUE ENDURANCE
W.S. 160 UPPER SURFACE

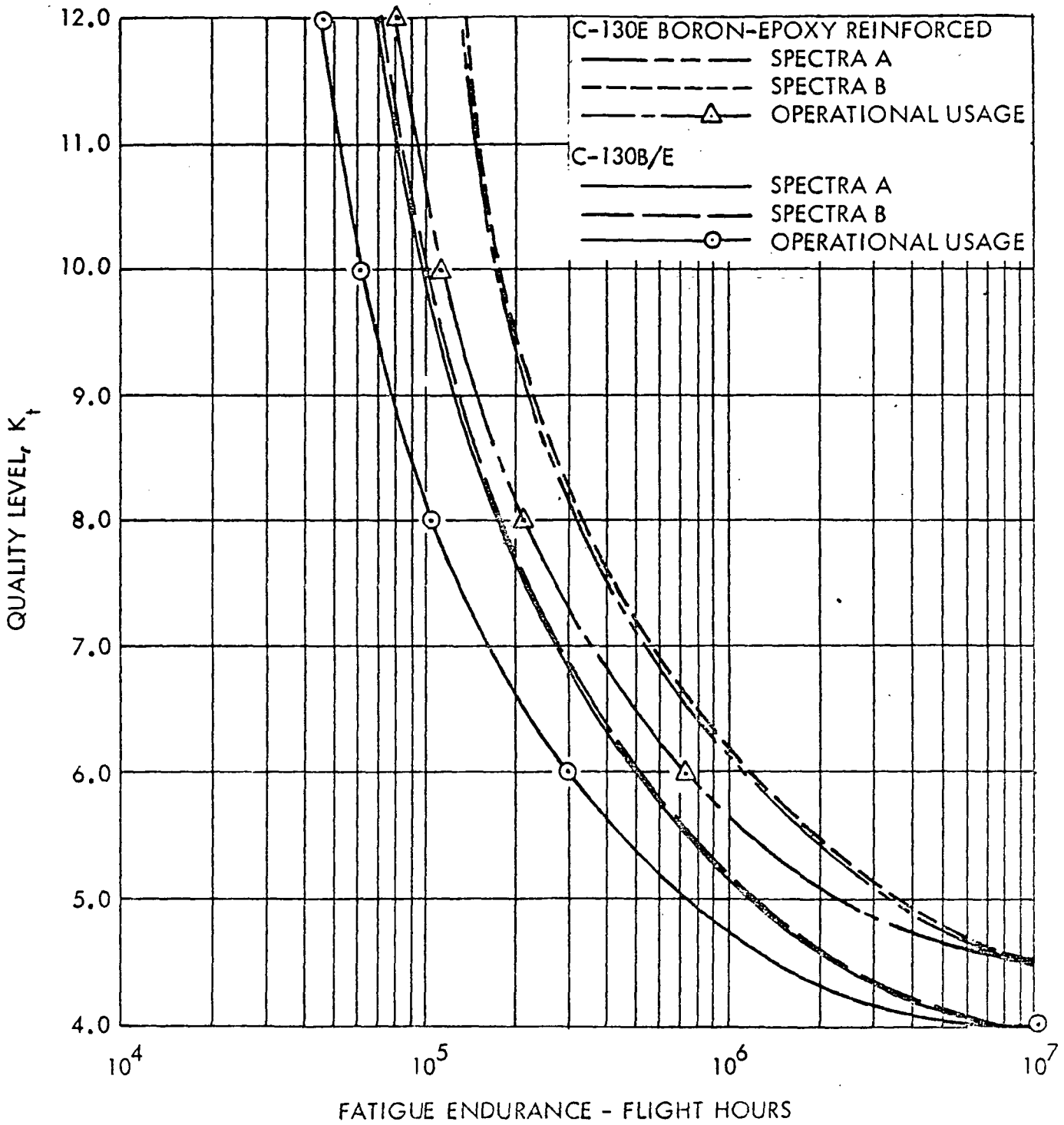

FIGURE C-12. - QUALITY LEVEL VERSUS FATIGUE ENDURANCE
W.S. 180 UPPER SURFACE

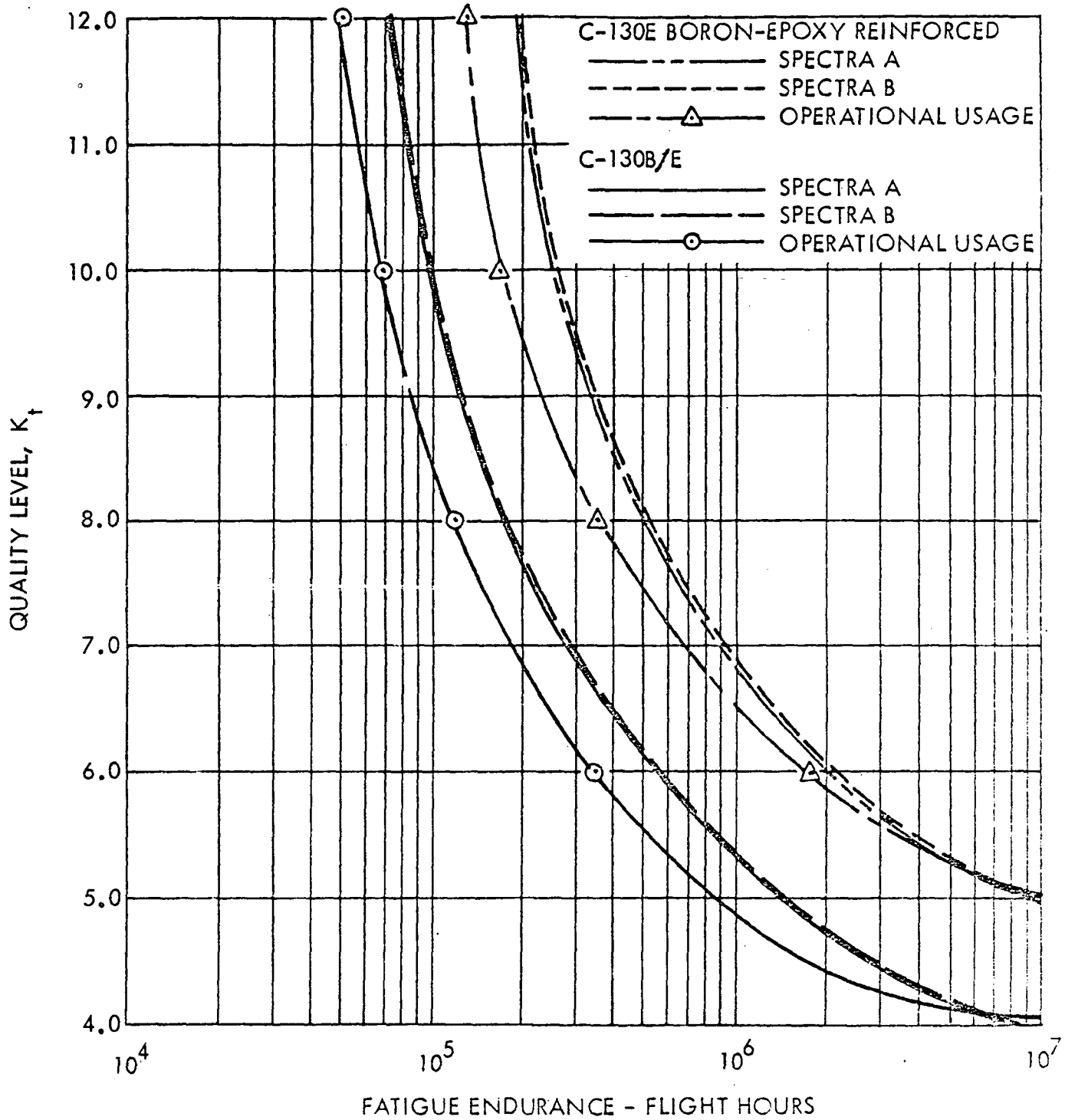

FIGURE C-13. - QUALITY LEVEL VERSUS FATIGUE ENDURANCE
W.S. 200 UPPER SURFACE

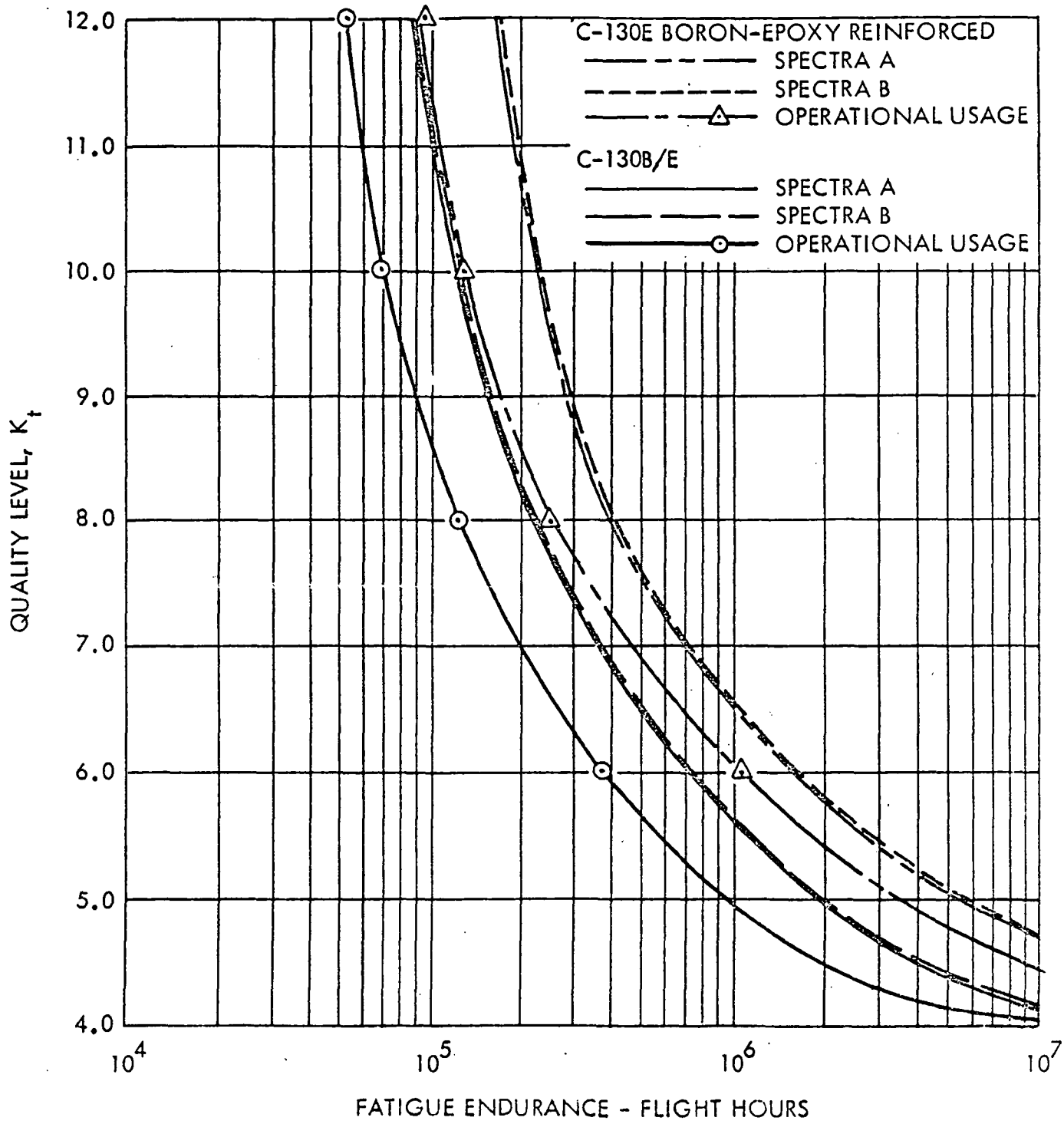

FIGURE C-14. - QUALITY LEVEL VERSUS FATIGUE ENDURANCE
W.S. 214 UPPER SURFACE

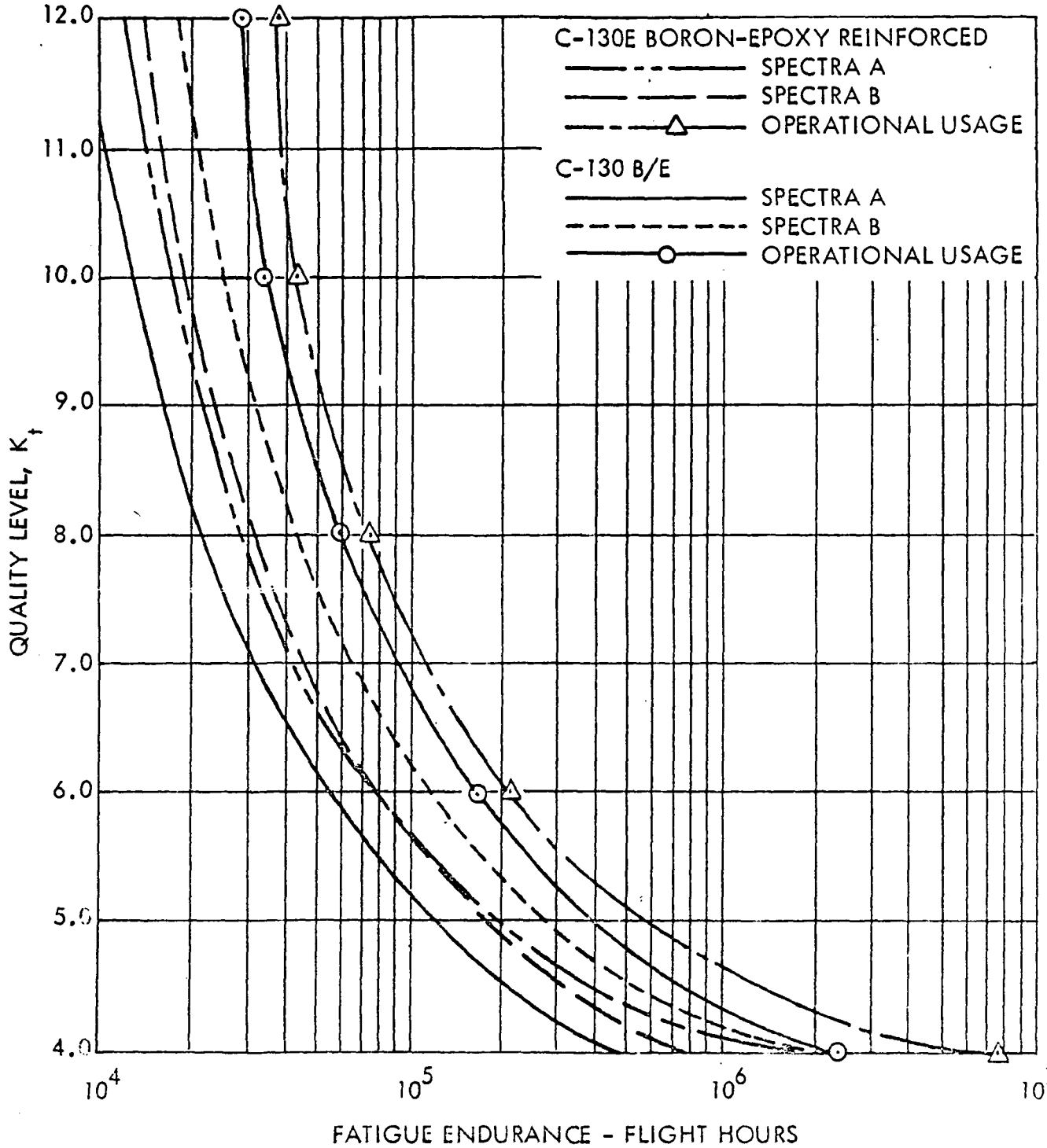

FIGURE C-15. - QUALITY LEVEL VERSUS FATIGUE ENDURANCE W.S. 40 LOWER SURFACE

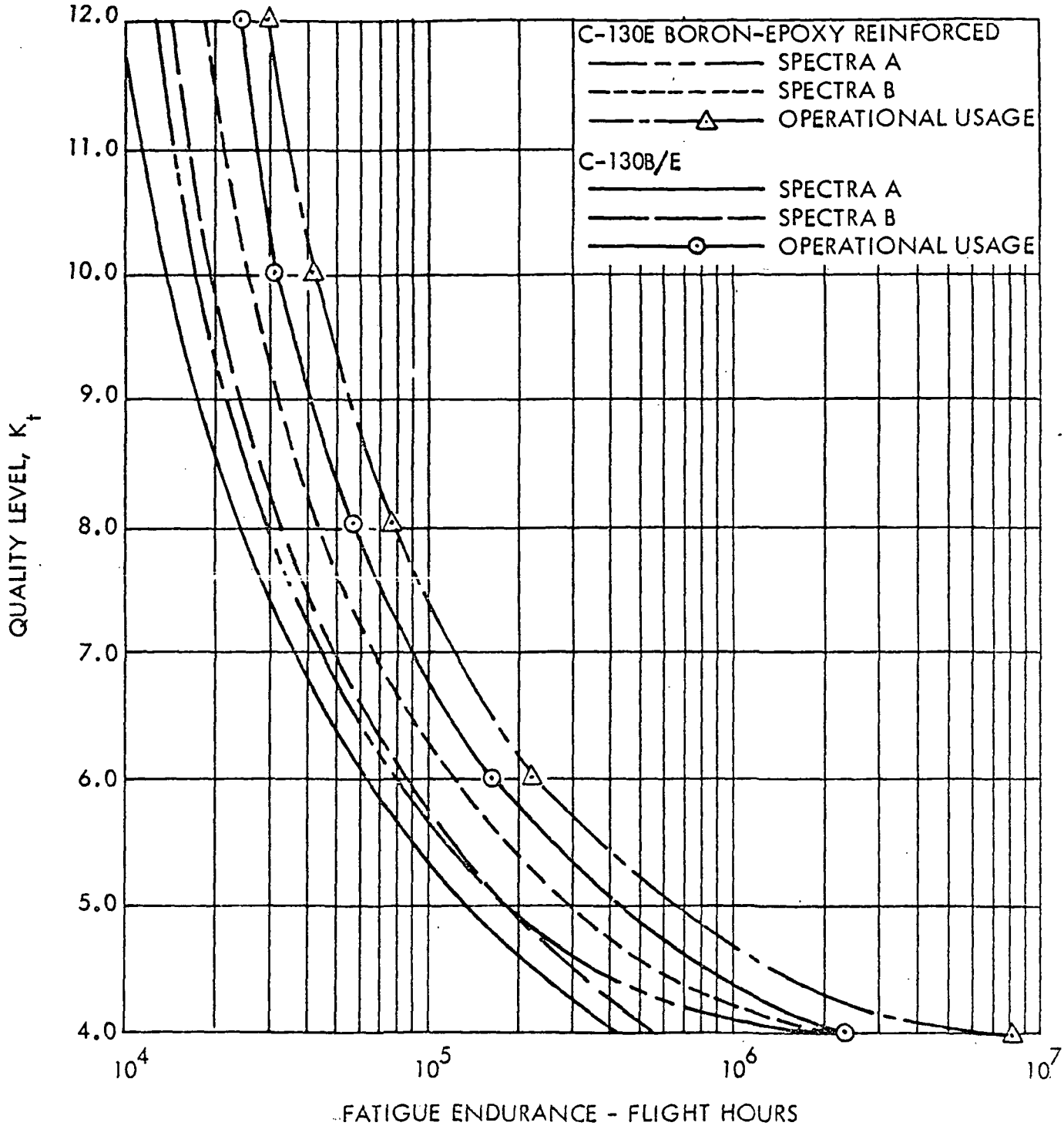

FIGURE C-16. - QUALITY LEVEL VERSUS FATIGUE ENDURANCE
W.S. 60 LOWER SURFACE

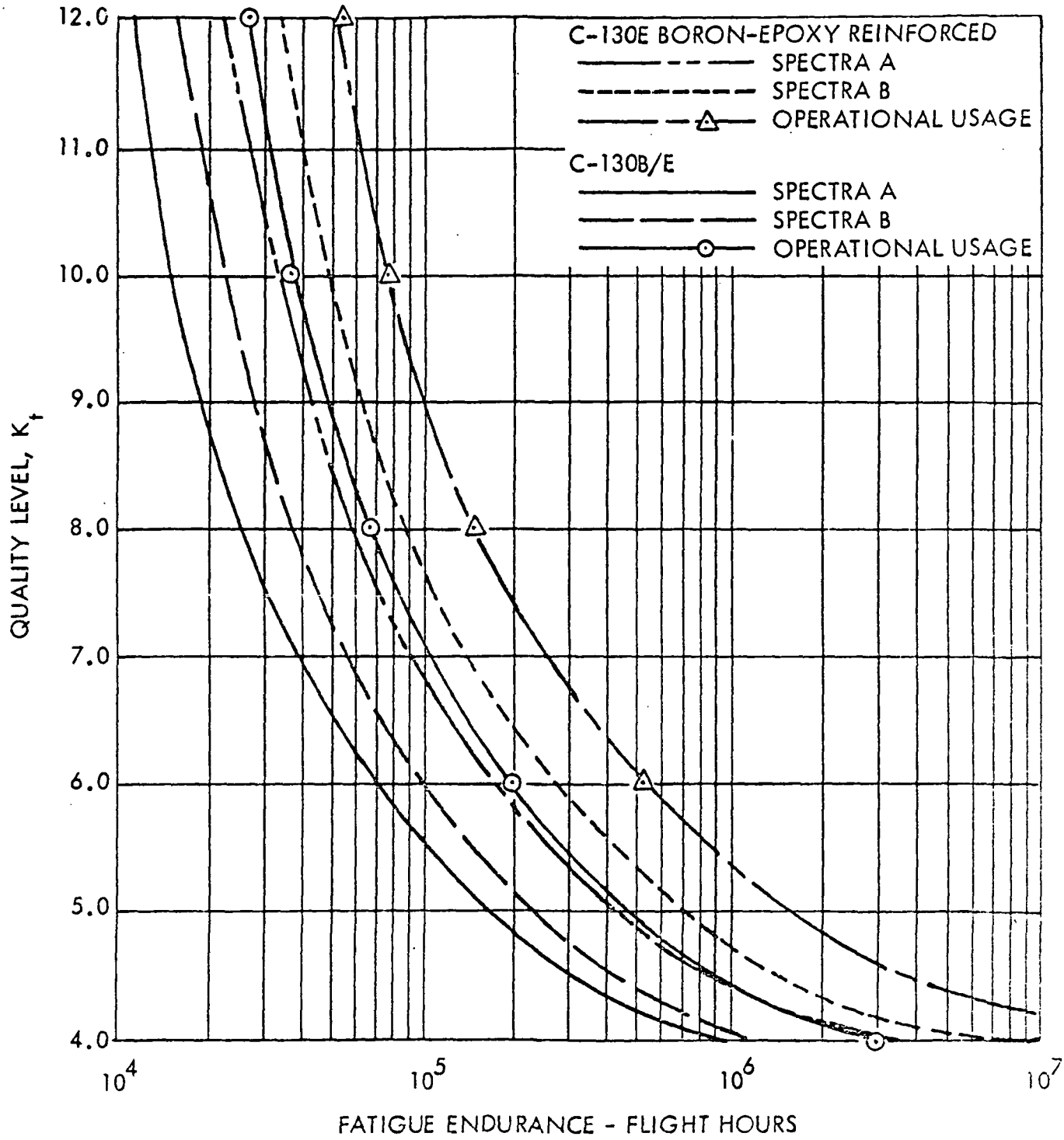

FIGURE C-17. - QUALITY LEVEL VERSUS FATIGUE ENDURANCE
W.S. 80 LOWER SURFACE

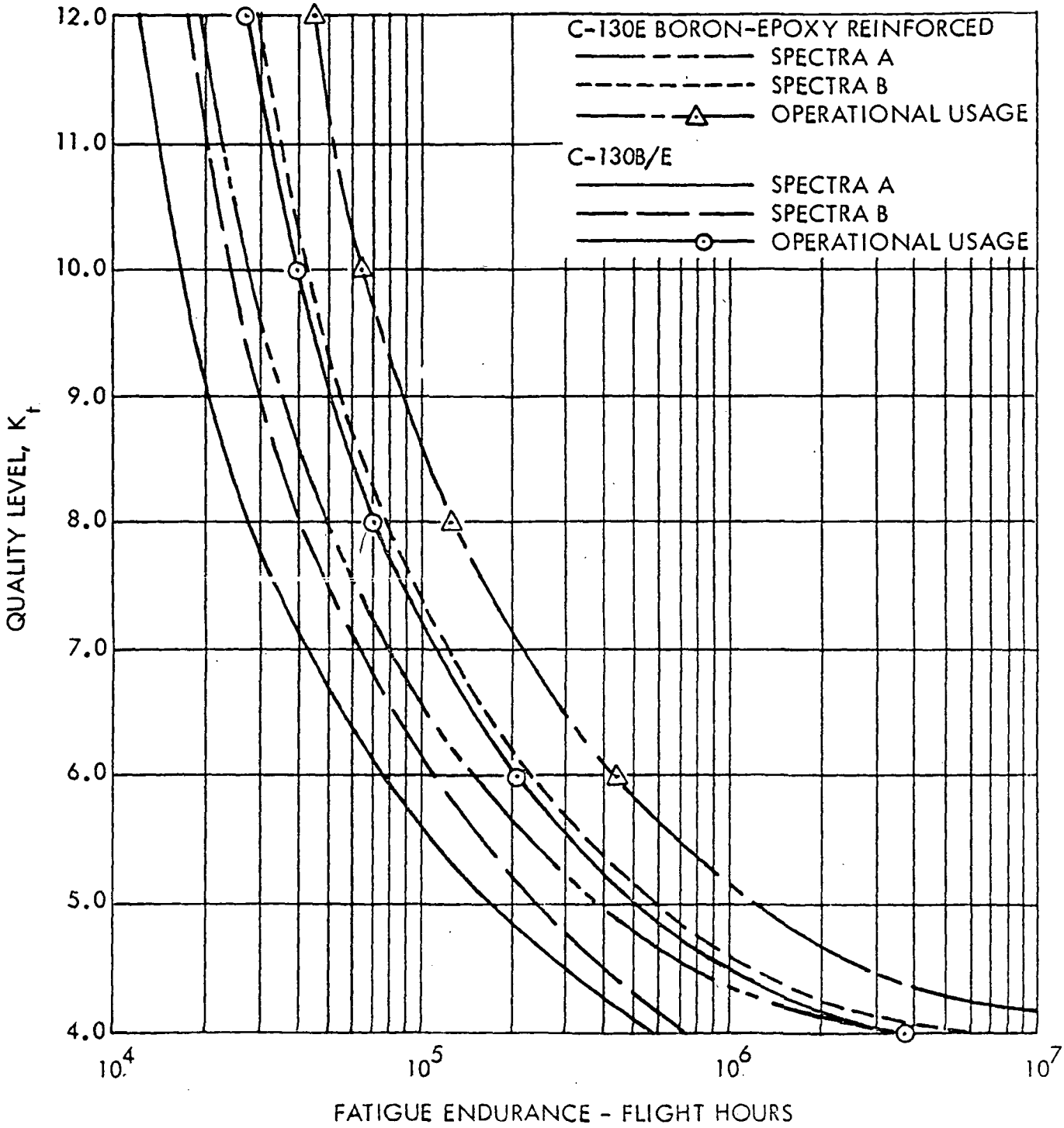

FIGURE C-18. - QUALITY LEVEL VERSUS FATIGUE ENDURANCE
W.S. 100 LOWER SURFACE

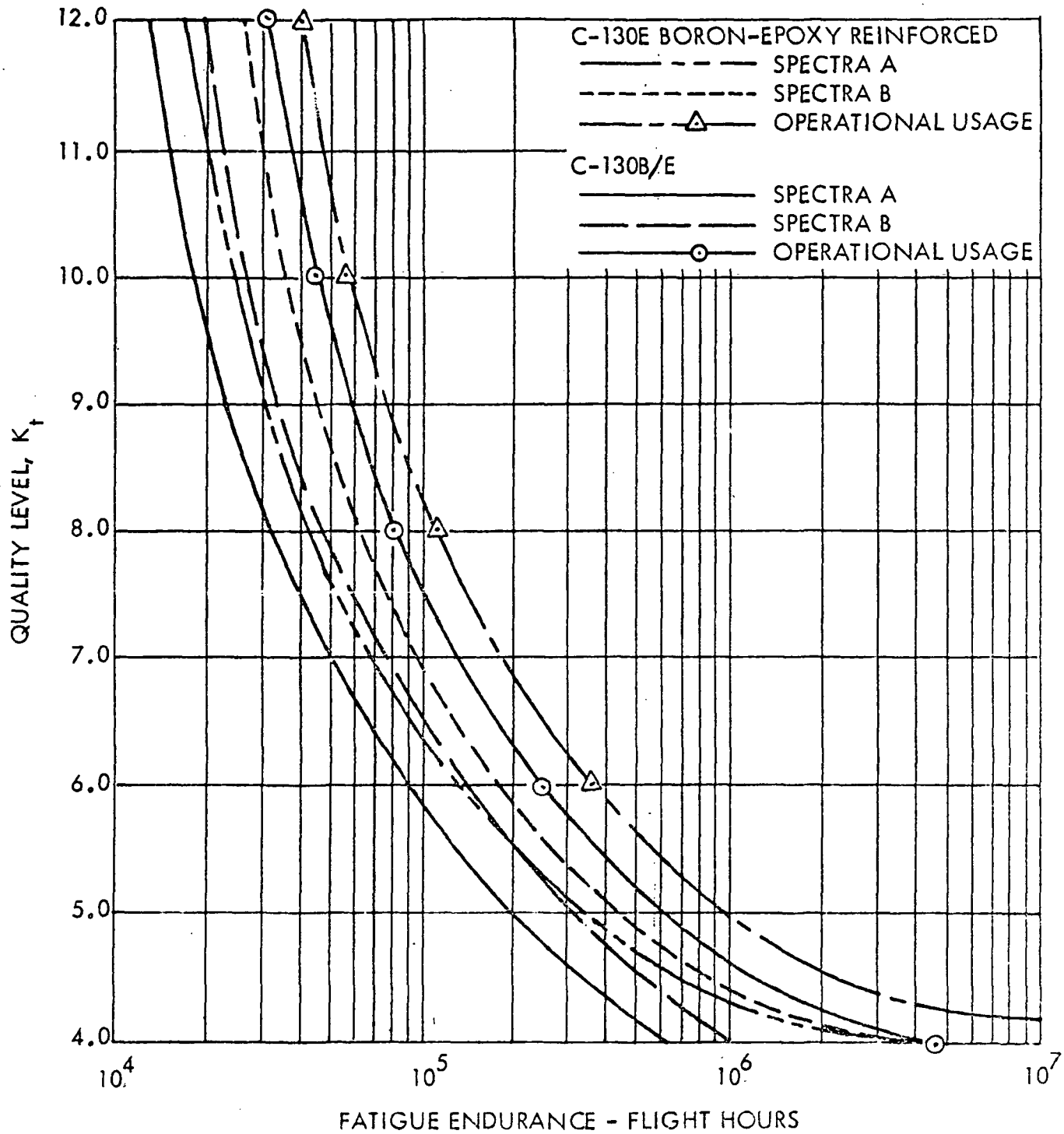

FIGURE C-19. -QUALITY LEVEL VERSUS FATIGUE ENDURANCE
W.S. 120 LOWER SURFACE

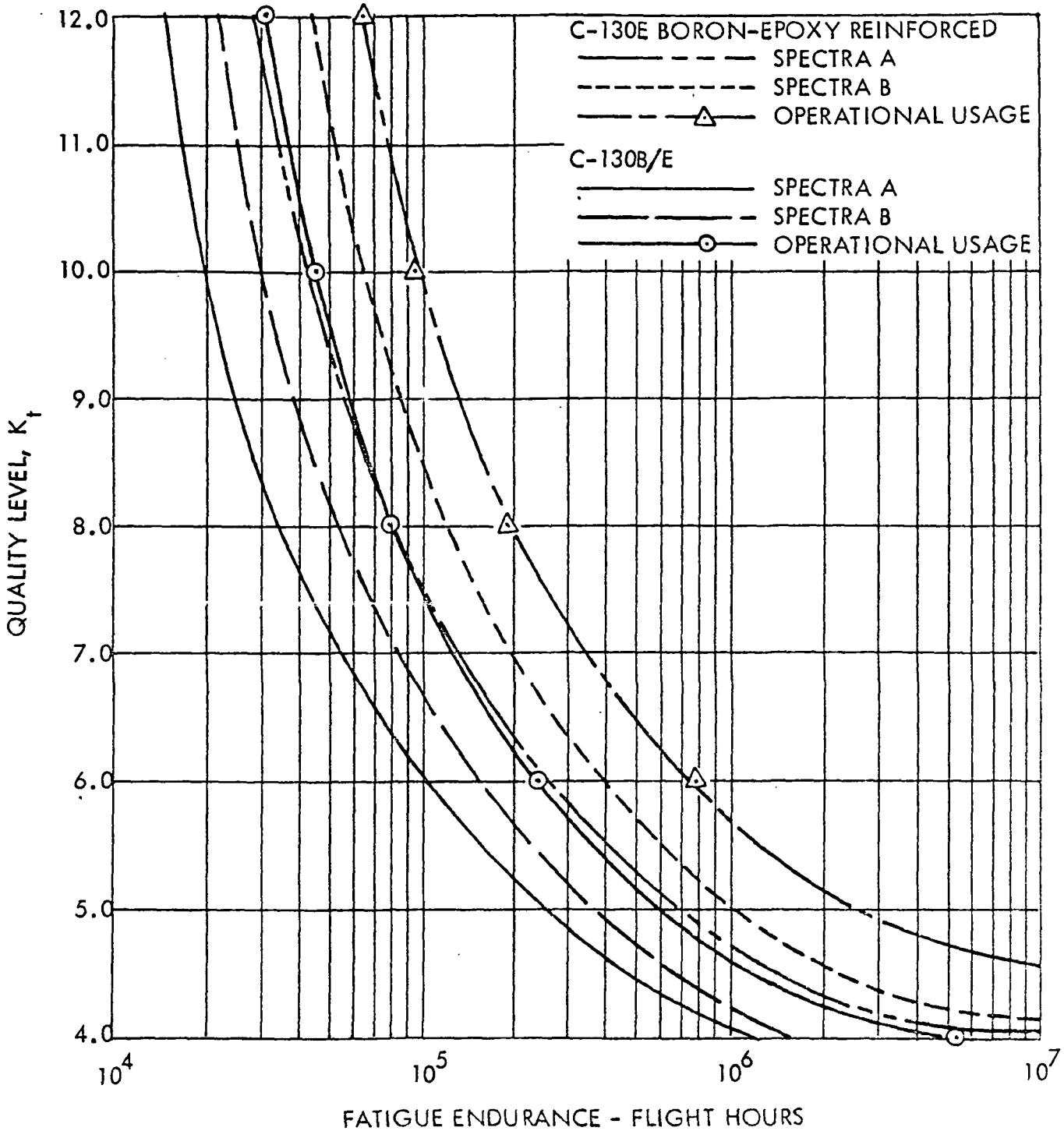

FIGURE C-20. - QUALITY LEVEL VERSUS FATIGUE ENDURANCE
W.S. 140 LOWER SURFACE

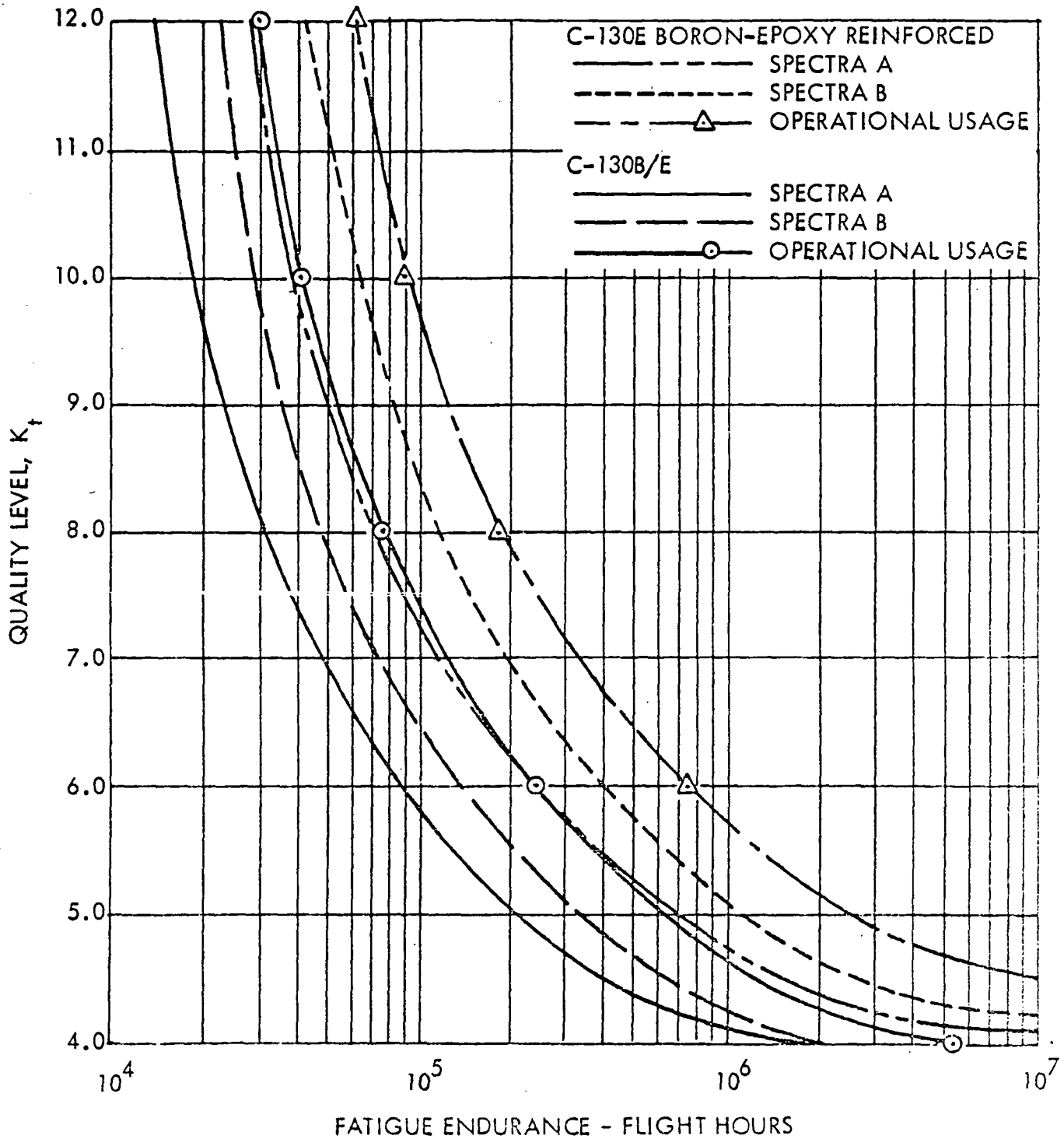

FIGURE C-21. - QUALITY LEVEL VERSUS FATIGUE ENDURANCE
W.S. 160 LOWER SURFACE

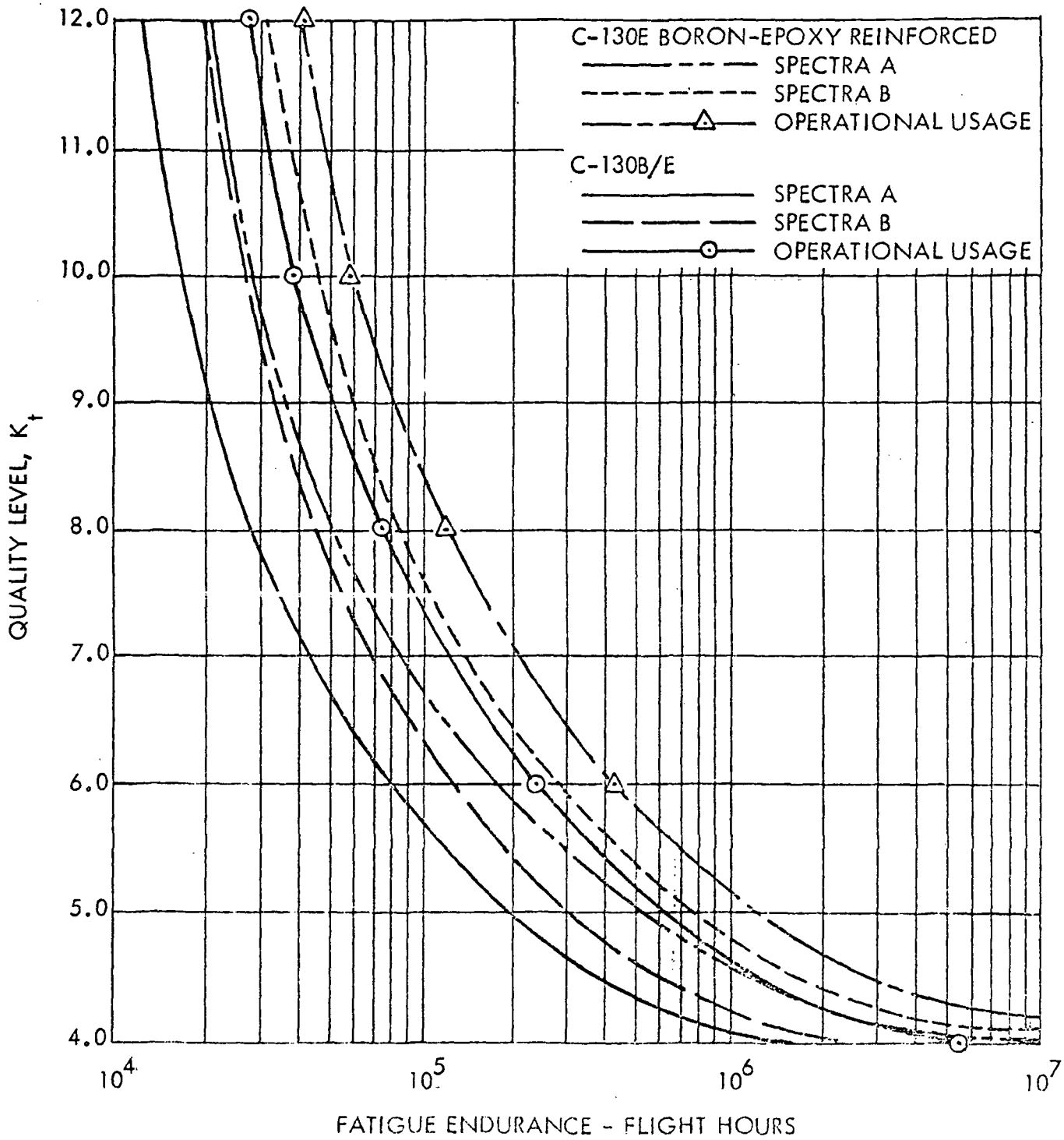

FIGURE C-22. -QUALITY LEVEL VERSUS FATIGUE ENDURANCE
W.S. 180 LOWER SURFACE

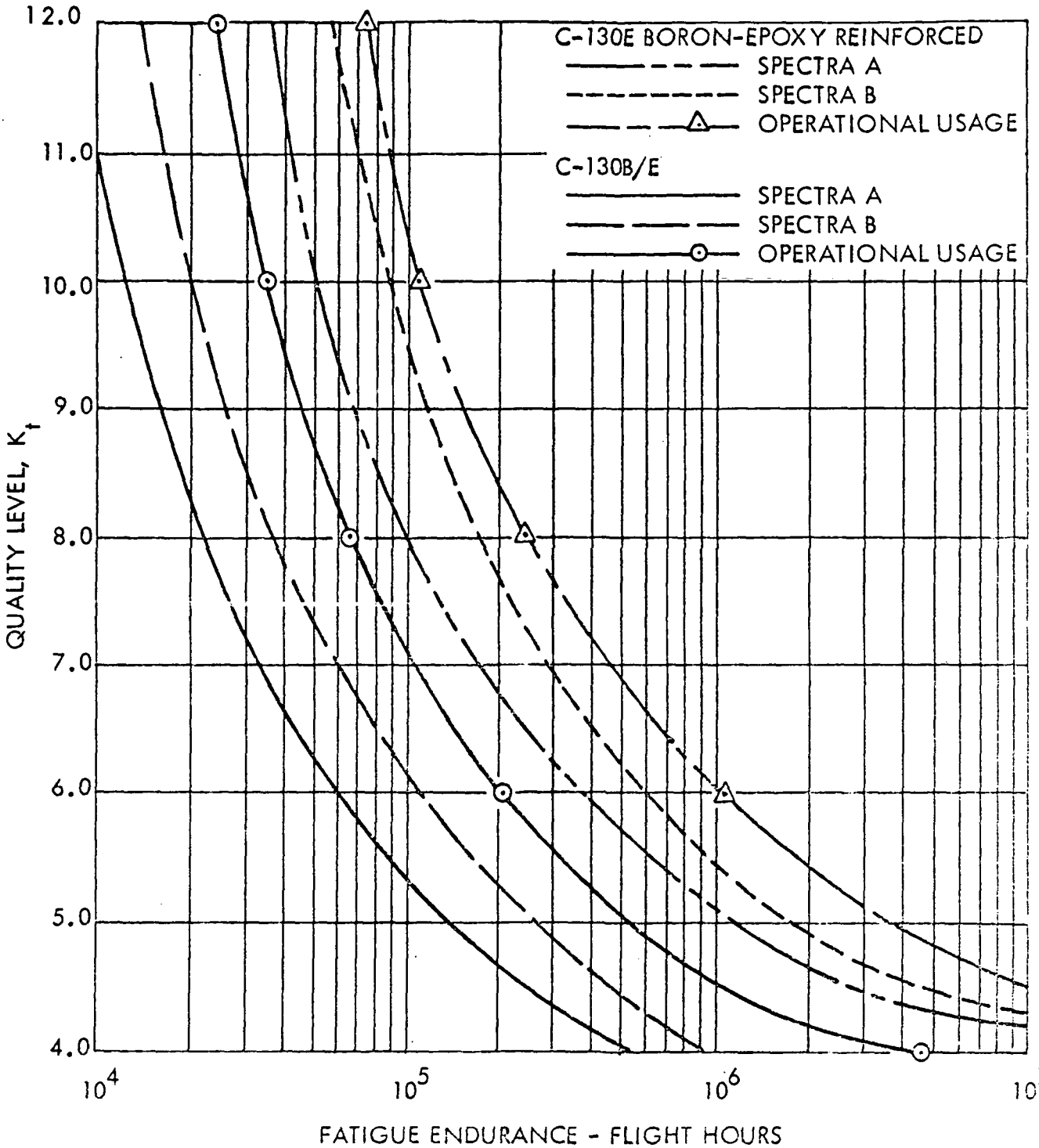

FIGURE C-23. - QUALITY LEVEL VERSUS FATIGUE ENDURANCE
W.S. 200 LOWER SURFACE

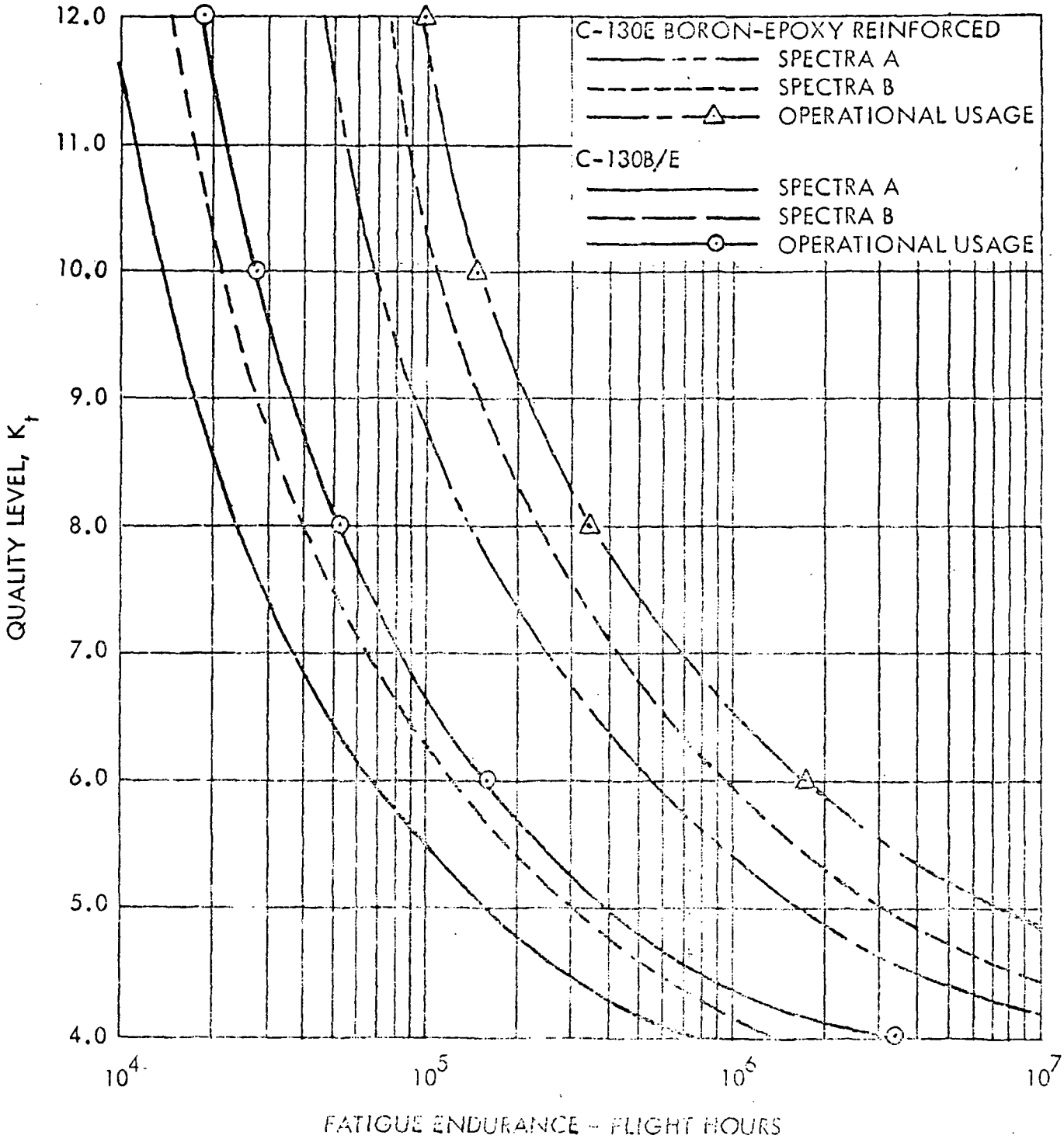

FIGURE C-24. - QUALITY LEVEL VERSUS FATIGUE ENDURANCE
W.S. 214 LOWER SURFACE